



HAL
open science

GPR88 signatures in mouse neuronal connectivity and behavior: a potential therapeutic target for psychiatric disorders

Tanzil Mahmud Arefin

► **To cite this version:**

Tanzil Mahmud Arefin. GPR88 signatures in mouse neuronal connectivity and behavior: a potential therapeutic target for psychiatric disorders. Neurobiology. Université de Strasbourg; Albert-Ludwigs-Universität (Freiburg im Breisgau, Allemagne), 2017. English. NNT : 2017STRAJ101 . tel-01775072

HAL Id: tel-01775072

<https://theses.hal.science/tel-01775072>

Submitted on 24 Apr 2018

HAL is a multi-disciplinary open access archive for the deposit and dissemination of scientific research documents, whether they are published or not. The documents may come from teaching and research institutions in France or abroad, or from public or private research centers.

L'archive ouverte pluridisciplinaire **HAL**, est destinée au dépôt et à la diffusion de documents scientifiques de niveau recherche, publiés ou non, émanant des établissements d'enseignement et de recherche français ou étrangers, des laboratoires publics ou privés.

ÉCOLE DOCTORALE SCIENCES DE LA VIE ET DE LA SANTE

Institut de génétique et de biologie moléculaire et cellulaire (IGBMC)

THÈSE présentée par :

Tanzil Mahmud AREFIN

soutenue le : **20 November, 2017**

pour obtenir le grade de : **Docteur de l'université de Strasbourg**

Discipline/ Spécialité : **Neuroscience**

TITRE de la thèse

Signatures du récepteur GPR88 sur la connectivité fonctionnelle et structurelle
du cerveau chez la souris : implications pour le développement de la
dépendance à l'alcool

THÈSE dirigée par :

Mme Ipek Yalcin, PhD. Université de Strasbourg

M. Ad Aertsen, PhD. University of Freiburg

RAPPORTEURS :

Mme Tracey D. Farr, PhD. University of Nottingham

Mme Ilka Diester, PhD. University of Freiburg

AUTRES MEMBRES DU JURY :

M. Yann Herault, PhD. Université de Strasbourg

Mme Laura-Adela Harsan, PhD. Université de Strasbourg

GPR88 signatures in mouse neuronal connectivity and behavior: A potential therapeutic target for psychiatric disorders

Inaugural-Dissertation

**Faculty of Biology
Albert-Ludwigs-Universität Freiburg
Freiburg, Germany**

**École Doctorale des Sciences de la Vie et de
la Santé Université de Strasbourg
Strasbourg, France**



**Submitted by
Tanzil Mahmud Arefin**

Contents

List of manuscripts	4
Summary	5
Chapter 1: Introduction	8
1.1 G-protein coupled receptor (GPCR) – GPR88.....	10
1.1.1 GPR88 – a novel therapeutic for psychiatric disorders	11
1.1.2 Behavioral studies on GPR88 receptor deficient mice.....	13
1.1.3 Generation of <i>Gpr88</i> ^{-/-} mice	15
1.2 The concept of brain connectivity and brain networks.....	16
1.3 Brain imaging techniques	19
1.3.1 Structural connectivity assessment via diffusion tensor imaging (DTI) and fiber tractography....	19
1.3.2 Functional connectivity assessment via resting state functional MRI (rsfMRI)	20
1.3.2.1 Default mode network	22
1.3.2.2 Central executive network	23
1.3.2.3 Salience network.....	24
1.3.2.4 Reward/aversion network.....	24
1.4 Rodents in neuroscience/neuroimaging research	26
1.4.1 rsfMRI and DTI in rodents.....	26
1.4.2 Rodents in behavioral neuroscience	27
1.4.2.1 IntelliCage.....	27
1.4.2.2 IntelliCage – software overview	29
1.5 Implications of GPR88 receptor in alcohol addiction.....	30
1.6 Integration of the introduced techniques into my work.....	31
Chapter 2: Results	33
2.1 Characterization of the impact of GPR88 receptor on the mouse brain connectivity.....	35
2.2 Behavioral studies with the <i>Gpr88</i> ^{-/-} mice.....	39
2.2.1 Increased alcohol seeking in mice lacking <i>Gpr88</i> involves dysfunctional addiction networks	39
2.2.2 Home cage behavioral phenotyping of <i>Gpr88</i> ^{-/-} female mice in group-housed condition	42
2.3 <i>Gpr88</i> signatures on the brain reward network connectivity after alcohol exposure in mice	46
2.4 Deletion of the mu opioid receptor gene in mice reshapes the reward–aversion connectome.....	48

Chapter 3: Discussion	50
Conclusion and future perspective	59
References	60
Acknowledgements	85
Chapter 4: Annex	86
4.1 Abbreviations	87
4.2 Tables.....	90
4.3 Figures	96
4.4 Experimental procedures	98
4.4.1 Construction of Gpr88 ^{-/-} mice.....	98
4.4.2 Animal preparation and MRI data acquisition	98
4.4.3 MRI data processing	99
4.4.3.1 Data pre-processing	99
4.4.3.2 Data post-processing.....	101
4.4.4 Mouse behavioral experiments.....	103
4.4.4.1 Experiments with alcohol.....	103
4.4.4.2 IntelliCage – system overview	103
4.4.4.3 Behavioral experiments with IntelliCage.....	109
4.4.4.4 IntelliCage data analysis	110
4.5 Principles of MRI.....	110
4.5.1 MR imaging.....	110
4.5.2 Relevant basic pulse sequences	112
4.5.3 Resting-state functional magnetic resonance imaging (rsfMRI)	113
4.5.4 T ₂ -weighted MRI.....	115
4.5.5 Diffusion tensor magnetic resonance imaging (DT-MRI) and fiber tracking.....	115

List of manuscripts

1. **Tanzil M. Arefin**, Anna E Mechling, Carole Meirsman, Thomas Bienert, Neele Hübner, Hsu-Lei Lee, Sami Ben Hamida, Aliza Ehrlich, Dan Roquet, Jürgen Hennig, Dominik v. Elverfeldt, Brigitte Lina Kieffer and Laura-Adela Harsan

Remodeling of sensorimotor brain connectivity in Gpr88 deficient mice (Arefin T. et al., 2017, Brain Connectivity, <https://doi.org/10.1089/brain.2017.0486>)

Own contribution: I designed the study, performed all experiments, analyzed data and wrote the manuscript in close collaboration with my supervisor.

2. Sami Ben Hamida, Sueli Netto, **Tanzil M. Arefin**, Md. Taufiq Nasseef, Laura-Joy Boulos, Michael McNicholas, Aliza Toby Ehrlich, Luc Moquin, Alain Gratton, Emanuel Darcq, Laura-Adela Harsan, Rafael Maldonado and Brigitte Kieffer.

Increased alcohol seeking in mice lacking Gpr88 involves dysfunctional mesocorticolimbic networks (Ben Hamida et al., 2018, Molecular Psychiatry, <https://doi.org/10.1016/j.biopsych.2018.01.026>)

Own contribution: I performed MRI experiments, analyzed data and wrote the manuscript parts related to rsfMRI in close collaboration with my supervisor.

3. Aliza T. Ehrlich, Meriem Semache, Julie Bailly, Stefan Wojcik, **Tanzil M. Arefin**, Christine Colley, Christian Le Gouill, Florence Gross, Viktoriya Lukasheva, Mireille Hogue, Emmanuel Darcq, Laura-Adela Harsan, Michel Bouvier and Brigitte L. Kieffer

Mapping GPR88-Venus illuminates a novel role for GPR88 in Sensory processing (Ehrlich et al., 2017, Brain structure and function, <https://doi.org/10.1007/s00429-017-1547-3>)

Own contribution: I performed MRI experiments, analyzed data and wrote the manuscript parts related to MRI in close collaboration with my supervisor.

4. Gregoire Maroteaux*, **Tanzil M. Arefin***, Sami Ben Hamida, Laura-Adela Harsan, Emmanuel Darcq, Brigitte Kieffer. *Co-1st authors

Lack of anticipatory behavior in Gpr88 knockout mice revealed by automatized home cage phenotyping (Maroteaux et al., 2018, Genes, Brain and Behavior, <https://doi.org/10.1111/gbb.12473>)

Own contribution: I designed the study, performed all experiments, analyzed data and wrote the manuscript in close collaboration with my supervisor.

5. Anna E. Mechling, **Tanzil Arefin**, Hsu-Lei Lee, Thomas Bienert, Marco Reisert, Sami Ben Hamida, Emmanuel Darcq, Aliza Ehrlich, Claire Gaveriaux-Ruff, Maxime J. Parent, Pedro Rosa Neto, Jürgen Hennig, Dominik von Elverfeldt, Brigitte Lina Kieffer and Laura-Adela Harsan.

Deletion of the mu opioid receptor gene in mice reshapes the reward-aversion connectome (Mechling et al., 2016, PNAS, doi:10.1073/pnas.1601640113)

Summary

Recent studies have demonstrated that the pathological perturbations of the brain and the expression or mutation of single gene influence spatially distinct regions via axonal pathways and result in the modification of overall brain functional and structural network architecture (Cao et al., 2015; Mechling et al., 2016; Richiardi et al., 2015; Thompson et al., 2013, Arefin et al., 2017). Functional and structural connectivity mapping of the brain thus offer a prevailing framework for localizing pathology, identifying the brain regions affected by pathological processes as well as tracking the patterns of psychiatric disorders that disturb higher cognitive functions (Biswal et al., 2010; Craddock et al., 2013; Sporns et al., 2005).

Resting-state functional magnetic resonance imaging (rsfMRI) is a technique that detects low frequency fluctuations (LFFs) of less than 0.1 Hz in the blood oxygen level dependent signal (BOLD) signal and measures functional connectivity (FC) between brain regions as the level of synchrony of spontaneous fMRI time-series during rest (Biswal et al., 1995, 1997; Greicius et al., 2003; Salvador et al., 2005). Diffusion tensor imaging (DTI) on the other hand is a three-dimensional noninvasive imaging modality that measures the diffusion of water molecules as a probe to infer the microstructural features. By combining the directional information and magnitude of anisotropic diffusion of the individual voxels, the course of fiber tracts can be reconstructed, which is known as tractography. Therefore, DTI and fiber tractography provides a unique opportunity to study the fiber architecture in vivo and characterize microstructural changes or differences with neuropathology and treatment. Both the rsfMRI and DTI have been widely used for functional and structural brain connectivity mapping in human (Fair et al., 2007; Fox and Raichle, 2007; Alexander et al., 2007; Mori et al., 2001), rodents (Jonckers et al., 2011; Mechling et al., 2014, 2016; Harsan et al., 2006, 2010, 2013, Arefin et al., 2017) and primates (Hutchison et al., 2012; Shi et al., 2013; Zhang et al., 2013).

In this study, we combined mouse mutagenesis with functional and structural magnetic resonance imaging (MRI) to determine whether targeted inactivation of a single gene would modify whole-brain connectivity in live animals and how it translates at the behavioral level. The targeted gene encodes GPR88 - an orphan G-protein coupled receptor, robustly expressed in the dorsal and ventral striatum as well as in the amygdala, olfactory tubercle, inferior olive nucleus and neocortex (Ghate et al., 2007; Meirsman et al., 2016; Mizushima et al., 2000) in rodents, monkeys and human being during development and adulthood (Massart et al., 2009). The striatum is a major entry into the basal ganglia (BG) and plays important role in the initiation and patterning of many behaviors. Striatum receives excitatory cortical glutamatergic and thalamic glutamatergic inputs as well as modulatory dopaminergic input from substantia nigra and ventral tegmental area. These glutamatergic inputs together with inhibitory inputs from interneurons are integrated and relayed to other BG components via GABAergic medium spiny neurons (MSNs). MSNs express D1- or D2-dopamine receptors (D1R and D2R), founding the striatonigral (direct) and striatopallidal (indirect) pathways (Gerfen, 1992). GPR88 is abundant in MSNs expressing D1R and D2R (Massart et al., 2009). GPR88 thus plays potential role in psychiatric and

neurodegenerative diseases such as schizophrenia, depression, hyperactivity, addiction and bipolar disorder (Del Zompo et al., 2014; Ingallinesi et al., 2015; Logue et al., 2009; Massart et al., 2009; Meirsmann et al., 2016; Quintana et al., 2012). However, much remains to be clarified regarding the specific cellular and physiologic roles of GPR88, and its pathophysiologic relevance to brain disorders.

Therefore, the first objective of my PhD project was to investigate the role of GPR88 receptor in living mouse brain structural and functional communication. This comprised, imaging the Gpr88 gene knock-out ($Gpr88^{-/-}$) mice and their wild-type littermates (CTRL or $Gpr88^{+/+}$ - mice normally expressing the GPR88 receptor) by means of rsfMRI and DTI with tractography techniques respectively.

Secondly, I investigated the involvement of GPR88 in the development of alcohol seeking and drinking behavior. $Gpr88^{-/-}$ and their littermates $Gpr88^{+/+}$ mice were exposed to alcohol to examine whether Gpr88 deletion alters alcohol-taking and seeking behaviors. These mice were further imaged to investigate the involvement of GPR88 receptor in neurocircuitries modifications due to alcohol intake. Neuronal connectivity alterations were assessed following similar MR based neuroimaging approaches similar to the first part of my study.

Additionally, $Gpr88$ deficient mice were characterized by investigating the effects of $Gpr88$ gene in mouse behaviors using computer-based, fully automated testing apparatus - IntelliCage. It is an automated home cage that monitors group-housed mice implanted with radio frequency identification chips and allows studying multi-dimensional aspects of mice behavior. This longitudinal study was designed to investigate the striatum and hippocampus mediated behaviors with group-housed mice in 4 consecutive phases (free adaptation, nosepoke adaptation, place learning and fixed schedule drinking).

My work provided the first evidence of GPR88 involvement in remodeling the mouse brain functional and structural brain networks, primitive to the repertoire behavior observed in $Gpr88^{-/-}$ mice (Arefin T. et al., 2017). Deletion of $Gpr88$ in mice resulted extensive remodeling of intracortical and cortico-subcortical networks. Most prominent modifications were observed in retrosplenial cortex connectivity, a core player of the default mode network (DMN). Indeed, FC modifications in the DMN is considered a hallmark of many psychiatric conditions (Brady et al., 2016; Castellanos et al., 2008; Fair et al., 2010; Garrity et al., 2007). Furthermore, somatosensory and motor cortical networks showed remarkable FC modifications suggesting sensorimotor gating deficiency reported in mutant animals (Logue et al., 2009; Meirsmann et al., 2016a), and also likely underlie their hyperactivity phenotype. Apart from the cortical network, alterations within hippocampal and dorsal striatum FC underscore a specific learning deficit previously reported in $Gpr88^{-/-}$ animals (Meirsmann et al., 2016a). Moreover, amygdala connectivity with cortex and striatum was weakened, perhaps underlying the “risk-taking” behavior of these animals (Meirsmann et al., 2016b). This study hence implies GPR88 as a core player in brain communication.

In addition, we observed that Gpr88 deletion disrupts executive, reward and emotional networks in a configuration that reduces alcohol reward and promotes alcohol seeking and drinking. The FC signature is reminiscent of alterations observed in individuals at-risk for alcohol use disorders (AUDs). The Gpr88 gene, therefore, may represent a vulnerability/resilience factor for AUDs, and a potential drug target for AUDs treatment (Ben Hamida et al., 2018).

Moreover, through the development of IntelliCage protocols, we perceived hyperactivity, non-habituation, repetitive behavior and learning alteration that were previously described using different classical behavioral tests. The novel finding of this study is the lack of anticipatory behavior in mice lacking GPR88 receptor (Maroteaux et al., 2018).

This is the first study demonstrating that GPR88 activity shapes the mouse brain functional as well as structural connectome and how it translates at the behavioral level. Most importantly, the concordance between connectivity alterations and behavior deficits observed in Gpr88-deficient mice suggests Gpr88 as a potential therapeutic target for psychiatric disorders.

Chapter 1

Introduction

The PhD project presented here relates to the interdisciplinary field of research, merging non-invasive neuroimaging techniques and behavioral investigations in genetically modified mice. This comprised: mapping brain functional and microstructural network by means of resting state functional magnetic resonance imaging (rsfMRI) and high angular resolution diffusion imaging (HARDI) as well as global tractography. Moreover, GPR88 mediated mouse behavioral and cognitive functions were investigated using a computer-based automated system – IntelliCage and mouse behavior in response to alcohol exposure was assessed using conventional type-III cages. Mice exposed to alcohol were further scanned to examine whether deletion of Gpr88 gene remodels the brain functional and structural connectivity. This chapter provides an introductory view of the entire study.

Section 1.1 introduces the novel GPR88 receptor and its expression in the mouse brain, followed by the importance of examining this gene as a therapeutic target for psychiatric disorders (1.1.1). Section 1.1.2 describes behavioral studies characterizing the influence of GPR88 in mouse behavior and thus highlighting the significance of investigating the role of this gene in brain communication.

Section 1.2 briefly describes the concept of brain connectivity and brain networks.

Section 1.3 introduces one of the most widely used non-invasive magnetic resonance imaging (MRI) technique to map the brain connectivity or networks. This section further includes 2 more sub-sections: 1.3.1 illustrates the principles of mapping the brain structural network using diffusion tensor imaging (DTI) and tractography approach and the subsequent section (1.3.2) describes the concept of rsfMRI and some of the methods commonly used for brain functional connectivity mapping, such as: seed correlation analysis, independent component analysis (ICA) and partial correlation analysis. These methods used in my studies to characterize the mouse brain connectivity have been also extensively used in humans, as well as rodents and primates to identify the functional brain networks. Three of the major functional networks: default mode network (DMN), central executive network (CEN) and salience network (SN), have been briefly introduced in the succeeding sub-sections 1.3.2.1, 1.3.2.2 and 1.3.2.3 respectively.

Section 1.4 describes the use of rodents in neuroscience research, particularly in the neuroimaging (rsfMRI and DTI) and behavioral neuroscience (1.4.1 and 1.4.2). Next, sub-sections introduce the computer-based automated system – IntelliCage, used for screening the behavioral and cognitive functions of group-housed mice. This includes the hardware and software of the IntelliCage as well as some of the salient features of this system.

Section 1.5 demonstrates the implication of GPR88 receptor in the development of alcohol addiction.

Section 1.6 finally elucidates how these techniques have been implemented and integrated into my work.

1.1 G-protein coupled receptor (GPCR) – GPR88

G protein-coupled receptors (GPCRs) are the most common targets of the neuro-pharmacological drugs in the central nervous system (CNS). GPCRs are activated by manifold neurotransmitters, and their activation in turn evokes slow synaptic transmission. GPR88 is an orphan G-protein coupled receptor that was first identified in rat brain by Mizushima et al. (Mizushima et al., 2000). Gpr88 gene is initially describes as having almost exclusive expression in dorsal and ventral striatum in rodents and human (Figure 1)

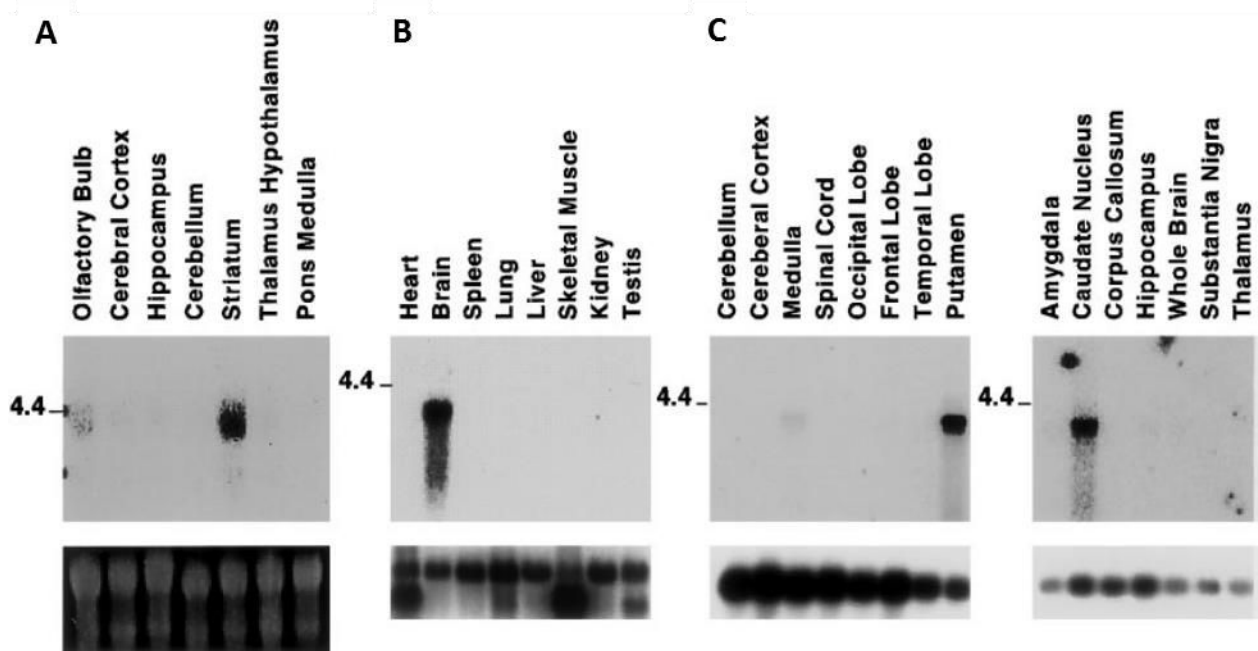


Figure 1: **Northern blot hybridization analysis for strg/GPR88 expression:** (A) Distribution of rStrg/rGpr88 mRNA in rat central nervous system. (B) Distribution of mStrg/mGpr88 mRNA in adult mouse tissues. (C) Distribution of human STRG/GPR88 mRNA in human brain tissues. The lower panels show the ethidium bromide-stained gel to confirm the quality and relative amount of the RNA in each lane (A) and control hybridization with the b-actin probe (B, C). [Adapted from (Mizushima et al., 2000)].

Further studies validate GPR88 expression in the amygdala, olfactory tubercle, inferior olive nucleus, as well as in neocortex (Figure 2, Arefin T. et al., 2017) (Ghate et al., 2007; Aura C. Meersman et al., 2016; Mizushima et al., 2000) in rodents, monkeys and human being during development and adulthood (Massart et al., 2009).

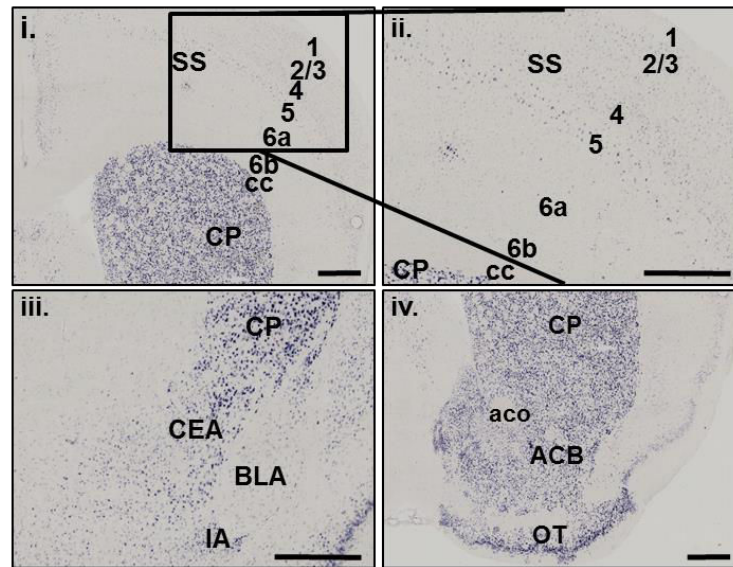


Figure 2: **Localization of GPR88 receptor via In situ hybridization (ISH):** ISH expression of GPR88 in cortical and subcortical regions: **i.** Cortical regions of GPR88 expression in the layers 4 and 5 of somatosensory cortex (SS), and caudate putamen (CP). **ii.** The SS layer 4 and 5 enrichment of GPR88. **iii.** Amygdalar GPR88 expression is predominately localized to the central extended amygdala areas (CEA) and intercalated amygdalar nucleus (IA) compared with the lack of expression in basolateral amygdala (BLA). **iv.** GPR88 is expressed in the nucleus accumbens (ACB) and olfactory tubercle (OT). Corpus callosum (cc) and anterior commissure (aco) is included for anatomical reference of the regions. Scale bar is 500 μ m.

1.1.1 GPR88 – a novel therapeutic for psychiatric disorders

The striatum is a major entry into the basal ganglia (BG) and plays important role in the initiation and patterning of many behaviors. Dorsal striatum (Caudoputamen – CP) contributes directly to decision making, especially to action selection and initiation, through the integration of sensorimotor, cognitive, and motivational/emotional information within specific cortico-striatal circuits involving discrete regions of striatum (Balleine and Killcross, 2006; Barnes et al., 2005; Cromwell and Schultz, 2003; Hikosaka et al., 1989; Jog et al., 1999; Kawagoe et al., 1998; Killcross and Coutureau, 2003; Shidara et al., 1998). Nucleus accumbens (ACB), the ventral striatal complex on the other hand serves as a critical region where motivations derived from limbic regions interface with motor control circuitry to regulate appropriate goal-directed behavior (Groenewegen et al., 1996; Mogenson et al., 1980; Nicola et al., 2000; Wise, 2004a; Zahm, 2000).

The olfactory tubercle is interconnected with endocrine, sensory, and cognitive related centers in the brain (Luskin and Price, 1983; Reep and Winans, 1982; Santiago and Shammah-Lagnado,

2004; Scott et al., 1980; Ubeda-Bañon et al., 2008; White, 1965). It is also heavily interconnected with the reward system (Ikemoto, 2007).

The amygdala is particularly important for conditioned forms of learning. It helps to establish associations between environmental cues and whether or not that particular experience is rewarding or aversive. It also interacts with the ventral tegmental area (VTA) – ACB reward pathway to determine the rewarding or aversive value of an environmental stimulus (natural reward, drug of abuse, stress) (Adolphs et al., 1995, 1995; Baxter and Murray, 2002; Berridge and Kringelbach, 2008; Ikemoto, 2007; LeDoux et al., 1990). Some other studies suggest that the projection from amygdala to ACB modulates cue-triggered motivated behaviors and thus facilitates reward seeking (Ambroggi et al., 2008; Cador et al., 1989; Di Ciano and Everitt, 2004; Stuber et al., 2011).

Optimal functioning of somatosensory system is crucial for learning and development of cognitive functions (Yochman et al., 2006). Several studies have documented on abnormal somatosensory processing in children with attention deficit hyperactivity disorder (ADHD) (Miyazaki et al., 2007; Mostofsky et al., 2006; Parush et al., 1997, 2007; Visser and Geuze, 2000; Yochman et al., 2006).

Robust expression of GPR88 in the striatal MSNs, amygdala, somatosensory area and olfactory tubercle, highlighted this gene as a potential target to treat several neuropsychiatric diseases that are caused due to abnormal function of striatal GABAergic MSNs, as well as malfunctioning of somatosensory system such as Parkinson's, Huntington's, bipolar disorder, learning disabilities, ADHD and addiction (Di Chiara and Imperato, 1988; Everitt et al., 2001; Gerfen, 1992; Graybiel et al., 1994; Ingallinesi et al., 2015; Joshi et al., 2009; Surmeier et al., 2009; Wise, 1996). Moreover, in recent years, it has attracted considerable attention because of its modulated expression observed in several anti-depressant therapies and pharmacological interventions (Befort et al., 2008; Böhm et al., 2006; Conti et al., 2006) and induced both by glutamate and dopamine (Logue et al., 2009; Massart et al., 2009). In humans, GPR88 was associated with bipolar disorders and schizophrenia (Del Zompo et al., 2014). Additionally, it has been reported that GPR88 deficiency alters sensory-motor gating in mice (Logue et al., 2009). These findings highlight the involvement of GPR88 in multiple psychiatric/neurodegenerative disorders and promote further investigations to unveil the neurobiological functions and molecular mechanisms of GPR88.

1.1.2 Behavioral studies on GPR88 receptor deficient mice

Up to date, emerging investigations have been carried out to reveal the implication of GPR88 in rodents behavior as listed in Annex: Table 1. Figure 3 summarizes some of the behavioral characteristics of Gpr88 gene knock-out mice reported earlier. It has been shown that in the absence of GPR88, MSNs have increased glutamatergic excitation and reduced GABAergic inhibition that together promote enhanced firing rates in vivo (Quintana et al., 2012). In mice, deletion of the GPR88 has been studied with a primary focus of striatal-mediated behaviors and null mutant mice show hyperactivity, poor motor-coordination, and impaired cue-based learning (Ingallinesi et al., 2015; Logue et al., 2009; Massart et al., 2009; Quintana et al., 2012). For example, mice were placed in activity chambers for 48 hours to elucidate the role of GPR88 in basal locomotor activity. Gpr88^{Cre/Cre} (Gpr88-knockout) mice were more active during the first few hours, reflecting the response to novelty (Figure 3A; adapted from (Quintana et al., 2012)). All animals increased their activity during the nocturnal cycle, however greater in Gpr88^{Cre/Cre} mice and daytime activities were comparable (Figure 3B; adapted from (Quintana et al., 2012)). As a step forward, mice were placed on top of an accelerating rod and the latency to fall was scored to assess the motor coordination and balance. While control group (GPR8^{+/+}) improved their performance with each experimental session, Gpr88^{Cre/Cre} mice fell more quickly and showed no improvement with training (Figure 3C; adapted from (Quintana et al., 2012)), confirming impairments in motor coordination or strength of Gpr88^{Cre/Cre} mice.

Logue et al., showed that Gpr88^{-/-} mice have lower pre-pulse inhibition (PPI) (Figure 3D (i), adapted from (Logue et al., 2009)), which can then be rescued by treating the mice with D2 antagonists (Figure 3D (ii), adapted from (Logue et al., 2009)).

Meirsman et al., demonstrates that Gpr88^{-/-} mice show improved hippocampal-dependent learning and reduced anxiety levels (Aura C. Meirsman et al., 2016). Striatum and hippocampus compete to drive during learning and memory (Poldrack and Packard, 2003). Thus, altered striatal functions in the GPR88 receptor deficient mice may influence hippocampal mediated behaviors as well. Meirsman et al., evaluated the hippocampal dependent behaviors in the Gpr88^{-/-} mice through several ways. For example, by scoring spontaneous attention in Y-maze revealed that knock-out mice entered into arms of the maze more often than the control group (Figure 3E; adapted from (Aura C. Meirsman et al., 2016)), consistent with locomotor hyperactivity observed in former study (Quintana et al., 2012). Mutant mice showed a trend toward higher spontaneous alteration and returned significantly less into the same arm, indicative of less preservative errors, while alternate arms returns were unchanged. Hippocampal/striatal balance in learning was specifically assessed by testing mutant mice in a dual-solution cross-maze task. Performance at early stage of the experiment reveals hippocampal facilitated allocentric strategy (place), whereas striatal conditioned egocentric strategy (response) during later stages. Gpr88^{-/-} mice showed longer choice latencies, however, acquired the task more rapidly and reached higher levels of performance than Gpr8^{+/+} mice. A probe trail after eight training sessions showed that knockout mice shifted toward an egocentric strategy to solve the task, while the control mice still used the

allocentric strategy at the same stage, suggesting higher levels of performance in mutant mice compared to the control. Interestingly, probe trial performed after two reversal sessions indicated that mutant mice reshifted to an allocentric strategy (Figure 3F; adapted from (Aura C. Meersman et al., 2016).

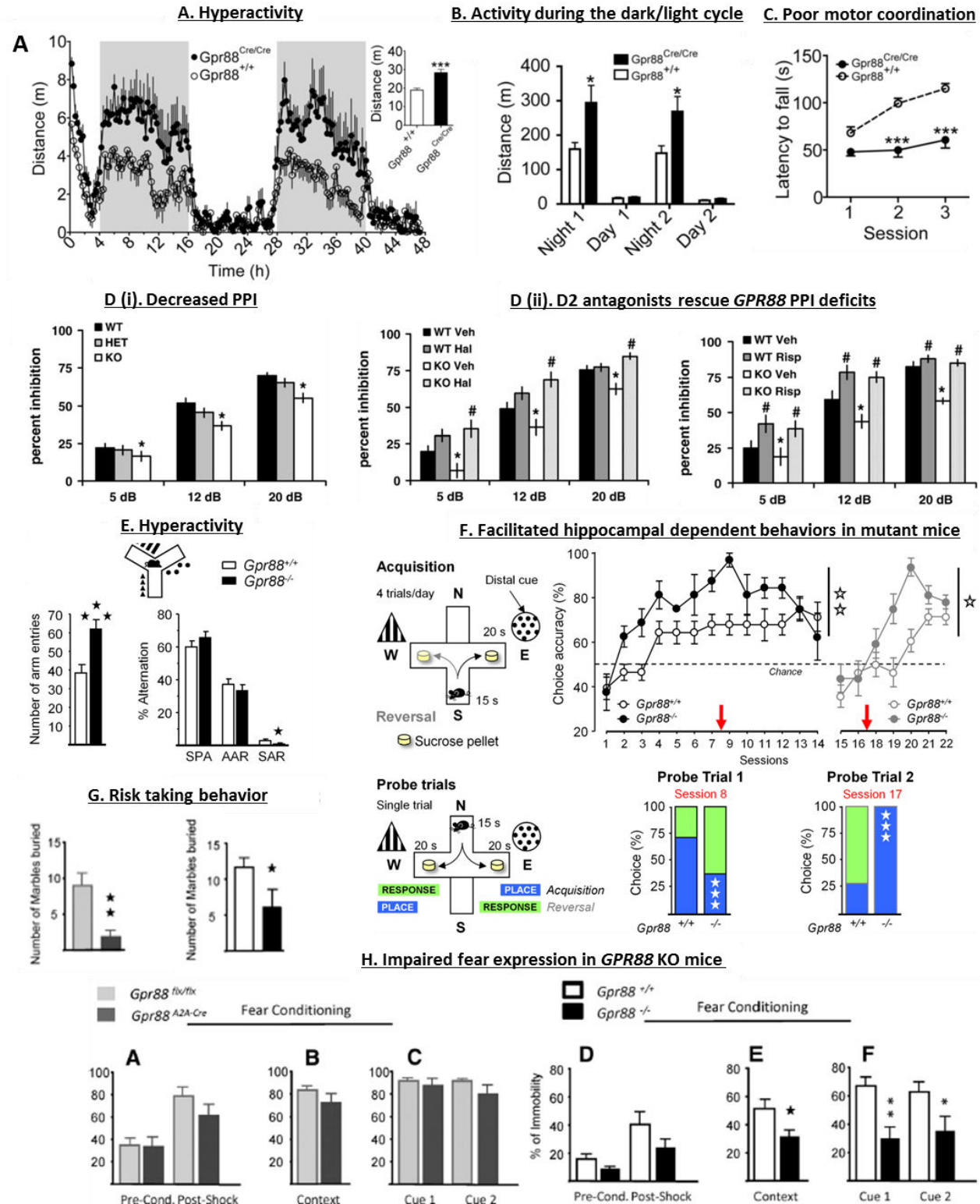


Figure 3: Impact of GPR88 receptor in mice behavior: (A) $Gpr88^{Cre/Cre}$ mice are more active than the $Gpr88^{+/+}$ mice. (B) Animals from both group increased their activities during the nocturnal cycle, however greater response was observed in $Gpr88^{Cre/Cre}$ mice. (C) $Gpr88^{Cre/Cre}$ mice show poor motor coordination in rotarod performance test. (D (i)) GPR88 receptor lacking mice show decreased pre-pulse inhibition (PPI) than the wild-type (WT). (D (ii)) D2 antagonists rescue PPI deficiency in the $Gpr88^{-/-}$ mice. (E) When exploring a Y-maze, mutant mice display more arm entries, evoking hyperactivity, and make less perseverative arm reentries. (F) Mutant animals acquire earlier and better a dual solution cross-maze task using distal extra-maze cues, shift sooner to a response strategy to solve the task (probe trial 1), and reacquire more rapidly this task after spatial reversal than $Gpr88^{+/+}$ animals, by shifting sooner to an allocentric strategy (probe trial 2). AAR, alternate arm return; E, east; N, north; S, south; SAR, same arm return; SPA, spontaneous alternation; W, west. (G) $Gpr88^{-/-}$ and $Gpr88^{A2A-Cre}$ mice show increased risk taking behavior. (H) $Gpr88^{-/-}$ but not A2AR- $Gpr88^{-/-}$ mice impairs fear expression.

These findings suggest GPR88 receptor lacking mice have facilitated hippocampus dependent behaviors. Recent work from the same group reports decreased threat avoidance and exhibit increased risk-taking behavior in both the $Gpr88^{-/-}$ and $Gpr88^{A2A-Cre}$ mice. However, impaired fear conditioning in the $Gpr88^{-/-}$ but not $Gpr88^{A2A-Cre}$ mice (Figure 3G and 3H; adapted from (Aura Carole Meirsman et al., 2016).

This receptor, therefore, controls a much larger behavior repertoire than initially anticipated and, beyond motor activity, also engages spatial learning, emotional processing, sensorimotor gating and fear conditioning as well as in the risk-taking behavior. Nevertheless, the impact of $Gpr88$ gene in brain connectivity has not been reported yet, promoting further investigations to address how this receptor reshapes the neural architecture at structural and functional level. Implications of GPR88 in brain communication may underscore the molecular mechanisms underlying the behavioral traits observed in $Gpr88^{-/-}$ mice. Thus, one of the main objectives of my study was to assess the brain connectivity modifications in response to the deletion of GPR88 in living mouse brain.

1.1.3 Generation of $Gpr88^{-/-}$ mice

GPR88 floxed mice ($Gpr88^{fl/fl}$) were generated at the Institut Clinique de la Souris (Strasbourg) using Cre-LoxP technology. Briefly, exon 2 was flanked by loxP sites and a LoX-flippase recognition target neomycin-resistance cassette was inserted downstream exon 2 using homologous recombination (Figure 4, adapted from Aura C. Meirsman et al., 2016). F1 heterozygous $Gpr88^{fl/+}$ mice were bred with CMV-Flip mice to remove the neomycin cassette and produce a conditional GPR88 floxed line. For this study, constitutive knockout animals were further created by breeding conditional animals with a general CMV-Cre driver

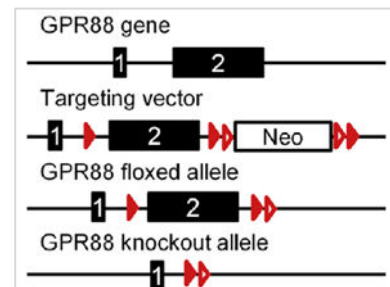


Figure 4: Gene targeting strategy to generate $GPR88^{-/-}$ mouse line.

line (Gaveriaux-Ruff et al., 2011; Metzger and Chambon, 2001). This led to germline deletion of GPR88 exon 2 on a hybrid 50% C57BL/6J-50% 129Sv genetic background. $Gpr88^{fl/fl} \times CMV-Cre^{Tg/+}$ and $Gpr88^{+/+} \times CMVCre^{0/+}$ were used as experimental ($Gpr88^{-/-}$ mice) and control ($Gpr88^{+/+}$: CTRL) animals, respectively (see Annex 3.4 for details).

1.2 The concept of brain connectivity and brain networks

Brain networks consist of spatially distributed but functionally connected regions that process information through their afferent and efferent connections in an orchestrated manner and thus enabling different sensorimotor and cognitive tasks to be performed.

Structural connectivity (SC) is defined as the formation of networks through synaptic contacts between neighboring neurons or fiber tracks connecting neuron pools in spatially distant brain regions. *Functional connectivity (FC)* on the other hand, is defined as the temporal dependency of neuronal activation patterns of anatomically separated brain regions (Friston, 1994). It reflects statistical dependencies between distinct and distant regions of information processing neuronal populations. A central paradigm in modern neuroscience is that structural and functional connections between brain regions are organized in a way such that information processing is near optimal.

Brain networks can be defined based on the structural connectivity or functional interdependence between brain regions. The structural network organization of the brain is based on the anatomical linkage of its neurons that are connected locally by synapses from short axons, dendrites and gap junctions. Although neuronal populations throughout the brain have a variety of different internal circuitry configurations, they can be represented as network nodes if they have a uniquely identifiable local structural organization. Large-scale functional network on the other hand can be defined as a collection interconnected brain areas that interact to perform circumscribed functions. Large-scale brain networks therefore provide a comprehensive description of the brain's structural and functional connections among brain areas that expedites signaling along preferred pathways in the service of specific cognitive tasks. It is essential to identify the brain areas that constitute structural network nodes and the connecting pathways that serve as structural network edges to know which configurations of interacting areas are possible. Graphical representation of a brain network provides quantitative information on how the network is structured or organized in order to segregate and integrate information among brain regions (Newman, 2006; Rubinov and Sporns, 2010, 2011; Sporns, 2013; Watts and Strogatz, 1998). Several parameters are used to characterize a brain network.

Nodes: Nodes in a network represent brain areas, however, their definition slightly differs while characterizing in structural and functional large-scale network. The nodes of large-scale structural networks are typically considered to be brain areas defined by: (i) cytoarchitectonics; (ii) local circuit connectivity; (iii) output projection target commonality; and (iv) input projection source commonality. A network node in a functional brain network can be a circumscribed brain region

displaying elevated metabolism in positron emission tomography (PET) recordings or elevated blood perfusion in functional magnetic resonance imaging (fMRI) or regions of interest (ROIs) based on anatomical knowledge or brain regions identified via independent component analysis (ICA) in resting state fMRI (rsfMRI) (Bressler and Menon, 2010).

Edges: The *edges* are the long-range axonal-fiber (white matter) pathways that connect brain areas in large-scale structural networks. Network edges are directed because axonal fiber pathways have directionality from the somata to the synapses, and can be bidirectional when fiber pathways run in both directions between brain areas. All blobs in figure 5 (adapted from (Sporns, 2013; Watts and Strogatz, 1998)), represent the nodes, connected via lines that are termed as edges.

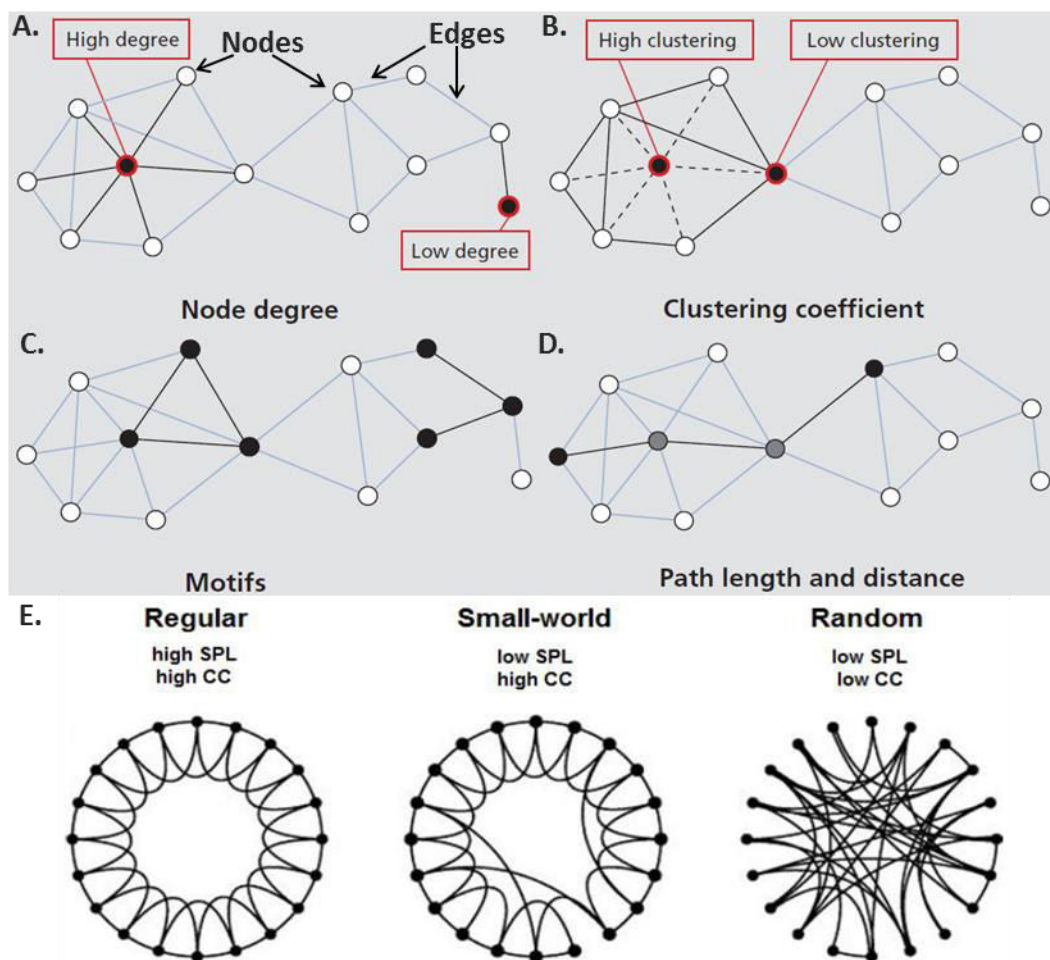


Figure 5: **Characterization of a brain network:** (A) Nodes, edges and the degree of nodes in a network. (B) Clustering coefficient expresses the extent to which a node's topological neighbors are connected among themselves. (C) Motifs – the subgraph of a network. (D) Path length and distance of a network. (E) Network configuration. Regular, small-world and random network are represented considering identical number of nodes and edges.

Node degree: The node degree is the number of edges attached to a specific node. Higher number of edges from a node denotes the higher degree of that corresponding node and vice-versa (Figure 5A).

Clustering coefficient (CC): It is the measure of density of connections among a node's topological neighbors (Figure 5B). If the neighbors of a given node are densely interconnected, they are said to form a cluster. The average of clustering coefficients over all nodes defines the clustering coefficients of the network.

Motifs: Motifs constitute the subgraph of a network. Every network can thus be subdivided into a set of motifs of a given size (Figure 5C).

Path, path length, shortest and characteristics path length: Path is the sequence of edges that connects two nodes with each other. Path length is therefore defined as the number of steps or the sum of the edge lengths in a network (Figure 5D). The length of the shortest path between each pair of nodes resembles their distance and referred to as the shortest path length (SPL). The global average of all distances across the entire network is called the characteristic path length.

Brain network features: Depending on the CC and SPL, the feature of a given brain network can be determined. Small-world feature of a network is a standard of complexity and efficiency of global network structures (Watts and Strogatz, 1998). Small world networks have a topology with a level of randomness between that of a regular and random network (Figure 5E). A small world topology with high local clustering of links and still short travel distances between any links of the network has been demonstrated for living organisms brain in former studies (Bullmore and Sporns, 2009; Mechling et al., 2014). Furthermore, this small-world feature has been investigated in several human brain disorders and indeed, alterations could be demonstrated in dementia, multiple sclerosis, traumatic brain injury or epilepsy (Stam, 2014). In contrast to the small-world network, regular network exhibits high SPL and CC, while these parameters are low in the random network (Figure 5E).

Modern noninvasive imaging techniques applied to humans and animals brain allow the mapping of such complex structural and functional brain networks. Emerging studies demonstrate disrupted brain communication between distinct regions due to psychiatric illness. Analysis of the neuronal connectivity within a brain network is thus important to understand the organization of brain, as well as to reorganization during disease, learning and aging. Additionally, insight to the brain functional and structural connectivity alterations due to the expression or restriction of specific gene, treatments with drugs and/or through disease modelling may endorse pathologies and potential treatment regimes.

Recent years have seen a dramatic increase in the advances and applications of non-invasive neuroimaging techniques, such as Magnetic Resonance Imaging (MRI), Electro/Magneto-encephalogram (EEG/MEG) as well as other invasive techniques like Computed Tomography (CT), Positron Emission Tomography (PET) or Single-Photon Emission Computed Tomography (SPECT). With the advent of these techniques, brain connectional fingerprints have become accessible, offering the unique possibility to identify altering brain functions and structures

persuaded by numerous factors including experience, pathology or genetics (Greenough, 1984; Kolb et al., 1998; Thompson et al., 2013).

1.3 Brain imaging techniques

MRI is one of the most widely used non-invasive imaging techniques in clinical and pre-clinical research now-a-days for mapping the brain structural and functional connectivity. In medicine, MRI is primarily used to produce structural images of organs, including the central nervous system (CNS), but it can also provide information on the physico-chemical state of tissues, their vascularization, and perfusion. Emergence of functional MRI (fMRI) - to measure the hemodynamic changes after enhanced neural activity in response to a task or stimulus, as well as in the absence of task (during rest), namely resting state functional MRI (rsfMRI) and diffusion tensor imaging (DTI) with fiber tracking - to study the brain microstructural modifications, had a real impact on basic cognitive neuroscience research. Since then, these techniques have been remarkably applied in the clinical and pre-clinical research. In my study, rsfMRI as well as DTI and fiber tracking techniques were implemented in the Gpr88 gene knockout living mouse brain, to map the functional and structural fingerprints respectively. The combined analysis of structural and functional connectivity provides insight on how brain structure shapes the brain function, to what degree brain function feeds back to change its structure, and what functional or structural aspects of physiology ultimately drive cognition and behavior (Sui et al., 2014). Following two sections (1.3.1 and 1.3.2) describe the principles of these techniques and how to map the large-scale structural and functional brain network respectively.

1.3.1 Structural connectivity assessment via diffusion tensor imaging (DTI) and fiber tractography

The brain contains more than 100 billion neurons that communicate with each other via axons and forms complex neural networks. The structural mapping of such networks during health and disease states is crucial for understanding brain function. In animal studies, histology followed by light or electron microscopy has been one of the most widely used imaging methods. Besides, numerous staining techniques can highlight the locations of proteins and genes of interests, and electron microscopy can encompass our observation to objects at the molecular level. However, histology-based imaging is invasive and labor-intensive, which makes it a non-ideal choice for examining the entire brain or for performing quantitative three-dimensional analyses. Diffusion tensor imaging (DTI) on the other hand is a three-dimensional noninvasive imaging modality used to characterize the entire brain anatomy. DTI was introduced in the mid1990s (Basser et al., 1994) and since then, this technique has been widely applied in characterizing structural fingerprints of rodents (Ahrens et al., 1998; Harsan et al., 2006, 2010, 2013; Mechling et al., 2016; Mori et al., 2001; Nair et al., 2005; Wu et al., 2014; Wu and Zhang, 2016; Zhang et al., 2012) and human brain (Alexander et al., 2007; Mori et al., 2001; Mukherjee and McKinstry,

2006; Pierpaoli et al., 1996; Tang et al., 2014; Tuch et al., 2001), as well as in the primates (D'Arceuil et al., 2007; Shi et al., 2013; Zhang et al., 2013).

The term 'diffusion' represents random thermal motion of water molecules. Diffusion of water is anisotropic (directionally dependent) in white matter (WM) fiber tracts, as axonal membranes and myelin sheaths present barriers to the motion of water molecules in directions not parallel to their own orientation. Diffusion tensor of WM tracts are considered as a three-dimensional structure with three principal diffusivities (eigenvalues, $\lambda_1, \lambda_2, \lambda_3$), associated with three mutually perpendicular principal directions (eigenvectors, e_1, e_2, e_3). Fractional anisotropy (FA) is another parameter, defined as the ratio of the anisotropic component of the diffusion tensor to the whole diffusion tensor and serves as a rotationally invariant scalar that quantifies the shape of the diffusion tensor. Thus FA measures the degree of directionality of diffusion that varies between zero and one. Zero represents maximal isotropic diffusion as in a perfect sphere and one represent maximal anisotropic diffusion. By combining the directional information and magnitude of anisotropic diffusion of the individual voxels, the course of fiber tracts can be reconstructed, which is known as tractography. This technique relies on the assumption that voxels with a similar orientation of their principal anisotropic diffusion direction are likely part of the same fiber tract. Therefore, DTI and fiber tractography provides a unique opportunity to study the fiber architecture in vivo and characterize microstructural changes or differences with neuropathology and treatment.

1.3.2 Functional connectivity assessment via resting state functional MRI (rsfMRI)

Neuronal activity causes local changes in cerebral blood flow, blood volume, and blood oxygenation. MRI is sensitive to changes in cerebral blood flow and blood oxygenation. Functional magnetic resonance imaging (fMRI) technique uses the blood oxygen level dependent (BOLD) contrast (Ogawa et al., 1990) to detect changes in blood oxygenation in response to a task or stimulus and thus measure the brain activity (Kwong et al., 1992; Ogawa et al., 1992).

In recent years, there has been an increase in interest in the application of this technique at rest, which is termed as resting-state fMRI (rsfMRI). This technique detects low frequency fluctuations (LFFs) of less than 0.1 Hz in the BOLD signal and measures FC between brain regions as the level of co-activation of spontaneous fMRI time-series during rest (Biswal et al., 1995, 1997; Greicius et al., 2003; Lowe et al., 2000; Salvador et al., 2005). These brain regions working together form a functional network, also called the resting state network (RSN), with a high level strongly correlated spontaneous neuronal activity in the absence of a task or stimulus (Fox and Raichle, 2007). These patterns of resting-state correlations are hypothesized to reflect the stable and intrinsic functional architecture of the brain (Buckner et al., 2009). Biswal et al., was the first to demonstrate ongoing neural activity that occurs at rest throughout functionally connected regions of the brain when they revealed a high correlation between the BOLD time-series of the left and right hemispheric regions of the primary motor network in the absence of a

task (Biswal et al., 1995). Several studies have since replicated these results, propelling extensive use of the technique in human (Fair et al., 2007, 2008; Fox and Raichle, 2007; Greicius et al., 2003; Koyama et al., 2011). It is also widely used in mapping rodents (Jonckers et al., 2011; Mechling et al., 2014, 2016; Sforazzini et al., 2014; Shah et al., 2015) and primates brain FC as well (Hutchison et al., 2012; Mantini et al., 2011; Wang et al., 2013).

Identification of functional networks from fMRI data obtained during cognition or resting state is critical for understanding and characterizing how different brain regions communicate with each other.

Analysis of rsfMRI data

In recent years, several methods have been developed to characterize functional brain networks and connectivity.

Model-based method: *Seed-based analysis* is one of the straight-forward methods of mapping whole brain connectivity from a specific region of interest (ROI). Thus it correlates the resting state time-series of a pre-defined ROI against the time-series of all other brain regions, resulting in a whole brain FC map (Biswal et al., 1997). Similar approach is also applied to the rsfMRI data and termed as resting state FC (rsFC) map. The FC or rsFC map provides information about the regions to which the seed region is functionally connected, and to what extent. The simplicity of this analysis affords a strong advantage for seed-dependent methods; however, the information obtained from the rsFC map is limited to the functional connections of the selected ROI only, making it difficult to examine the whole-brain functional architecture (Buckner and Vincent, 2007). Moreover, the selection of a priori ROI can be a challenge to the researchers as it requires having profound knowledge on the brain anatomy and in addition, one has to use a priori knowledge for selecting the seeds.

Model-free methods: Evaluation of whole-brain connectivity patterns is also possible using model-free method such as, independent component analysis (ICA). ICA decomposes the entire BOLD signal into number of spatially independent components ((ICs) or sources (Beckmann and Smith, 2004; Calhoun et al., 2001). Thus, it requires the investigator to estimate the number of components and then to look for the existence of spatial sources of resting-state signals that vary together over time and are maximally distinguishable from other sets of signals (Beckmann et al., 2005). The advantage of using ICA is its application to whole-brain voxel-wise data and high consistency among the RSNs (Damoiseaux et al., 2006). In contrast, complex representation of ICA derived data may complicate translation of results to clinical relevance (Fox and Raichle, 2007).

Brain regions identified by ICA, can be used directly to compute FC between multiple regions by partial correlation. It provides an estimation of the linear conditional dependence between brain regions, removing the linear influence of other regions. The resulting correlation coefficients are usually converted to z-scores using the fisher transformation and then thresholded to identify statistically significant network connections (Supekar et al., 2008). Positive correlations between regions indicate that those regions are typically co-modulated, whereas anti-correlations between

regions indicate them temporarily modulated in opposite directions (Fox et al., 2006). However, zero correlation between two brain regions represents these regions are conditionally independent given temporal fluctuations in other brain regions considered (Peng et al., 2009). Several previous imaging studies have used partial correlations for estimating functional connectivity (Hampson et al., 2002; Huang et al., 2010; Marrelec et al., 2006, 2007).

These methods have been extensively applied to identify major functional networks or circuitry, such as the primary motor, visual, and auditory networks, in addition to higher order cognitive systems (Cordes et al., 2000; Fox and Raichle, 2007; Greicius et al., 2003). Default mode network (DMN), central executive network (CEN), and salience network (SN) are considered to represent the major portion of higher-order functional brain networks. Such complex network is susceptible to many external or internal sources, like experience, influences, physiological and psychological changes or immunological events which all can result in connectivity alterations. Indeed, the impact of pathology on brain connectivity networks has been addressed for several neurological or psychiatric disorders (Guye et al., 2010, 2010; Stam, 2014).

1.3.2.1 Default mode network

Default mode network (DMN) is of particular interest which comprises a group of brain regions appear to be more active during rest compared with a cognitively active state (Raichle et al., 2001). It denotes the intrinsic activity of the brain when the subject is at rest. In other words, DMN exhibits task-induced deactivations and thus also named as task-negative network, which has been associated with processes such as self-reflection and mind wandering.

Extensive studies have been carried out in humans and animals to understand the function of DMN and identify its major anatomical subdivisions. These include: the medial prefrontal cortex (mPFC: the dmPFC, the rostral anterior cingulate, and parts of the anterior and ventral mPFC), medial parietal cortex (the posterior cingulate and retrosplenial cortex), medial temporal lobe (the hippocampus and parahippocampal cortices), lateral parietal and temporal cortex (Gusnard et al., 2001a, 2001b; Lu et al., 2012; Ongür and Price, 2000; Popa et al., 2009; Raichle et al., 2001; Schilbach et al., 2008; Sforazzini et al., 2014; Shannon et al., 2013; Shulman et al., 1997; Vincent et al., 2006). Figure 6 (adapted from (Lu et al., 2012; Sforazzini et al., 2014)) summarizes the DMN reported in rat, mouse, monkey and human brain.

Alterations in DMN connectivity patterns lead to cognitive dysfunctions in neurologic and psychiatric disorders. Changes in DMN FC have been reported in multiple psychiatric and neurologic disorders including depression (Greicius et al., 2008; Kühn and Gallinat, 2012; Lui et al., 2011), schizophrenia (Garrity et al., 2007; Kühn and Gallinat, 2012; Whitfield-Gabrieli and Ford, 2012), Alzheimer's disease (Greicius et al., 2004; Hedden et al., 2009), epilepsy (Waites et al., 2006; Z. Zhang et al., 2010), disorders of consciousness (Soddu et al., 2011) including coma (Norton et al., 2012), multiple sclerosis (Lowe et al., 2002), amyotrophic lateral sclerosis (Mohammadi et al., 2009), autism (Cherkassky et al., 2006; Murdaugh et al., 2012) and blindness (Liu et al., 2007). Emerging studies also demonstrate ADHD as DMN disorder (Castellanos et al., 2008; Fair et al., 2010; Sonuga-Barke and Castellanos, 2007) as well as decreased DMN

connectivity in ADHD patients (Castellanos et al., 2008; Castellanos and Proal, 2012; Fassbender et al., 2009).

DMN thus serves as an elucidating and critical system for identifying treatment targets and aiding in the clinical diagnosis and development of treatment strategies.

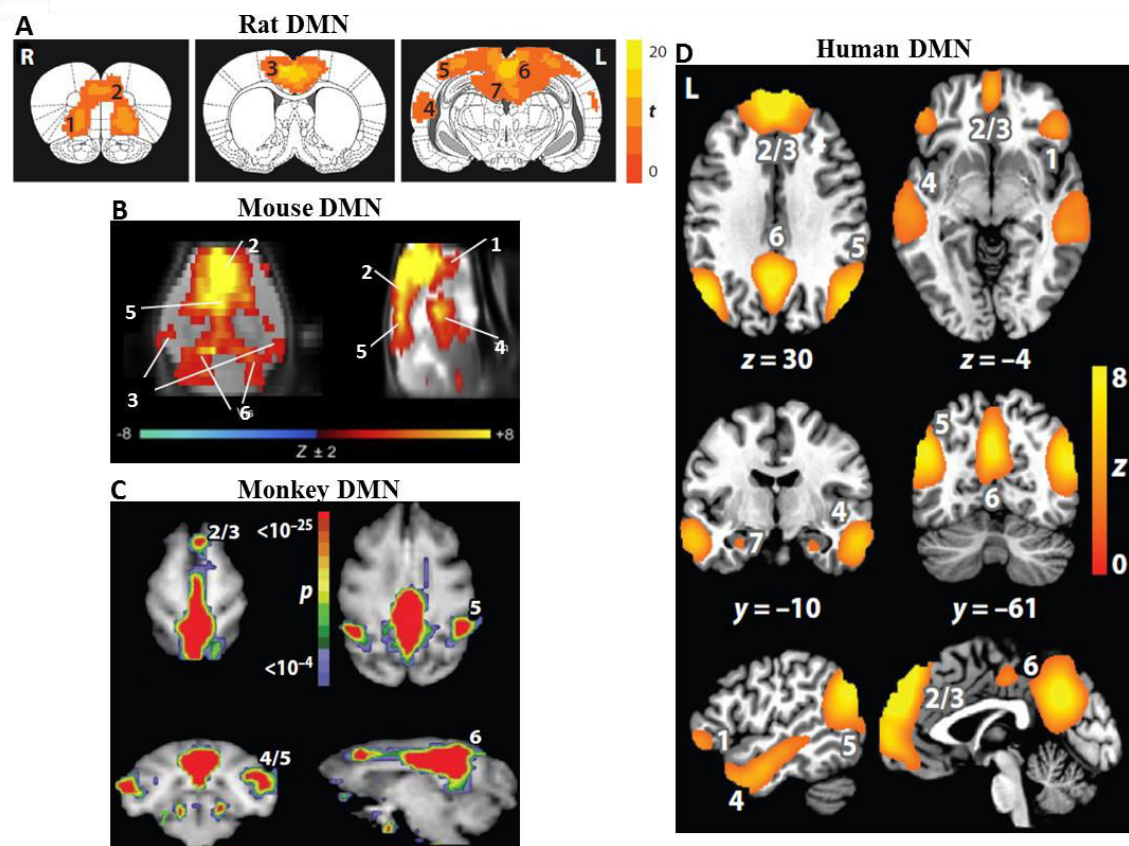


Figure 6: **Default mode network (DMN):** (A) In rat brain: 1. orbital cortex, 2. pre-limbic cortex (PL), 3. cingulate area (ACA), 4. auditory/temporal association area (TEa), 5. posterior parietal association area (PTLp), 6. retrosplenial area (RSA), corresponds to the posterior cingulate cortex (PCC) in human, 7. hippocampus (CA1 – part of hippocampal formation (HPF)). (B) In mouse brain: 1. orbito-frontal cortex (OFC), 2. ACA, 3. TEa, 4. thalamus (TH), 5. RSA, 6. visual area (VIS). (C) In monkey brain: 2/3. dorso-medial prefrontal cortex (mPFC), 4/5. lateral temporoparietal cortex, 6. RSA, 7. Posterior parahippocampal cortex. (D) In human brain: 1. OFC, 2/3. mPFC/ACA, 4. lateral temporal cortex, 5. inferior parietal lobe, 6. RSA, 7. HPF.

1.3.2.2 Central executive network

Dorsolateral prefrontal cortex (dlPFC), and posterior parietal cortex (PTLp) are the key nodes of central executive network (CEN), also termed as task-positive network (TPN) or frontoparietal network (FPN). CEN nodes show strong intrinsic functional coupling as well as strong co-activation during cognitively challenging tasks, while decrease in activation during rest. In

particular, the CEN is critical for active maintenance and manipulation of information in working memory, for judgment and decision-making in the context of goal directed behavior (Koechlin and Summerfield, 2007; Miller and Cohen, 2001; Müller and Knight, 2006; Petrides, 2005).

1.3.2.3 Salience network

Anterior and posterior part of agranular insular area (AI), potentially together with the anterior cingulate area (ACA) serves as the salience network (SN) (Seeley et al., 2007). This network is associated with the detection of novel, salient stimuli, and is thought to play a role in coordinating an adequate response by recruiting appropriate brain networks. Therefore, some authors suggest it might play a role in coordinating between DMN and CEN activity (Bonnelle et al., 2012; Menon and Uddin, 2010). Neuroimaging studies have provided the evidence for prominent SN dysfunction in many psychopathologies, including frontotemporal dementia (Zhou et al., 2010), Alzheimer’s disease (Zhou and Seeley, 2014), mood (Hamilton et al., 2013) and anxiety disorders (Paulus and Stein, 2006; Stein et al., 2007), posttraumatic stress disorder (Peterson et al., 2014), schizophrenia (Manoliu et al., 2014), drug addiction (Sutherland et al., 2012), and chronic pain (Otti et al., 2013).

1.3.2.4 Reward/aversion network

Reward/aversion network is comprised of several brain regions that connect with each other through dopaminergic and opioidergic projections. This network is very well known to play important roles in addiction.

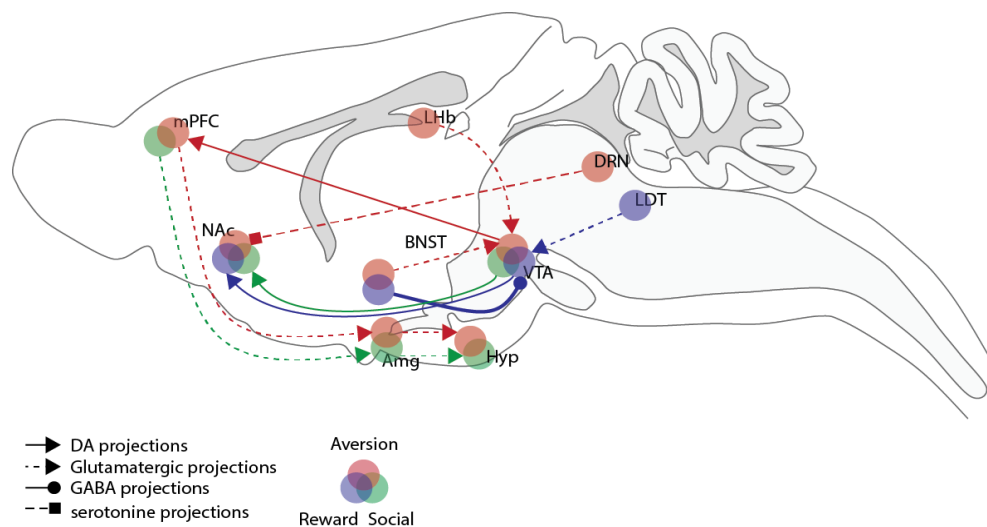


Figure 7: **Schematic diagram of the reward/aversion network:** Blue, red and green circle represents the regions belonging to the reward, aversion, and social system respectively. Dopaminergic, glutamatergic, GABA-ergic and serotonin projections from/to the brain regions have been shown via solid or dashed lines as mentioned in the figure.

Figure 7 demonstrates a schematic diagram of the reward/aversion network. Ventral tegmental area (VTA) plays the central role in the reward and aversion system as it sends and receives projections from different brain regions. Dopamine neurons of the VTA target important structures, such as ACB and medial prefrontal cortex (mPFC), involved in reward (blue) and aversion (red) response behavior (Bromberg-Martin et al., 2010) and receives reward- and aversive-related input from the latero-dorsal tegmental nucleus (LDT) and lateral habenula (LHb) respectively (Lammel et al., 2012a). Glutamatergic and GABAergic neurons from bed nuclei of the stria terminalis (BST) to VTA are activated in response to aversive and rewarding stimulus (Jennings et al., 2013). Dorsal raphe nucleus (DRN) serotonergic neurons projecting onto the ACB produces aversion and potentiates cocaine reward (Lutz and Kieffer, 2013).

Alteration in social interaction is often related with several psychiatric disorders such as autism, schizophrenia, depression and social anxiety disorder. However, little is known on the neuronal circuit involved in social interactions. The brain regions involved in social interactions are often related to the RAC (Gunaydin et al., 2014; Kumar et al., 2014). A recent study coupling optogenetic and fiber photometry in mice managed to identify the involvement of the VTA's projections to the ACB in social interactions (Green). The modulation of the social interaction was mediated by D1R signaling downstream in the ACB (Gunaydin et al., 2014). ACB opioid receptors were shown to be necessary and sufficient for morphine to increase social play (Trezza et al., 2011). Another study showed that the variability in PFC function underlies individual differences in vulnerability of stress induced by chronic social defeat and also demonstrated that the response properties of the glutamatergic projections between PFC to the amygdala, involved in modulation fear and stress response, correspond to naturally occurring differences in vulnerability to chronic social defeat (Kumar et al., 2014). Medial amygdala (MEA) and its projections to the hypothalamic regions are involved in innate social and asocial behavior (Newman, 2006; Swanson, 2000) and in conditioned fear (Duvarci and Pare, 2014). A recent study showed that glutamatergic subpopulation inhibits social interaction independently of its promoting effect on self-grooming while the GABAergic subpopulation promotes aggression and inhibits self-grooming even in a non-social context (Hong et al., 2014).

Assessment of neuronal connectivity impairments in large-scale brain network and their impact in brain communication within or between the networks is therefore essential to understand the underlying molecular mechanisms of the neurodegenerative and psychiatric diseases. Combining neuroimaging technologies with animal models of neurological disorders provides unique opportunities to comprehend the pathophysiology of human neurological disorders. One of the main advantages of animal studies is group homogeneity, which cannot be easily achieved in clinical (human) studies. Moreover, animal models can interact and react to stimuli that can provide an idea of how those stimuli might react in a human being. In addition, how the restriction or expression of genes can reshape human brain connectivity is possible to image using animal models. It allows thus to investigate the spatial and temporal dynamics of disease-specific functional and molecular events longitudinally in intact living organisms.

1.4 Rodents in neuroscience/neuroimaging research

1.4.1 rsfMRI and DTI in rodents

A multitude of animal models have been established to mimic human neurodegenerative and psychiatric disorders. These animal models range from interventional models (such as xenograft, neurotoxic or mechanical lesion models) to knockout and transgenic (mono-, bi- or trigenic through crossbreeding) animals. With the advance of these animal models, non-invasive techniques for the evaluation of disease-associated functional, biochemical and anatomical changes through a variety of dedicated small animal imaging scanners with high sensitivity, specificity and resolution have become indispensable. Over the past century, the mouse has developed into the premier mammalian model system for genetic research. Scientists from a wide range of biomedical fields have gravitated to the mouse because of its close genetic and physiological similarities to humans, as well as the ease with which its genome can be manipulated and analyzed. Consequently, utilization of rsfMRI and DTI methods in mouse models of psychiatric disorders provide considerable benefits for the identification of disease-associated brain circuits and metabolic changes. Despite these advantages of using mouse models, there are some major challenges need to consider especially while performing rsfMRI and DTI studies on living animals.

Anesthesia plays an important role in brain connectivity. Even though it implies restrictions on fMRI, experiments with conscious rodents (Becerra et al., 2011; N. Zhang et al., 2010) also have their limitations (Berwick et al., 2002). For example, even after habituation to the apparatus, animals are still stressed by the fixation or noise from the scanner itself, which may subsequently have an impact on the investigated brain functions, suggesting the need of anesthesia or light sedation to minimize stress level as well as to avoid movement related artifacts. Previous studies on humans and rodents brain functional connectivity report that the level of consciousness during the experiment, influences RSN patterns and activity (Guldenmund et al., 2012; Ma et al., 2017; Nasrallah et al., 2012, 2014). Both the BOLD response as well as the temporal correlation of LFFs between brain regions can be affected by the choice (and level) of anesthesia in rodents (Jonckers et al., 2014; Williams et al., 2010). Therefore, it is very crucial to select the appropriate type of anesthesia and dosage level to avoid strong anesthetic induced effects on brain connectivity.

Maintaining stable physiological conditions, such as, body temperature, respiration rate and blood oxygenation level throughout the rsfMRI and DTI study is very important. Fluctuations in body temperature can contribute to drifts in the BOLD signal baseline, even when the temperature changes are within physiological ranges (Vanhoutte et al., 2006). Respiratory and cardiac cycles are known to contribute to the rsfMRI signal and can introduce unwanted correlations (Birn et al., 2006; Shmueli et al., 2007; Wise et al., 2004). Hence, physiological parameters should be monitored and controlled (to the extent possible) during an experiment.

Rodent models play an important role in understanding the neural basis of BOLD correlations and are likely to continue to do so. Brain connectivity studies with rodents are rapidly expanding into the wide realm of animal models of brain disorders. This will facilitate the transfer of knowledge between rodent and human research. The non-invasive nature of rsfMRI and DTI, together with the advantages of using rodent models allows us to develop biomarkers that can be quickly examined in the human population. Additionally, the neurophysiological basis of alterations observed in humans can be determined in animal models. Caution is necessary, however, particularly in with regards to maintaining animal physiology and accounting for the effects of anesthesia.

1.4.2 Rodents in behavioral neuroscience

Rats and mice are among the most commonly used animal models in behavioral neuroscience research. They are well suited model organisms, as they display a variety of behaviors with relevance to human disease. Thus behavioral characterization of genetically modified mice and rats as well as wild-type strains has become a powerful tool for investigating not only the molecular bases of normal brain functions but also the pathogenesis and treatment of neurophysiological disorders (Crawley, 2007; Holmes et al., 2002; Picciotto and Wickman, 1998; Takao et al., 2007; Watase and Zoghbi, 2003; Wolfer et al., 2002). There are a wide variety of behavioral tests available for laboratory rodents, from tests of basic locomotor and sensory function, to analyses of more complex behavior related to cognition and emotionality. However, the standardization and reproducibility of the testing methods for mouse behavioral assessment is still inadequate (Brunner et al., 2002; J. C. Crabbe et al., 1999; Novak et al., 2015; Sorge et al., 2014; Wahlsten et al., 2003). Introduction of IntelliCage by NewBehavior (NewBehavior AG) in the field of behavioral neuroscience permitted the researchers to overcome this problem.

In my study, I successfully implemented this technology for screening behavioral and cognitive functions of the GPR88 deficient mice. This is the first study assessing on the real time measurement of the GPR88^{-/-} mice behavior. I optimized and adjusted several behavioral test protocols, consisting the adaptation phases, followed by the cognitive performance and spatial learning evaluation phase. Each protocol was designed with the ‘IntelliCage Designer’ software and the experiments were monitored online through the ‘IntelliCage Controller’ module. Data saved by the controller during the experimentation, was extracted at the end of each experiment using the ‘IntelliCage Analyzer’ software and further processed for statistical analysis. Following sections provide an overview of the IntelliCage hardware and software packages that were used to design the experiment, monitor mice activities online and data processing respectively.

1.4.2.1 IntelliCage

IntelliCage is a newly developed computer-based, fully automated testing apparatus that allows automated cognitive and behavioral screening of mutant or treated mice living in social groups. It is a large standard plastic cage ($55 \times 37.5 \times 20.5 \text{ cm}^3$) (Figure 8A) equipped with four triangular operant learning chambers ($15 \times 15 \times 21 \text{ cm}^3$) (Figure 8B) that fit into each corner of

the cage. Subcutaneously injected radio frequency identification (RFID) readers (Figure 8C) and other type of sensors (Figure 8D) allow simultaneous monitoring of up to 16 transponder-tagged mice living in the same cage. Mice have access to enter the corner through a short narrow tunnel that functions as an RFID antenna. In this unit, only one mouse can enter a corner at a time because of the limited size of the corner and tunnel. In the inner space of the corner, there are two nose-poke holes with an infrared beam-break response detector. Nose-poke triggers the opening of a motorized access gate to water-bottle spouts. In IntelliCage, the time and duration of each behavioral event (number of visits in each corner, duration of stay in each corner, number of nose-pokes, number of licks and licking duration), mouse ID and corner ID are automatically recorded through RFID readers, infrared sensors and lickometers respectively. Thus it provides the real time measure of the mouse activities, which is a unique feature of the IntelliCage over the traditional cages. Figure 8 was adapted from (“Info - Home - TSE Systems,”)

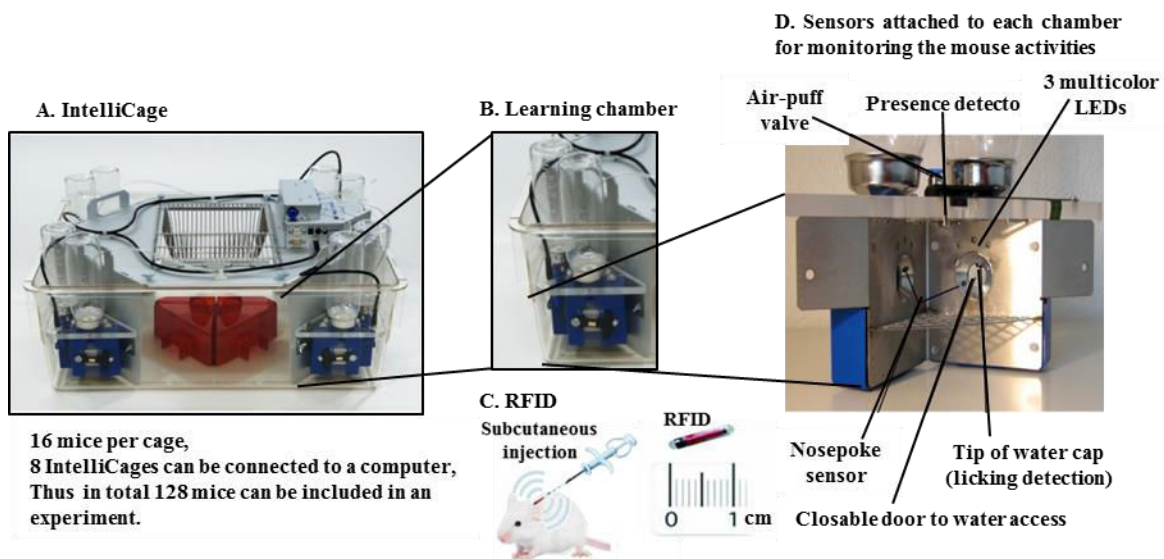


Figure 8: **Overview of the IntelliCage system:** (A) IntelliCage system apparatus: mice are group-housed in the cage and their behavioral responses (corner visits, nosepokes, and lickings) are monitored in a fully automated manner. (B) Learning chamber: each corner of the IntelliCage contains a learning chamber that holds 2 bottles for drinking, and other monitoring sensors. Only one mouse can enter the chamber at a time through a hole. (C) Radio frequency identification reader (RFID) of 1 cm in length is subcutaneously injected into the mouse shoulder. Each RFID has a unique identification number that is registered each time in response to the activity of the mouse. (D) Interior of the learning chamber: multiple sensors are attached in each chamber. Each time a transponder-tagged mouse enters the learning chamber; all activities are recorded by the system which can further be analyzed using the designated IntelliCage software modules. Several features of IntelliCage have made this automated system as a powerful tool for the behavioral characterization of mice or rats.

1. It is possible to achieve a sensitive and highly standardized experiment by minimizing the artifacts that arise from unavoidable differences among experimenters or other laboratory-specific conditions.
2. Long term monitoring of mouse behavior can be performed in less stressful environment.

3. High-throughput testing is possible by analyzing a maximum of 16 mice per cage simultaneously. It is conceivable to connect 8 IntelliCages in series to a single computer, thus in total 128 mice can be included in an experiment.
4. Experimenters can design and use their own original cognitive task depending on their research objective, which is a unique feature of the IntelliCage.
5. IntelliCage can be run in a fully automated manner, utilizing sensors and four operant conditioning units placed in each corner of the cage. Thus it permits to monitor individual learning over long time periods in real time.

Therefore, IntelliCages offer online monitoring of the mouse activities providing a comprehensive view of the mouse behaviors with minimized artefactual effects on the results.

1.4.2.2 IntelliCage – software overview

Designer: ‘Designer’ software is used to design the cognitive test of the mouse. All mice are registered into the system using the designer software by specifying the RFID numbers that are detected each time, in response to any activities of the respective mouse in any of the corners. This software also allows stipulating the hardware settings according to the experiment objective. For example, access to water, sucrose or alcohol from bottles placed in each corner – as positive reinforcement and air-puff can be introduced as – negative reinforcement. 3 LEDs of different colors (red, green, blue and yellow) attached in each side of the corner, can be used as conditional stimuli. Each side of the corner can further be defined as correct, neutral or incorrect in order to assess the learning ability of the mouse, which is known as ‘cluster’ that represents the status of the cage components for each mouse assigned to that particular cluster. All events in specific corners are defined by creating individual modules. Animal behaviors (visit, nose-poke and lick) can be linked to trigger hardware events (door opening, air-puffs, switching LEDs on), resulting in full control over conditioning behavior. Several modules can be created for an experiment and linked to each other. Switching between the clusters and/or modules can be driven by the specific behavior of mice. Furthermore, creating day patterns link or switch the modules or clusters automatically at specific time of the day. Thus it does not require the experimenters to change the status of the experiment manually, facilitating mice to be in stress free environment and more importantly reducing the experimenters biased artifacts.

Controller: The ‘controller’ software is used to extract all on-going behavioral events (visits, nose-pokes and licks) during the experiment. It provides an overview of the state of the Intellicage corresponding to the mice activities in each cage, allowing online monitoring of events and developments. Therefore, the controller software is used to execute the designed experiment and monitor the status and progress of the experiment in real-time. Controller saves the experimental data into zip-archive format that can be used to process the data afterwards.

Analyzer: Data saved by the controller can be accessed by the ‘analyzer’ software. This software can be used to analyze mouse specific activities in hour-by-hour or daily basis, using the filter option. It creates specific mouse or group-wise charts or graphs. Filtered data can be saved for further statistical analysis using external statistical packages.

Detailed description of the IntelliCage system including software modules are provided in the Annex, section 4.4.4.2.

1.5 Implications of GPR88 receptor in alcohol addiction

Alcohol use disorder (AUD) is a chronic relapsing disorder, characterized by excessive alcohol drinking and loss of control over consumption, and has dramatic consequences for individuals' health and productivity, their families, and society. Only few treatments are available (Maisel et al., 2013; Johnson, 2010), which target glutamatergic, gamma-aminobutyric acidergic, dopaminergic, or opioid systems; efficacy is low and variable; and the search for novel therapeutic strategies is largely open. In rodent research, gene knockout approaches have identified a number of genes that causally contribute to alcohol drinking-related behaviors (Mayfield et al., 2016; Ron and Barak, 2016).

At the neurobiological level, alcohol acts as a complex drug that modifies the activity of multiple molecular targets and triggers broad alterations of gene expression and synaptic plasticity in neural networks responsible for reward, mood, and decision making (Ron and Barak, 2016; Spanagel, 2009). Remarkably, Gpr88 is essentially expressed in these brain circuits (Koob and Volkow, 2016). The Gpr88 transcript is most enriched in the striatum of both rodent (Mizushima et al., 2000) and human (Ehrlich et al., 2017) brains, and also in the central amygdala (Becker et al., 2008; Befort et al., 2008) and cortex (Massart et al., 2016), although with lower density. Gpr88 transcript levels are altered upon pharmacological treatment using antidepressants (Conti et al., 2007) and mood stabilizers (Brandish et al., 2005; Ogden et al., 2004), as well as chronic exposure to drugs of abuse, including alcohol (Le Merrer et al., 2012). To our knowledge, however, a potential role of this receptor in drug consumption, seeking, and dependence has not been examined.

Functional studies of GPR88 have used genetic approaches, as GPR88 drugs (Dzierba et al., 2015; Jin et al., 2014) with effective in vivo activity are lacking. Gpr88 gene knockout in the mouse leads to a range of phenotypes consistent with the strong striatal GPR88 expression. In brief, these include altered dopamine (DA) signaling and enhanced MSNs excitability, increased basal activity and locomotor responses to psychostimulants, increased stereotypies and motor coordination deficits, and altered cue-based and procedural learning (Logue et al., 2009; Quintana et al., 2012; Meirsmann et al., 2016a). Sensorimotor gating (Logue et al., 2009) and sensory processing (Ehrlich et al., 2017) deficits are also observed in Gpr88 knockout mice, possibly related to cortical GPR88 expression. Finally, these mutant mice display reduced anxiety-related responses together with increased approach behaviors, leading to a risk-taking phenotype (Meirsmann et al., 2016a), and perseverative (Meirsmann et al., 2016a) and compulsive-like behavior. In sum, the Gpr88 expression pattern overlapping brain networks of addiction, and the phenotypic traits of Gpr88 knockout mice involving dysfunctional motivation, mood regulation,

and higher-order integration, prompted us to hypothesize that GPR88 may contribute to alcohol-drinking behaviors.

In this context, one of the major objectives of my study was to investigate whether GPR88 deletion alters alcohol-taking and alcohol-seeking behaviors as well as the underlying neuronal connectivity patterns that may promote this phenotype. To address this question, alcohol drinking behavior of mice was tested in IGBMC, Strasbourg, France and the dynamic of the brain networks alterations were assessed using MR based imaging approaches (as described in section 1.3) at the Department of Radiology in University Medical Center Freiburg.

1.6 Integration of the introduced techniques into my work

My doctoral study was designed in 3 individual phases comprising in-vivo mouse brain imaging (via rsfMRI and DTI), behavioral studies of *Gpr88*^{-/-} mice using IntelliCage and the assessment of mouse brain connectivity and behavior in response to alcohol exposure.

The first part of my project was aimed to characterize the GPR88 receptor deficient mice. This included MR-based neuroimaging of *Gpr88*^{-/-} mice to assess how the deletion of GPR88 receptor impacts on the neuronal connectivity both structurally and functionally. Subsequently, the effects of *Gpr88* gene in mouse behavior were assessed with GPR88 receptor deficient mice living in social groups using IntelliCage. In parallel, a different cohort of mice (CTRL and *Gpr88*^{-/-}) was exposed to alcohol in traditional type-III cages using 2-bottle choice continuous and intermittent access paradigms. Finally, mice exposed to alcohol were imaged (rsfMRI and DTI) to investigate the participation of GPR88 receptor in alcohol induced alterations/remodeling of neuronal connectivity.

Therefore, I combined brain MRI, genetics and animal behavior in order to assess the implication of GPR88 receptor in brain structural and functional connectivity modifications that underpin large range of behavioral characteristics observed in *Gpr88*^{-/-} mice.

Mouse brain imaging: Cutting edge mouse brain rsfMRI and DTI experiments were conducted in/at the Department of Radiology, Medical Physics, University Medical Center Freiburg, Germany. Non-invasive mouse brain DTI and fiber tracking was used to map the structural connectivity. The functional relevance of any identified alterations was assessed by means of rsfMRI methodology. All mouse brain imaging was carried out using a high field 7T small bore animal scanner (Biospec 70/20, Bruker, Germany) and a mouse brain adapted CryoCoil (Bruker, Germany). I optimized and adapted the methodological framework for mapping the brain structural and functional networks, that includes: optimization of anesthetic regime and obtaining stable physiological conditions of the mouse during the experiment sessions.

Mouse behavioral studies and alcohol drinking experiments: I implemented the IntelliCage system for automated behavioral and cognitive testing of mice, for the first time at the laboratory of Prof. Kieffer in IGBMC. This study involved several phases, including adaptation period and

cognitive learning tests. Additionally, mouse behavior due to alcohol exposure was evaluated through continuous access, followed by intermittent access to alcohol in a two-bottle choice drinking paradigm. This experiment was designed to investigate whether deletion of GPR88 receptor impacts on mouse alcohol drinking behavior.

Chapter 2

Results

This chapter illustrates the results obtained during my doctoral study.

Section 2.1 summarizes salient findings from first phase of the study: functional and structural connectivity mapping of the $Gpr88^{-/-}$ mice (See attached: Arefin T. et al., 2017, Brain Connectivity). This includes:

- i. Identification of the resting state functional networks via Independent component analysis (ICA).
- ii. Whole brain evaluation of functional connectivity (FC): mapping of the brain functional connectivity matrix by partial correlation analysis:
 - a) Evaluation of whole brain functional network architecture in the $Gpr88^{-/-}$ mice which reveals massive modifications in the brain FC, particularly in the intra-cortical area.
 - b) Identification and ranking of brain regions showing significantly altered FC.
- iii. Region specific whole brain functional connectivity mapping using seed correlation analysis:
 - a) Default mode network (DMN) specification which shows DMN alterations in response to deletion of $Gpr88$ gene deletion.
 - b) Functional connectivity mapping of the motor and sensory areas, underscoring the hyperactivity phenotype observed in the $GPR88$ deficient mice.
 - c) Assessment of striatal and hippocampal functional connectivity endorsing the learning deficiency in the $Gpr88^{-/-}$ mice.
- iv. Structural connectivity assessment via DTI with fiber tracking approaches.

Section 2.2 describes the behavioral studies carried out with the $GPR88$ deficient mice. Firstly, deletion of $GPR88$ receptor increases alcohol-seeking and drinking behavior in mice (2.2.1 and see attached: Ben Hamida et al., 2018, Biological Psychiatry). Furthermore, behavioral studies performed with the IntelliCage revealed delayed habituation, repetitive and less anticipatory but more persistent behavior in $Gpr88^{-/-}$ mice (2.2.2 and see attached: Maroteaux et al., 2018, Genes, Brain and Behavior).

Section 2.3 demonstrates the preliminary results on the neural architecture modifications observed in mice after alcohol exposure.

Section 2.4 reviews how the deletion of mu opioid receptor reshapes brain neuronal connectivity, particularly the reward-aversion network (See attached: Mechling et al., 2016, PNAS).

2.1 Characterization of the impact of GPR88 receptor on the mouse brain connectivity

Remodeling of sensorimotor brain connectivity in Gpr88 deficient mice (Arefin T. et al., 2017, Brain Connectivity, doi:10.1089/brain.2017.0486)

Former studies report region specific GPR88 receptor facilitated behaviors, particularly striatum, amygdala and striatal-hippocampal mediated behaviors in mice (described in section 1.1.2 and see Annex 4.2: Table 1). Together these findings highlight the potential role of Gpr88 gene in psychiatric disorders. Nevertheless, the mechanisms underlying such phenomena and the participation of GPR88 receptor in neuronal connectivity remained unfolded. To bridge this gap, the major objective of this study was to characterize the impact of GPR88 receptor in living mouse brain communication (see attached manuscript: Arefin T., et al., 2017, Brain Connectivity).

GPR88 expression in mouse brain

Expression of Gpr88 in the CTRL mice was verified by in situ hybridization (Figure S1a). In support of formerly reported literatures (Becker et al., 2008; Ghate et al., 2007; Massart et al., 2016; Mizushima et al., 2000), we also observed the expression of Gpr88 in the layers 4 and 5 of somatosensory cortex, striatum, amygdala as well as in the olfactory tubercle.

Assessment of resting state functional networks (RSN) in Gpr88^{-/-} mice

Based on the 100-ICASSO analysis of rsfMRI datasets from control and Gpr88^{-/-} mice (see Annex section 4.4.3.2), 88 reliable functional clusters with spatial pattern covering neuroanatomical regions were identified (Figure S2). Remaining 12 components were excluded from the study based on their artifactual pattern, related to CSF, movement or vascular origin. The robustness of the components was tested and validated using ICASSO algorithm (Himberg et al., 2004) (see Annex 4.2: Table 2). Furthermore, reproducibility of the group ICASSO patterns in each animal and in each experimental group was validated via back-reconstruction that demonstrated low intra-groups variability of the components pattern (Figure S1b and S1c). Anatomically well-defined brain regions were further used as nodes in the generation of resting state brain functional connectivity (rsFC) matrices (two sided one-sample t-test, $p < 0.05$) of CTRL and Gpr88^{-/-} group of animals (Figure 1a – above and below the diagonal) using partial correlation analysis (see Annex: 4.4.3.2 and Arefin et al., 2017, Brain Connectivity, for details).

Topological characteristics of Gpr88^{-/-} mouse brain resting state network

Considering both positive and negative correlations, graph-based network analysis (graph theory) revealed modification in the segregation of modules in the knock-out animals. 5 modules were detected in the CTRL group whereas 7 modules were identified in the Gpr88^{-/-} group. Furthermore, the connectional architecture of the mouse brain was assessed by computing

clustering coefficient (CC) and shortest path length (SPL) for both groups. This calculation resulted in a high value of CC with short minimum path length for both groups:

CTRL: $CC = 2.52 * C_{rand} \Rightarrow CC/C_{rand} = 2.52$; $SPL = 1.06 * L_{rand} \Rightarrow SPL/L_{rand} = 1.06$

Gpr88^{-/-}: $CC = 2.83 * C_{rand} \Rightarrow CC/C_{rand} = 2.83$; $SPL = 1.06 * L_{rand} \Rightarrow SPL/L_{rand} = 1.06$

The ratio of these two metrics $\sigma_{CTRL} = (CC/C_{rand}) / (SPL/L_{rand}) = 2.52/1.06 = 2.37 > 1$ and $\sigma_{Gpr88^{-/-}} = (CC/C_{rand}) / (SPL/L_{rand}) = 2.83/1.06 = 2.66 > 1$, suggest that small-worldness features of functional network are preserved in both groups.

Mapping of the Gpr88^{-/-} mouse brain architecture

In order to elucidate how GPR88 receptor reshapes the whole brain network, connectivity matrices obtained for each group from the partial correlation analysis were further statistically compared. The 2D matrix shown in figure 1b represents the causal effect on whole-brain networks in response to the deletion of GPR88 receptor. This matrix contains only the regions that showed significant FC alterations between groups (CTRL vs Gpr88^{-/-}) (two-sample t-test, $p < 0.01$, FDR corrected). Furthermore, ranking the brain areas on the basis of the number of statistically significant differences in connectivity across the two genotypes provided an insight into the mouse brain connectome (Figure 1c). Functional connectivity modifications in the intra-cortical brain regions were dominant over the sub-cortical brain regions. Among all, retrosplenial area (RSP) showed the strongest modifications toward other brain regions (Figure 1c, rank 1). RSP serves a range of cognitive functions and is one of the core components of the default mode network (DMN) (Buckner et al., 2008; Raichle, 2015). Along with this area, visual area (VIS, rank 4, Figure 1c), thalamus (TH, rank 5, Figure 1c), temporal association area (TEa, rank 6, Figure 1c), hippocampal formation (HPF, rank 8, Figure 1c) and anterior cingulate area (ACA, rank 9, Figure 1c) are brain regions present in the top-10 of the hierarchy which were previously described as part of a DM-like network in the C57Bl/6 mouse strain (Liska et al., 2015). These findings highlighted the DMN to be strongly modified in the Gpr88^{-/-} mice. In order to validate and strengthen this finding RSP specific whole brain connectivity was mapped using seed correlation analysis.

Remodeled DMN pattern in the Gpr88^{-/-} mouse brain

DMN is considered as one of the major functional brain networks. In the Gpr88^{-/-} mouse brain, DMN was non-invasively probed using bi-lateral RSP as the seed region (two-tailed t-test, $p < 0.001$) likewise used in human (Fox et al., 2005) and mouse (Sforazzini et al., 2014). This quantitative approach revealed RSP as a core area positively connected with other cortical and sub-cortical brain regions such as ACA, HPF, TEa and VIS in the CTRL group (Figure 2a & 2b), consistent with the posterior DMN obtained in humans (Di and Biswal, 2014). In contrast, reduced RSP connectivity with ACA, TEa, HPF, and TH was observed in the mutant group (Figure 2b). Findings from the partial correlation and seed based RSP resting state functional

connectivity (rsFC) analysis together suggest that DMN is strongly vulnerable in mice lacking Gpr88 gene.

Sensory and motor functional connectivity modifications correlate with hyperactivity in Gpr88 deficient mice

Inter-group comparison from the partial correlation analysis revealed somatosensory (SS) and motor (MO) area as two of the most altered brain regions (ranked second and third respectively in the quantification of FC alterations) (Figure 1c). The extent of these modifications with respect to seed areas placed in the MO and SS in both groups was investigated using seed correlation analysis. This approach displayed widespread cortical and sub-cortical rsFC modifications in the Gpr88^{-/-} group (Figure 3a and 3c). Statistical significance of the alterations was verified using voxel-level general linear modeling (GLM), corrected for multiple comparisons ($p < 0.001$) (Figure 3b and 3d). MO showed decreased positive correlation with the frontal cortex, limbic area and caudal RSP as well as parietal cortex (PTLp) in Gpr88^{-/-} group (Figure 3a-correlations from 0 to 1 and Figure 3b-positive correlation, CTRL > Gpr88^{-/-}). However, stronger rsFC (Figure 3b-positive correlation, CTRL < Gpr88^{-/-}) was quantified between MO and CP, MO and SS as well as within the MO. Notably, MO exhibited modified FC toward the striatum in Gpr88^{-/-} mice (Figure 3a, positive correlation) and these strong modifications of the striato-motor connectivity are particularly relevant to highest GPR88 expression in the striatum and the hyperactive phenotype observed in this model. Modifications in the striatal-motor connectivity are particularly relevant to the highest GPR88 expression in the striatum and the hyperactive phenotype observed in this model (Logue et al., 2009; Aura C. Meirsman et al., 2016; Quintana et al., 2012).

Somatosensory area ranked third among mostly altered top ten brain regions obtained from the partial correlation analysis. Therefore, whole brain connectivity from the SS seed was mapped that showed significant modifications in positive correlations predominantly toward the cortical regions, such as, MO, RSP and VIS areas (Figure 3c-correlations from 0 to 1 and Figure 3d-positive correlation, CTRL > Gpr88^{-/-}), however stronger in Gpr88^{-/-} group with the rostral isocortex and SS (Figure 3d-positive correlation, CTRL < Gpr88^{-/-}). In contrast, sub-cortical regions showed modified anti-correlations with SS (Figure 3c and 3d). These intra-cortical modifications of rsFC in Gpr88^{-/-} group correlate with modifications of the brain connectivity matrix derived from ICASSO analysis (Figure 1b). Altered motor – sensory connectivity observed in the Gpr88 deficient mice suggests sensorimotor gating deficiency. Intact sensorimotor gating is an important adaptive function, critical for an individual to be able to screen out internal and external distracting stimuli and also to appropriately attend to and process relevant stimuli (Braff et al., 1978; Perry and Braff, 1994; Venables, 1984). In contrast, sensorimotor gating abnormalities are thought to manifest clinically as symptoms of abnormal cognition and motor function (Swerdlow and Koob, 1987) and exhibited by schizophrenic patients as well as their first-degree relatives (Braff et al., 2001; Cadenhead et al., 2000a, 2000b; Wynn et al., 2004).

Modified striatal and hippocampal functional connectivity in *Gpr88*^{-/-} mice

Recent study from Meirsman et al., reported that *Gpr88*^{-/-} mice perform better in the allocentric versus egocentric component of the task for both acquisition and reversal learning, demonstrating facilitation of hippocampus-dependent behavior at the expense of striatal-dependent responses (Aura C. Meirsman et al., 2016). Thus, these two regions were particularly used to generate whole brain FC which revealed extensive rsFC modifications in the mutant group (Figure 4).

Seed based analysis from CP revealed strongly decreased rsFC between HPF, TH, as well as MB area in the *Gpr88*^{-/-} group (Figure 4b, positive correlation: CTRL > *Gpr88*^{-/-}), whereas increased connectivity towards ACA, rostral subcortical area, including septal complex (S), Pallidum (PAL), bed nuclei of the stria terminalis (BST) and agranular insular area (AI) (Figure 4b-positive correlation: CTRL < *Gpr88*^{-/-}). From negative correlation analysis, CP exhibited weaker connectivity with AMY, entorhinal (ENT) and VIS including SC, as well as pontine olivary nuclei (P) in the mutant mice (Figure 4b, anti-correlation: CTRL > *Gpr88*^{-/-}). However stronger anti-correlations were observed between CP and ACB along with MO, SS, ACA and PTLp (Figure 4b, anti-correlation, CTRL < *Gpr88*^{-/-}).

HPF on the other hand showed stronger positive correlations with the AMY, ENT, TEa, rostral TH and MB in the CTRL group, while toward the caudal TH, as well as SC and PG in the knockout group (Figure 4d, positive correlation: CTRL > *Gpr88*^{-/-} and CTRL < *Gpr88*^{-/-}). From negative correlation analysis HPF displayed decreased negative connectivity toward the frontal limbic system, including orbital (ORB), PL, and ACB areas, as well as ACA, MO, SS, RSP and PTLp cortical regions in the *Gpr88*^{-/-} mice (Figure 4d, anti-correlation: CTRL > *Gpr88*^{-/-}). Increased anti-correlated rsFC was however quantified between HPF and CP, lateral septal nuclei (LSx) and ILA (Figure 4d, anti-correlation: CTRL < *Gpr88*^{-/-}). Altogether, robust striato-hippocampal rsFC modifications underscore altered striato-hippocampal learning phenotype that was observed earlier in the *Gpr88*^{-/-} mice.

Annex 4.2: Table 3, summarizes all brain regions that showed significant FC modifications with MO, SS, CP and HPF.

Assessment of brain microstructure

Modifications in the microstructure of brain functional networks due to the deletion of *Gpr88* receptor was assessed by means of DTI and fiber tractography. Fiber density (FD) (Figure 6, Arefin et al., 2017) and fractional anisotropy (FA) (Annex 4.3: Figure2) were measured for the assessment of such structural connectivity modifications (Figure 6). Significant increase of FD and FA values was detected in *Gpr88*^{-/-} animals compared to CTRL group (voxel-wise statistical group comparison, $p < 0.01$, FWE corrected, contrast CTRL < *Gpr88*^{-/-}), in brain areas with altered rsFC. These areas included: CP, MO, SS, HPF, parts of TH and MB. However, no significant changes in FD and FA could be detected when examining the CTRL > *Gpr88*^{-/-}.

2.2 Behavioral studies with the Gpr88^{-/-} mice

2.2.1 Increased alcohol seeking in mice lacking Gpr88 involves dysfunctional mesocorticolimbic networks (Ben Hamida et al., 2018, Biological Psychiatry, doi: 10.1016/j.biopsych.2018.01.026.)

Based on the hypothesis that GPR88 receptor plays potential role in alcohol seeking and drinking behavior, mice were exposed to alcohol by following two consecutive alcohol drinking paradigms (see attached manuscript: Ben Hamida et al., 2018, Biological Psychiatry).

Two-bottle choice – continuous access: We first investigated if the level of moderate voluntary alcohol intake alters in Gpr88 deficient mice (Gpr88^{-/-}) compared to the wild-type (Gpr88^{+/+}) mice using 10% alcohol continuous access two-bottle-choice drinking paradigm in the home cage. Total deletion of Gpr88 in mice increased daily alcohol consumption compared to Gpr88^{+/+} mice (Figure 1a, left panel). The right panel of Figure 1a depicts the mean daily alcohol intake during the whole experiment and showed a significant increase of 39.9 % in Gpr88^{-/-} mice compared to Gpr88^{+/+} ($p < 0.001$). However, water intake was comparable in both groups (Figure 1b).

Two-bottle choice – intermittent access: This paradigm was used to examine whether deletion of GPR88 affects excessive alcohol intake, a hallmark of alcohol mediated disorders. Same group of wild-type mice were used in both paradigms. This procedure leads to escalation of the mean daily alcohol intake in both Gpr88^{-/-} (76.3%) and CTRL (57 %) compared to continuous access procedure (Figure 1c). This increase in the level of alcohol intake was more pronounced in Gpr88^{-/-} mice. Similar to the findings under continuous access procedure, no difference in water consumption was found (Figure 1d). These results together demonstrate that the Gpr88 gene deletion increases both moderate and excessive voluntary alcohol drinking.

One week after the alcohol-drinking study, mice were further examined to justify whether excessive alcohol intake by Gpr88^{-/-} mice was a consequence of an alteration of taste perception. All animals were tested for saccharin (0.066%) (sweet) or quinine (0.06 mM) (bitter) intake. Mice lacking GPR88 and the control animals drank similar amounts and expressed an equivalent preference for saccharin (Figure 1e) and quinine (Figure 1f), meaning that total deletion of GPR88 did not affect taste palatability. The increased level of alcohol intake observed in Gpr88^{-/-} mice can also be explained by a change in the sensitivity to this drug. To assess this hypothesis, the effect of an intoxicating/hypnotic dose of alcohol (3.2 g/Kg, 20% v/v solution, i.p.) on the latency and duration of the LORR were tested. There was no difference in the latency and duration (Figure 1g) of the LORR between Gpr88^{-/-} and CTRL mice. Furthermore, blood alcohol levels obtained in a separate cohort of mice showed no difference between the GPR88 deficient mice and CTRL group (Figure 1h). This result indicates that alcohol clearance is not affected by total deletion of GPR88 receptor and suggests that higher alcohol consumption in Gpr88^{-/-} mice is not due to alteration of alcohol metabolism.

Home cage free-choice bottle drinking models provide a measure of consummatory aspects and *Gpr88*^{-/-} exhibited excessive alcohol drinking behaviors. Whether this consummatory behavior was associated with increased operant self-administration (SA) of alcohol, drug-taking and drug-seeking behaviors between *Gpr88*^{-/-} and control mice, were tested during alcohol self-administration and progressive ratio test.

The timeline of the 10% alcohol operant self-administration in CTRL and *Gpr88*^{-/-} mice under fixed ratio 3 (FR3) and FR5 schedules is presented in Figure 2a. No differences were found in the pattern of pure saccharine intake (number of licks) between *Gpr88*^{-/-} mice (168 ± 84) compared to the CTRL (177 ± 72). However, increased lever responding and licks for saccharine/alcohol mixtures in *Gpr88*^{-/-} mice compared to controls were consistently observed (Figure 2b). Saccharine was omitted when alcohol concentration reached 10%. *Gpr88*^{-/-} mice made significantly higher number of lever presses for alcohol on the active lever in both FR schedules (Figure 2c). Compared to the controls, mutant mice also showed increased activity on the inactive lever (Figure 2c). Furthermore, number of licks in both FR schedules was higher for *Gpr88*^{-/-} mice (Figure 2d and 2e). These findings suggest that both alcohol seeking and drinking were increased in *Gpr88* deficient mice.

Together, these results led to the hypothesis that mice lacking GPR88 receptor express higher incentive motivation for alcohol drinking. To test this hypothesis, a progressive ratio (PR) session (response requirements increased number of presses after each reward) was undertaken to determine the breakpoint values of each genotype. These results revealed that the breakpoint (final ratio completed) was significantly enhanced in mice lacking GPR88 (Figure 2f). As a step forward, we examined whether the alcohol phenotype is substance-specific. We observed that both groups of mice acquired and maintained comparable operant responding for a natural reward (food) (Figure 2g) and the criteria for acquisition of this operant responding were reached upon the same number of sessions (Figure 2h).

All together, these results indicate that deletion of GPR88 change the incentive properties of alcohol that motivate alcohol seeking behavior in mice.

GPR88 deletion decreases alcohol-induced conditioned place preference (CPP)

We therefore tested whether deletion of GPR88 receptor in mice affects the expression and/or development of alcohol-induced CPP, to understand the underlying mechanisms of increased alcohol seeking and drinking (Figure 3a). During the preconditioning day, no side preference occurred in both genotypes (data not shown). However, mutant mice had lower CPP scores and spent less time in the alcohol-paired compartment than control mice. These data suggest that *Gpr88*^{-/-} mice show reduced development and/or expression of alcohol CPP, indicating reduced alcohol rewards in these animals.

Decreased dopamine (DA) response to alcohol in Gpr88^{-/-} mice

We further tested the consequences of Gpr88 deletion on basal and alcohol-enhanced extracellular levels of nucleus accumbens (NAC) dopamine (DA) (Figure 3b) and its metabolites DOPAC and HVA in the NAC (Figure 3c). Alcohol administration increased extracellular DA in both groups of mice. Notably, Gpr88^{-/-} mice exhibited significantly lower DA-elevating response to the high alcohol dose. Except for the two alcohol doses (insert for figure 3b), there was no difference in DOPAC or HVA (data not shown) levels between the groups in response to alcohol administration. Significant reduction of both alcohol place conditioning and NAC DA response to alcohol indicate that alcohol reward is diminished in mutant mice – a mechanism that could partly contribute to enhanced alcohol administration.

Gpr88 deletion weakens rsFC of the mesocorticolimbic circuitry

In order to investigate the molecular mechanisms underlying the high alcohol drinking behavior observed in Gpr88 deficient mice, we further compared the rsFC patterns of key mesolimbic brain regions. We selected four seed regions from the reward network, namely, prefrontal cortex (PFC), ventral tegmental area (VTA), NAC and amygdala (AMY). For all these seeds, rsFC was predominantly weakened (Gpr88^{-/-} < CTRL) in mutant mice (Figure 4a, voxel-level general linear model, corrected for multiple comparisons, p<0.001).

PFC showed reduced rsFC with the sub-cortical regions (CP, NAC, AMY, GP, LSX and TH) in the mutant group. VTA also showed reduced rsFC toward the cortical (MO, SS and AI) and sub-cortical (CP, NAC and TH) area. However, VTA – AMY rsFC were strengthened and weakened depending on the considered voxel groups. Furthermore, AMY showed significant FC alterations with CP and HPF, as well as with the cortex. Intriguingly, NAC rsFC was modified toward MO, SS and CP in the Gpr88^{-/-} group, however, no modification was detected toward the mesocorticolimbic regions of interest. Figure 4b summarizes the rsFC modifications observed from these seeds.

Diminished effective connectivity from VTA to NAC and AMY in Gpr88^{-/-} mice

To gain further insight into modified mesolimbic rsFC patterns of mutant mice, the causal influence of one region of interest on other regions (effective connectivity) was evaluated based on a pre-defined model (Figure 4c). Average effective connectivity parameters (t-test, p<0.001, FDR corrected) of the model are shown for CTRL (Figure 4c) and Gpr88^{-/-} mice (Figure 4d). Group comparison showed significantly reduced effective connectivity strength in mutant animals for both VTA to AMY and VTA to NAC connections (paired t-test, p<0.05), whereas no significant increase was detected within the small network. These findings suggest that deletion of Gpr88 gene limits the information flow from VTA to NAC and AMY.

2.2.2 Home cage behavioral phenotyping of Gpr88^{-/-} female mice in group-housed condition (Maroteaux G*, Arefin T*, et al., Genes, Brain and Behavior, 2018. *co-1st authors)

This study was aimed to investigate the behavior of Gpr88 deficient mice using IntelliCage, an automated behavioral assessment system (NewBehavior AG, Zurich, Switzerland).

In total of 32 female mice (control: n = 16, Gpr88^{-/-}: n = 16), 7 – 8 weeks old, were separated in groups of 8 of identical genotype and monitored in 4 Intellicages. The study was done with female mice as they have a greater compatibility in a social home cage setting and the long-term monitoring will most likely cancel most of the fluctuation due to their 5-days long estrous cycle (Kobayashi et al., 2013). Radio frequency identification transponders (Planet ID GmbH, Essen, Germany) were implanted subcutaneously in the dorso-cervical region under isoflurane inhalation anesthesia. Thereafter, the mice were allowed to recover for 1 week, in standard Type III cages (Tecniplast, Buguggiate, Italy), with water and food available ad libitum. Animals were then placed into the IntelliCages and maintained on a 12-hour light/dark cycle (lights on at 7:00 am) at a controlled temperature (22°C ± 1°C). Food and water were available ad libitum throughout the experiments. Recording chamber in each corner of the Intellicage contained two bottles filled with water or sucrose or alcohol solution. Mice activity was recorded using unique RFID tracking to register individual's visits of the conditioning corners. A visit is defined by antenna reading and presence signal. A nose-poke was count each time the mouse inserted its nose in the round opening, whether the door opened or not. Licks were registered by a lickometer, each time a mouse touched the drinking spout. The apparatus was controlled by the IntelliCage software 2.1, described previously (Krackow et al., 2010; Voikar et al., 2010). In this study the measure of activity is associated to the number of visits in the different corner as previous study suggested that visits of a corner via a small entrance and locomotor activity are correlated (G. Maroteaux et al., 2012). The protocol was divided into 3 phases free adaptation, nose-poke conditioning and fixed schedule drinking (Fig. 1). Experimental procedures and data processing techniques have been illustrated in (Maroteaux G*, Arefin T*, et al., 2018, Genes, Brain and Behavior)

Gpr88^{-/-} mice exhibited delayed habituation and repetitive behavior in the Intellicage

Former studies report both the male and female Gpr88^{-/-} mice as hyperactive (Aura Carole Meirsmann et al., 2016; Aura C. Meirsmann et al., 2016; Quintana et al., 2012). Habituation in the IntelliCage was assessed from the activities of mice during the free adaptation phase. The analysis was performed separately between the active – dark period (D) and the resting – light period (L). Diurnal activity of both groups was overall similar with peaks of activity during the dark periods and deeps in the activity during light periods (Fig. S1). Strikingly, Gpr88^{-/-} mice showed less number of corner visits on the first day during dark period, but did not decrease their number of visits over time (from dark 1 (D1) to D4) compared to their counterpart and thus showed higher number of visits on D4 (Figure 2Ai). In contrast, both groups showed increased

number of visits during the light periods (light1 (L1) to L3) (Fig. 2Aii). However, no difference in the total number of visits was observed (Fig. 2Aiii). A similar pattern was observed while comparing the number of nose-pokes between groups. CTRL mice significantly decreased their number of nose-pokes over time whereas *Gpr88^{-/-}* mice showed no difference over the four days resulting in a higher number of nose-pokes on D3 and D4 (Fig. 2Bi). However, CTRL mice showed stable pattern of nose-pokes during the light periods throughout the free adaptation phase (L1 to L3), but an increase from 94 ± 22 to 228 ± 47 nose-pokes for *Gpr88^{-/-}* mice on L3 (Fig. 2Bii), as well as higher number of total nose-pokes (Fig. 2Biii). The total number of licks representing the drinking behavior was higher in *Gpr88^{-/-}* mice. Interestingly, cumulative data plot revealed that *Gpr88^{-/-}* mice took more time to start drinking from the water bottles (5 out of 15 mice almost did not drink during the first 3 days) and drastically increasing their number of licks on the last dark period and catching up with the mouse have the highest number of licks (> 32000) (Fig. 2C).

Based on the model of the Y-maze to test hippocampal-dependent navigation, four identical corners of the IntelliCage were used to look at spontaneous alternations over the first hundred visits of each mouse. Alternations were divided in 3 specific conditions: 1) spontaneous corner alternation (SCA), 2) alternate corner return (ACR) and 3) same corner return (SCR). CTRL mice made a significantly higher number of SCA compared to ACR (Fig. 2D). No difference was observed in the total number of alternations between the groups (Fig. 2E). However, over the four days of free adaptation phase, CTRL mice made significantly more SCA and ACR than *Gpr88^{-/-}* mice. In contrast, *Gpr88^{-/-}* made significantly more SCR than SCA and ACR (Fig. 2F). Total number of alternations over 4 days of free adaptation phase was lower for *Gpr88^{-/-}* group (Fig. 2G).

In summary, during the free adaptation phase, CTRL mice showed decreased number of visits and nose-pokes during the dark periods and exploration pattern with more SCA at first suggesting a clear habituation pattern. On the contrary, this habituation pattern was not observed in the *Gpr88^{-/-}* mice as they showed stable number of visits and an increase in the number of nose-pokes throughout this phase. Moreover, a sub-group of *Gpr88^{-/-}* showed delayed use of the drinking spouts resulting in compensation in the number of licks on the last day of that phase. In addition, *Gpr88^{-/-}* displayed a preference to return to the previously visited corner. These findings are in consistent with the previously described non-habituation behavior and repetitive behavior of mice lacking GPR88 receptor (Aura C. Meirsman et al., 2016).

GPR88 deficient mice were more active in the IntelliCage over time

In the second phase of the experiment, mice were trained for 3 days to perform 5s nose-pokes to access the water bottles. CTRL mice decreased the number of visits over time. *Gpr88^{-/-}* mice on the other hand, showed a tendency to decrease the number of visits initially, however, significantly increased on D7 compared to the CTRL mice (Fig. 3Ai). During the light cycles, both groups had significantly lower number of visits (Fig. 3Aii). Similar to the free adaptation phase, no significant difference was observed in the total number of visits between genotypes

(Fig. 3Aiii). While comparing the number of nose-pokes, CTRL mice showed no difference throughout the phase, whereas *Gpr88*^{-/-} mice showed significantly higher number of nose-pokes on D5, followed by a drastic drop on D6 but an increase on D7 (Fig. 3Bi). This might result from the fact that few mice did not drink for 3 days in the first phase and hence compensated during the nose-poke adaptation phase. Both groups showed decreased number of nose-pokes over the light cycles (Figure 3Bii). Total number of nose-poke showed a difference on the edge of significance between the two groups, over this period (Fig. 3Biii). Figure 3C shows the cumulative licks for both groups during the nose-poke adaptation phase. Higher number of licks by *Gpr88*^{-/-} group on D5 was biased by the compensating mice, yet the pairwise comparison showed still a higher number of licks on D7 (Fig. S3). All together, these results suggest that CTRL mice reduced the number of visits gradually and stabilized the number of nose-pokes over time, whereas GPR88 receptor deficient mice showed more activity with significantly higher numbers of visits, nose-pokes and licks on the dark cycle of day 7. However, both groups showed no difficulties to adapt 5s nose-poke conditioning to get water.

Gpr88 deficiency does not affect mice cognitive abilities

Two consecutive phases of 3 days each: place learning and place reversal test were performed to test the cognitive abilities of mice due to the deletion of GPR88 (Fig. 1A). During the first phase, mice had only access in one corner consisting one bottle of water and another with 8% sucrose solution. To avoid following behavior, pairs of cage-mates were assigned to one corner (correct corner) in which they could access water or sucrose in response to a 5s nose-poke.

Total number of visits was stable for both groups, but *Gpr88*^{-/-} displayed higher number of visits (306 ± 35) on D10 compared to CTRL (177 ± 18) (Fig. 4Ai). During the light periods, both groups showed similar patterns of visits (Fig. 4Aii). However, CTRL mice increased their percentage of visits in the correct corner between D8 ($27 \pm 2\%$) and D9 ($34 \pm 2\%$) ($p = 0.007$), developing a preference for the correct corner (25% is the chance level). Whereas, *Gpr88*^{-/-} did not show any clear preference with stable percentage of correct visits (between D8 and D10) (Figure 4Bi). During the light periods, both groups showed a preference for the correct corner with a percentage of visits between 29% and 34% (Fig. 4Bii).

Number of nose-pokes differed between CTRL and *Gpr88*^{-/-}. During the dark periods, CTRL mice decreased the number of nose-pokes over time, whereas *Gpr88*^{-/-} showed stable number of nose-pokes, but a higher number of nose-pokes on D10 compared to CTRL (Fig. 4Ci). However, both groups performed similar number of nose-pokes during the light periods (Fig. 4Cii).

Additionally, no major difference was observed in the number of nose-pokes in the correct corner where both water and sucrose solution were accessible (dark period-Fig. 4Di and light period-Fig. 4Dii). Compared to the total number of nose-pokes in the four corners, not *Gpr88*^{-/-}, but CTRL mice increased their percentage of nose-pokes in the correct corner over the days during the dark periods (Fig. 4Ei). No difference was observed during the light periods (Fig. 4Eii). Moreover, both groups exhibited similar percentage of nose-pokes in the sucrose side during the dark (Fig.

4Fi) and light (Fig. 4Fii) periods, in particular, showing high preference for sucrose on D10 (CTRL = $62 \pm 7\%$ and Gpr88^{-/-} = $69 \pm 4\%$).

Both groups showed stable number of licks (sucrose + water) during the dark (Fig. 4Gi) and light (Fig. 4Gii) periods. However, higher preference to sucrose with more than 72% of licks in the sucrose side was observed for both groups on D10 (dark period-Fig. 4Hi and light period-Fig. 4Hii). In summary, both CTRL and Gpr88^{-/-} learned to find the corner with sucrose and water available and preferred the sucrose solution more than water.

This learning phase was followed by a reversal learning phase, in which the correct corner was switched to the opposite corner. During the dark and light periods, total number of visits (dark period-Fig. 5Ai and light period-Fig. 5Aii) and percentage of correct corner visits (dark period-Fig. 5Bi and light period-Fig. 5Bii) were similar between groups.

Total number of nose-pokes (dark period- Fig. 5Ci and light period-Fig. 5Cii) and the number of nose-pokes to the correct corner (dark period- Fig. 5Di and light period-Fig. 5Dii) were higher in Gpr88^{-/-} group compared to the CTRL. However, the percentage of nose-pokes in the correct corner was similar for both groups as shown in figure 5Ei (dark) and 5Eii (light). Notably, both groups displayed a preference to nose-poke in the new correct corner (>42% on D13). During the dark periods, Gpr88^{-/-} showed higher percentage of nose-pokes in the sucrose side on D11 but not on D12 and D13 compared to CTRL (Fig. 5Fi), but there was no significant differences during the light periods (Fig. 5Fii). Both groups showed again a high preference for the sucrose solution (on D13: CTRL = $65 \pm 4\%$ and Gpr88^{-/-} = $64 \pm 5\%$).

Total number of licks during the dark and light periods was similar for both groups (dark period-Fig. 5Gi and light period-Fig. 5Gii) and showed high preference to sucrose with more than 69% of licks in the sucrose side on D13 (dark period- Fig. 5Hi and light period-Fig. 5Hii). These results suggest GPR88 deficiency does not modify the learning abilities and preference to sucrose.

Gpr88^{-/-} mice exhibit less anticipatory but more persistent behavior

In order to test temporal learning abilities as well as natural reward response, mice were given access to water in 2 separate 1 hour (1h) session at 11 am and 4 pm during the light cycle and all doors remained closed for rest of the time. Both groups of mice showed similar pattern of drinking water during these 1h sessions and significantly higher number of licks during the 1h session at 11 am compared to 4 pm. During this fixed schedule drinking (FSD) period, all mice were monitored to ensure that they drink water. 86% mice visited corners to drink during 11 am drinking session as compared to 43% on average during 4 pm session over 9 days long FSD phase (Figure 6A). This observation ensures us that all mice had restricted access to water and were drinking sufficiently. Interestingly, CTRL mice showed a striking change in the pattern of corner visits. Particularly after 4 days, the difference in visits between dark and light cycles disappeared. Gpr88^{-/-} mice also decreased visiting corners during the dark cycles, however, the

number of visits were comparable between dark and light cycles (Figure 6B). Both groups showed stable pattern for nose-pokes during dark and light cycles, but the CTRL mice after day 16 and *Gpr88*^{-/-} mice after day 18 (Figure 6C). To refine the findings, visits and nose-pokes to the corners were evaluated, specifically on the hour just before and after the mice had access to water. Until day 17 both genotypes visited the corners equally between 10 am and 11 am (during the hour just before the mice had access to water). However, from day 18 to 21, CTRL mice exhibited higher number of visits compared to *Gpr88*^{-/-} (Figure 6D, upper left panel). During the 1h drinking session at 11 am, CTRL mice showed significantly higher number of visits than *Gpr88*^{-/-} mice only on day 14, but similar pattern of visits were observed for the rest of the days of FSD (Figure 6D, upper middle panel). Interestingly, *Gpr88*^{-/-} group exhibited higher number of visits and nose-pokes (Figure 6D and 6E, upper right panel) from day 15 to 19 compared to the CTRL. However, during the drinking session at 4 pm, only 50% mice had licks to water making the statistics less robust, whereas it was 87% during 11 am drinking session. Therefore, we concluded that 11am was the important part of the FSD phase. Taken together, these data show that *Gpr88*^{-/-} mice have a delay in developing an anticipatory behavior before the water-accessible hour and were more persistent with more visits and nose-pokes during the hour after that drinking session.

2.3 *Gpr88* signatures on the brain reward network connectivity after alcohol exposure in mice

Previous studies showed modulated expression of GPR88 following various treatments with antidepressants or mood regulators, addictive drugs including alcohol (Befort et al., 2008; Conti et al., 2006). In addition, our recent study (as described in section 2.2.1, Ben Hamida et al., 2018) also highlights *Gpr88* gene as a potential target for alcohol use disorder. Therefore, in this study we further aimed to examine whether GPR88 deletion remodels the rsFC of the brain regions associated with the reward network and mediates vulnerability to alcohol drinking behavior in mice.

Mice were exposed to alcohol for 2 months during the second phase of my study in IGBMC (as described in section 2.2.1). These mice were then scanned to map the structural and functional brain connectivity by means of rsfMRI and DTI with tractography (for details: see Annex 4.4). Mice exposed to water were scanned at any time point of the week (after 2months), however the mice exposed to alcohol were scanned on the day immediately after the last drinking session (for details: see section 2.2.1).

rsfMRI and DTI data were acquired from a total of 40 mice separated equally in 4 individual groups provided with water and alcohol respectively (n = 10 CTRL-water, n = 10 CTRL-alcohol, n = 10 *GPR88*^{-/-}-water and n = 10 *GPR88*^{-/-}-alcohol). Details experimental procedures and data processing methods are described in annex 4.4 and Arefin T. et al., 2017, respectively.

Deletion of GPR88 in mice increased daily alcohol consumption, however did not affect water intake compared to GPR88^{+/+} mice (see Ben Hamida et al., 2017, Figure 1). To investigate whether GPR88 reshapes reward resting state brain network connectivity, rsFC patterns of ventral tegmental area (VTA) and central amygdala (CEA) via seed correlation analysis (for details: see Arefin T. et al., 2017 and Annex section 4.4.3.2). These regions are well known core players of the reward processing. Seed analysis quantified strong VTA (Figure1) and CEA (Figure 2) rsFC modifications due to alcohol consumption in both GPR88^{+/+} and GPR88^{-/-} groups, predominantly toward the orbito-frontal cortex, striatum, amygdala, thalamus and midbrain area (p<0.001).

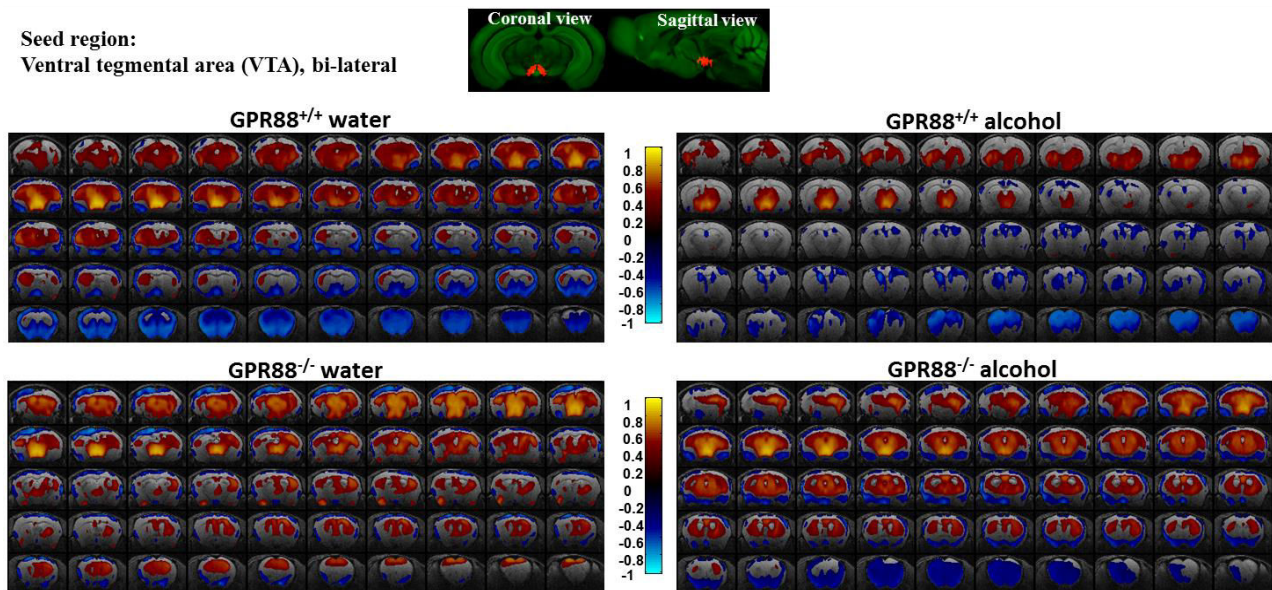


Figure 1: Alcohol consumption modifies the VTA connectivity in GPR88^{+/+} and GPR88^{-/-} groups: Seed region (bi-lateral VTA, extracted from Allen mouse brain atlas) is shown in coronal and sagittal plane. BOLD rsfMRI correlation maps ($p < 0.001$) of the (from top left to bottom right) GPR88^{+/+} water, GPR88^{+/+} alcohol, GPR88^{-/-} water and GPR88^{-/-} alcohol group were over-laid on a T₂-weighted anatomical brain slices. The color scale indicates the T-value (positive correlations from 0 to +1: dark red to yellow and negative correlations from 0 to -1: dark blue to turquoise).

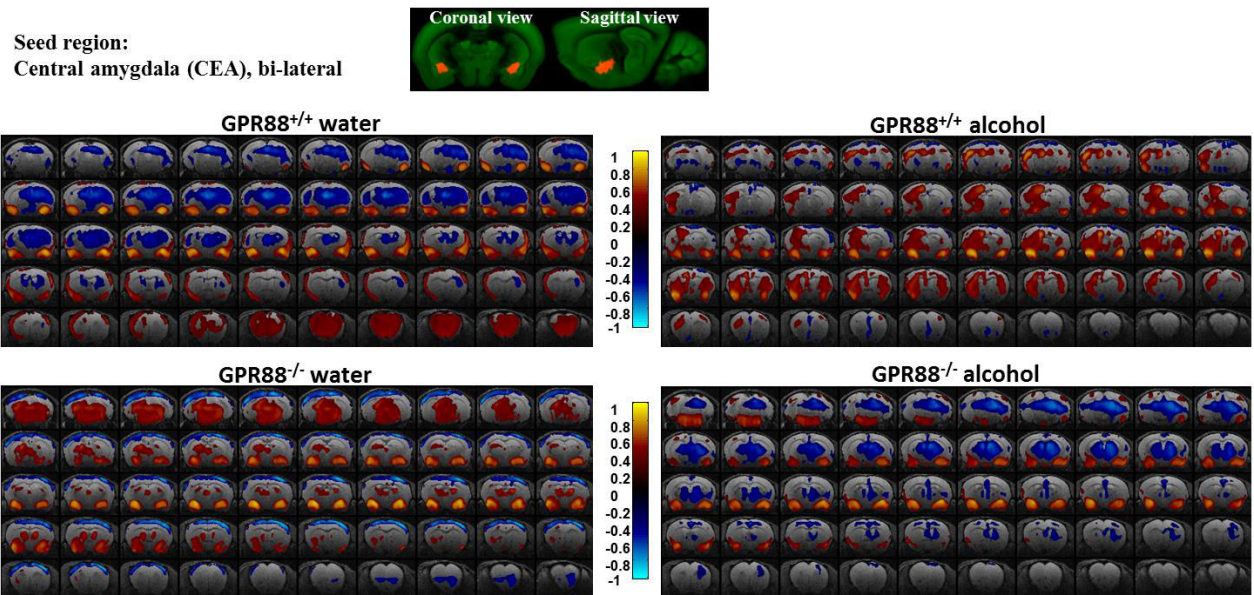


Figure 2: **Modified CEA connectivity due to alcohol intake in GPR88^{+/+} and GPR88^{-/-} groups:** Seed region (bi-lateral CEA, extracted from Allen mouse brain atlas) is shown in coronal and sagittal plane. BOLD rsfMRI correlation maps ($p < 0.001$) of the (from top left to bottom right) GPR88^{+/+} water, GPR88^{+/+} alcohol, GPR88^{-/-} water and GPR88^{-/-} alcohol group were overlaid on a T₂-weighted anatomical brain slices. The color scale indicates the T-value (positive correlations from 0 to +1: dark red to yellow and negative correlations from 0 to -1: dark blue to turquoise).

2.4 Deletion of the mu opioid receptor gene in mice reshapes the reward-aversion connectome (Mechling A. et al., 2016)

This study was based on the hypothesis that MOR contributes in the modifications of reward and addiction related functional network (Mechling et al., 2016). From the 100-ICASSO analysis rsfMRI data of 14 MOR knock-out mice (*Oprm1*^{-/-}) animals and respective 14 controls, 87 functional clusters were identified as pattern of neurological origin (see Supplementary Figure 1, Mechling et al., 2016). These brain regions were used as nodes to evaluate direct whole brain functional connectivity network via partial correlation analysis. Combining partial correlation and graph theory, modularity and small-worldness features were revealed to be conserved in both groups. The brain network hubs (nodes considered as relays of the functional network) were identified based on their associated normalized connectional strength and diversity (see methods, Mechling et al., 2016). From positive correlation analysis, nucleus accumbens (ACB) and prefrontal cortex (PFC), midbrain reticular nucleus (MRN)/ periaqueductal gray (PAG), habenula (HB) and somatosensory areas (SS) were identified as hubs in the control group. In contrast,

several sub-cortical brain regions, such as, caudoputamen (CP), bed nuclei of stria terminalis (BST), hippocampal formation (HPF) and peri-HPF cortex, thalamus (TH), superior colliculus (SC)/PAG, MRN/SC/PAG) appeared as functional hubs only specific to the *Oprm1*^{-/-} group. These hubs covered brain regions integrated into the core aversion-related network (Hayes and Northoff, 2012). PAG – a major opioid-sensitive pain-modulatory structure in both rodents (Fields, 2004) as well as humans (Wager et al., 2007) and is engaged in aversive learning (Roy et al., 2014), appeared entirely remodeled in the mutant group. Notably, considering both positive and negative correlations in the hub analysis – as stronger exclusion criteria, revealed ventromedial rostral MRN/PAG – a core node of pain/aversion network as the sole remaining *oprm1*-dependent functional hub.

Direct statistical inter-group comparison of controls and *Oprm1*^{-/-} correlation matrices was performed (two-sample t-test, $p < 0.05$, FDR corrected) and a ranking of the brain regions according to the number of their significantly changed connections was assembled (Figure 1d and Supplementary Video 1, Mechling et al., 2016). The highest number of changes was found in PAG - the core region of the pain/aversion network. Interestingly, the top 10 components of the hierarchy were predominantly from the aversion-related network (Borsook et al., 2007; Lammel et al., 2012b) and thus leading similar conclusion as hub analysis.

Habenula (HB) and ventral tegmental area/Interpeduncular (VTA/IPN) are the major nodes of the reward/aversion circuitry (RAC), express the highest density of MORs in the brain (Figure 3C and 3D, Mechling et al., 2016). Significant remodeling of habenula – ventral tegmental area/Interpeduncular nucleus (Hb – VTA/IPN) functional pathway (Figure 3A and 3B, Mechling et al., 2016) suggests concerted perturbation of the entire dorsal diencephalic conduction pathway in MOR deficient mice.

Furthermore, changes in the mouse brain microstructure were evaluated by high-resolution fiber mapping of the structural connectivity via high angular-resolution diffusion imaging (HARDI) and fiber tracking algorithm (Harsan et al., 2013; Reisert et al., 2011). We found only subtle modifications of structural scaffolding (Figure 4, Mechling et al., 2016), contrasting the rich FC remodeling and consistent with the neuromodulatory nature of the single missing gene (Navratilova et al., 2015; Navratilova and Porreca, 2014).

In conclusion, this study combines genetic and non-invasive brain imaging modalities and provides a comprehensive insight into the MOR deficient mouse brain functional and structural network.

Chapter 3

Discussion

Characterization of the impact of GPR88 receptor on the mouse brain connectivity

Genetic influences in psychiatric illnesses alter the phenotype in a complex manner, however, may not be broadly involved in the neurodevelopmental process but may instead interact with specific neural pathways resulting in the disruption of neural architecture that is behaviorally expressed. Identifications of the mechanisms through which these factors affect neural connectivity are important to develop novel therapeutic strategies. Emerging studies indicate that robust expression of GPR88 in the medium spiny neurons of striatum does not only regulate the striatal mediated behaviors but even in a larger repertoire. Nevertheless, the neuropharmacological/neuroadaptive mechanisms of GPR88 in psychiatric diseases are still under investigations. Therefore, the very first study was aimed to investigate the resting state functional and structural network amendments in GPR88 deficient mice via rsfMRI and DTI with tractography respectively.

In this study, resting state functional clusters were identified using hypothesis-free paradigm independent component analysis (ICA). Resting state data was decomposed into 100 spatial components using group ICA. However, estimation of the number of independent components appropriate to resting-state data is very important. Underestimation of the number of components may lead in combining several components together (Margulies et al., 2010; McKeown et al., 1998), while overestimation may split a reliable network (Esposito et al., 2003; Moritz et al., 2005) and thus decreasing the stability of IC estimates (Li et al., 2007). This challenge was handled by conducting a vigorous analysis of the mouse brain rsfMRI data using ICASSO (Himberg et al., 2004). This enabled the visualization of component clustering with a quantitative measure of robustness of ICs by evaluating the value of ‘stability index (I_q)’, ranging from 0 to 1 and highlighted unstable components. Furthermore, reproducibility of the group ICASSO patterns in each experimental group was verified by exploiting information and results generated with GIFT tools (Group ICA of fMRI Toolbox - v1.3i, <http://www.nitrc.org/projects/gift/>) via back reconstruction. The back reconstructed individual spatial maps were used to create “incidence maps” for each independent component (Figure S1b, S1c). The results demonstrated low intra-groups variability of the components pattern and extremely high similarity between groups. This approach revealed the spatial pattern of some of these components with areas strongly expressing GPR88 receptors in normal conditions (Figure S1b).

Anatomically well-defined brain regions obtained from the ICA were used to evaluate the whole brain functional connectivity architecture in the *Gpr88* deficient mice. Quantitative analysis of rsFC revealed RSP as mostly altered brain region among all (Figure 1c). RSP comprises the entire posterior cingulate cortex in rodents (Vogt and Peters, 1981) and the central part of DMN (Buckner et al., 2008). It is involved in cognition (Buckner et al., 2008; Raichle et al., 2001; Vann et al., 2009) and several studies report that RSP plays role in most common neurological disorders that impair learning and memory (Maguire, 2001; Nelson et al., 2014, 2015; Vann et al., 2009). Multiple neuroimaging studies also show perturbation in coherent activity of DMN in a range of neurological and psychiatric disorders including schizophrenia, autism, ageing,

attention deficit hyperactivity disorder (ADHD) and depression (Buckner et al., 2008; Greicius et al., 2008). Emerging studies also report ADHD as DMN disorder (Sonuga-Barke and Castellanos, 2007) and decreased DMN connectivity with ADHD patients (Castellanos et al., 2008; Castellanos and Proal, 2012; Fassbender et al., 2009).

Apart from the DMN, modifications in the sensory and motor area were noticeable. In particular, somato-motor connectivity (SS-MO) and SS-MO-ACA functional connections, linked with the observed sensorimotor gating deficiency (Logue et al., 2009; Aura C. Meirsmann et al., 2016) and risk-taking behavior (Aura Carole Meirsmann et al., 2016; Aura C. Meirsmann et al., 2016) of *Gpr88^{-/-}* mice. Beyond the widespread whole brain functional disconnections detected in schizophrenic patients (Liang et al., 2006; Welsh et al., 2010), several studies report specific rsFC disruption in DMN and sensorimotor networks (Kaufmann et al., 2015; Tang et al., 2012) similar to our findings in mice lacking the GPR88 receptor. Sensorimotor gating is the process of screening or gating of the sensory and motor/cognitive information to enable uninterrupted processing of the most salient aspects of the external and internal environment (Butler et al., 1990). Pre-pulse inhibition (PPI) is a well validated operational measure of sensorimotor gating in human and animals (Geyer et al., 2001), found disrupted in *Gpr88^{-/-}* mice (Logue et al., 2009).

Interestingly, here we perceived extensive intra-cortical connectivity modifications in mice lacking GPR88 despite of its robust expression in the striatum. This is because, GPR88 presents a classical GPCR plasma membrane/cytoplasmic localization in the cortical plate of the developing cortex that shifts on the day of birth to nuclei of neurons progressively settling during post-natal development, principally in layers V to II. Thus, it is likely that GPR88 influences the development of intra-cortical functional communication to some extent and that deletion of the receptor in the *Gpr88^{-/-}* mice leads to remodeling of cortical functional pathways, as seen here.

Apart from the intra-cortical rsFC modifications, cortico-striatal connectivity (particularly MO-striatum FC) is strongly perturbed in the *Gpr88^{-/-}* mice congruent to the fundamental resting state-network perturbations perceived in ADHD (Castellanos et al., 2006; Castellanos and Proal, 2012; Oldehinkel et al., 2016). ADHD is a highly prevalent neurobehavioral disorder in children and adolescents, which frequently persists into adulthood and manifests with symptoms of inattention and/or hyperactivity and impulsivity (Polanczyk et al., 2007) due to the deficiency in executive functions such as response inhibition, working memory (Willcutt et al., 2005), reward processing (Sonuga-Barke, 2005), and motor function (Stray et al., 2013). Dorsal and ventral part of striatum (CP and ACB) is the key brain regions related with these functions. Striatum receives projections from distinct cerebral regions (Alexander et al., 1986; Di Martino et al., 2008; Helmich et al., 2010). CP connectivity with MO regulates motor functions (Alexander et al., 1986). Precisely, anterior part of CP connectivity with ACA and MO (Helmich et al., 2010) has been associated with higher order cognitive aspects of motor control including learning and initiating new movements (Aramaki et al., 2011), whereas the posterior CP-MO connectivity has been related to the execution of well-learned, skilled movements (Tricomi et al., 2009, Helmich et al., 2010). These cortico-striatal networks are implicated in behavior that is often impaired in patients with

ADHD and thus, have been suggested as potential neural circuitry underpinning ADHD-related deficits (Cubillo et al., 2012). Several rsfMRI studies have demonstrated aberrant functional connectivity of striatum and motor regions in ADHD (Oldehinkel et al., 2013). Furthermore, atypical functional connectivity of striatum has been associated with severity of symptoms of hyperactivity/impulsivity and inattention (Costa Dias et al., 2013; Tomasi and Volkow, 2012). Taken together, these studies suggest dysfunction of cortico-striatal networks in ADHD. However, aberrant brain responses from one or more regions within cortico-striatal network do not necessarily imply dysfunction of the entire network. Instead, these dysfunctions might be primarily related to impairments in within striatum cross-talk, based on the assumption that striatal regions modulate each other via striato-nigro-striatal connections (Aarts et al., 2011; Haber et al., 2000).

Another salient finding of this study is the reduction in amygdala connectivity toward somatosensory and motor cortical area as well as caudate putamen, is consistent with the notion that amygdala might now drive increased risk taking (RT) behavior in potentially dangerous environment, leading to an apparent reduced anxiety in *Gpr88^{-/-}* mice (Aura C. Meersman et al., 2016). In addition, hyper-synchrony of the BOLD signal in the striatum of *Gpr88^{-/-}* mice, as observed in our study (Figure 4) has been reported earlier as a major contributor to adolescent RT behavior (Galvan, 2010).

Furthermore, both the hypothesis-free partial correlation (Figure 1c) and hypothesis-driven seed correlation analysis (Figure 4) revealed robust rsFC modifications in CP and HPF. Dorsal striatum (CP) is a major hub of the basal ganglia network, involved in several functional domains including learning, cognition and motivation (Mestres-Missé et al., 2012; Miyachi et al., 2002; Yin et al., 2009). In rodents, CP lesions disrupt acquisition of habits and impair goal-directed learning (Yin et al., 2004, 2005). Human neuroimaging studies also report the involvement of CP activity in the development of habits and goal directed behavior (Liljeholm et al., 2011; Tanaka et al., 2008; Tricomi et al., 2009). Hippocampus on the other hand plays crucial roles in working and episodic memory (Aggleton and Brown, 2006; Cabeza and Nyberg, 2000). Therefore, aberrant cross-talk between CP-HPF along with prefrontal cortex, limbic area and MB area, together with altered HPF rsFC, might underlie the modified learning phenotype of *Gpr88^{-/-}* mice, observed in a behavioral test that specifically addresses the striatum-hippocampus balance in learning (Quintana et al., 2012).

Thus far, cortical and sub-cortical resting state network modifications correlated with hyperactive characteristics in the *Gpr88^{-/-}* mice as observed previously evocating connectivity amendments observed in ADHD patients. Disrupted functional communications between brain regions is often accompanied by micro-structural abnormalities in the white matter (WM), which are thought to contribute to behavioral functioning in ADHD patients (Nagel et al., 2011). Fiber density (FD) and fractional anisotropy are the most common quantitative indices used to measure structural integrity (Konrad and Eickhoff, 2010; Nagel et al., 2011) with diffusion based tractography. Therefore, FD and FA were further mapped to measure the microstructural integrity in the *Gpr88^{-/-}*

^{-/-} mouse brain via DTI and fiber tractography (Harsan et al., 2013). Both FD (Figure 6) and FA (Annex 4.3: Figure2) were significantly higher in *Gpr88*^{-/-} mice (two-sample t-test, $p < 0.05$, FWE corrected) particularly along striato-cortical pathway (Figure 6) linking the striatum (CP) and cortical areas, like MO and SS. Former studies report disturbed structural connectivity of the cortico-striatal network in both adults and children with ADHD in comparison with the healthy subjects (Konrad and Eickhoff, 2010; Tamm et al., 2012). Taken together, functional and structural connectivity modifications in the sensorimotor and cortico-striatal circuitry observed in *Gpr88*^{-/-} mice are consistent with the prevailing neurobiological hypothesis of ADHD, which identifies these networks as a probable substrate for cognitive and behavioral impairments seen in ADHD patients (Bush et al., 2005; Castellanos et al., 2006; Castellanos and Proal, 2012; Holstein et al., 2013; Oldehinkel et al., 2016; van Ewijk et al., 2012).

Increased alcohol seeking in mice lacking *Gpr88* involves dysfunctional mesocorticolimbic networks

In this study we report that mice lacking *Gpr88* gene show increased alcohol-seeking and –taking behavior. Tackling mechanisms underlying this behavior, we next show lower alcohol-induced conditioned place preference (CPP) associated with reduced augmentation of extracellular DA levels by alcohol in the nucleus accumbens (NAC), suggesting that alcohol reward is decreased in mutant mice. Extending our study to the broader circuits of addiction, using rsfMRI in live animals, we finally demonstrate altered rsFC within the mesocorticolimbic circuitry of live knockout mice, in a pattern suggestive to network alterations observed in individuals at risk for AUD.

Gpr88^{-/-} mice exhibited higher levels of voluntary alcohol drinking and higher alcohol intake in operant SA, which together indicate significant alteration of processes that promote approach behaviors to alcohol. Importantly, we did not find any genotype differences in daily sucrose intake and thus, observed phenotypes could not be attributed to a general alteration of appetitive learning or taste sensitivity. Also, both mutant and control mice similarly acquired and maintained stable operant responding for food and chocolate pellets, and showed comparable preference for non-alcohol tastes (saccharine and quinine). In addition, food and chocolate operant responding as well as sucrose intake were unchanged, indicating that neither hyperactivity nor generalized responding to rewarding stimuli could explain the higher motivation for alcohol in SA experiments.

The progressive ratio break point during alcohol SA, considered a measure of motivation for the reward, was also enhanced in *Gpr88*^{-/-} mice. Increased motivation for alcohol may be due to higher or lower rewarding effects of alcohol, as SA studies show that higher drug-seeking behavior can be associated with either higher or lower drug reward (Berridge and Kringelbach, 2008; Lack et al., 2008). Here we find that, parallel to increased motivation for alcohol, mutant mice show reduced alcohol place preference in a conditioning paradigm, and also, importantly, reduced DA extracellular levels release in the NAC upon alcohol administration. Because extracellular DA levels in the NAC classically reflect drug reward related to abuse potential

(Abraham et al., 2012; Adamantidis et al., 2011), we propose that alcohol reward is indeed reduced in *Gpr88*^{-/-} mice. This, in turn, would contribute to augmenting both voluntary intake and operant responding for alcohol, to reach in mutant mice alcohol-rewarding effects similar to those achieved by control animals. Paralleling our findings, previous rodent studies showed that reduced drug reward together with reduced drug-induced DA responses is associated to higher motivation for cocaine (Lack et al., 2008). In humans, both reduced DA response to a psychostimulant (Casey et al., 2014) and low response to an alcohol challenge in young humans with a family history of AUD (Schickel, 1994) are predictive of a higher risk for addiction. The *Gpr88* knockout mouse phenotype may therefore be interpreted along a similar line (de Wit H., and Phillips T.J., 2012). This mechanism, however, is unlikely to be the only cause for higher alcohol seeking and taking in *Gpr88* knockout mice, and a second conclusion from this study is that GPR88 is critical in regulating functional activity of a number of brain networks.

We particularly focused on the rsFC patterns of the mesocorticolimbic networks. The most salient finding is a broad reduction of brainwide rsFC for the VTA, PFC, and AMY seeds, providing circuit-level mechanisms to explain excessive alcohol seeking and taking in mutant animals. First, VTA seed-based connectivity showed decreased correlation/anticorrelation with the NAC and AMY regions and, further, information flow from VTA to NAC (EF) was significantly reduced in *Gpr88*^{-/-} mice. These data are consistent with neurochemical analysis showing a lower increase of NAC DA levels upon alcohol treatment, and support the notion that reduced alcohol reward in mutant mice promotes increased alcohol-drinking behavior. Second, the PFC seed also showed reduced rsFC with the NAC and AMY seeds, as well as the somatosensory area, motor area, caudate putamen, and hippocampal formation, which remarkably correlate with previously reported behavioral deficits of *Gpr88*-deficient mice (Logue et al., 2009; Quintana et al., 2012; Meirnsman et al., 2016a and 2016b). This finding strongly suggests that top-down controls are disrupted in mutant mice, a hallmark of behavioral modification in addiction research (Baler and Volkow, 2006). Third, the AMY seed showed reduced correlation with the PFC and caudate putamen. Conversely, the PFC and VTA seeds showed either decreased or increased rsFC with the AMY. Also, EF from the VTA to the AMY was strongly reduced, and together, these multiple modifications of AMY rsFC are suggestive of altered emotional processing. In sum, the genetic deletion of *Gpr88* leads to significant modifications of brain networks contributing to reward processing, executive controls, and emotional regulation, and all concur to regulate addiction-related behaviors. Whether GPR88 activity regulates neuronal connectivity and effectiveness of these circuits during development, and/or is an active brain modulator in the adult, remains to be established. The observation of developmental stage-dependent *Gpr88* expression (Ehrlich et al., 2017) certainly includes the former. In the future inducible gene knockout experiments may clarify the respective contributions of developmental and tonic GPR88 activities in shaping addiction-related networks. Alternatively, pharmacology may adequately address this question, should specific and bioavailable agonists/antagonists become available.

Our behavioral, neurochemical, and functional connectivity analyses of *Gpr88* knockout mice together suggest that deletion of the *Gpr88* gene creates an alcohol vulnerability phenotype in

mice. The impaired interplay among reward, emotional, and executive functioning in Gpr88 mutant mice also characterizes the premorbid condition of at-risk human subjects. Our study represents a first step toward the establishment of translatable FC signatures, or biomarkers that may also provide mechanistic clues for abnormal alcohol-related behavior.

Gpr88 signatures on the brain reward network connectivity after alcohol exposure in mice

In order to investigate the underlying molecular mechanisms which intercede increased alcohol seeking and drinking behavior due to the deletion of GPR88 receptor, functional and structural networks of alcohol exposed mice were further non-invasively probed via rsfMRI and DT-MRI.

Seed-based analysis quantified extensive rsFC modifications in ventral tegmental area (VTA) and central amygdala (CEA) – two core players of the brain reward processing. VTA is the major hub of the brain reward network projects DA neurons to the limbic (amygdala, hippocampus), dorsal and ventral striatum and prefrontal regions (Beitner-Johnson et al., 1992; Epping-Jordan et al., 1998; Floresco and Tse, 2007). Activity of DA neurons is influenced by novel stimuli and responds to unexpected natural rewards and conditioned cues that predict reward (Horvitz, 2000; Ikemoto, 2007; Wise, 2004b). Plasticity in this system is strongly implicated in addictive disorders that involve compulsive drug-seeking (Wolf et al., 2004; Zweifel et al., 2008). The CEA functions as an integrative hub that converts emotionally-relevant sensory information about the external and internal environment into behavioral and physiological responses. CEA microcircuitry receives and integrates complex multi-modal information to produce behavioral responses. Medial part of the CEA (CEAm) is the major output nucleus of the amygdala that connects regions responsible for producing behavioral and physiological responses to emotionally relevant events (Jolkkonen and Pitkänen, 1998; Pape and Pare, 2010). Recent study also suggests GABAergic projections from the lateral CEA (CEAl) to behavioral and physiological effector regions (Penzo et al., 2014). CEA microcircuitry is thus critical for emotional processing, especially for interpretation of emotionally relevant stimuli or the attachment of emotional relevance to otherwise neutral stimuli. Dysfunction in amygdala circuitry implicated in both anxiety disorders (Tye et al., 2011) and substance abuse (Koob, 2008). In summary, extensive modifications in VTA and CEA rsFC might be part of the reward related pathways underlying the susceptibility to alcohol intake behavior observed in the Gpr88^{-/-} mice. These preliminary results support further investigations of the rsFC of other brain regions controlling reward related behavior in order to have a comprehensive picture of the resting state brain reward network modifications. Additionally, using hypothesis-free paradigms, such as, ICA and partial correlation analysis will provide the whole brain rsFC remodeling in response to the exposure of alcohol in mice. To achieve this goal, as a first step, resting state functional clusters were assessed via 100-ICASSO. 87 reliable functional components associated with anatomically well-defined brain areas were identified (see Annex: section 4.3, Figure 1). Remaining 13 components were excluded from the study based on their artifactual pattern, related to CSF, movement or vascular origin. The robustness of the components was tested and validated using ICASSO algorithm (Himberg et al., 2004). These 87 brain regions will be used as nodes to create

the brain FC matrix via partial correlation analysis. Apart from the functional connectivity assessment, evaluation of the DTI and fiber tractography derived parameters (fiber density – FD and fractional anisotropy – FA) as measures for structural connectivity modifications will reveal how the deletion of GPR88 gene impacts the underlying microstructure of brain functional networks. Taken together, this study will expand our knowledge on the brain adaptations to alcohol as well as the implications of GPR88 in alcoholism.

Home cage behavioral phenotyping of Gpr88^{-/-} female mice in group-housed condition

Psychiatric disorders are complex multi-factorial-dependent disorders (Karl and Arnold, 2014; Kim and Leventhal, 2015). Their diagnosis, treatment and recovery are long lasting processes and sensitive to environmental factors. However, most standard behavioral tests used to investigate mouse models of psychiatric disorders, take snapshots of their behavior (lasting between 5 to 60 min) (Barnes, 1979; Crawley and Goodwin, 1980b; Hall, 1932; Pellow et al., 1985). Therefore, to describe the effect of genetic background, mutation or drug on behavior, a battery of tests is required to tap into different aspects of behavior such as motor, sensory, cognitive and circadian functions (Rogers et al., 1999). Yet, the succession of tests in those batteries involves several major confounders such as repetitive human handling, testing during mice's rest period (during the light phase) and sometimes single-housing the animals. These external stressors influence the rodents behavioral response and should be carefully taken into account as they are source of variation in the results that may lead to different interpretations (J C Crabbe et al., 1999; Turner and Burne, 2013; Wahlsten, 2010; Würbel, 2002). A solution to reduce confounding factors effect is to observe mice behavior in their home cage. The development of automated home cage monitoring allows repetitive, objective, and consistent measurement of mice behavior over days or even weeks, rather than minutes or hour. In addition, continuous recording allows investigation of multi-dimensional aspects of behavior, in a freely moving animal, from the basal activity, its everyday life pattern, to challenged behavior (de Visser et al., 2006; Endo et al., 2012; Grégoire Maroteaux et al., 2012). Under such conditions, the motivation of the animal is intrinsic; the animal is not forced to react to a novel environment and its reaction is not biased by any handling. In order to investigate mice in a social and environmental adequate situation and reduce the influence of external factors, behavioral and cognitive performance of GPR88 receptor deficient mice were tested using the IntelliCage. It is an automated home cage that monitors group-housed mice implanted with radio frequency identification chips and allows investigating multi-dimensional aspects of mice behavior (habituation, baseline and challenged behavior).

This longitudinal study was designed in 4 consecutive phases with group-housed female mice lacking GPR88 receptor and investigates the striatum and hippocampus mediated behaviors. Thus far, behavioral investigations on the GPR88 deficient mice were carried out using conventional type III cages that provided a snapshot of the mouse behavior (Del Zompo et al., 2014; Ingallinesi et al., 2015; Logue et al., 2009; Massart et al., 2009; Aura Carole Meirsman et al., 2016; Aura C. Meirsman et al., 2016; Quintana et al., 2012). To our best knowledge, this is the first IntelliCage study with female Gpr88^{-/-} mice that provided real time measurement of the

mouse activities and revealed several important behavioral aspects of this specific genotype. Salient findings from this study include:

- *Gpr88*^{-/-} mice displayed an altered habituation pattern during the free adaptation phase.
- These mice exhibited increased activity over time, however, no deficit in the nose-poke conditioning compared to the counterparts.
- GPR88 deficiency does not alter the cognitive function in mice
- During the FSD phase, *Gpr88* receptor lacking mice did not show learning deficiency, yet, significant differences in activities during dark and light cycles and less anticipatory but more persistent behavior before and after the 1h drinking session compared to the CTRL mice.

Most of the previous studies report *Gpr88*^{-/-} mice as hyperactive. This study does not explicitly show *Gpr88*^{-/-} female mice hyperactive, however, non-habituation behavior was observed during the nose-poke adaptation and FSD phase. Repetitive behavior observed in the GPR88 deficient mice are consistent with the previous findings (Aura C. Meirsmann et al., 2016). Importantly, this study demonstrates the impact of GPR88 receptor on the striatum mediated non-habituation and repetitive behavior. In addition, *Gpr88*^{-/-} mice showed similar decrease in the number of visits and nose-pokes during the dark cycles of FSD phase as well as similar number of licks at 11 am and 4 pm drinking session and thus exhibiting no learning deficiency during the FSD phase. Furthermore, IntelliCage system allowed narrowing down the experiment to investigate the mouse behavior particularly at the hour before and after the fixed schedule drinking session (11 am and 4 pm respectively). CTRL mice increased the number of visits on the hour prior to 1h drinking session as an anticipation of the up-coming event (water access), while *Gpr88*^{-/-} mice did not significantly increase their number of visits. Moreover, on the hour after the 1h drinking session, CTRL mice decreased their number of visits and nose-pokes, whereas *Gpr88*^{-/-} mice had significantly higher activities, showing more perseverative behavior. Previous study demonstrated altered basal dopamine and phosphoDARPP-32 levels in the striatum of the GPR88 deficient mice (Logue et al., 2009), suggesting major modifications of the dopaminergic system. The mesolimbic dopaminergic system has a key role in natural reward and is activated in response to ingestive behavior (Pitchers et al., 2010; Yoshida et al., 1992). Moreover, dopamine levels in lateral hypothalamic area and nucleus accumbens were correlated to anticipatory and consummatory phases of feeding (Legrand et al., 2015). Salient findings from this study along with the evidences from the former studies point toward the fact that lack of GPR88 in mice results in a modification of the reward response towards a natural reward such as drinking after a long period of restriction.

Conclusion and future perspective

This study combines brain magnetic resonance imaging (MRI), genetic and molecular approaches to investigate the involvement of GPR88 receptor in mouse brain connectivity to behavior. In-vivo non-invasive mouse brain imaging approaches (rsfMRI, DTI and fiber tracking) were applied to map the functional and micro-structural connectivity fingerprints. This is the first study demonstrating the impact of GPR88 receptor in reshaping the mouse brain functional and structural circuitry, closely resembling human network alterations observed in some psychiatric disorders, particularly relevant to ADHD. Additionally, remodeled resting state reward network suggests GPR88 receptor as a potential contributor in the modifications of brain connectivity after alcohol exposure in mice and further supports the observation of increased vulnerability to alcohol in *Gpr88*^{-/-} mice. Moreover, less anticipatory but more persistent behavior exhibited by *Gpr88* deficient mice is a novel finding of this study. In summary, this study signifies the GPR88 receptor as a potential target for pharmacological treatment of multiple psychiatric disorders.

Despite of these intriguing findings, yet, there are still some questions to be addressed in future. For instance:

- It has been shown that acute methylphenidate (MPH) administration reverses hyperactivity trait of *Gpr88*^{-/-} mice. Therefore, it is important to investigate whether ritaline treatment restores striato-cortical connectivity in the *GPR88*^{-/-} mice.
- Somatosensory - thalamus rsFC was decreased in the *GPR88*^{-/-} mice, however the inverse was true for PAG, which is an important structure in terms of pain inhibition. Hence, this could be a prospective pathway to investigate whether *Gpr88* also contribute in pain inhibition or not.
- In the present study, alcohol was exposed to single-housed mouse. In future, it will be interesting to develop longitudinal alcohol-drinking paradigm with group housed mice using IntelliCage. This will allow the real time measurement of mice activities in the acquisition and development of alcohol dependency.
- In addition, examination of the pathological brain neurocircuitry changes in mouse models that mimic the various stages of alcohol addiction cycle, such as, recreational alcohol drinking, excessive alcohol drinking and alcohol intoxication models.

This study demonstrates the potential of rsfMRI and DTI to noninvasively probe the brain functional and structural networks in genetically modified mice. Further research using *Gpr88*^{-/-} mice will significantly contribute to the understanding about the implication of GPR88 on the development of neurological or psychiatric disorders including alcohol addiction.

References

- Aarts, E., van Holstein, M., Cools, R., 2011. Striatal Dopamine and the Interface between Motivation and Cognition. *Front. Psychol.* 2. doi:10.3389/fpsyg.2011.00163
- Abrahamo, K.P., Quadros, I.M.H., Andrade, A.L.M., Souza-Formigoni, M.L.O., 2012. Accumbal dopamine D2 receptor function is associated with individual variability in ethanol behavioral sensitization. *Neuropharmacology* 62, 882–889. doi:10.1016/j.neuropharm.2011.09.017
- Adamantidis, A.R., Tsai, H.-C., Boutrel, B., Zhang, F., Stuber, G.D., Budygin, E.A., Touriño, C., Bonci, A., Deisseroth, K., de Lecea, L., 2011. Optogenetic interrogation of dopaminergic modulation of the multiple phases of reward-seeking behavior. *J. Neurosci. Off. J. Soc. Neurosci.* 31, 10829–10835. doi:10.1523/JNEUROSCI.2246-11.2011
- Adolphs, R., Tranel, D., Damasio, H., Damasio, A.R., 1995. Fear and the human amygdala. *J. Neurosci. Off. J. Soc. Neurosci.* 15, 5879–5891.
- Aggleton, J.P., Brown, M.W., 2006. Interleaving brain systems for episodic and recognition memory. *Trends Cogn. Sci.* 10, 455–463. doi:10.1016/j.tics.2006.08.003
- Ahrens, E.T., Laidlaw, D.H., Readhead, C., Brosnan, C.F., Fraser, S.E., Jacobs, R.E., 1998. MR microscopy of transgenic mice that spontaneously acquire experimental allergic encephalomyelitis. *Magn. Reson. Med.* 40, 119–132.
- Alexander, A.L., Lee, J.E., Lazar, M., Field, A.S., 2007. Diffusion Tensor Imaging of the Brain. *Neurother. J. Am. Soc. Exp. Neurother.* 4, 316–329. doi:10.1016/j.nurt.2007.05.011
- Alexander, G.E., DeLong, M.R., Strick, P.L., 1986. Parallel Organization of Functionally Segregated Circuits Linking Basal Ganglia and Cortex. *Annu. Rev. Neurosci.* 9, 357–381. doi:10.1146/annurev.ne.09.030186.002041
- Ambroggi, F., Ishikawa, A., Fields, H.L., Nicola, S.M., 2008. Basolateral amygdala neurons facilitate reward-seeking behavior by exciting nucleus accumbens neurons. *Neuron* 59, 648–661. doi:10.1016/j.neuron.2008.07.004
- Aramaki, Y., Haruno, M., Osu, R., Sadato, N., 2011. Movement Initiation-Locked Activity of the Anterior Putamen Predicts Future Movement Instability in Periodic Bimanual Movement. *J. Neurosci.* 31, 9819–9823. doi:10.1523/JNEUROSCI.4473-10.2011
- Arefin, T., Mechling, A.E., Meirsmann, C.A., Bienert, T., Huebener, N.S., Lee H.L., Ben Hamida, S., Ehrlich, A., Roquet, D., Hennig, J., von Elverfeldt, D., Kieffer, BL., Harsan, LA., 2017. Remodeling of Sensorimotor Brain Connectivity in Gpr88 Deficient Mice. *Brain Connectivity*. doi:10.1089/brain.2017.0486 [Epub ahead of print]
- Baler R.D., Volkow, N.D., 2006. Drug addiction: The neurobiology of disrupted self-control. *Trends Mol Med* 12:559-566
- Balleine, B.W., Killcross, S., 2006. Parallel incentive processing: an integrated view of amygdala function. *Trends Neurosci.* 29, 272–279. doi:10.1016/j.tins.2006.03.002
- Barnes, C.A., 1979. Memory deficits associated with senescence: a neurophysiological and behavioral study in the rat. *J. Comp. Physiol. Psychol.* 93, 74–104.
- Barnes, T.D., Kubota, Y., Hu, D., Jin, D.Z., Graybiel, A.M., 2005. Activity of striatal neurons reflects dynamic encoding and recoding of procedural memories. *Nature* 437, 1158–1161. doi:10.1038/nature04053
- Basser, P.J., Mattiello, J., LeBihan, D., 1994. MR diffusion tensor spectroscopy and imaging. *Biophys. J.* 66, 259–267. doi:10.1016/S0006-3495(94)80775-1

- Bateup, H.S., Santini, E., Shen, W., Birnbaum, S., Valjent, E., Surmeier, D.J., Fisone, G., Nestler, E.J., Greengard, P., 2010. Distinct subclasses of medium spiny neurons differentially regulate striatal motor behaviors. *Proc. Natl. Acad. Sci. U. S. A.* 107, 14845–14850. doi:10.1073/pnas.1009874107
- Baxter, M.G., Murray, E.A., 2002. The amygdala and reward. *Nat. Rev. Neurosci.* 3, 563–573. doi:10.1038/nrn875
- Becerra, L., Pendse, G., Chang, P.-C., Bishop, J., Borsook, D., 2011. Robust reproducible resting state networks in the awake rodent brain. *PloS One* 6, e25701. doi:10.1371/journal.pone.0025701
- Beckmann, C.F., DeLuca, M., Devlin, J.T., Smith, S.M., 2005. Investigations into resting-state connectivity using independent component analysis. *Philos. Trans. R. Soc. Lond. B. Biol. Sci.* 360, 1001–1013. doi:10.1098/rstb.2005.1634
- Beckmann, C.F., Smith, S.M., 2004. Probabilistic independent component analysis for functional magnetic resonance imaging. *IEEE Trans. Med. Imaging* 23, 137–152. doi:10.1109/TMI.2003.822821
- Befort, K., Filliol, D., Ghate, A., Darcq, E., Matifas, A., Muller, J., Lardenois, A., Thibault, C., Dembele, D., Le Merrer, J., Becker, J. a. J., Poch, O., Kieffer, B.L., 2008. Mu-opioid receptor activation induces transcriptional plasticity in the central extended amygdala. *Eur. J. Neurosci.* 27, 2973–2984. doi:10.1111/j.1460-9568.2008.06273.x
- Beitner-Johnson, D., Guitart, X., Nestler, E.J., 1992. Neurofilament proteins and the mesolimbic dopamine system: common regulation by chronic morphine and chronic cocaine in the rat ventral tegmental area. *J. Neurosci. Off. J. Soc. Neurosci.* 12, 2165–2176.
- Ben Hamida, S., Netto, S., Arefin T., Nasseef, T., Boulos, L., McNicholas M., Ehrlich, A., Moquin, L., Gratton, A., Darcq, E., Harsan, LA., Maldonado R., and Kieffer, B., 2017. Increased alcohol seeking in mice lacking Gpr88 involves dysfunctional mesocorticolimbic networks, *Biological Psychiatry* (2018), doi: 10.1016/j.biopsych.2018.01.026.
- Berridge, K.C., Kringelbach, M.L., 2008. Affective neuroscience of pleasure: reward in humans and animals. *Psychopharmacology (Berl.)* 199, 457–480. doi:10.1007/s00213-008-1099-6
- Berwick, J., Martin, C., Martindale, J., Jones, M., Johnston, D., Zheng, Y., Redgrave, P., Mayhew, J., 2002. Hemodynamic response in the unanesthetized rat: intrinsic optical imaging and spectroscopy of the barrel cortex. *J. Cereb. Blood Flow Metab. Off. J. Int. Soc. Cereb. Blood Flow Metab.* 22, 670–679. doi:10.1097/00004647-200206000-00005
- Birn, R.M., Diamond, J.B., Smith, M.A., Bandettini, P.A., 2006. Separating respiratory-variation-related fluctuations from neuronal-activity-related fluctuations in fMRI. *NeuroImage* 31, 1536–1548. doi:10.1016/j.neuroimage.2006.02.048
- Biswal, B., Yetkin, F.Z., Haughton, V.M., Hyde, J.S., 1995. Functional connectivity in the motor cortex of resting human brain using echo-planar MRI. *Magn. Reson. Med.* 34, 537–541.
- Biswal, B.B., Mennes, M., Zuo, X.-N., Gohel, S., Kelly, C., et al., 2010. Toward discovery science of human brain function. *Proc. Natl. Acad. Sci. U. S. A.* 107, 4734–4739. doi:10.1073/pnas.0911855107
- Biswal, B.B., Van Kylen, J., Hyde, J.S., 1997. Simultaneous assessment of flow and BOLD signals in resting-state functional connectivity maps. *NMR Biomed.* 10, 165–170.
- Bloch, F., 1946. Nuclear Induction. *Phys. Rev.* 70, 460–474. doi:10.1103/PhysRev.70.460
- Böhm, C., Newrzella, D., Herberger, S., Schramm, N., Eisenhardt, G., Schenk, V., Sonntag-Buck, V., Sorgenfrei, O., 2006. Effects of antidepressant treatment on gene expression

- profile in mouse brain: cell type-specific transcription profiling using laser microdissection and microarray analysis. *J. Neurochem.* 97 Suppl 1, 44–49. doi:10.1111/j.1471-4159.2006.03750.x
- Bonnelle, V., Ham, T.E., Leech, R., Kinnunen, K.M., Mehta, M.A., Greenwood, R.J., Sharp, D.J., 2012. Salience network integrity predicts default mode network function after traumatic brain injury. *Proc. Natl. Acad. Sci. U. S. A.* 109, 4690–4695. doi:10.1073/pnas.1113455109
- Borowsky, I.W., Collins, R.C., 1989. Metabolic anatomy of brain: a comparison of regional capillary density, glucose metabolism, and enzyme activities. *J. Comp. Neurol.* 288, 401–413. doi:10.1002/cne.902880304
- Borsook, D., Becerra, L., Carlezon, W.A., Shaw, M., Renshaw, P., Elman, I., Levine, J., 2007. Reward-aversion circuitry in analgesia and pain: implications for psychiatric disorders. *Eur. J. Pain Lond. Engl.* 11, 7–20. doi:10.1016/j.ejpain.2005.12.005
- Brady, R.O., Tandon, N., Masters, G.A., Margolis, A., Cohen, B.M., Keshavan, M., Öngür, D., 2016. Differential brain network activity across mood states in bipolar disorder. *J. Affect. Disord.* 207, 367–376. doi:10.1016/j.jad.2016.09.041
- Braff, D., Stone, C., Callaway, E., Geyer, M., Glick, I., Bali, L., 1978. Prestimulus effects on human startle reflex in normals and schizophrenics. *Psychophysiology* 15, 339–343.
- Braff, D.L., Geyer, M.A., Swerdlow, N.R., 2001. Human studies of prepulse inhibition of startle: normal subjects, patient groups, and pharmacological studies. *Psychopharmacology (Berl.)* 156, 234–258.
- Brandish PE, Su M, Holder DJ, Hodor P, Szumiloski J, Kleinhanz RR, et al. (2005): Regulation of gene expression by lithium and depletion of inositol in slices of adult rat cortex. *Neuron* 45:861–872.
- Bressler, S.L., Menon, V., 2010. Large-scale brain networks in cognition: emerging methods and principles. *Trends Cogn. Sci.* 14, 277–290. doi:10.1016/j.tics.2010.04.004
- Bromberg-Martin, E.S., Matsumoto, M., Hikosaka, O., 2010. Dopamine in motivational control: rewarding, aversive, and alerting. *Neuron* 68, 815–834. doi:10.1016/j.neuron.2010.11.022
- Brunner, D., Nestler, E., Leahy, E., 2002. In need of high-throughput behavioral systems. *Drug Discov. Today* 7, S107-112.
- Buckner, R.L., Andrews-Hanna, J.R., Schacter, D.L., 2008. The brain’s default network: anatomy, function, and relevance to disease. *Ann. N. Y. Acad. Sci.* 1124, 1–38. doi:10.1196/annals.1440.011
- Buckner, R.L., Sepulcre, J., Talukdar, T., Krienen, F.M., Liu, H., Hedden, T., Andrews-Hanna, J.R., Sperling, R.A., Johnson, K.A., 2009. Cortical hubs revealed by intrinsic functional connectivity: mapping, assessment of stability, and relation to Alzheimer’s disease. *J. Neurosci. Off. J. Soc. Neurosci.* 29, 1860–1873. doi:10.1523/JNEUROSCI.5062-08.2009
- Buckner, R.L., Vincent, J.L., 2007. Unrest at rest: default activity and spontaneous network correlations. *NeuroImage* 37, 1091-1096-1099. doi:10.1016/j.neuroimage.2007.01.010
- Bullmore, E., Sporns, O., 2009. Complex brain networks: graph theoretical analysis of structural and functional systems. *Nat. Rev. Neurosci.* 10, 186–198. doi:10.1038/nrn2575
- Bush, G., Valera, E.M., Seidman, L.J., 2005. Functional neuroimaging of attention-deficit/hyperactivity disorder: a review and suggested future directions. *Biol. Psychiatry* 57, 1273–1284. doi:10.1016/j.biopsych.2005.01.034
- Butler, R.W., Braff, D.L., Rausch, J.L., Jenkins, M.A., Sprock, J., Geyer, M.A., 1990. Physiological evidence of exaggerated startle response in a subgroup of Vietnam veterans

- with combat-related PTSD. *Am. J. Psychiatry* 147, 1308–1312. doi:10.1176/ajp.147.10.1308
- Buxton, R.B., Uludağ, K., Dubowitz, D.J., Liu, T.T., 2004. Modeling the hemodynamic response to brain activation. *NeuroImage* 23 Suppl 1, S220–233. doi:10.1016/j.neuroimage.2004.07.013
- Cabeza, R., Nyberg, L., 2000. Imaging cognition II: An empirical review of 275 PET and fMRI studies. *J. Cogn. Neurosci.* 12, 1–47.
- Cadenhead, K.S., Light, G.A., Geyer, M.A., Braff, D.L., 2000a. Sensory gating deficits assessed by the P50 event-related potential in subjects with schizotypal personality disorder. *Am. J. Psychiatry* 157, 55–59. doi:10.1176/ajp.157.1.55
- Cadenhead, K.S., Swerdlow, N.R., Shafer, K.M., Diaz, M., Braff, D.L., 2000b. Modulation of the startle response and startle laterality in relatives of schizophrenic patients and in subjects with schizotypal personality disorder: evidence of inhibitory deficits. *Am. J. Psychiatry* 157, 1660–1668. doi:10.1176/appi.ajp.157.10.1660
- Cador, M., Robbins, T.W., Everitt, B.J., 1989. Involvement of the amygdala in stimulus-reward associations: interaction with the ventral striatum. *Neuroscience* 30, 77–86.
- Calhoun, V.D., Adali, T., Pearlson, G.D., Pekar, J.J., 2001. A method for making group inferences from functional MRI data using independent component analysis. *Hum. Brain Mapp.* 14, 140–151.
- Casey, K.F., Benkelfat, C., Cherkasova, M.V., Baker, G.B., Dagher, A., Leyton, M., 2014. Reduced dopamine response to amphetamine in subjects at ultra-high risk for addiction. *Biol Psychiatry.* 76, 23–30.
- Cao, M., Wang, Z., He, Y., 2015. Connectomics in psychiatric research: advances and applications. *Neuropsychiatr. Dis. Treat.* 11, 2801–2810. doi:10.2147/NDT.S63470
- Castellanos, F.X., Margulies, D.S., Kelly, C., Uddin, L.Q., Ghaffari, M., Kirsch, A., Shaw, D., Shehzad, Z., Di Martino, A., Biswal, B., Sonuga-Barke, E.J.S., Rotrosen, J., Adler, L.A., Milham, M.P., 2008. Cingulate-precuneus interactions: a new locus of dysfunction in adult attention-deficit/hyperactivity disorder. *Biol. Psychiatry* 63, 332–337. doi:10.1016/j.biopsych.2007.06.025
- Castellanos, F.X., Proal, E., 2012. Large-scale brain systems in ADHD: beyond the prefrontal-striatal model. *Trends Cogn. Sci.* 16, 17–26. doi:10.1016/j.tics.2011.11.007
- Castellanos, F.X., Sonuga-Barke, E.J.S., Milham, M.P., Tannock, R., 2006. Characterizing cognition in ADHD: beyond executive dysfunction. *Trends Cogn. Sci.* 10, 117–123. doi:10.1016/j.tics.2006.01.011
- Chavhan, G.B., Babyn, P.S., Thomas, B., Shroff, M.M., Haacke, E.M., 2009. Principles, techniques, and applications of T2*-based MR imaging and its special applications. *Radiogr. Rev. Publ. Radiol. Soc. N. Am. Inc* 29, 1433–1449. doi:10.1148/rg.295095034
- Cherkassky, V.L., Kana, R.K., Keller, T.A., Just, M.A., 2006. Functional connectivity in a baseline resting-state network in autism. *Neuroreport* 17, 1687–1690. doi:10.1097/01.wnr.0000239956.45448.4c
- Choi, J., Jeong, B., Lee, S.W., Go, H.-J., 2013. Aberrant development of functional connectivity among resting state-related functional networks in medication-naïve ADHD children. *PloS One* 8, e83516. doi:10.1371/journal.pone.0083516
- Conti, B., Maier, R., Barr, A.M., Morale, M.C., Lu, X., Sanna, P.P., Bilbe, G., Hoyer, D., Bartfai, T., 2006. Region-specific transcriptional changes following the three antidepressant treatments electro convulsive therapy, sleep deprivation and fluoxetine. *Mol. Psychiatry* 12, 167–189. doi:10.1038/sj.mp.4001897

- Cordes, D., Haughton, V.M., Arfanakis, K., Wendt, G.J., Turski, P.A., Moritz, C.H., Quigley, M.A., Meyerand, M.E., 2000. Mapping functionally related regions of brain with functional connectivity MR imaging. *AJNR Am. J. Neuroradiol.* 21, 1636–1644.
- Costa Dias, T.G., Wilson, V.B., Bathula, D.R., Iyer, S.P., Mills, K.L., et al., 2013. Reward circuit connectivity relates to delay discounting in children with attention-deficit/hyperactivity disorder. *Eur. Neuropsychopharmacol. J. Eur. Coll. Neuropsychopharmacol.* 23, 33–45. doi:10.1016/j.euroneuro.2012.10.015
- Crabbe, J.C., Wahlsten, D., Dudek, B.C., 1999. Genetics of mouse behavior: interactions with laboratory environment. *Science* 284, 1670–1672.
- Crabbe, J.C., Wahlsten, D., Dudek, B.C., 1999. Genetics of mouse behavior: interactions with laboratory environment. *Science* 284, 1670–1672.
- Craddock, R.C., Jbabdi, S., Yan, C.-G., Vogelstein, J.T., Castellanos, F.X., Di Martino, A., Kelly, C., Heberlein, K., Colcombe, S., Milham, M.P., 2013. Imaging human connectomes at the macroscale. *Nat. Methods* 10, 524–539. doi:10.1038/nmeth.2482
- Crawley, J., Goodwin, F.K., 1980a. Preliminary report of a simple animal behavior model for the anxiolytic effects of benzodiazepines. *Pharmacol. Biochem. Behav.* 13, 167–170.
- Crawley, J., Goodwin, F.K., 1980b. Preliminary report of a simple animal behavior model for the anxiolytic effects of benzodiazepines. *Pharmacol. Biochem. Behav.* 13, 167–170.
- Crawley, J.N., 2007. Mouse behavioral assays relevant to the symptoms of autism. *Brain Pathol. Zurich Switz.* 17, 448–459. doi:10.1111/j.1750-3639.2007.00096.x
- Cromwell, H.C., Schultz, W., 2003. Effects of expectations for different reward magnitudes on neuronal activity in primate striatum. *J. Neurophysiol.* 89, 2823–2838. doi:10.1152/jn.01014.2002
- Cubillo, A., Halari, R., Smith, A., Taylor, E., Rubia, K., 2012. A review of fronto-striatal and fronto-cortical brain abnormalities in children and adults with Attention Deficit Hyperactivity Disorder (ADHD) and new evidence for dysfunction in adults with ADHD during motivation and attention. *Cortex J. Devoted Study Nerv. Syst. Behav.* 48, 194–215. doi:10.1016/j.cortex.2011.04.007
- Damoiseaux, J.S., Rombouts, S.A.R.B., Barkhof, F., Scheltens, P., Stam, C.J., Smith, S.M., Beckmann, C.F., 2006. Consistent resting-state networks across healthy subjects. *Proc. Natl. Acad. Sci. U. S. A.* 103, 13848–13853. doi:10.1073/pnas.0601417103
- D’Arceuil, H.E., Westmoreland, S., de Crespigny, A.J., 2007. An approach to high resolution diffusion tensor imaging in fixed primate brain. *NeuroImage* 35, 553–565. doi:10.1016/j.neuroimage.2006.12.028
- de Visser, L., van den Bos, R., Kuurman, W.W., Kas, M.J.H., Spruijt, B.M., 2006. Novel approach to the behavioural characterization of inbred mice: automated home cage observations. *Genes Brain Behav.* 5, 458–466. doi:10.1111/j.1601-183X.2005.00181.x
- Del Zompo, M., Deleuze, J.-F., Chillotti, C., Cousin, E., Niehaus, D., et al., Faucon Biguet, N., Mallet, J., Meloni, R., 2014. Association study in three different populations between the GPR88 gene and major psychoses. *Mol. Genet. Genomic Med.* 2, 152–159. doi:10.1002/mgg3.54
- Di Chiara, G., Imperato, A., 1988. Drugs abused by humans preferentially increase synaptic dopamine concentrations in the mesolimbic system of freely moving rats. *Proc. Natl. Acad. Sci. U. S. A.* 85, 5274–5278.
- Di Ciano, P., Everitt, B.J., 2004. Direct interactions between the basolateral amygdala and nucleus accumbens core underlie cocaine-seeking behavior by rats. *J. Neurosci. Off. J. Soc. Neurosci.* 24, 7167–7173. doi:10.1523/JNEUROSCI.1581-04.2004

- Di Martino, A., Scheres, A., Margulies, D.S., Kelly, A.M.C., Uddin, L.Q., et al., 2008. Functional connectivity of human striatum: a resting state fMRI study. *Cereb. Cortex N. Y. N* 1991 18, 2735–2747. doi:10.1093/cercor/bhn041
- Di, X., Biswal, B.B., 2014. Modulatory interactions between the default mode network and task positive networks in resting-state. *PeerJ* 2, e367. doi:10.7717/peerj.367
- Durieux, P.F., Bearzatto, B., Guiducci, S., Buch, T., Waisman, A., Zoli, M., Schiffmann, S.N., de Kerchove d'Exaerde, A., 2009. D2R striatopallidal neurons inhibit both locomotor and drug reward processes. *Nat. Neurosci.* 12, 393–395. doi:10.1038/nn.2286
- Durieux, P.F., Schiffmann, S.N., de Kerchove d'Exaerde, A., 2012. Differential regulation of motor control and response to dopaminergic drugs by D1R and D2R neurons in distinct dorsal striatum subregions. *EMBO J.* 31, 640–653. doi:10.1038/emboj.2011.400
- Duvarci, S., Pare, D., 2014. Amygdala microcircuits controlling learned fear. *Neuron* 82, 966–980. doi:10.1016/j.neuron.2014.04.042
- Dzierba CD, Bi Y, Dasgupta B, Hartz RA, Ahuja V, Cianchetta G, et al. (2015): Design, synthesis, and evaluation of phenylglycinols and phenyl amines as agonists of GPR88. *Bioorg Med Chem Lett* 25:1448–1452.
- Endo, T., Kakeyama, M., Uemura, Y., Haijima, A., Okuno, H., Bito, H., Tohyama, C., 2012. Executive Function Deficits and Social-Behavioral Abnormality in Mice Exposed to a Low Dose of Dioxin In Utero and via Lactation. *PLOS ONE* 7, e50741. doi:10.1371/journal.pone.0050741
- Epping-Jordan, M.P., Markou, A., Koob, G.F., 1998. The dopamine D-1 receptor antagonist SCH 23390 injected into the dorsolateral bed nucleus of the stria terminalis decreased cocaine reinforcement in the rat. *Brain Res.* 784, 105–115.
- Esposito, F., Seifritz, E., Formisano, E., Morrone, R., Scarabino, T., Tedeschi, G., Cirillo, S., Goebel, R., Di Salle, F., 2003. Real-time independent component analysis of fMRI time-series. *NeuroImage* 20, 2209–2224.
- Everitt, B.J., Dickinson, A., Robbins, T.W., 2001. The neuropsychological basis of addictive behaviour. *Brain Res. Brain Res. Rev.* 36, 129–138.
- Fair, D.A., Cohen, A.L., Dosenbach, N.U.F., Church, J.A., Miezin, F.M., Barch, D.M., Raichle, M.E., Petersen, S.E., Schlaggar, B.L., 2008. The maturing architecture of the brain's default network. *Proc. Natl. Acad. Sci. U. S. A.* 105, 4028–4032. doi:10.1073/pnas.0800376105
- Fair, D.A., Dosenbach, N.U.F., Church, J.A., Cohen, A.L., Brahmbhatt, S., Miezin, F.M., Barch, D.M., Raichle, M.E., Petersen, S.E., Schlaggar, B.L., 2007. Development of distinct control networks through segregation and integration. *Proc. Natl. Acad. Sci. U. S. A.* 104, 13507–13512. doi:10.1073/pnas.0705843104
- Fair, D.A., Posner, J., Nagel, B.J., Bathula, D., Dias, T.G.C., Mills, K.L., Blythe, M.S., Giwa, A., Schmitt, C.F., Nigg, J.T., 2010. Atypical default network connectivity in youth with attention-deficit/hyperactivity disorder. *Biol. Psychiatry* 68, 1084–1091. doi:10.1016/j.biopsych.2010.07.003
- Farber, N.E., Harkin, C.P., Niedfeldt, J., Hudetz, A.G., Kampine, J.P., Schmeling, W.T., 1997. Region-specific and agent-specific dilation of intracerebral microvessels by volatile anesthetics in rat brain slices. *Anesthesiology* 87, 1191–1198.
- Fassbender, C., Zhang, H., Buzy, W.M., Cortes, C.R., Mizuiri, D., Beckett, L., Schweitzer, J.B., 2009. A lack of default network suppression is linked to increased distractibility in ADHD. *Brain Res.* 1273, 114–128. doi:10.1016/j.brainres.2009.02.070

- Fields, H., 2004. State-dependent opioid control of pain. *Nat. Rev. Neurosci.* 5, 565–575. doi:10.1038/nrn1431
- Floresco, S.B., Tse, M.T., 2007. Dopaminergic regulation of inhibitory and excitatory transmission in the basolateral amygdala-prefrontal cortical pathway. *J. Neurosci. Off. J. Soc. Neurosci.* 27, 2045–2057. doi:10.1523/JNEUROSCI.5474-06.2007
- Fowler, T., Shelton, K., Lifford, K., Rice, F., McBride, A., Nikolov, I., Neale, M.C., Harold, G., Thapar, A., van den Bree, M.B.M., 2007. Genetic and environmental influences on the relationship between peer alcohol use and own alcohol use in adolescents. *Addict. Abingdon Engl.* 102, 894–903. doi:10.1111/j.1360-0443.2007.01824.x
- Fox, M.D., Corbetta, M., Snyder, A.Z., Vincent, J.L., Raichle, M.E., 2006. Spontaneous neuronal activity distinguishes human dorsal and ventral attention systems. *Proc. Natl. Acad. Sci. U. S. A.* 103, 10046–10051. doi:10.1073/pnas.0604187103
- Fox, M.D., Raichle, M.E., 2007. Spontaneous fluctuations in brain activity observed with functional magnetic resonance imaging. *Nat. Rev. Neurosci.* 8, 700–711. doi:10.1038/nrn2201
- Fox, M.D., Snyder, A.Z., Vincent, J.L., Corbetta, M., Van Essen, D.C., Raichle, M.E., 2005. The human brain is intrinsically organized into dynamic, anticorrelated functional networks. *Proc. Natl. Acad. Sci. U. S. A.* 102, 9673–9678. doi:10.1073/pnas.0504136102
- Friston, K.J., 1994. Functional and effective connectivity in neuroimaging: A synthesis. *Hum. Brain Mapp.* 2, 56–78. doi:10.1002/hbm.460020107
- Galsworthy, M.J., Amrein, I., Kuptsov, P.A., Poletaeva, I.I., Zinn, P., Rau, A., Vyssotski, A., Lipp, H.-P., 2005. A comparison of wild-caught wood mice and bank voles in the Intellicage: assessing exploration, daily activity patterns and place learning paradigms. *Behav. Brain Res.* 157, 211–217. doi:10.1016/j.bbr.2004.06.021
- Galvan, A., 2010. Adolescent development of the reward system. *Front. Hum. Neurosci.* 4, 6. doi:10.3389/neuro.09.006.2010
- Garrity, A.G., Pearlson, G.D., McKiernan, K., Lloyd, D., Kiehl, K.A., Calhoun, V.D., 2007. Aberrant “default mode” functional connectivity in schizophrenia. *Am. J. Psychiatry* 164, 450–457. doi:10.1176/ajp.2007.164.3.450
- Gaveriaux-Ruff, C., Nozaki, C., Nadal, X., Hever, X.C., Weibel, R., Matifas, A., Reiss, D., Filliol, D., Nassar, M.A., Wood, J.N., Maldonado, R., Kieffer, B.L., 2011. Genetic ablation of delta opioid receptors in nociceptive sensory neurons increases chronic pain and abolishes opioid analgesia. *Pain* 152, 1238–1248. doi:10.1016/j.pain.2010.12.031
- Gerfen, C.R., 1992. The neostriatal mosaic: multiple levels of compartmental organization. *Trends Neurosci.* 15, 133–139.
- Gerlai, R., 2001. Behavioral tests of hippocampal function: simple paradigms complex problems. *Behav. Brain Res.* 125, 269–277. doi:10.1016/S0166-4328(01)00296-0
- Geyer, M.A., Krebs-Thomson, K., Braff, D.L., Swerdlow, N.R., 2001. Pharmacological studies of prepulse inhibition models of sensorimotor gating deficits in schizophrenia: a decade in review. *Psychopharmacology (Berl.)* 156, 117–154.
- Ghate, A., Befort, K., Becker, J. a. J., Filliol, D., Bole-Feysot, C., Demebele, D., Jost, B., Koch, M., Kieffer, B.L., 2007. Identification of novel striatal genes by expression profiling in adult mouse brain. *Neuroscience* 146, 1182–1192. doi:10.1016/j.neuroscience.2007.02.040
- GIFT Software [WWW Document], n.d. URL <http://mialab.mrn.org/software/gift/documentation.html> (accessed 10.19.16).

- Graybiel, A.M., Aosaki, T., Flaherty, A.W., Kimura, M., 1994. The basal ganglia and adaptive motor control. *Science* 265, 1826–1831.
- Greenough, W.T., 1984. Structural correlates of information storage in the mammalian brain: a review and hypothesis. *Trends Neurosci.* 7, 229–233. doi:10.1016/S0166-2236(84)80211-8
- Greicius, M.D., Kiviniemi, V., Tervonen, O., Vainionpää, V., Alahuhta, S., Reiss, A.L., Menon, V., 2008. Persistent default-mode network connectivity during light sedation. *Hum. Brain Mapp.* 29, 839–847. doi:10.1002/hbm.20537
- Greicius, M.D., Krasnow, B., Reiss, A.L., Menon, V., 2003. Functional connectivity in the resting brain: a network analysis of the default mode hypothesis. *Proc. Natl. Acad. Sci. U. S. A.* 100, 253–258. doi:10.1073/pnas.0135058100
- Greicius, M.D., Srivastava, G., Reiss, A.L., Menon, V., 2004. Default-mode network activity distinguishes Alzheimer’s disease from healthy aging: evidence from functional MRI. *Proc. Natl. Acad. Sci. U. S. A.* 101, 4637–4642. doi:10.1073/pnas.0308627101
- Gremel, C.M., Cunningham, C.L., 2007. Role of test activity in ethanol-induced disruption of place preference expression in mice. *Psychopharmacology (Berl.)* 191, 195–202. doi:10.1007/s00213-006-0651-5
- Groenewegen, H.J., Wright, C.I., Beijer, A.V., 1996. The nucleus accumbens: gateway for limbic structures to reach the motor system? *Prog. Brain Res.* 107, 485–511.
- Grubb, R.L., Raichle, M.E., Eichling, J.O., Ter-Pogossian, M.M., 1974. The effects of changes in PaCO₂ on cerebral blood volume, blood flow, and vascular mean transit time. *Stroke J. Cereb. Circ.* 5, 630–639.
- Guldenmund, P., Vanhaudenhuyse, A., Boly, M., Laureys, S., Soddu, A., 2012. A default mode of brain function in altered states of consciousness. *Arch. Ital. Biol.* 150, 107–121.
- Gunaydin, L.A., Grosenick, L., Finkelstein, J.C., Kauvar, I.V., Fenno, L.E., Adhikari, A., Lammel, S., Mirzabekov, J.J., Airan, R.D., Zalocusky, K.A., Tye, K.M., Anikeeva, P., Malenka, R.C., Deisseroth, K., 2014. Natural neural projection dynamics underlying social behavior. *Cell* 157, 1535–1551. doi:10.1016/j.cell.2014.05.017
- Gusnard, D.A., Akbudak, E., Shulman, G.L., Raichle, M.E., 2001a. Medial prefrontal cortex and self-referential mental activity: relation to a default mode of brain function. *Proc. Natl. Acad. Sci. U. S. A.* 98, 4259–4264. doi:10.1073/pnas.071043098
- Gusnard, D.A., Raichle, M.E., Raichle, M.E., 2001b. Searching for a baseline: functional imaging and the resting human brain. *Nat. Rev. Neurosci.* 2, 685–694. doi:10.1038/35094500
- Guye, M., Bettus, G., Bartolomei, F., Cozzone, P.J., 2010. Graph theoretical analysis of structural and functional connectivity MRI in normal and pathological brain networks. *Magma N. Y.* N 23, 409–421. doi:10.1007/s10334-010-0205-z
- Haber, S.N., Fudge, J.L., McFarland, N.R., 2000. Striatonigrostriatal pathways in primates form an ascending spiral from the shell to the dorsolateral striatum. *J. Neurosci. Off. J. Soc. Neurosci.* 20, 2369–2382.
- Hall, C., 1932. A study of the rat’s behavior in a field. A contribution to method in comparative psychology. *Univ. Calif. Publ. Psychol.* 6, 1–12.
- Hamilton, J.P., Chen, M.C., Gotlib, I.H., 2013. Neural systems approaches to understanding major depressive disorder: an intrinsic functional organization perspective. *Neurobiol. Dis.* 52, 4–11. doi:10.1016/j.nbd.2012.01.015
- Hampson, M., Peterson, B.S., Skudlarski, P., Gatenby, J.C., Gore, J.C., 2002. Detection of functional connectivity using temporal correlations in MR images. *Hum. Brain Mapp.* 15, 247–262.

- Harsan, L.-A., Dávid, C., Reisert, M., Schnell, S., Hennig, J., von Elverfeldt, D., Staiger, J.F., 2013. Mapping remodeling of thalamocortical projections in the living reeler mouse brain by diffusion tractography. *Proc. Natl. Acad. Sci. U. S. A.* 110, E1797-1806. doi:10.1073/pnas.1218330110
- Harsan, L.-A., Paul, D., Schnell, S., Kreher, B.W., Hennig, J., Staiger, J.F., von Elverfeldt, D., 2010. In vivo diffusion tensor magnetic resonance imaging and fiber tracking of the mouse brain. *NMR Biomed.* 23, 884–896. doi:10.1002/nbm.1496
- Harsan, L.A., Poulet, P., Guignard, B., Steibel, J., Parizel, N., de Sousa, P.L., Boehm, N., Grucker, D., Ghandour, M.S., 2006. Brain dysmyelination and recovery assessment by noninvasive in vivo diffusion tensor magnetic resonance imaging. *J. Neurosci. Res.* 83, 392–402. doi:10.1002/jnr.20742
- Hayes, D.J., Northoff, G., 2012. Common brain activations for painful and non-painful aversive stimuli. *BMC Neurosci.* 13, 60. doi:10.1186/1471-2202-13-60
- Hedden, T., Van Dijk, K.R.A., Becker, J.A., Mehta, A., Sperling, R.A., Johnson, K.A., Buckner, R.L., 2009. Disruption of functional connectivity in clinically normal older adults harboring amyloid burden. *J. Neurosci. Off. J. Soc. Neurosci.* 29, 12686–12694. doi:10.1523/JNEUROSCI.3189-09.2009
- Heinz, A., Siessmeier, T., Wrase, J., Hermann, D., Klein, S., Grüsser, S.M., Grüsser-Sinopoli, S.M., Flor, H., Braus, D.F., Buchholz, H.G., Gründer, G., Schreckenberger, M., Smolka, M.N., Rösch, F., Mann, K., Bartenstein, P., 2004. Correlation between dopamine D(2) receptors in the ventral striatum and central processing of alcohol cues and craving. *Am. J. Psychiatry* 161, 1783–1789. doi:10.1176/appi.ajp.161.10.1783
- Helmich, R.C., Derikx, L.C., Bakker, M., Scheeringa, R., Bloem, B.R., Toni, I., 2010. Spatial remapping of cortico-striatal connectivity in Parkinson's disease. *Cereb. Cortex N. Y. N* 1991 20, 1175–1186. doi:10.1093/cercor/bhp178
- Hennig, J., Nauerth, A., Friedburg, H., 1986. RARE imaging: a fast imaging method for clinical MR. *Magn. Reson. Med.* 3, 823–833.
- Hikosaka, O., Sakamoto, M., Usui, S., 1989. Functional properties of monkey caudate neurons. II. Visual and auditory responses. *J. Neurophysiol.* 61, 799–813.
- Himberg, J., Hyvärinen, A., Esposito, F., 2004. Validating the independent components of neuroimaging time series via clustering and visualization. *NeuroImage* 22, 1214–1222. doi:10.1016/j.neuroimage.2004.03.027
- Holmes, A., Wrenn, C.C., Harris, A.P., Thayer, K.E., Crawley, J.N., 2002. Behavioral profiles of inbred strains on novel olfactory, spatial and emotional tests for reference memory in mice. *Genes Brain Behav.* 1, 55–69.
- Holstein, D.H., Vollenweider, F.X., Geyer, M.A., Csomor, P.A., Belser, N., Eich, D., 2013. Sensory and sensorimotor gating in adult attention-deficit/hyperactivity disorder (ADHD). *Psychiatry Res.* 205, 117–126. doi:10.1016/j.psychres.2012.08.013
- Hong, W., Kim, D.-W., Anderson, D.J., 2014. Antagonistic control of social versus repetitive self-grooming behaviors by separable amygdala neuronal subsets. *Cell* 158, 1348–1361. doi:10.1016/j.cell.2014.07.049
- Horvitz, J.C., 2000. Mesolimbocortical and nigrostriatal dopamine responses to salient non-reward events. *Neuroscience* 96, 651–656.
- Huang, S., Li, J., Sun, L., Ye, J., Fleisher, A., Wu, T., Chen, K., Reiman, E., Alzheimer's Disease Neuroimaging Initiative, 2010. Learning brain connectivity of Alzheimer's disease by sparse inverse covariance estimation. *NeuroImage* 50, 935–949. doi:10.1016/j.neuroimage.2009.12.120

- Hutchison, R.M., Womelsdorf, T., Gati, J.S., Leung, L.S., Menon, R.S., Everling, S., 2012. Resting-state connectivity identifies distinct functional networks in macaque cingulate cortex. *Cereb. Cortex N. Y. N* 1991 22, 1294–1308. doi:10.1093/cercor/bhr181
- Hyman, S.E., Malenka, R.C., 2001. Addiction and the brain: the neurobiology of compulsion and its persistence. *Nat. Rev. Neurosci.* 2, 695–703. doi:10.1038/35094560
- Ikemoto, S., 2007. Dopamine reward circuitry: two projection systems from the ventral midbrain to the nucleus accumbens-olfactory tubercle complex. *Brain Res. Rev.* 56, 27–78. doi:10.1016/j.brainresrev.2007.05.004
- Info - Home - TSE Systems [WWW Document], n.d. URL <http://www.tse-systems.com/> (accessed 10.20.16).
- Ingallinesi, M., Le Bouil, L., Biguet, N.F., Thi, A.D., Mannoury la Cour, C., Millan, M.J., Ravassard, P., Mallet, J., Meloni, R., 2015. Local inactivation of Gpr88 in the nucleus accumbens attenuates behavioral deficits elicited by the neonatal administration of phencyclidine in rats. *Mol. Psychiatry* 20, 951–958. doi:10.1038/mp.2014.92
- Jennings, J.H., Sparta, D.R., Stamatakis, A.M., Ung, R.L., Pleil, K.E., Kash, T.L., Stuber, G.D., 2013. Distinct extended amygdala circuits for divergent motivational states. *Nature* 496, 224–228. doi:10.1038/nature12041
- Jin C, Decker AM, Huang XP, Gilmour BP, Blough BE, Roth BL, et al. (2014): Synthesis, pharmacological characterization, and structure-activity relationship studies of small molecular agonists for the orphan GPR88 receptor. *ACS Chem Neurosci* 5:576–587.
- Jog, M.S., Kubota, Y., Connolly, C.I., Hillegaart, V., Graybiel, A.M., 1999. Building neural representations of habits. *Science* 286, 1745–1749.
- Johnson BA (2010): Medication treatment of different types of alcoholism. *Am J Psychiatry* 167:630–639.
- Jolkkonen, E., Pitkänen, A., 1998. Intrinsic connections of the rat amygdaloid complex: projections originating in the central nucleus. *J. Comp. Neurol.* 395, 53–72.
- Jonckers, E., Delgado y Palacios, R., Shah, D., Guglielmetti, C., Verhoye, M., Van der Linden, A., 2014. Different anesthesia regimes modulate the functional connectivity outcome in mice. *Magn. Reson. Med.* 72, 1103–1112. doi:10.1002/mrm.24990
- Jonckers, E., Van Audekerke, J., De Visscher, G., Van der Linden, A., Verhoye, M., 2011. Functional connectivity fMRI of the rodent brain: comparison of functional connectivity networks in rat and mouse. *PloS One* 6, e18876. doi:10.1371/journal.pone.0018876
- Joshi, P.R., Wu, N.-P., André, V.M., Cummings, D.M., Cepeda, C., et al., 2009. Age-Dependent Alterations of Corticostriatal Activity in the YAC128 Mouse Model of Huntington Disease. *J. Neurosci.* 29, 2414–2427. doi:10.1523/JNEUROSCI.5687-08.2009
- Kalivas, P.W., Volkow, N.D., 2005. The neural basis of addiction: a pathology of motivation and choice. *Am. J. Psychiatry* 162, 1403–1413. doi:10.1176/appi.ajp.162.8.1403
- Karl, T., Arnold, J.C., 2014. Schizophrenia: a consequence of gene-environment interactions? *Front. Behav. Neurosci.* 8. doi:10.3389/fnbeh.2014.00435
- Kaufmann, T., Skåtun, K.C., Alnæs, D., Doan, N.T., Duff, E.P., et al., 2015. Disintegration of Sensorimotor Brain Networks in Schizophrenia. *Schizophr. Bull.* 41, 1326–1335. doi:10.1093/schbul/sbv060
- Kawagoe, R., Takikawa, Y., Hikosaka, O., 1998. Expectation of reward modulates cognitive signals in the basal ganglia. *Nat. Neurosci.* 1, 411–416. doi:10.1038/1625
- Khalili-Mahani, N., Zoethout, R.M.W., Beckmann, C.F., Baerends, E., de Kam, et al., 2012. Effects of morphine and alcohol on functional brain connectivity during “resting state”: a

- placebo-controlled crossover study in healthy young men. *Hum. Brain Mapp.* 33, 1003–1018. doi:10.1002/hbm.21265
- Killcross, S., Coutureau, E., 2003. Coordination of actions and habits in the medial prefrontal cortex of rats. *Cereb. Cortex N. Y. N* 13, 400–408.
- Kim, S.-G., Ogawa, S., 2012. Biophysical and physiological origins of blood oxygenation level-dependent fMRI signals. *J. Cereb. Blood Flow Metab. Off. J. Int. Soc. Cereb. Blood Flow Metab.* 32, 1188–1206. doi:10.1038/jcbfm.2012.23
- Kim, Y.S., Leventhal, B.L., 2015. Genetic Epidemiology and Insights into Interactive Genetic and Environmental Effects in Autism Spectrum Disorders. *Biol. Psychiatry* 77, 66–74. doi:10.1016/j.biopsych.2014.11.001
- Kimmel, H.L., O'Connor, J.A., Carroll, F.I., Howell, L.L., 2007. Faster onset and dopamine transporter selectivity predict stimulant and reinforcing effects of cocaine analogs in squirrel monkeys. *Pharmacol. Biochem. Behav.* 86, 45–54. doi:10.1016/j.pbb.2006.12.006
- Kiviniemi, V., Jauhiainen, J., Tervonen, O., Pääkkö, E., Oikarinen, J., Vainionpää, V., Rantala, H., Biswal, B., 2000. Slow vasomotor fluctuation in fMRI of anesthetized child brain. *Magn. Reson. Med.* 44, 373–378.
- Kobayashi, Y., Sano, Y., Vannoni, E., Goto, H., Suzuki, H., Oba, A., Kawasaki, H., Kanba, S., Lipp, H.-P., Murphy, N.P., Wolfer, D.P., Itohara, S., 2013. Genetic dissection of medial habenula-interpeduncular nucleus pathway function in mice. *Front. Behav. Neurosci.* 7, 17. doi:10.3389/fnbeh.2013.00017
- Koechlin, E., Summerfield, C., 2007. An information theoretical approach to prefrontal executive function. *Trends Cogn. Sci.* 11, 229–235. doi:10.1016/j.tics.2007.04.005
- Kolb, B., Forgie, M., Gibb, R., Gorny, G., Rowntree, S., 1998. Age, Experience and the Changing Brain. *Neurosci. Biobehav. Rev.* 22, 143–159. doi:10.1016/S0149-7634(97)00008-0
- Konrad, K., Eickhoff, S.B., 2010. Is the ADHD brain wired differently? A review on structural and functional connectivity in attention deficit hyperactivity disorder. *Hum. Brain Mapp.* 31, 904–916. doi:10.1002/hbm.21058
- Koob, G.F., 2008. A role for brain stress systems in addiction. *Neuron* 59, 11–34. doi:10.1016/j.neuron.2008.06.012
- Koob, G.F., Le Moal, M., 2001. Drug addiction, dysregulation of reward, and allostasis. *Neuropsychopharmacol. Off. Publ. Am. Coll. Neuropsychopharmacol.* 24, 97–129. doi:10.1016/S0893-133X(00)00195-0
- Koob, G.F., Volkow, N.D., 2016. Neurobiology of addiction: A neuro-circuitry analysis. *Lancet Psychiatry* 3: 760–773
- Koyama, M.S., Martino, A.D., Zuo, X.-N., Kelly, C., Mennes, M., Jutagir, D.R., Castellanos, F.X., Milham, M.P., 2011. Resting-State Functional Connectivity Indexes Reading Competence in Children and Adults. *J. Neurosci.* 31, 8617–8624. doi:10.1523/JNEUROSCI.4865-10.2011
- Krackow, S., Vannoni, E., Codita, A., Mohammed, A.H., Cirulli, F., et al., 2010. Consistent behavioral phenotype differences between inbred mouse strains in the IntelliCage. *Genes Brain Behav.* 9, 722–731. doi:10.1111/j.1601-183X.2010.00606.x
- Kühn, S., Gallinat, J., 2012. The neural correlates of subjective pleasantness. *NeuroImage* 61, 289–294. doi:10.1016/j.neuroimage.2012.02.065

- Kumar, S., Hultman, R., Hughes, D., Michel, N., Katz, B.M., Dzirasa, K., 2014. Prefrontal cortex reactivity underlies trait vulnerability to chronic social defeat stress. *Nat. Commun.* 5, 4537. doi:10.1038/ncomms5537
- Kwong, K.K., Belliveau, J.W., Chesler, D.A., Goldberg, I.E., Weisskoff, R.M., Poncelet, B.P., Kennedy, D.N., Hoppel, B.E., Cohen, M.S., Turner, R., 1992. Dynamic magnetic resonance imaging of human brain activity during primary sensory stimulation. *Proc. Natl. Acad. Sci. U. S. A.* 89, 5675–5679.
- Lack, C.M., Jones, S.R., Roberts, D.C.S., 2008. Increased breakpoints on a progressive ratio schedule reinforced by IV cocaine are associated with reduced locomotor activation and reduced dopamine efflux in nucleus accumbens shell in rats. *Psychopharmacology (Berl.)* 195, 517–525. doi:10.1007/s00213-007-0919-4
- Lammel, S., Lim, B.K., Ran, C., Huang, K.W., Betley, M.J., Tye, K.M., Deisseroth, K., Malenka, R.C., 2012a. Input-specific control of reward and aversion in the ventral tegmental area. *Nature* 491, 212–217. doi:10.1038/nature11527
- Lammel, S., Lim, B.K., Ran, C., Huang, K.W., Betley, M.J., Tye, K.M., Deisseroth, K., Malenka, R.C., 2012b. Input-specific control of reward and aversion in the ventral tegmental area. *Nature* 491, 212–217. doi:10.1038/nature11527
- Lauterbur, P.C., 1989. Image formation by induced local interactions. Examples employing nuclear magnetic resonance. 1973. *Clin. Orthop.* 3–6.
- Le Bihan, D., Breton, E., Lallemand, D., Grenier, P., Cabanis, E., Laval-Jeantet, M., 1986. MR imaging of intravoxel incoherent motions: application to diffusion and perfusion in neurologic disorders. *Radiology* 161, 401–407. doi:10.1148/radiology.161.2.3763909
- LeDoux, J.E., Cicchetti, P., Xagoraris, A., Romanski, L.M., 1990. The lateral amygdaloid nucleus: sensory interface of the amygdala in fear conditioning. *J. Neurosci. Off. J. Soc. Neurosci.* 10, 1062–1069.
- Legrand, R., Lucas, N., Breton, J., Déchelotte, P., Fetissov, S.O., 2015. Dopamine release in the lateral hypothalamus is stimulated by α -MSH in both the anticipatory and consummatory phases of feeding. *Psychoneuroendocrinology* 56, 79–87. doi:10.1016/j.psyneuen.2015.02.020
- Lein, E.S., Hawrylycz, M.J., Ao, N., Ayres, M., Bensinger, A., et al., 2007. Genome-wide atlas of gene expression in the adult mouse brain. *Nature* 445, 168–176. doi:10.1038/nature05453
- Le Merrer J, Befort K, Gardon O, Filliol D, Darcq E, Dembele D, et al. (2012): Protracted abstinence from distinct drugs of abuse shows regulation of a common gene network. *Addict Biol* 17:1–12.
- Li, Y.-O., Adali, T., Calhoun, V.D., 2007. Estimating the number of independent components for functional magnetic resonance imaging data. *Hum. Brain Mapp.* 28, 1251–1266. doi:10.1002/hbm.20359
- Liang, M., Zhou, Y., Jiang, T., Liu, Z., Tian, L., Liu, H., Hao, Y., 2006. Widespread functional disconnectivity in schizophrenia with resting-state functional magnetic resonance imaging. *Neuroreport* 17, 209–213.
- Liljeholm, M., Tricomi, E., O'Doherty, J.P., Balleine, B.W., 2011. Neural correlates of instrumental contingency learning: differential effects of action-reward conjunction and disjunction. *J. Neurosci. Off. J. Soc. Neurosci.* 31, 2474–2480. doi:10.1523/JNEUROSCI.3354-10.2011
- Liska, A., Galbusera, A., Schwarz, A.J., Gozzi, A., 2015. Functional connectivity hubs of the mouse brain. *NeuroImage* 115, 281–291. doi:10.1016/j.neuroimage.2015.04.033

- Liu, Y., Yu, C., Liang, M., Li, J., Tian, L., Zhou, Y., Qin, W., Li, K., Jiang, T., 2007. Whole brain functional connectivity in the early blind. *Brain J. Neurol.* 130, 2085–2096. doi:10.1093/brain/awm121
- Logothetis, N.K., Pauls, J., Augath, M., Trinath, T., Oeltermann, A., 2001. Neurophysiological investigation of the basis of the fMRI signal. *Nature* 412, 150–157. doi:10.1038/35084005
- Logothetis, N.K., Wandell, B.A., 2004. Interpreting the BOLD signal. *Annu. Rev. Physiol.* 66, 735–769. doi:10.1146/annurev.physiol.66.082602.092845
- Logue, S.F., Grauer, S.M., Paulsen, J., Graf, R., Taylor, N., et al., 2009. The orphan GPCR, GPR88, modulates function of the striatal dopamine system: a possible therapeutic target for psychiatric disorders? *Mol. Cell. Neurosci.* 42, 438–447. doi:10.1016/j.mcn.2009.09.007
- Lowe, M.J., Dzemidzic, M., Lurito, J.T., Mathews, V.P., Phillips, M.D., 2000. Correlations in low-frequency BOLD fluctuations reflect cortico-cortical connections. *NeuroImage* 12, 582–587. doi:10.1006/nimg.2000.0654
- Lowe, M.J., Phillips, M.D., Lurito, J.T., Mattson, D., Dzemidzic, M., Mathews, V.P., 2002. Multiple sclerosis: low-frequency temporal blood oxygen level-dependent fluctuations indicate reduced functional connectivity initial results. *Radiology* 224, 184–192. doi:10.1148/radiol.2241011005
- Lu, H., Zou, Q., Gu, H., Raichle, M.E., Stein, E.A., Yang, Y., 2012. Rat brains also have a default mode network. *Proc. Natl. Acad. Sci. U. S. A.* 109, 3979–3984. doi:10.1073/pnas.1200506109
- Lui, S., Wu, Q., Qiu, L., Yang, X., Kuang, W., Chan, R.C.K., Huang, X., Kemp, G.J., Mechelli, A., Gong, Q., 2011. Resting-state functional connectivity in treatment-resistant depression. *Am. J. Psychiatry* 168, 642–648. doi:10.1176/appi.ajp.2010.10101419
- Luskin, M.B., Price, J.L., 1983. The topographic organization of associational fibers of the olfactory system in the rat, including centrifugal fibers to the olfactory bulb. *J. Comp. Neurol.* 216, 264–291. doi:10.1002/cne.902160305
- Lutz, P.-E., Kieffer, B.L., 2013. The multiple facets of opioid receptor function: implications for addiction. *Curr. Opin. Neurobiol.* 23, 473–479. doi:10.1016/j.conb.2013.02.005
- Ma, Y., Hamilton, C., Zhang, N., 2017. Dynamic Connectivity Patterns in Conscious and Unconscious Brain. *Brain Connect.* 7, 1–12. doi:10.1089/brain.2016.0464
- Maguire, E.A., 2001. The retrosplenial contribution to human navigation: a review of lesion and neuroimaging findings. *Scand. J. Psychol.* 42, 225–238.
- Mailliard, W.S., Diamond, I., 2004. Recent advances in the neurobiology of alcoholism: the role of adenosine. *Pharmacol. Ther.* 101, 39–46.
- Maisel NC, Blodgett JC, Wilbourne PL, Humphreys K, Finney JW (2013): Meta-analysis of naltrexone and acamprosate for treating alcohol use disorders: When are these medications most helpful? *Addiction* 108:275–293.
- Manoliu, A., Riedl, V., Zherdin, A., Mühlau, M., Schwerthöffer, D., Scherr, M., Peters, H., Zimmer, C., Förstl, H., Bäuml, J., Wohlschläger, A.M., Sorg, C., 2014. Aberrant dependence of default mode/central executive network interactions on anterior insular salience network activity in schizophrenia. *Schizophr. Bull.* 40, 428–437. doi:10.1093/schbul/sbt037
- Mantini, D., Gerits, A., Nelissen, K., Durand, J.-B., Joly, O., Simone, L., Sawamura, H., Wardak, C., Orban, G.A., Buckner, R.L., Vanduffel, W., 2011. Default Mode of Brain Function in Monkeys. *J. Neurosci.* 31, 12954–12962. doi:10.1523/JNEUROSCI.2318-11.2011

- Margulies, D.S., Böttger, J., Long, X., Lv, Y., Kelly, C., Schäfer, A., Goldhahn, D., Abbushi, A., Milham, M.P., Lohmann, G., Villringer, A., 2010. Resting developments: a review of fMRI post-processing methodologies for spontaneous brain activity. *Magma N. Y. N* 23, 289–307. doi:10.1007/s10334-010-0228-5
- Maroteaux, G., Loos, M., van der Sluis, S., Koopmans, B., Aarts, E., van Gassen, K., Geurts, A., Largaespada, D.A., Spruijt, B.M., Stiedl, O., Smit, A.B., Verhage, M., 2012. High throughput phenotyping of avoidance learning in mice discriminates different genotypes and identifies a novel gene. *Genes Brain Behav.* doi:10.1111/j.1601-183X.2012.00820.x
- Maroteaux, G., Arefin TM., Harsan, L.-A., Emmanuel D., Ben Hamida, S., Kieffer, B., 2018. Lack of anticipatory behavior in Gpr88 knockout mice revealed by automated home cage phenotyping. *Genes Brain Behav.* <https://doi.org/10.1111/gbb.12473>
- Marrelec, G., Horwitz, B., Kim, J., Pélégrini-Issac, M., Benali, H., Doyon, J., 2007. Using partial correlation to enhance structural equation modeling of functional MRI data. *Magn. Reson. Imaging* 25, 1181–1189. doi:10.1016/j.mri.2007.02.012
- Marrelec, G., Krainik, A., Duffau, H., Pélégrini-Issac, M., Lehericy, S., Doyon, J., Benali, H., 2006. Partial correlation for functional brain interactivity investigation in functional MRI. *NeuroImage* 32, 228–237. doi:10.1016/j.neuroimage.2005.12.057
- Massart, R., Guilloux, J.-P., Mignon, V., Sokoloff, P., Diaz, J., 2009. Striatal GPR88 expression is confined to the whole projection neuron population and is regulated by dopaminergic and glutamatergic afferents. *Eur. J. Neurosci.* 30, 397–414. doi:10.1111/j.1460-9568.2009.06842.x
- Massart, R., Mignon, V., Stanic, J., Munoz-Tello, P., Becker, J.A.J., Kieffer, B.L., Darmon, M., Sokoloff, P., Diaz, J., 2016. Developmental and adult expression patterns of the G-protein-coupled receptor GPR88 in the rat: Establishment of a dual nuclear-cytoplasmic localization. *J. Comp. Neurol.* 524, 2776–2802. doi:10.1002/cne.23991
- Mayfield J, Arends MA, Harris RA, Blednov YA (2016): Genes and alcohol consumption: Studies with mutant mice. *Int Rev Neurobiol* 126:293–355.
- McKeown, M.J., Makeig, S., Brown, G.G., Jung, T.P., Kindermann, S.S., Bell, A.J., Sejnowski, T.J., 1998. Analysis of fMRI data by blind separation into independent spatial components. *Hum. Brain Mapp.* 6, 160–188.
- McLeod, K.R., Langevin, L.M., Goodyear, B.G., Dewey, D., 2014. Functional connectivity of neural motor networks is disrupted in children with developmental coordination disorder and attention-deficit/hyperactivity disorder. *NeuroImage Clin.* 4, 566–575. doi:10.1016/j.nicl.2014.03.010
- Mechan, A.O., Wyss, A., Rieger, H., Mohajeri, M.H., 2009. A comparison of learning and memory characteristics of young and middle-aged wild-type mice in the IntelliCage. *J. Neurosci. Methods* 180, 43–51. doi:10.1016/j.jneumeth.2009.02.018
- Mechling, A.E., Arefin, T., Lee, H.-L., Bienert, T., Reisert, M., Ben Hamida, S., Darcq, E., Ehrlich, A., Gaveriaux-Ruff, C., Parent, M.J., Rosa-Neto, P., Hennig, J., von Elverfeldt, D., Kieffer, B.L., Harsan, L.-A., 2016. Deletion of the mu opioid receptor gene in mice reshapes the reward-aversion connectome. *Proc. Natl. Acad. Sci. U. S. A.* 113, 11603–11608. doi:10.1073/pnas.1601640113
- Mechling, A.E., Hübner, N.S., Lee, H.-L., Hennig, J., von Elverfeldt, D., Harsan, L.-A., 2014. Fine-grained mapping of mouse brain functional connectivity with resting-state fMRI. *NeuroImage* 96, 203–215. doi:10.1016/j.neuroimage.2014.03.078
- Meersman, A.C., Le Merrer, J., Pellissier, L.P., Diaz, J., Clesse, D., Kieffer, B.L., Becker, J.A.J., 2016. Mice Lacking GPR88 Show Motor Deficit, Improved Spatial Learning, and Low

- Anxiety Reversed by Delta Opioid Antagonist. *Biol. Psychiatry* 79, 917–927. doi:10.1016/j.biopsych.2015.05.020
- Meirsman, A.C., Robé, A., de Kerchove d’Exaerde, A., Kieffer, B.L., 2016. GPR88 in A2AR Neurons Enhances Anxiety-Like Behaviors. *eNeuro* 3. doi:10.1523/ENEURO.0202-16.2016
- Menon, V., Uddin, L.Q., 2010. Saliency, switching, attention and control: a network model of insula function. *Brain Struct. Funct.* 214, 655–667. doi:10.1007/s00429-010-0262-0
- Mestres-Missé, A., Turner, R., Friederici, A.D., 2012. An anterior-posterior gradient of cognitive control within the dorsomedial striatum. *NeuroImage* 62, 41–47. doi:10.1016/j.neuroimage.2012.05.021
- Metzger, D., Chambon, P., 2001. Site- and time-specific gene targeting in the mouse. *Methods San Diego Calif* 24, 71–80. doi:10.1006/meth.2001.1159
- Miller, E.K., Cohen, J.D., 2001. An integrative theory of prefrontal cortex function. *Annu. Rev. Neurosci.* 24, 167–202. doi:10.1146/annurev.neuro.24.1.167
- Miyachi, S., Hikosaka, O., Lu, X., 2002. Differential activation of monkey striatal neurons in the early and late stages of procedural learning. *Exp. Brain Res.* 146, 122–126. doi:10.1007/s00221-002-1213-7
- Miyazaki, M., Fujii, E., Saijo, T., Mori, K., Hashimoto, T., Kagami, S., Kuroda, Y., 2007. Short-latency somatosensory evoked potentials in infantile autism: evidence of hyperactivity in the right primary somatosensory area. *Dev. Med. Child Neurol.* 49, 13–17. doi:10.1111/j.1469-8749.2007.0059a.x
- Mizushima, K., Miyamoto, Y., Tsukahara, F., Hirai, M., Sakaki, Y., Ito, T., 2000. A novel G-protein-coupled receptor gene expressed in striatum. *Genomics* 69, 314–321. doi:10.1006/geno.2000.6340
- Mogenson, G.J., Jones, D.L., Yim, C.Y., 1980. From motivation to action: functional interface between the limbic system and the motor system. *Prog. Neurobiol.* 14, 69–97.
- Mohammadi, B., Kollwe, K., Samii, A., Krampfl, K., Dengler, R., Münte, T.F., 2009. Changes of resting state brain networks in amyotrophic lateral sclerosis. *Exp. Neurol.* 217, 147–153. doi:10.1016/j.expneurol.2009.01.025
- Mongrain, S., Standing, L., 1989. Impairment of cognition, risk-taking, and self-perception by alcohol. *Percept. Mot. Skills* 69, 199–210. doi:10.2466/pms.1989.69.1.199
- Moonat, S., Starkman, B.G., Sakharkar, A., Pandey, S.C., 2010. Neuroscience of alcoholism: molecular and cellular mechanisms. *Cell. Mol. Life Sci. CMLS* 67, 73–88. doi:10.1007/s00018-009-0135-y
- Mori, S., Itoh, R., Zhang, J., Kaufmann, W.E., van Zijl, P.C., Solaiyappan, M., Yarowsky, P., 2001. Diffusion tensor imaging of the developing mouse brain. *Magn. Reson. Med.* 46, 18–23.
- Moritz, C.H., Carew, J.D., McMillan, A.B., Meyerand, M.E., 2005. Independent component analysis applied to self-paced functional MR imaging paradigms. *NeuroImage* 25, 181–192. doi:10.1016/j.neuroimage.2004.11.009
- Mostofsky, S.H., Dubey, P., Jerath, V.K., Jansiewicz, E.M., Goldberg, M.C., Denckla, M.B., 2006. Developmental dyspraxia is not limited to imitation in children with autism spectrum disorders. *J. Int. Neuropsychol. Soc. JINS* 12, 314–326.
- Mukherjee, P., McKinstry, R.C., 2006. Diffusion tensor imaging and tractography of human brain development. *Neuroimaging Clin. N. Am.* 16, 19–43, vii. doi:10.1016/j.nic.2005.11.004

- Müller, N.G., Knight, R.T., 2006. The functional neuroanatomy of working memory: contributions of human brain lesion studies. *Neuroscience* 139, 51–58. doi:10.1016/j.neuroscience.2005.09.018
- Müller-Oehring, E.M., Jung, Y.-C., Pfefferbaum, A., Sullivan, E.V., Schulte, T., 2014. The Resting Brain of Alcoholics. *Cereb. Cortex* bhu134. doi:10.1093/cercor/bhu134
- Murdaugh, D.L., Shinkareva, S.V., Deshpande, H.R., Wang, J., Pennick, M.R., Kana, R.K., 2012. Differential deactivation during mentalizing and classification of autism based on default mode network connectivity. *PloS One* 7, e50064. doi:10.1371/journal.pone.0050064
- Nagel, B.J., Bathula, D., Herting, M., Schmitt, C., Kroenke, C.D., Fair, D., Nigg, J.T., 2011. Altered white matter microstructure in children with attention-deficit/hyperactivity disorder. *J. Am. Acad. Child Adolesc. Psychiatry* 50, 283–292. doi:10.1016/j.jaac.2010.12.003
- Nair, G., Tanahashi, Y., Low, H.P., Billings-Gagliardi, S., Schwartz, W.J., Duong, T.Q., 2005. Myelination and long diffusion times alter diffusion-tensor-imaging contrast in myelin-deficient shiverer mice. *NeuroImage* 28, 165–174. doi:10.1016/j.neuroimage.2005.05.049
- Nasrallah, F.A., Tan, J., Chuang, K.-H., 2012. Pharmacological modulation of functional connectivity: α 2-adrenergic receptor agonist alters synchrony but not neural activation. *NeuroImage* 60, 436–446. doi:10.1016/j.neuroimage.2011.12.026
- Nasrallah, F.A., Tay, H.-C., Chuang, K.-H., 2014. Detection of functional connectivity in the resting mouse brain. *NeuroImage* 86, 417–424. doi:10.1016/j.neuroimage.2013.10.025
- Navratilova, E., Porreca, F., 2014. Reward and motivation in pain and pain relief. *Nat. Neurosci.* 17, 1304–1312. doi:10.1038/nn.3811
- Navratilova, E., Xie, J.Y., Meske, D., Qu, C., Morimura, K., Okun, A., Arakawa, N., Ossipov, M., Fields, H.L., Porreca, F., 2015. Endogenous opioid activity in the anterior cingulate cortex is required for relief of pain. *J. Neurosci. Off. J. Soc. Neurosci.* 35, 7264–7271. doi:10.1523/JNEUROSCI.3862-14.2015
- Nelson, A.J.D., Hindley, E.L., Haddon, J.E., Vann, S.D., Aggleton, J.P., 2014. A novel role for the rat retrosplenial cortex in cognitive control. *Learn. Mem.* 21, 90–97. doi:10.1101/lm.032136.113
- Nelson, A.J.D., Hindley, E.L., Pearce, J.M., Vann, S.D., Aggleton, J.P., 2015. The effect of retrosplenial cortex lesions in rats on incidental and active spatial learning. *Front. Behav. Neurosci.* 9. doi:10.3389/fnbeh.2015.00011
- Newman, M.E.J., 2006. Modularity and community structure in networks. *Proc. Natl. Acad. Sci. U. S. A.* 103, 8577–8582. doi:10.1073/pnas.0601602103
- Nicola, S.M., Surmeier, J., Malenka, R.C., 2000. Dopaminergic modulation of neuronal excitability in the striatum and nucleus accumbens. *Annu. Rev. Neurosci.* 23, 185–215. doi:10.1146/annurev.neuro.23.1.185
- Norton, L., Hutchison, R.M., Young, G.B., Lee, D.H., Sharpe, M.D., Mirsattari, S.M., 2012. Disruptions of functional connectivity in the default mode network of comatose patients. *Neurology* 78, 175–181. doi:10.1212/WNL.0b013e31823fcd61
- Novak, J., Bailoo, J.D., Melotti, L., Rommen, J., Würbel, H., 2015. An Exploration Based Cognitive Bias Test for Mice: Effects of Handling Method and Stereotypic Behaviour. *PloS One* 10, e0130718. doi:10.1371/journal.pone.0130718
- Ogawa, S., Lee, T.M., Kay, A.R., Tank, D.W., 1990. Brain magnetic resonance imaging with contrast dependent on blood oxygenation. *Proc. Natl. Acad. Sci. U. S. A.* 87, 9868–9872.

- Ogawa, S., Tank, D.W., Menon, R., Ellermann, J.M., Kim, S.G., Merkle, H., Ugurbil, K., 1992. Intrinsic signal changes accompanying sensory stimulation: functional brain mapping with magnetic resonance imaging. *Proc. Natl. Acad. Sci. U. S. A.* 89, 5951–5955.
- Ogden CA, Rich ME, Schork NJ, Paulus MP, Geyer MA, Lohr JB, et al. (2004): Candidate genes, pathways and mechanisms for bipolar (manic-depressive) and related disorders: An expanded convergent functional genomics approach. *Mol Psychiatry* 9:1007–1029.
- Oldehinkel, M., Beckmann, C.F., Pruim, R.H.R., Oort, E.S.B. van, Franke, B., Hartman, C.A., Hoekstra, P.J., Oosterlaan, J., Heslenfeld, D., Buitelaar, J.K., Mennes, M., 2016. Attention-Deficit/Hyperactivity Disorder Symptoms Coincide With Altered Striatal Connectivity. *Biol. Psychiatry Cogn. Neurosci. Neuroimaging* 1, 353–363. doi:10.1016/j.bpsc.2016.03.008
- Oldehinkel, M., Franx, W., Beckmann, C.F., Buitelaar, J.K., Mennes, M., 2013. Resting state fMRI research in child psychiatric disorders. *Eur. Child Adolesc. Psychiatry* 22, 757–770. doi:10.1007/s00787-013-0480-0
- Ongür, D., Price, J.L., 2000. The organization of networks within the orbital and medial prefrontal cortex of rats, monkeys and humans. *Cereb. Cortex N. Y. N* 10, 206–219.
- Otti, A., Guendel, H., Wohlschläger, A., Zimmer, C., Noll-Hussong, M., 2013. Frequency shifts in the anterior default mode network and the salience network in chronic pain disorder. *BMC Psychiatry* 13, 84. doi:10.1186/1471-244X-13-84
- Pan, W.-J., Billings, J.C.W., Grooms, J.K., Shakil, S., Keilholz, S.D., 2015. Considerations for resting state functional MRI and functional connectivity studies in rodents. *Front. Neurosci.* 9. doi:10.3389/fnins.2015.00269
- Pape, H.-C., Pare, D., 2010. Plastic synaptic networks of the amygdala for the acquisition, expression, and extinction of conditioned fear. *Physiol. Rev.* 90, 419–463. doi:10.1152/physrev.00037.2009
- Parush, S., Sohmer, H., Steinberg, A., Kaitz, M., 2007. Somatosensory function in boys with ADHD and tactile defensiveness. *Physiol. Behav.* 90, 553–558. doi:10.1016/j.physbeh.2006.11.004
- Parush, S., Sohmer, H., Steinberg, A., Kaitz, M., 1997. Somatosensory functioning in children with attention deficit hyperactivity disorder. *Dev. Med. Child Neurol.* 39, 464–468.
- Pauling, L., Coryell, C.D., 1936. The Magnetic Properties and Structure of Hemoglobin, Oxyhemoglobin and Carbonmonoxyhemoglobin. *Proc. Natl. Acad. Sci. U. S. A.* 22, 210–216.
- Paulus, M.P., Stein, M.B., 2006. An insular view of anxiety. *Biol. Psychiatry* 60, 383–387. doi:10.1016/j.biopsycho.2006.03.042
- Pellow, S., Chopin, P., File, S.E., Briley, M., 1985. Validation of open:closed arm entries in an elevated plus-maze as a measure of anxiety in the rat. *J. Neurosci. Methods* 14, 149–167.
- Peng, J., Wang, P., Zhou, N., Zhu, J., 2009. Partial Correlation Estimation by Joint Sparse Regression Models. *J. Am. Stat. Assoc.* 104, 735–746. doi:10.1198/jasa.2009.0126
- Penzo, M.A., Robert, V., Li, B., 2014. Fear conditioning potentiates synaptic transmission onto long-range projection neurons in the lateral subdivision of central amygdala. *J. Neurosci. Off. J. Soc. Neurosci.* 34, 2432–2437. doi:10.1523/JNEUROSCI.4166-13.2014
- Perry, W., Braff, D.L., 1994. Information-processing deficits and thought disorder in schizophrenia. *Am. J. Psychiatry* 151, 363–367. doi:10.1176/ajp.151.3.363
- Peterson, A., Thome, J., Frewen, P., Lanius, R.A., 2014. Resting-state neuroimaging studies: a new way of identifying differences and similarities among the anxiety disorders? *Can. J. Psychiatry Rev. Can. Psychiatr.* 59, 294–300.

- Petrides, M., 2005. Lateral prefrontal cortex: architectonic and functional organization. *Philos. Trans. R. Soc. Lond. B. Biol. Sci.* 360, 781–795. doi:10.1098/rstb.2005.1631
- Picciotto, M.R., Wickman, K., 1998. Using knockout and transgenic mice to study neurophysiology and behavior. *Physiol. Rev.* 78, 1131–1163.
- Pierpaoli, C., Jezzard, P., Basser, P.J., Barnett, A., Di Chiro, G., 1996. Diffusion tensor MR imaging of the human brain. *Radiology* 201, 637–648. doi:10.1148/radiology.201.3.8939209
- Pitchers, K.K., Balfour, M.E., Lehman, M.N., Richtand, N.M., Yu, L., Coolen, L.M., 2010. Neuroplasticity in the mesolimbic system induced by natural reward and subsequent reward abstinence. *Biol. Psychiatry* 67, 872–879. doi:10.1016/j.biopsych.2009.09.036
- Polanczyk, G., de Lima, M.S., Horta, B.L., Biederman, J., Rohde, L.A., 2007. The worldwide prevalence of ADHD: a systematic review and metaregression analysis. *Am. J. Psychiatry* 164, 942–948. doi:10.1176/ajp.2007.164.6.942
- Poldrack, R.A., Packard, M.G., 2003. Competition among multiple memory systems: converging evidence from animal and human brain studies. *Neuropsychologia* 41, 245–251.
- Popa, D., Popescu, A.T., Paré, D., 2009. Contrasting activity profile of two distributed cortical networks as a function of attentional demands. *J. Neurosci. Off. J. Soc. Neurosci.* 29, 1191–1201. doi:10.1523/JNEUROSCI.4867-08.2009
- Quintana, A., Sanz, E., Wang, W., Storey, G.P., Güler, A.D., Wanat, M.J., Roller, B.A., La Torre, A., Amieux, P.S., McKnight, G.S., Bamford, N.S., Palmiter, R.D., 2012. Lack of GPR88 enhances medium spiny neuron activity and alters motor- and cue-dependent behaviors. *Nat. Neurosci.* 15, 1547–1555. doi:10.1038/nn.3239
- Raichle, M.E., 2015. The brain's default mode network. *Annu. Rev. Neurosci.* 38, 433–447. doi:10.1146/annurev-neuro-071013-014030
- Raichle, M.E., MacLeod, A.M., Snyder, A.Z., Powers, W.J., Gusnard, D.A., Shulman, G.L., 2001. A default mode of brain function. *Proc. Natl. Acad. Sci. U. S. A.* 98, 676–682.
- Reep, R.L., Winans, S.S., 1982. Efferent connections of dorsal and ventral agranular insular cortex in the hamster, *Mesocricetus auratus*. *Neuroscience* 7, 2609–2635.
- Reisert, M., Mader, I., Anastasopoulos, C., Weigel, M., Schnell, S., Kiselev, V., 2011. Global fiber reconstruction becomes practical. *NeuroImage* 54, 955–962. doi:10.1016/j.neuroimage.2010.09.016
- Richardson, N.R., Roberts, D.C., 1996. Progressive ratio schedules in drug self-administration studies in rats: a method to evaluate reinforcing efficacy. *J. Neurosci. Methods* 66, 1–11.
- Richiardi, J., Altmann, A., Milazzo, A.-C., Chang, C., Chakravarty, M.M., et al., 2015. Correlated gene expression supports synchronous activity in brain networks. *Science* 348, 1241–1244. doi:10.1126/science.1255905
- Rogers, D.C., Jones, D.N., Nelson, P.R., Jones, C.M., Quilter, C.A., Robinson, T.L., Hagan, J.J., 1999. Use of SHIRPA and discriminant analysis to characterise marked differences in the behavioural phenotype of six inbred mouse strains. *Behav. Brain Res.* 105, 207–217.
- Ron, D., Barak, S., 2016. Molecular mechanisms underlying alcohol-drinking behaviours. *Nat Rev Neurosci* 17:576-591.
- Roy, M., Shohamy, D., Daw, N., Jepma, M., Wimmer, G.E., Wager, T.D., 2014. Representation of aversive prediction errors in the human periaqueductal gray. *Nat. Neurosci.* 17, 1607–1612. doi:10.1038/nn.3832
- Rubinov, M., Sporns, O., 2011. Weight-conserving characterization of complex functional brain networks. *NeuroImage* 56, 2068–2079. doi:10.1016/j.neuroimage.2011.03.069

- Rubinov, M., Sporns, O., 2010. Complex network measures of brain connectivity: uses and interpretations. *NeuroImage* 52, 1059–1069. doi:10.1016/j.neuroimage.2009.10.003
- Sagvolden, T., Russell, V.A., Aase, H., Johansen, E.B., Farshbaf, M., 2005. Rodent models of attention-deficit/hyperactivity disorder. *Biol. Psychiatry* 57, 1239–1247. doi:10.1016/j.biopsych.2005.02.002
- Salvador, R., Suckling, J., Coleman, M.R., Pickard, J.D., Menon, D., Bullmore, E., 2005. Neurophysiological architecture of functional magnetic resonance images of human brain. *Cereb. Cortex N. Y. N 1991* 15, 1332–1342. doi:10.1093/cercor/bhi016
- Santiago, A.C., Shammah-Lagnado, S.J., 2004. Efferent connections of the nucleus of the lateral olfactory tract in the rat. *J. Comp. Neurol.* 471, 314–332. doi:10.1002/cne.20028
- Sawiak, S.J., Wood, N.I., Williams, G.B., Morton, A.J., Carpenter, T.A., 2013. Voxel-based morphometry with templates and validation in a mouse model of Huntington’s disease. *Magn. Reson. Imaging* 31, 1522–1531. doi:10.1016/j.mri.2013.06.001
- Schilbach, L., Eickhoff, S.B., Rotarska-Jagiela, A., Fink, G.R., Voegeley, K., 2008. Minds at rest? Social cognition as the default mode of cognizing and its putative relationship to the “default system” of the brain. *Conscious. Cogn.* 17, 457–467. doi:10.1016/j.concog.2008.03.013
- Schuckit, M.A., 1994. Low level of response to alcohol as a predictor of future alcoholism. *Am J Psychiatry.* 151: 184–189.
- Scott, J.W., McBride, R.L., Schneider, S.P., 1980. The organization of projections from the olfactory bulb to the piriform cortex and olfactory tubercle in the rat. *J. Comp. Neurol.* 194, 519–534. doi:10.1002/cne.901940304
- Seeley, W.W., Menon, V., Schatzberg, A.F., Keller, J., Glover, G.H., Kenna, H., Reiss, A.L., Greicius, M.D., 2007. Dissociable intrinsic connectivity networks for salience processing and executive control. *J. Neurosci. Off. J. Soc. Neurosci.* 27, 2349–2356. doi:10.1523/JNEUROSCI.5587-06.2007
- Sforzini, F., Schwarz, A.J., Galbusera, A., Bifone, A., Gozzi, A., 2014. Distributed BOLD and CBV-weighted resting-state networks in the mouse brain. *NeuroImage* 87, 403–415. doi:10.1016/j.neuroimage.2013.09.050
- Shah, D., Blockx, I., Guns, P.-J., De Deyn, P.P., Van Dam, D., Jonckers, E., Delgado Y Palacios, R., Verhoye, M., Van der Linden, A., 2015. Acute modulation of the cholinergic system in the mouse brain detected by pharmacological resting-state functional MRI. *NeuroImage* 109, 151–159. doi:10.1016/j.neuroimage.2015.01.009
- Shannon, B.J., Dosenbach, R.A., Su, Y., Vlessenko, A.G., Larson-Prior, L.J., Nolan, T.S., Snyder, A.Z., Raichle, M.E., 2013. Morning-evening variation in human brain metabolism and memory circuits. *J. Neurophysiol.* 109, 1444–1456. doi:10.1152/jn.00651.2012
- Shi, Y., Short, S.J., Knickmeyer, R.C., Wang, J., Coe, C.L., Niethammer, M., Gilmore, J.H., Zhu, H., Styner, M.A., 2013. Diffusion tensor imaging-based characterization of brain neurodevelopment in primates. *Cereb. Cortex N. Y. N 1991* 23, 36–48. doi:10.1093/cercor/bhr372
- Shidara, M., Aigner, T.G., Richmond, B.J., 1998. Neuronal Signals in the Monkey Ventral Striatum Related to Progress through a Predictable Series of Trials. *J. Neurosci.* 18, 2613–2625.
- Shmuel, A., Leopold, D.A., 2008. Neuronal correlates of spontaneous fluctuations in fMRI signals in monkey visual cortex: Implications for functional connectivity at rest. *Hum. Brain Mapp.* 29, 751–761. doi:10.1002/hbm.20580

- Shmueli, K., van Gelderen, P., de Zwart, J.A., Horovitz, S.G., Fukunaga, M., Jansma, J.M., Duyn, J.H., 2007. Low-frequency fluctuations in the cardiac rate as a source of variance in the resting-state fMRI BOLD signal. *NeuroImage* 38, 306–320. doi:10.1016/j.neuroimage.2007.07.037
- Shulman, G.L., Fiez, J.A., Corbetta, M., Buckner, R.L., Miezin, F.M., Raichle, M.E., Petersen, S.E., 1997. Common Blood Flow Changes across Visual Tasks: II. Decreases in Cerebral Cortex. *J. Cogn. Neurosci.* 9, 648–663. doi:10.1162/jocn.1997.9.5.648
- Soares-Cunha, C., Coimbra, B., Sousa, N., Rodrigues, A.J., 2016. Reappraising striatal D1- and D2-neurons in reward and aversion. *Neurosci. Biobehav. Rev.* 68, 370–386. doi:10.1016/j.neubiorev.2016.05.021
- Soddu, A., Vanhaudenhuyse, A., Demertzi, A., Bruno, M.-A., Tshibanda, L., Di, H., Mélanie, B., Papa, M., Laureys, S., Noirhomme, Q., 2011. Resting state activity in patients with disorders of consciousness. *Funct. Neurol.* 26, 37–43.
- Sonuga-Barke, E.J.S., 2005. Causal Models of Attention-Deficit/Hyperactivity Disorder: From Common Simple Deficits to Multiple Developmental Pathways. *Biol. Psychiatry* 57, 1231–1238. doi:10.1016/j.biopsych.2004.09.008
- Sonuga-Barke, E.J.S., Castellanos, F.X., 2007. Spontaneous attentional fluctuations in impaired states and pathological conditions: a neurobiological hypothesis. *Neurosci. Biobehav. Rev.* 31, 977–986. doi:10.1016/j.neubiorev.2007.02.005
- Sorge, R.E., Martin, L.J., Isbester, K.A., Sotocinal, S.G., Rosen, S., Tuttle, A.H., Wieskopf, J.S., Acland, E.L., Dokova, A., Kadoura, B., Leger, P., Mapplebeck, J.C.S., McPhail, M., Delaney, A., Wigerblad, G., Schumann, A.P., Quinn, T., Frasnelli, J., Svensson, C.I., Sternberg, W.F., Mogil, J.S., 2014. Olfactory exposure to males, including men, causes stress and related analgesia in rodents. *Nat. Methods* 11, 629–632. doi:10.1038/nmeth.2935
- Spanagel R., 2009. Alcoholism: A systems approach from molecular physiology to addictive behavior. *Physiol Rev* 89:649-705
- SPM - Statistical Parametric Mapping [WWW Document], n.d. URL <http://www.fil.ion.ucl.ac.uk/spm/> (accessed 10.18.16).
- SPM Mouse [WWW Document], n.d. URL <http://www.spmouse.org/> (accessed 10.18.16).
- Sporns, O., 2013. Structure and function of complex brain networks. *Dialogues Clin. Neurosci.* 15, 247–262.
- Sporns, O., Tononi, G., Kötter, R., 2005. The human connectome: A structural description of the human brain. *PLoS Comput. Biol.* 1, e42. doi:10.1371/journal.pcbi.0010042
- Stam, C.J., 2014. Modern network science of neurological disorders. *Nat. Rev. Neurosci.* 15, 683–695. doi:10.1038/nrn3801
- Stein, M.B., Simmons, A.N., Feinstein, J.S., Paulus, M.P., 2007. Increased amygdala and insula activation during emotion processing in anxiety-prone subjects. *Am. J. Psychiatry* 164, 318–327. doi:10.1176/ajp.2007.164.2.318
- Stray, L.L., Kristensen, Ø., Lomeland, M., Skorstad, M., Stray, T., Tønnessen, F.E., 2013. Motor regulation problems and pain in adults diagnosed with ADHD. *Behav. Brain Funct.* 9, 18. doi:10.1186/1744-9081-9-18
- Stuber, G.D., Sparta, D.R., Stamatakis, A.M., van Leeuwen, W.A., Hardjoprajitno, J.E., Cho, S., Tye, K.M., Kempadoo, K.A., Zhang, F., Deisseroth, K., Bonci, A., 2011. Amygdala to nucleus accumbens excitatory transmission facilitates reward seeking. *Nature* 475, 377–380. doi:10.1038/nature10194

- Sui, J., Huster, R., Yu, Q., Segall, J.M., Calhoun, V.D., 2014. Function-structure associations of the brain: evidence from multimodal connectivity and covariance studies. *NeuroImage* 102 Pt 1, 11–23. doi:10.1016/j.neuroimage.2013.09.044
- Supekar, K., Menon, V., Rubin, D., Musen, M., Greicius, M.D., 2008. Network Analysis of Intrinsic Functional Brain Connectivity in Alzheimer’s Disease. *PLoS Comput. Biol.* 4. doi:10.1371/journal.pcbi.1000100
- Surmeier, D.J., Ding, J., Day, M., Wang, Z., Shen, W., 2007. D1 and D2 dopamine-receptor modulation of striatal glutamatergic signaling in striatal medium spiny neurons. *Trends Neurosci.* 30, 228–235. doi:10.1016/j.tins.2007.03.008
- Surmeier, D.J., Plotkin, J., Shen, W., 2009. Dopamine and synaptic plasticity in dorsal striatal circuits controlling action selection. *Curr. Opin. Neurobiol.* 19, 621–628. doi:10.1016/j.conb.2009.10.003
- Sutherland, M.T., McHugh, M., Pariyadath, V., Stein, E.A., 2012. Resting State Functional Connectivity in Addiction: Lessons Learned and a Road Ahead. *NeuroImage* 62, 2281–2295. doi:10.1016/j.neuroimage.2012.01.117
- Swanson, L.W., 2000. Cerebral hemisphere regulation of motivated behavior1. *Brain Res., Towards 2010, A brain Odyssey, The 3rd Brain Research Interactive* 886, 113–164. doi:10.1016/S0006-8993(00)02905-X
- Swerdlow, N.R., Koob, G.F., 1987. Lesions of the dorsomedial nucleus of the thalamus, medial prefrontal cortex and pedunculopontine nucleus: effects on locomotor activity mediated by nucleus accumbens-ventral pallidal circuitry. *Brain Res.* 412, 233–243.
- Takao, K., Yamasaki, N., Miyakawa, T., 2007. Impact of brain-behavior phenotyping of genetically-engineered mice on research of neuropsychiatric disorders. *Neurosci. Res.* 58, 124–132. doi:10.1016/j.neures.2007.02.009
- Tamm, L., Barnea-Goraly, N., Reiss, A.L., 2012. Diffusion tensor imaging reveals white matter abnormalities in Attention-Deficit/Hyperactivity Disorder. *Psychiatry Res.* 202, 150–154. doi:10.1016/j.psychres.2012.04.001
- Tanaka, S.C., Balleine, B.W., O’Doherty, J.P., 2008. Calculating consequences: Brain systems that encode the causal effects of actions. *J. Neurosci. Off. J. Soc. Neurosci.* 28, 6750–6755. doi:10.1523/JNEUROSCI.1808-08.2008
- Tang, X., Yoshida, S., Hsu, J., Huisman, T.A.G.M., Faria, A.V., Oishi, K., Kuttner, K., Poretti, A., Li, Y., Miller, M.I., Mori, S., 2014. Multi-contrast multi-atlas parcellation of diffusion tensor imaging of the human brain. *PloS One* 9, e96985. doi:10.1371/journal.pone.0096985
- Tang, Y., Wang, L., Cao, F., Tan, L., 2012. Identify schizophrenia using resting-state functional connectivity: an exploratory research and analysis. *Biomed. Eng. OnLine* 11, 50. doi:10.1186/1475-925X-11-50
- Thompson, P.M., Ge, T., Glahn, D.C., Jahanshad, N., Nichols, T.E., 2013. Genetics of the connectome. *NeuroImage* 80, 475–488. doi:10.1016/j.neuroimage.2013.05.013
- Tomasi, D., Volkow, N.D., 2012. Abnormal Functional Connectivity in Children with Attention-Deficit/Hyperactivity Disorder. *Biol. Psychiatry, Autism and Attention-Deficit/Hyperactivity Disorder: Mechanisms and Circuits* 71, 443–450. doi:10.1016/j.biopsych.2011.11.003
- Trezza, V., Damsteegt, R., Achterberg, E.J.M., Vanderschuren, L.J.M.J., 2011. Nucleus accumbens μ -opioid receptors mediate social reward. *J. Neurosci. Off. J. Soc. Neurosci.* 31, 6362–6370. doi:10.1523/JNEUROSCI.5492-10.2011

- Tricomi, E., Balleine, B.W., O'Doherty, J.P., 2009. A specific role for posterior dorsolateral striatum in human habit learning. *Eur. J. Neurosci.* 29, 2225–2232. doi:10.1111/j.1460-9568.2009.06796.x
- Tuch, D.S., Wedeen, V.J., Dale, A.M., George, J.S., Belliveau, J.W., 2001. Conductivity tensor mapping of the human brain using diffusion tensor MRI. *Proc. Natl. Acad. Sci. U. S. A.* 98, 11697–11701. doi:10.1073/pnas.171473898
- Turner, K.M., Burne, T.H.J., 2013. Interaction of genotype and environment: effect of strain and housing conditions on cognitive behavior in rodent models of schizophrenia. *Front. Behav. Neurosci.* 7, 97. doi:10.3389/fnbeh.2013.00097
- Tye, K.M., Prakash, R., Kim, S.-Y., Fenno, L.E., Grosenick, L., Zarabi, H., Thompson, K.R., Gradinaru, V., Ramakrishnan, C., Deisseroth, K., 2011. Amygdala circuitry mediating reversible and bidirectional control of anxiety. *Nature* 471, 358–362. doi:10.1038/nature09820
- Ubeda-Bañon, I., Novejarque, A., Mohedano-Moriano, A., Pro-Sistiaga, P., Insausti, R., Martinez-Garcia, F., Lanuza, E., Martinez-Marcos, A., 2008. Vomeronasal inputs to the rodent ventral striatum. *Brain Res. Bull.* 75, 467–473. doi:10.1016/j.brainresbull.2007.10.028
- van de Ven, V.G., Formisano, E., Prvulovic, D., Roeder, C.H., Linden, D.E.J., 2004. Functional connectivity as revealed by spatial independent component analysis of fMRI measurements during rest. *Hum. Brain Mapp.* 22, 165–178. doi:10.1002/hbm.20022
- van Ewijk, H., Heslenfeld, D.J., Zwiers, M.P., Buitelaar, J.K., Oosterlaan, J., 2012. Diffusion tensor imaging in attention deficit/hyperactivity disorder: a systematic review and meta-analysis. *Neurosci. Biobehav. Rev.* 36, 1093–1106. doi:10.1016/j.neubiorev.2012.01.003
- Vanhoutte, G., Verhoye, M., Van der Linden, A., 2006. Changing body temperature affects the T2* signal in the rat brain and reveals hypothalamic activity. *Magn. Reson. Med.* 55, 1006–1012. doi:10.1002/mrm.20861
- Vann, S.D., Aggleton, J.P., Maguire, E.A., 2009. What does the retrosplenial cortex do? *Nat. Rev. Neurosci.* 10, 792–802. doi:10.1038/nrn2733
- Venables, P.H., 1984. Cerebral mechanisms, autonomic responsiveness, and attention in schizophrenia. *Neb. Symp. Motiv.* 31, 47–91.
- Vincent, J.L., Snyder, A.Z., Fox, M.D., Shannon, B.J., Andrews, J.R., Raichle, M.E., Buckner, R.L., 2006. Coherent spontaneous activity identifies a hippocampal-parietal memory network. *J. Neurophysiol.* 96, 3517–3531. doi:10.1152/jn.00048.2006
- Visser, J., Geuze, R.H., 2000. Kinaesthetic acuity in adolescent boys: a longitudinal study. *Dev. Med. Child Neurol.* 42, 93–96.
- Vogt, B.A., Peters, A., 1981. Form and distribution of neurons in rat cingulate cortex: areas 32, 24, and 29. *J. Comp. Neurol.* 195, 603–625. doi:10.1002/cne.901950406
- Voikar, V., Colacicco, G., Gruber, O., Vannoni, E., Lipp, H.-P., Wolfer, D.P., 2010. Conditioned response suppression in the IntelliCage: assessment of mouse strain differences and effects of hippocampal and striatal lesions on acquisition and retention of memory. *Behav. Brain Res.* 213, 304–312. doi:10.1016/j.bbr.2010.05.019
- Volkow, N.D., Wang, G.-J., Begleiter, H., Porjesz, B., Fowler, J.S., Telang, F., Wong, C., Ma, Y., Logan, J., Goldstein, R., Alexoff, D., Thanos, P.K., 2006. High levels of dopamine D2 receptors in unaffected members of alcoholic families: possible protective factors. *Arch. Gen. Psychiatry* 63, 999–1008. doi:10.1001/archpsyc.63.9.999

- Volkow, N.D., Wang, G.J., Fowler, J.S., Logan, J., Hitzemann, R., Ding, Y.S., Pappas, N., Shea, C., Piscani, K., 1996. Decreases in dopamine receptors but not in dopamine transporters in alcoholics. *Alcohol. Clin. Exp. Res.* 20, 1594–1598.
- Wager, T.D., Scott, D.J., Zubieta, J.-K., 2007. Placebo effects on human mu-opioid activity during pain. *Proc. Natl. Acad. Sci. U. S. A.* 104, 11056–11061. doi:10.1073/pnas.0702413104
- Wahlsten, D., 2010. *Mouse Behavioral Testing: How to Use Mice in Behavioral Neuroscience.* Academic Press.
- Wahlsten, D., Rustay, N.R., Metten, P., Crabbe, J.C., 2003. In search of a better mouse test. *Trends Neurosci.* 26, 132–136. doi:10.1016/S0166-2236(03)00033-X
- Waites, A.B., Briellmann, R.S., Saling, M.M., Abbott, D.F., Jackson, G.D., 2006. Functional connectivity networks are disrupted in left temporal lobe epilepsy. *Ann. Neurol.* 59, 335–343. doi:10.1002/ana.20733
- Wang, Z., Chen, L.M., Négyessy, L., Friedman, R.M., Mishra, A., Gore, J.C., Roe, A.W., 2013. The relationship of anatomical and functional connectivity to resting-state connectivity in primate somatosensory cortex. *Neuron* 78, 1116–1126. doi:10.1016/j.neuron.2013.04.023
- Watase, K., Zoghbi, H.Y., 2003. Modelling brain diseases in mice: the challenges of design and analysis. *Nat. Rev. Genet.* 4, 296–307. doi:10.1038/nrg1045
- Watts, D.J., Strogatz, S.H., 1998. Collective dynamics of “small-world” networks. *Nature* 393, 440–442. doi:10.1038/30918
- Weber, A.M., Soreni, N., Noseworthy, M.D., 2014. A preliminary study on the effects of acute ethanol ingestion on default mode network and temporal fractal properties of the brain. *Magma N. Y.* N 27, 291–301. doi:10.1007/s10334-013-0420-5
- Welsh, R.C., Chen, A.C., Taylor, S.F., 2010. Low-frequency BOLD fluctuations demonstrate altered thalamocortical connectivity in schizophrenia. *Schizophr. Bull.* 36, 713–722. doi:10.1093/schbul/sbn145
- White, L.E., 1965. Olfactory bulb projections of the rat. *Anat. Rec.* 152, 465–479. doi:10.1002/ar.1091520406
- Whitfield-Gabrieli, S., Ford, J.M., 2012. Default mode network activity and connectivity in psychopathology. *Annu. Rev. Clin. Psychol.* 8, 49–76. doi:10.1146/annurev-clinpsy-032511-143049
- Willcutt, E.G., Doyle, A.E., Nigg, J.T., Faraone, S.V., Pennington, B.F., 2005. Validity of the Executive Function Theory of Attention-Deficit/Hyperactivity Disorder: A Meta-Analytic Review. *Biol. Psychiatry* 57, 1336–1346. doi:10.1016/j.biopsych.2005.02.006
- Williams, K.A., Magnuson, M., Majeed, W., LaConte, S.M., Peltier, S.J., Hu, X., Keilholz, S.D., 2010. Comparison of alpha-chloralose, medetomidine and isoflurane anesthesia for functional connectivity mapping in the rat. *Magn. Reson. Imaging* 28, 995–1003. doi:10.1016/j.mri.2010.03.007
- Wise, R.A., 2004a. Dopamine and food reward: back to the elements. *Am. J. Physiol. Regul. Integr. Comp. Physiol.* 286, R13. doi:10.1152/ajpregu.00590.2003
- Wise, R.A., 2004b. Dopamine, learning and motivation. *Nat. Rev. Neurosci.* 5, 483–494. doi:10.1038/nrn1406
- Wise, R.A., 1996. Neurobiology of addiction. *Curr. Opin. Neurobiol.* 6, 243–251.
- Wise, R.G., Ide, K., Poulin, M.J., Tracey, I., 2004. Resting fluctuations in arterial carbon dioxide induce significant low frequency variations in BOLD signal. *NeuroImage* 21, 1652–1664. doi:10.1016/j.neuroimage.2003.11.025

- Wolf, M.E., Sun, X., Mangiavacchi, S., Chao, S.Z., 2004. Psychomotor stimulants and neuronal plasticity. *Neuropharmacology* 47 Suppl 1, 61–79. doi:10.1016/j.neuropharm.2004.07.006
- Wolfer, D.P., Crusio, W.E., Lipp, H.P., 2002. Knockout mice: simple solutions to the problems of genetic background and flanking genes. *Trends Neurosci.* 25, 336–340.
- Worsley, K.J., Marrett, S., Neelin, P., Vandal, A.C., Friston, K.J., Evans, A.C., 1996. A unified statistical approach for determining significant signals in images of cerebral activation. *Hum. Brain Mapp.* 4, 58–73. doi:10.1002/(SICI)1097-0193(1996)4:1<58::AID-HBM4>3.0.CO;2-O
- Wu, D., Reisinger, D., Xu, J., Fatemi, S.A., van Zijl, P.C.M., Mori, S., Zhang, J., 2014. Localized diffusion magnetic resonance micro-imaging of the live mouse brain. *NeuroImage* 91, 12–20. doi:10.1016/j.neuroimage.2014.01.014
- Wu, D., Zhang, J., 2016. In vivo mapping of macroscopic neuronal projections in the mouse hippocampus using high-resolution diffusion MRI. *NeuroImage* 125, 84–93. doi:10.1016/j.neuroimage.2015.10.051
- Würbel, H., 2002. Behavioral phenotyping enhanced–beyond (environmental) standardization 1, 3–8.
- Wynn, J.K., Dawson, M.E., Schell, A.M., McGee, M., Salveson, D., Green, M.F., 2004. Prepulse facilitation and prepulse inhibition in schizophrenia patients and their unaffected siblings. *Biol. Psychiatry* 55, 518–523. doi:10.1016/j.biopsych.2003.10.018
- Yin, H.H., Knowlton, B.J., Balleine, B.W., 2004. Lesions of dorsolateral striatum preserve outcome expectancy but disrupt habit formation in instrumental learning. *Eur. J. Neurosci.* 19, 181–189.
- Yin, H.H., Mulcare, S.P., Hilário, M.R.F., Clouse, E., Holloway, T., Davis, M.I., Hansson, A.C., Lovinger, D.M., Costa, R.M., 2009. Dynamic reorganization of striatal circuits during the acquisition and consolidation of a skill. *Nat. Neurosci.* 12, 333–341. doi:10.1038/nn.2261
- Yin, H.H., Ostlund, S.B., Knowlton, B.J., Balleine, B.W., 2005. The role of the dorsomedial striatum in instrumental conditioning. *Eur. J. Neurosci.* 22, 513–523. doi:10.1111/j.1460-9568.2005.04218.x
- Yochman, A., Ornoy, A., Parush, S., 2006. Co-occurrence of developmental delays among preschool children with attention-deficit-hyperactivity disorder. *Dev. Med. Child Neurol.* 48, 483–488. doi:10.1017/S0012162206001034
- Yoshida, M., Yokoo, H., Mizoguchi, K., Kawahara, H., Tsuda, A., Nishikawa, T., Tanaka, M., 1992. Eating and drinking cause increased dopamine release in the nucleus accumbens and ventral tegmental area in the rat: measurement by in vivo microdialysis. *Neurosci. Lett.* 139, 73–76.
- Zahm, D.S., 2000. An integrative neuroanatomical perspective on some subcortical substrates of adaptive responding with emphasis on the nucleus accumbens. *Neurosci. Biobehav. Rev.* 24, 85–105.
- Zhang, D., Guo, L., Zhu, D., Li, K., Li, L., Chen, H., Zhao, Q., Hu, X., Liu, T., 2013. Diffusion tensor imaging reveals evolution of primate brain architectures. *Brain Struct. Funct.* 218, 1429–1450. doi:10.1007/s00429-012-0468-4
- Zhang, J., Aggarwal, M., Mori, S., 2012. Structural insights into the rodent CNS via diffusion tensor imaging. *Trends Neurosci.* 35, 412–421. doi:10.1016/j.tins.2012.04.010
- Zhang, N., Rane, P., Huang, W., Liang, Z., Kennedy, D., Frazier, J.A., King, J., 2010. Mapping resting-state brain networks in conscious animals. *J. Neurosci. Methods* 189, 186–196. doi:10.1016/j.jneumeth.2010.04.001

- Zhang, Z., Lu, G., Zhong, Y., Tan, Q., Liao, W., Wang, Z., Wang, Z., Li, K., Chen, H., Liu, Y., 2010. Altered spontaneous neuronal activity of the default-mode network in mesial temporal lobe epilepsy. *Brain Res.* 1323, 152–160. doi:10.1016/j.brainres.2010.01.042
- Zhao, F., Zhao, T., Zhou, L., Wu, Q., Hu, X., 2008. BOLD study of stimulation-induced neural activity and resting-state connectivity in medetomidine-sedated rat. *NeuroImage* 39, 248–260. doi:10.1016/j.neuroimage.2007.07.063
- Zhou, J., Greicius, M.D., Gennatas, E.D., Growdon, M.E., Jang, J.Y., Rabinovici, G.D., Kramer, J.H., Weiner, M., Miller, B.L., Seeley, W.W., 2010. Divergent network connectivity changes in behavioural variant frontotemporal dementia and Alzheimer’s disease. *Brain J. Neurol.* 133, 1352–1367. doi:10.1093/brain/awq075
- Zhou, J., Seeley, W.W., 2014. Network dysfunction in Alzheimer’s disease and frontotemporal dementia: implications for psychiatry. *Biol. Psychiatry* 75, 565–573. doi:10.1016/j.biopsych.2014.01.020
- Zweifel, L.S., Argilli, E., Bonci, A., Palmiter, R.D., 2008. Role of NMDA receptors in dopamine neurons for plasticity and addictive behaviors. *Neuron* 59, 486–496. doi:10.1016/j.neuron.2008.05.028

Acknowledgements

This acknowledgement note is the concluding touch on my thesis where I would like to reflect on the people who supported and helped me a lot during my doctoral study at the University of Freiburg, Germany and University of Strasbourg, France.

First, I would like to thank my supervisors Dr. Laura-Adela Harsan and Prof. Brigitte Kieffer for their aspiring guidance, invaluable constructive criticism, friendly advice and tremendous support throughout my PhD study. Your valuable instructions always helped me to choose the right directions and successfully accomplish my dissertation.

My sincere gratitude to the scientific director of the Department of Radiology – Medical Physics, Prof. Dr. Dr. h.c. Juergen Hennig and the head of the ‘Advanced Molecular Imaging Research’ (AMIR) group PD Dr. Dominik von Elverfeldt, for providing me the platform to conduct my research. It was the most intensive period of learning in my life.

Appreciation also goes out to my former colleague Anna, who helped me with setting up the MR experiments and supported during my hard times. I am also thankful to Dr. Sami Ben Hamida for his expert opinions and friendly support to set up all behavioral experiments at IGBMC in Strasbourg, France. I must acknowledge my other colleagues Neele, Thomas, Annette, Jochen, Meltem and Thiago who never denied helping me whenever I asked for.

I would also like to thank Dr. Domitille Boudard – the manager of the Erasmus Mundus NeuroTime program, BCF and Uniklinik Freiburg admins and Frau Renate Kendlinger for handling all administrative tasks regarding my project. Without their kind support I could not be able to run this project smoothly.

I am also grateful to my family. Particularly my parents, their motivation and encouragement are the stairs toward my dreams. I doubt being able to pay off their endless sacrifices and support, that they provided me through my entire life. My elder sister, whose unconditional help and motivation never let me feel down. I will always be grateful to her. I am thankful to my elder brother, for his valuable suggestions during the time I changed my academic track. Special thanks to my wife, Warda, for being with me during all ups and downs over the last two years. Without her encouragement, love and care, I would not have finished this thesis. I appreciate her patience and compassions.

Last but not the least; I would like to thank the Erasmus Mundus Joint Doctorate (EMJD) NeuroTime program, for funding my research.

Chapter 4

Annex

4.1 Abbreviations

Abbreviations of the brain regions (alphabetically) according to the Allen Mouse brain atlas:

ACA: Anterior cingulate area
ACAd: Anterior cingulate area – dorsal part
ACAv: Anterior cingulate area – ventral part
ACB: Nucleus accumbens
aco: Anterior commissure
AI: Agranular insular Area
AMY: Amygdala
AMY: Amygdala
BG: Basal ganglia
BLA: Basolateral amygdala
BST: Bed nuclei of the stria terminalis
CEA: Central amygdala
CP: Caudate putamen
CSF: Cerebrospinal fluid
dmPFC: Medial pre-frontal cortex – dorsal part
ENT: Entorhinal area
ENTl: Entorhinal area
GP: Global Pallidus
Hb: habenula
HPF: Hippocampal formation
HY: Hypothalamus
IA: Intercalated amygdalar nucleus
ILA: Infralimbic area
LHb: Lateral Habenula
LSr: Lateral septal complex – rostral part
LSx: Lateral septal complex
MB: Midbrain
MO: Motor area
mPFC: Medial pre-frontal cortex
OFC: Orbito-frontal cortex
OT: Olfactory tubercle
P: Pons
PAG: Pallidum
PAG: Peri-aqueductal gray
PG: Pontine gray
PL: Prelimbic area
PTLp: Posterior parietal association area
RSP: Retrosplenial area
RSPv: Retrosplenial area – ventral part

S: Septal complex
SC: Superior colliculus
SS: Somatosensory area
TEa: Temporal association area
TH: Thalamus
VIS: Visual area
VTA: Ventral tegmental area

Others (alphabetically):

AAR: Alternate arm return
ACR: Alternate corner return
ADHD: Attention deficit hyperactivity disorder
AMBA: Allen mouse brain atlas (<http://mouse.brain-map.org/static/atlas>)
BOLD: Blood oxygen level dependent
cc: clustering coefficient
CEN: Central network
CNS: Central nervous system
CPP: Conditioned place preference
CT: Computed Tomography
CTRL: Control
D: Dark cycle
DA: Dopamine
DMN: Default mode network
DTI: Diffusion Tensor Imaging
DWI: Diffusion weighted imaging
D1R: Dopamine receptor 1
D2R: Dopamine receptor 2
E: East
EEG: Electro-encephalogram
EPI: Echo planar imaging
ES: Embryonic stem
FA: Fractional anisotropy
FC: Functional connectivity
FD: Fiber density
FDR: False discovery rate
FID: Free induction decay
FLASH: Fast low angle shot
FSD: Fixed schedule drinking
fMRI: Functional magnetic resonance imaging
FPN: Fronto-parietal network
GM: Grey matter
GPCR: G protein-coupled receptor
GPR88: G protein-coupled receptor 88
FOV: Field of View
Hz: Hertz
IC: Independent components

ICA: Independent component analysis
I_q: Quality index
KO: Knock-out
L: Light cycle
LED: Light-emitting diode
LFF: Low frequency fluctuation
MBFC: Mouse brain functional connectivity
MD: Medetomidine
MEG: Magneto-encephalogram
Mm: Millimeter
Ms: Millisecond
Min: Minute
MR: Magnetic resonance
MRI: Magnetic resonance imaging
MSN: Medium spiny neuron
M_{xy}: Transverse magnetization
M_z: Longitudinal magnetization
N: North
NP: Nose-poke
PCR: Polymerase chain reaction
PET: Positron Emission Tomography
PPI: Pre-pulse inhibition
RARE: Rapid acquisition with relaxation enhancement
RF: Radio frequency
RFID: Radio frequency identification
ROI: Regions of interest
rsFC: Resting state functional connectivity
rsfMRI: Resting-state functional magnetic resonance imaging
RSN: Resting state network
s: Second
S: South
SAR: same arm return
SC: Structural connectivity
SCA: Spontaneous corner alternation
SCR: Same corner return
SN: Salience network
SPA: spontaneous alternation
SPECT: Single-Photon Emission Computed Tomography
SPL: Shortest path length
T: Tesla
TE: Echo time
TPN: Task positive network
TR: Repetition time
W: West
WM: White matter
WT: Wild type

4.2 Tables

Table 1: Behavioral characteristics observed in the *GPR88* deficient mice, adapted from several former studies as cited on the right most column of the table.

System	Behavioral Test	Behavior	Results	References
(i) Sensory	Prepulse inhibition of the acoustic startle response assay	Sensorimotor gating	<i>Gpr88</i> ^{-/-} mice have no difference in acoustic startle response but exhibit decreased PPI of the acoustic startle response that can be rescued by D2 antagonists.	Logue et al., 2009
(ii) Sensory/ Motor	Apomorphine induced Stereotypy	Apomorphine induced distinct stereotypic sniffing behavior	<i>Gpr88</i> ^{-/-} mice exhibited more stereotypy than WT mice. Haloperidol treatment was less effective in blocking <i>Gpr88</i> ^{-/-} stereotypy.	Logue et al., 2009
	Stereotypy	Numbers of rearing, burying, allogrooming, circling episodes and total time spent burying	<i>Gpr88</i> ^{-/-} mice exhibit increased stereotypy.	Meirsman et al., 2015
(iii) Activity Responses (motor, basal and DA agonists)	Basal locomotor activity	Basal locomotor activity was recorded over 48 hours in activity chambers	<i>Gpr88</i> ^{Cre/Cre} mice exhibit increased basal locomotor activity in novel and familiar environments, ameliorated by re-expression of GPR88 in the striatum.	Quintana et al., 2012
	Basal locomotor activity	Basal locomotor activity in a novel environment open-field	<i>Gpr88</i> ^{-/-} mice have increased locomotor activity and lack habituation to a novel environment.	Meirsman et al., 2015
	Basal locomotor activity	Basal locomotor activity in a novel environment open-field	<i>Gpr88</i> ^{-/-} and A2AR- <i>Gpr88</i> ^{-/-} mice have increased locomotor activity.	Meirsman et al., 2016

	Amphetamine induced hyperlocomotor activity	Amphetamine stimulated locomotor activity	Gpr88 ^{-/-} mice were more sensitive to amphetamine- stimulated locomotor activity than WT mice.	Logue et al., 2009
	Amphetamine induced hyperlocomotor activity	Locomotor activity (90 min) after daily (5-day) amphetamine administration	Gpr88 ^{Cre/Cre} mice have increased sensitivity to amphetamine induced hyperlocomotor activity.	Quintana et al., 2012
	Apomorphine induced Climbing	Apomorphine induces climbing behavior	Gpr88 ^{-/-} mice exhibited more climbing than WT mice.	Logue et al., 2009
	Dopamine D1 receptor agonist mediated hyperlocomotor activity	Hyperlocomotor activity (60 min) in response to increasing doses of D1R agonist, SKF-81297.	Gpr88 ^{Cre/Cre} mice have decreased sensitivity to D1 agonist induced hyperlocomotor activity.	Quintana et al., 2012
	Dopamine D2 receptor mediated effects on hypolocomotor activity	Hypolocomotor activity (3 h) in response to increasing doses of D2R agonist, quinpirole.	Gpr88 ^{Cre/Cre} mice have decreased sensitivity to D2 agonist induced hypolocomotor activity.	Quintana et al., 2012
(iv) Motor Coordinat ion	Haloperidol blockade of climbing activity	Haloperidol blocks climbing activity	Haloperidol is less effective in blocking climbing in Gpr88 ^{-/-} mice.	Logue et al., 2009
	Rotarod	Motor coordination and balance	Impaired motor coordination or strength in Gpr88 ^{Cre/Cre} mice. Striatal GPR88 re-expression decreased motor coordination impairment.	Quintana et al., 2012
	Rotarod	Motor coordination and balance	Gpr88 ^{-/-} mice have motor coordination and learning impairment. Reversible by chronic treatment with a Delta opioid receptor antagonist, Naltrindole.	Meirsman et al., 2015

	Grip test	Motor coordination and balance	Gpr88 ^{-/-} mice have no difference in muscle strength.	Meirsman et al., 2015
(v) Learning and Memory	Operant behavior, Two-way active avoidance procedure	Avoidance learning, acquisition and integration of visual or auditory cues	Impaired in Gpr88 ^{Cre/Cre} mice and rescued by GPR88 re-expression in striatum.	Quintana et al., 2012
	Morris water maze	Spatial learning and memory	Gpr88 ^{Cre/Cre} had mild impairment in initial performance of the task but visuospatial memory and learning were intact.	Quintana et al., 2012
	A water-based, U maze	Associative learning	Gpr88 ^{Cre/Cre} mice had impairments in cue-based learning.	Quintana et al., 2012
	Y-Maze	Willingness to explore new environments.	Gpr88 ^{-/-} increased Y-maze arm entry and reduced same arm entry. Reversible by chronic treatment with a Delta opioid receptor antagonist.	Meirsman et al., 2015
	Novel object recognition test	Ability to discriminate either novel objects or their spatial location. Learning and recognition memory.	Gpr88 ^{-/-} mice explore items more often suggesting improved learning and recognition memory.	Meirsman et al., 2015
	Dual solution cross-maze task	Ability to distinguish between goal-directed responses and habitual behavior	Gpr88 ^{-/-} mice displayed improved ability at this task.	Meirsman et al., 2015
	Fear conditioning	Ability to learn and remember an association between environmental cues and	Gpr88 ^{-/-} but not A2AR-Gpr88 ^{-/-} mice impair contextual fear and cue-related fear expression.	Meirsman et al., 2016

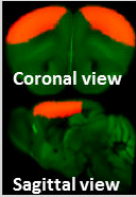
		aversive experiences		
(vi) Risk-taking/low anxiety	Elevated-plus Maze Test	Measure of anxiety-like behaviors	Gpr88 ^{-/-} mice exhibit reduced anxiety levels, not reversible by chronic treatment with a Delta opioid receptor antagonist, Naltrindole.	Meirsman et al., 2015
	Elevated-plus Maze Test	Measure of anxiety-like behaviors	Gpr88 ^{-/-} and A2AR-Gpr88 ^{-/-} mice have decreased anxiety behaviors.	Meirsman et al., 2016
	Light-Dark Test	Anxiety-like behavior	Gpr88 ^{-/-} and A2AR-Gpr88 ^{-/-} mice entered and spent more time exploring the aversive illuminated compartment, exhibit increased risk-taking behaviors.	Meirsman et al., 2016
	Marble-burying Test	Measure of anxiety-like behaviors	Gpr88 ^{-/-} mice bury less marbles, consistent with lower anxiety.	Meirsman et al., 2015
	Marble-burying Test	Measure of anxiety-like behaviors	Gpr88 ^{-/-} and A2AR-Gpr88 ^{-/-} mice display decreased threat avoidance and more risk-taking behaviors.	Meirsman et al., 2016
	Nest building	Nest building behavior as a measure of anxiety-like behaviors	Gpr88 ^{-/-} males display decreased anxiety evidenced by reduced nest building.	Meirsman et al., 2015
	Novelty preference	Novel environment exploration	Gpr88 ^{-/-} but not A2AR-Gpr88 ^{-/-} mice display increased novelty approach/low anxiety behaviors.	Meirsman et al., 2016
	Novelty-suppressed feeding Test	A conflict task challenging approach/avoidance behavior	Gpr88 ^{-/-} mice exhibit decreased conflict anxiety, reversible by chronic treatment with a Delta opioid receptor antagonist, Naltrindole.	Meirsman et al., 2015

	Novelty-suppressed feeding Test	A conflict task challenging approach/avoidance behavior	Gpr88 ^{-/-} but not A2AR-Gpr88 ^{-/-} mice display increased novelty approach/low anxiety behaviors.	Meirsman et al., 2016
	Social interaction test	Measure of anxiety-like behaviors	Gpr88 ^{-/-} and A2AR-Gpr88 ^{-/-} mice display increased social behaviors.	Meirsman et al., 2016

Table 2: Comparative analysis of the estimation of the number of ICs for different number of components (10, 15, 20, 40, 60, 80, 100 and 120 ICA) based on the stability index (I_q) ranging from 0 to 1.

ICA with bootstrapping and randomizing initial conditions (ICASSO – 20 repetitions)								
Quality index $I_q >$	% of stable components							
	10 ICA	15 ICA	20 ICA	40 ICA	60 ICA	80 ICA	100 ICA	120 ICA
0.6	100%	100%	100%	100%	100%	100%	100%	98%
0.7	100%	100%	100%	100%	98%	99%	99%	96%
0.8	100%	100%	100%	100%	97%	97.5%	96%	87%

Table 3: Brain regions that showed significantly modified functional connectivity (both positive and anti-correlations) with the seed regions: MO, SS, CP and HPF

Seed region	Correlation	CTRL > <i>GPR88</i> ^{-/-}	CTRL < <i>GPR88</i> ^{-/-}
a) Motor area 	Positive	OFC, AI, PL, ILA, ACB, RSP, PTLp	CP, SS, within MO
	Negative	AMY, TH (posterior)	HPF, MB, SC, PAG
b) Somatosensory area 	Positive	MO, RSP, VIS	MO, ACA
	Negative	AMY, TH (posterior), HY, MB	ACB, HPF, SC, PAG
c) Caudate putamen 	Positive	HPF, TH, MB	ACA, AI, S, PAL, BST
	Negative	AMY, ENT, VIS, SC, P	ACB, MO, SS, ACA, PTLp
d) Hippocampal formation 	Positive	AMY, ENT, TEa, rostral TH, MB	Caudal TH, SC, PG
	Negative	ORB, PL, ACB, ACA, MO, SS, RSP, PTLp	CP, LSx, ILA

4.3 Figures

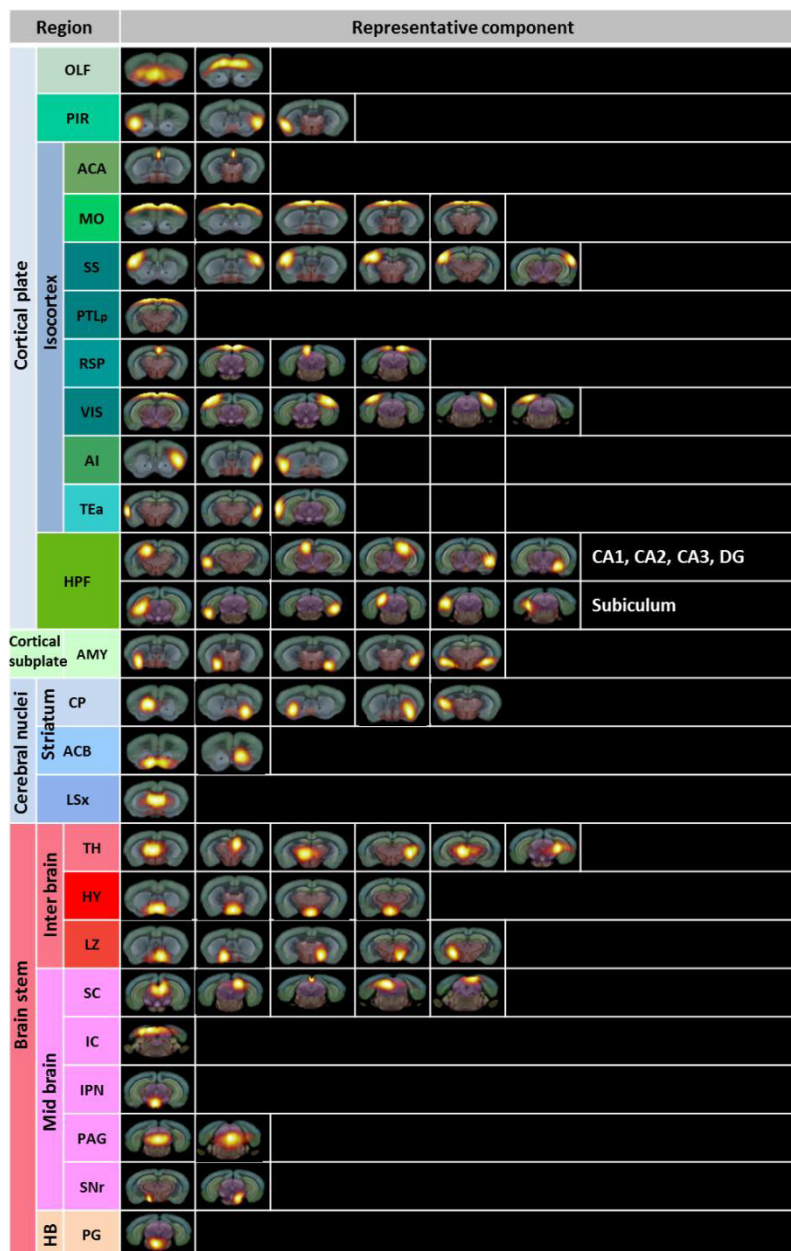


Figure 1: Independent component analysis (ICA) reveals anatomically well-defined brain components or nodes: Spatial ICA using ICASSO (Gift - Group ICA of fMRI Toolbox – v.1.3i, <http://www.nitrc.org/projects/gift/>) was performed on the datasets, obtained from 40 combined control (CTRL) and *Gpr88*^{-/-} group, housed with water or alcohol datasets. The analysis revealed 87 components or nodes, displayed as spatial color-coded z-maps (threshold 3.0) onto Allen Mouse Brain Atlas and are arranged according to their affiliation to broader brain areas: Isocortex, Hippocampal formation, Cortical subplate, Striatum, Inter brain regions (Thalamus, Hypothalamus, Hypothalamic lateral zone), Midbrain regions (Superior colliculus, Inferior colliculus, Interpeduncular Nucleus, Periaqueductal gray, Substantia Nigra) and Hindbrain (Pontine gray)

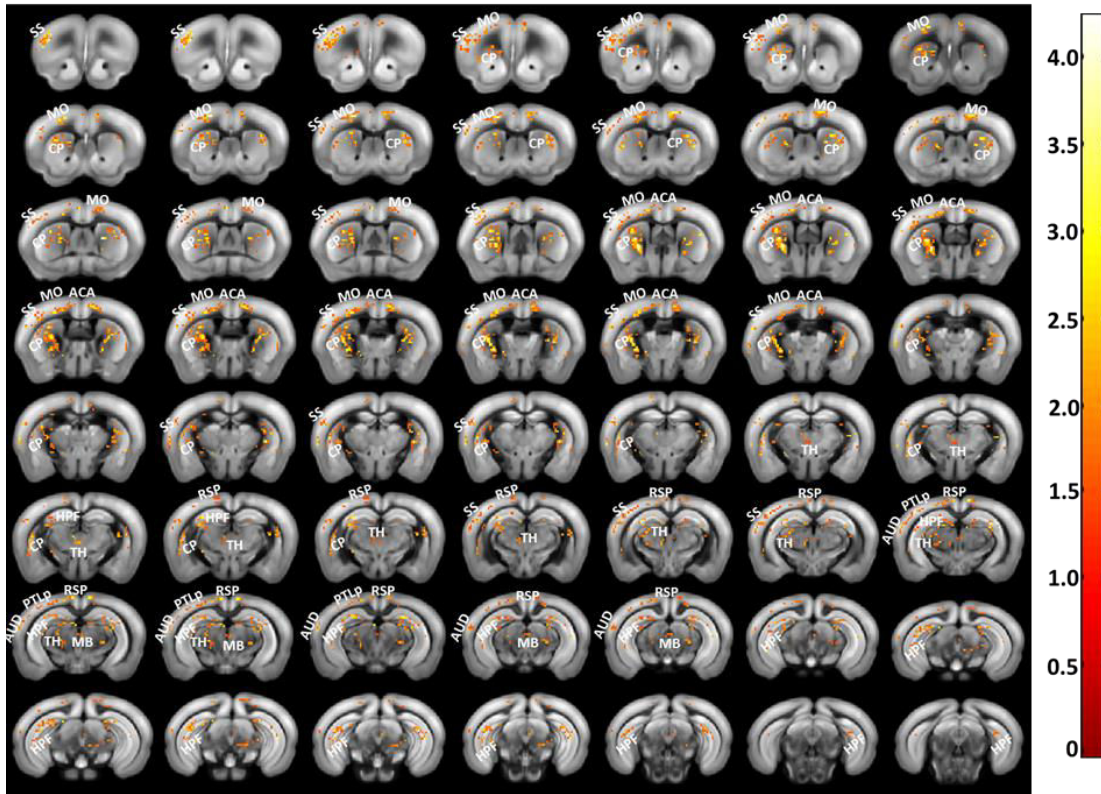


Figure 2: Significant alterations of the fractional anisotropy (FA) in *Gpr88*^{-/-} mice: Statistical significance was evaluated using two sample t-test ($p < 0.05$, FWE corrected). The panel shows the regions with higher fiber density in the mutant mice compared to the CTRL. Corresponding T value scale is shown.)

4.4 Experimental procedures

CTRL (control) and *Gpr88*^{-/-} mice used in this study were generated following the same technique at the Institut Clinique de la Souris, Strasbourg, France, as described in section 3.4.1. Anesthesia regime, scanning parameters and rsfMRI and DTI data processing methods were same for all mouse imaging studies as illustrated in 3.4.2 and 3.4.3 respectively. All *in-vivo* mouse brain imaging studies were performed at the Department of Radiology, Medical Physics in University Medical Center Freiburg, Germany. Mouse behavioral experiments with alcohol and IntelliCage (demonstrated in section 3.4.4) were carried out in IGBMC, Strasbourg, France. Section 3.5 describes the principles of MRI as well as some basic pulse sequences and MR imaging techniques.

4.4.1 Construction of *Gpr88*^{-/-} mice

GPR88 floxed mice (*GPR88*^{fl/fl}) were generated at the Institut Clinique de la Souris using Cre-LoxP technology. Mice with a floxed *GPR88* gene (*GPR88*^{fl/fl}) were first generated, where exon 2 is flanked by a loxP site (upstream) and a Lox-FRT neomycin-resistance cassette (downstream) (Figure 1A). A 9.6 kb genomic clone containing exons 1 and 2 of the *GPR88* gene was isolated from 129Sv genomic DNA and cloned into a targeting plasmid to generate the targeting vector. This clone was engineered to introduce a loxP site 230 bp upstream of exon 2 and 524 pb after the stop codon. The targeting vector was linearized for electroporation into 129Sv derived embryonic stem (ES) cells, which were selected with neomycin. Surviving cells were screened for homologous recombination by polymerase chain reaction (PCR). ES cells with the correct genotype were injected into C57BL/6J blastocysts, and resulting chimeric males were bred with C57BL/6J females to obtain germline transmission. F1 heterozygous *Gpr88*^{fl/+} mice were bred with CMV-Flip mice in order to remove the neomycin cassette, and the obtained animals were then crossed with CMV-Cre mice expressing Cre recombinase under the cytomegalovirus promoter (Gaveriaux-Ruff et al., 2011; Metzger and Chambon, 2001). This led to germ-line deletion of *GPR88* exon 2 on a hybrid 50% C57BL/6J–50% 129Sv genetic background. We obtain *Gpr88*^{fl/fl} × CMV-Cre^{Tg/+} (deletion of *GPR88* exon 2; *Gpr88*^{-/-} mice), *Gpr88*^{+/+} × CMV-Cre^{0/+} (*GPR88* wt allele; *Gpr88*^{+/+}), *Gpr88*^{+/+} × CMV-Cre^{Tg/+} and *Gpr88*^{fl/+} × CMV-Cre^{0/+} animals. *Gpr88*^{-/-} and *Gpr88*^{+/+} were used as experimental and control animals (CTRL) respectively.

4.4.2 Animal preparation and MRI data acquisition

2.4 – 3.2 volume % isoflurane with a debit of 1-1.2 litres of oxygen/air per minute was applied to anesthetize the mouse during the time of stereotaxic fixation on the mouse bed and attachment of physiological monitoring sensors. However, isoflurane was substituted by alpha-2 adrenergic agonist medetomidine (MD – Domitor, Pfizer, Karlsruhe, Germany) to avoid the negative side effect on the Blood-Oxygen-Level Dependent (BOLD) response as well as in the temporal correlation of Low Frequency Fluctuations (LFFs). An optimum sedation was maintained

throughout the resting state scanning session by an initial subcutaneous (s.c.) bolus of 0.3 mg MD/kg body weight (BW) in 100 μ l 0.9% NaCl solution, and after positioning the mouse in the scanner (head first) by a continuous s.c. infusion of 0.6 mg MD/kg BW, 200 μ l/hour through an MR compatible catheter inserted on the back of the mouse. The physiological conditions like body temperature, respiration, and blood oxygen saturation were monitored continually during the imaging session using a rectal probe, pressure sensitive pad placed underneath the mouse abdomen, and pulse oximeter (SA instruments, Inc. Stony Brook, NY) clipped on the hind paw respectively. To provide an additional control over the body temperature within the range of 36.5 – 37.5 $^{\circ}$ C, circulation of warm water was supplied along the lower part of the animal body. Breathing rates under MD remained within the range of 100 – 135 breaths per minute, and imaging data was acquired only at the blood oxygenation levels in the range of 97 – 100%. MD infusion was stopped and switched to isoflurane to perform Turbo RARE T₂ scan, followed by the DTI session and images were acquired on respiration triggering.

Mouse brain MRI data was acquired with a 7T small bore animal scanner (Biospec 70/20, Bruker, Germany) and a mouse head adapted CryoCoil (MRI CryoProbe, Bruker, Germany). Prior to the mouse brain imaging data acquisition, a whole brain shimming protocol using ParaVision 5.1 (PV 5.1) was applied including adjustment of basic frequency, reference pulse gain and field homogeneity.

rsfMRI was performed with T₂* - weighted single shot GE-EPI sequence (TE/TR = 10 ms/1700 ms). The mouse brain (excluding the cerebellum) was covered using 12 axial slices of 0.7 mm thickness, with a field of view (FOV) of 19.2 \times 12 mm² and a planar resolution of 150 \times 150 μ m². 200 volumes were recorded in interlaced fashion for each run. MD infusion was stopped after the rsfMRI scan.

Turbo RARE T₂ sequence (TE/TR = 50 ms/6514 ms) was applied on respiration triggering under ~2.5 Vol% of isoflurane to attain high resolution anatomical images of the mouse brain. The whole brain including cerebellum was covered using 48 slices (0.3 mm slice thickness) at planar spatial resolution of 51 \times 51 μ m² with a FOV of 1.3 \times 1.0 cm².

DTI session was carried out using DTI-EPI sequence with 25 axial slices of 0.5 mm thickness at a resolution of 94 \times 94 μ m³ covering the equivalent partition of the brain as for the rsfMRI scan (TE/TR= 20ms/7750ms); Δ = 10ms, diffusion gradient duration (δ) = 4ms, b factor of 1000s/mm², 30 non-collinear diffusion gradient directions.

4.4.3 MRI data processing

4.4.3.1 Data pre-processing

Statistical Parametric Mapping (“SPM - Statistical Parametric Mapping,” n.d.) with SPMmouse toolbox (“SPM Mouse,” n.d.) for MATLAB (The MathWorks, Natick, Massachusetts) was used to preprocess all imaging data acquired during this study which includes several steps as described below:

Coregistration: We used this function to align the DTI and rsfMRI (first time point only) volumes of each mouse to its respective T_2 image volume, in order to remove any movement artifacts, which might have occurred during the scanning session. We used the SPM8 co-registration with a normalized mutual information approach, a 4th degree B-Spline interpolation and a 6-parameter rigid body transformation (3 parameters for translation and 3 parameters for rotation). No warping was applied during this step.

Realignment: The SPM realignment function was used to realign each rsfMRI time point image volume to the first image of each subject's time series to remove movement artifacts. This realignment uses a least squares approach with a 6 parameter rigid body spatial transformation. These two alignments ensure that image volumes of each mouse are aligned to their respective T_2 scan, but there is still no alignment between different subjects. For that, we chose our in-house refined tissue probability maps (TPM, based on the SPMmouse TPM, (Sawiak et al., 2013)) to be the image volumes, on which all our mouse image volumes should be aligned to. These TPM give standard locations of grey matter (GM), white matter (WM) and cerebrospinal fluid (CSF).

Segmentation: We further used the SPM segmentation function with our TPM and the T_2 of each subject, to determine normalization parameters for a 12-parameter affine transformation and warping to best match the T_2 to the TPM. These parameters were computed for each subject (forward transformation) and their inverse transformation was calculated. This way we obtained the transformation parameters for a deformation from the TPM orientation to the individual mouse space. The quality of the segmentation was assessed by visual check of the TPM-aligned T_2 images using the SPM CheckReg function. If the warping introduced strong distortions, or the 12-parameter affine transformation did not produce a good overlap, we adjusted the TPM alignment and rerun the segmentation.

Deformation: The SPM deformation function was used to apply the subject specific forward transformation to the T_2 , DTI and rsfMRI volumes, thus generating images which are in alignment with the TPM. We also used the deformation function to reslice all volumes with a 4th degree B-spline interpolation to voxel sizes of $0.15 \times 0.15 \times 0.15$ mm, so that we can run voxel-wise statistics between all modalities without losing any physical information. This resolution was chosen because it has proven to be a good compromise between the resolutions of our three different modalities (T_2 , DTI, (rs)-fMRI).

Smoothing: We applied a Gaussian smoothing with a kernel of FWHM of $0.4 \times 0.4 \times 1$ mm (Mechling et al., 2014) to all TPM-aligned rsfMRI image volumes. This type of smoothing has proven to produce high quality index (I_q) values in the later ICA.

Brain mask: The segmentation function generates (according to the TPM) volumes corresponding to GM, WM and CSF determined from each T_2 . We added the volumes of GM and WM to generate subject specific masks excluding CSF and used them for further processing steps to improve the accuracy of the results by reducing the influence of non-BOLD signals.

Data coregistration with the Allen Mouse Brain Atlas (AMBA): The whole brain was parceled using an in house developed, MATLAB and AMBA (Lein et al., 2007) based mouse brain atlas

tool. The AMBA anatomical image volume was aligned to match our template using the SPM8 segmentation approach described above. The derived warping parameters were applied to all AMBA image volumes and the initial AMBA resolution of $528 \times 320 \times 456$ voxel was changed to the TPM defined resolution of $165 \times 230 \times 135$ voxel with a voxel size of $0.07 \times 0.07 \times 0.07$ mm³. This was necessary to retain consistency with our TPM.

4.4.3.2 Data post-processing

Pre-processed rsfMRI and DTI data were further processed in several steps. Resting state functional connectivity clusters were identified using a data-driven method, called ‘Independent component analysis’ (ICA). Functional connectivity between brain regions were assessed using partial correlation and further region specific whole brain connectivity were mapped by means of seed correlation analysis. Brain micro-structural organization was evaluated using global mouse brain fiber tractography.

Independent component analysis (ICA): ICA using GIFT toolbox was performed to define elementary functional clusters. Estimation of the number of components is an important step while decomposing the entire BOLD signal into spatially independent components (ICs) or sources. Underestimation of the components may result in mixing various components (Margulies et al., 2010; van de Ven et al., 2004), whereas overestimation can result in splitting reliable networks (Esposito et al., 2003; Moritz et al., 2005), decreasing the stability of IC estimates (Li et al., 2007). Therefore, we used ICASSO algorithm (Himberg et al., 2004) to assess the stability pattern via bootstrapping and randomizing initial conditions for different numbers of independent components. The ‘quality index’ I_q (values ranging from 0 to 1) was used as a quantitative measure of robustness of the identified components evaluating compactness and isolation of each cluster (Mechling et al., 2014). We verified the consistency of the results when progressively achieving a high spatial definition (in accordance to fine anatomical details) of the functional clustering patterns with 10, 15, 20, 40, 60, 80, 100 and 120-ICASSO, respectively. Furthermore, we tested the reproducibility of the group ICA patterns in each experimental group by exploiting information and results generated with GIFT tools (Group ICA of fMRI Toolbox - v1.3i) via back reconstruction. Indeed, the patterns of functional elementary clusters resulting from 100 - ICASSO represent group components. However, from these aggregate components and the original data, GIFT toolbox computes spatial back-reconstructed individual subject components using a spatial-temporal regression approach (details are given in the GIFT toolbox manual: (“GIFT Software,” n.d.)). We used the back reconstructed individual spatial maps to create “incidence maps” for each independent component. This approach revealed low intra-groups variability of the ICA patterns and extremely high similarity between group patterns. These results substantiate further approach of using the group ICA functional clusters as “nodes” in the generation of brain functional connectivity matrices for individual group of mice.

Pearson partial correlation (PC) analysis: PC analysis was used for direct connectivity analysis of the time courses of anatomically well-defined brain regions (ICs), obtained from ICA. Partial correlation matrix (PCM) was generated considering both positive (max. value +1) and

negative/anti correlation (min. value -1) for each experimental group. In order to have an overview of the group-level significant connectivity relationships over the whole brain, we performed two-sample t-test thresholding at 0.01 under false discovery rate (FDR) control for multiple comparisons. Additionally, we counted total number of correlation changes for each component towards the rest and ranked top ten mostly functionally altered brain regions.

Seed correlation analysis: Several regions of interest (ROIs) were further used for hypothesis driven whole brain FC mapping. Average resting state time series of each group was processed through de-trending, global signal regression and further temporally band-pass filtration (0.01 ~ 0.1 Hz). Seed regions were chosen from the ranking of the mostly altered brain regions (Obtained from partial correlation analysis). Correlation coefficients were then computed between the seed region and the averaged time series of the remaining whole brain and were converted to Z values using Fisher's r-to-z transformation. Furthermore, to evaluate the group effects, we segmented the ROI independently for each subject, according to grey matter probability map corresponding to that respective subject thresholding at 0.5. This approach allowed us to map the functional connectivity for a specific ROI or seed, for each subject in its native space, in place of the standard or group space. Thus, it reduced the between-subject differences of gray matter probabilities. Group effects were then estimated segregating positive and negative (anti) correlations for the respective seed using voxel-level general linear model, corrected for multiple comparisons via Random Field Theory approach (Worsley et al., 1996).

Network topology: Some other measures of interest include: *shortest path length (SPL)* – a measure of global connectedness, which is the length of the shortest connection between all pairs of nodes. *Clustering coefficient (CC)* – provides the level of local neighborhood clustering within a network, expressing how close the neighbors of node are connected with each other, indicating the level of local connectedness of a network. These parameters were further compared to the mean clustering coefficient (C_{rand}) and path length (L_{rand}) of a random network with the same number of nodes and edges to demonstrate the topological overview of the mouse brain. *Small world networks* have high clustering coefficients (>1) implying high level of local connectedness, but with a short average path length (~ 1). As such, this organization combines a high level local efficiency with a high level of global efficiency (Watts and Strogatz, 1998). Therefore, in our study, we also addressed this question whether the *GPR88^{-/-}* mouse brain displays the small world network's features or not.

Diffusion tensor tractography: This approach provided insight into the mouse brain structural network. HARDI data was acquired for all animals of our study and fiber tracking was performed via a global fiber tracking algorithm developed in our group (Reisert et al., 2011), optimized and validated for in-vivo mouse brain tractography (Harsan et al., 2013). As a general rule, the tractography approaches exploit the assumption that the water molecule's movement in tissue will be hindered to a higher extent across than along the axons. The directions of greatest diffusion in each voxel of the images are therefore used as estimates for fiber orientation. The method used in our study is reconstructing all fiber bundles simultaneously, for the whole brain,

without the requirement of defining seed or target regions. The approach is therefore offering resistance to the local imaging artifacts, avoiding the cumulative errors generally arising when sequentially integrating local fiber directions from pre-defined seed-points. It allows the reconstruction of a larger field of view when an ambiguous area has to be resolved. Furthermore, from the diffusion tensor, we determined three eigenvectors and the corresponding eigenvalues ($\lambda_1, \lambda_2, \lambda_3$), representing in each voxel the main diffusion directions and the magnitude of diffusivity in all three directions. Based on these three eigenvalues, we calculated fractional anisotropy (FA) that gives a measure for the anisotropy of diffusion within the voxel ($0 < FA < 1$, where 0 = isotropic condition).

4.4.4 Mouse behavioral experiments

4.4.4.1 Experiments with alcohol

Two-bottle choice – continuous access: Animals were single-housed under a 12 hour (12h) reversed light/dark cycle. Oral alcohol intake was determined using continuous access to alcohol in a two-bottle choice drinking paradigm. Drinking sessions were conducted 24h a day during 5 consecutive days, with one bottle containing tap water, while the other contained alcohol diluted to 20% alcohol (v/v) in tap water. The bottles were weighed every day and the mice were weighted at the beginning of the experiment. The position (left or right) of each solution was alternated between sessions as a control for side preference. Possible loss of solutions due to the handling of the bottles was controlled by weighting bottles in empty cages.

Two-bottle choice – intermittent access: 48h after the continuous access paradigm, mice were given 24h of concurrent access to one bottle of 20% alcohol (v/v) in tap water and another bottle of water starting at 12 a.m. on Monday, Wednesday and Friday with 24h or 48h (during the weekend) of alcohol-deprivation periods between the alcohol-drinking sessions. The water and alcohol bottles were weighed after 24h of access. The controls used for the continuous access were also used in this paradigm.

Data were analyzed with (GraphPad Prism) unpaired t test or two-way ANOVA with or without repeated measures (RM-ANOVA). Significant main effects and interactions of the ANOVAs were further investigated with the Bonferroni *post-hoc* test or method of contrast analysis. Statistical significance was set at $p < 0.05$.

4.4.4.2 IntelliCage – system overview

Intellcage is a novel automated learning apparatus assessing spontaneous and learning behavior of group-caged mice (NewBehavior AG). The system fits into a large standard rat cage (Techniplast 2000) measuring 55×37.5 cm at the base, 58×40 cm at the top, with a height of 20.5 cm (for a detailed description, see (Galsworthy et al., 2005)). A cover plate holds four operant learning chambers that fit into the corners of the housing cage, covering a triangular 15 cm \times 15 cm \times 21 cm area of floor space each. Access into the chamber is provided via a tubular antenna reading the transponder codes (50 mm outer and 30 mm inner diameter). This design

restricts access to the learning chamber for a single mouse only. The chamber, equipped with a proximity sensor, contains two openings of 13 mm diameter permitting access to the spouts of drinking bottles. These openings are crossed by photo beams recording nose-pokes of the mice. Access to the spouts can be barred by small motorized doors. Aversive stimulation can be delivered in forms of air-puffs directed to the head of the mouse through tubing controlled by electric valves. In addition, each cage contained a sleeping shelter in the center on which the animals could climb to reach the food (*ad libitum*). In my study, the whole set-up of 4 IntelliCages were controlled by a computer recognizing visits, nose-pokes, and spout-lickings of individual mouse, and delivering reward (by opening the access to water/sucrose/alcohol after a nose-poke or nose-pokes for 5s) according to preprogrammed schedules depending on the assignment of the mice to different test groups within the same cage. All cages were located in a dedicated room of the animal facilities only for the IntelliCage experiments. The system ran continually for several days, behavioral activity of the mice being monitored from the office via Intranet.

4.4.4.2.1 IntelliCage software

IntelliCage software consist 3 different modules: *designer* – to design the experiment, *controller* – to monitor animal's behavior during the experiment and *analyzer* – to analyze the data from the experiment.

Designer software allows for the definition of cognitive testing schedules that are applied to each transponder-marked animal in the IntelliCage individually. Different conditions based on the experiment requirements can be assigned using designer software. For example: access to water from bottles functions as positive reward, air-puffs for negative reinforcement and LEDs for conditional stimulation.

Controller extracts and stores the behavioral events from the incoming stream of sensor data and the output resulting from the controlling design. For example:

- Correct or incorrect presence of individuals in the conditioning apparatus.
- Location and correctness (according to conditioning scheme) of nose-pokes and licks
- The incidence and extent of drinking behavior (reward) and
- The occurrence of negative reinforcement (air-puffs).

Controller further visualizes the basic behavioral parameters during the ongoing experiment, allowing for online-monitoring of events and developments.

Analyzer software takes advantage of the stored behavioral sequence data in order to derive the temporal development of the animal's behavior in response to the designed conditioning schedules. The foremost focus of analyses is on responses to any of the potentially large number of designable conditioning schemes that might be used to investigate a plethora of questions regarding cognitive abilities and development, including:

- Discrimination learning.
- Procedural learning and memory.

- Spatial preference/avoidance learning and memory.
- Reversal and complex learning.

The analyzer software takes further advantage of the continuous information on animal activity allowing complex behavioral traits of the animals. For example:

- Circadian activity levels.
- Habituation and neophobia reactions.
- Explorative and anxiety scores and
- Spontaneous spatial or gustatory preferences.

Thus IntelliCage system provides the opportunity to design simple to complex conditioning tasks in a uniquely flexible manner and control for each animal. The individually tailored experimental protocols can be automatically run and analyzed for transponder-tagged animals in potentially large numbers of cages, simultaneously. This allows for testing experimental, phenotypic, or genotypic effects on cognitive abilities as well as activity patterns, as is frequently required in biomedical and basic behavioral, neurobiological and genetic research, with unprecedented efficiency and minimal work load.

4.4.4.2.2 Designing and monitoring the behavioral studies using IntelliCage

This section briefly illustrates how to design an experiment using IntelliCage designer software. IntelliCage – Designer software module provides graphical tools to design and store conditioning tasks, handling of animal ID, groups, clusters, and modules for the experiment.

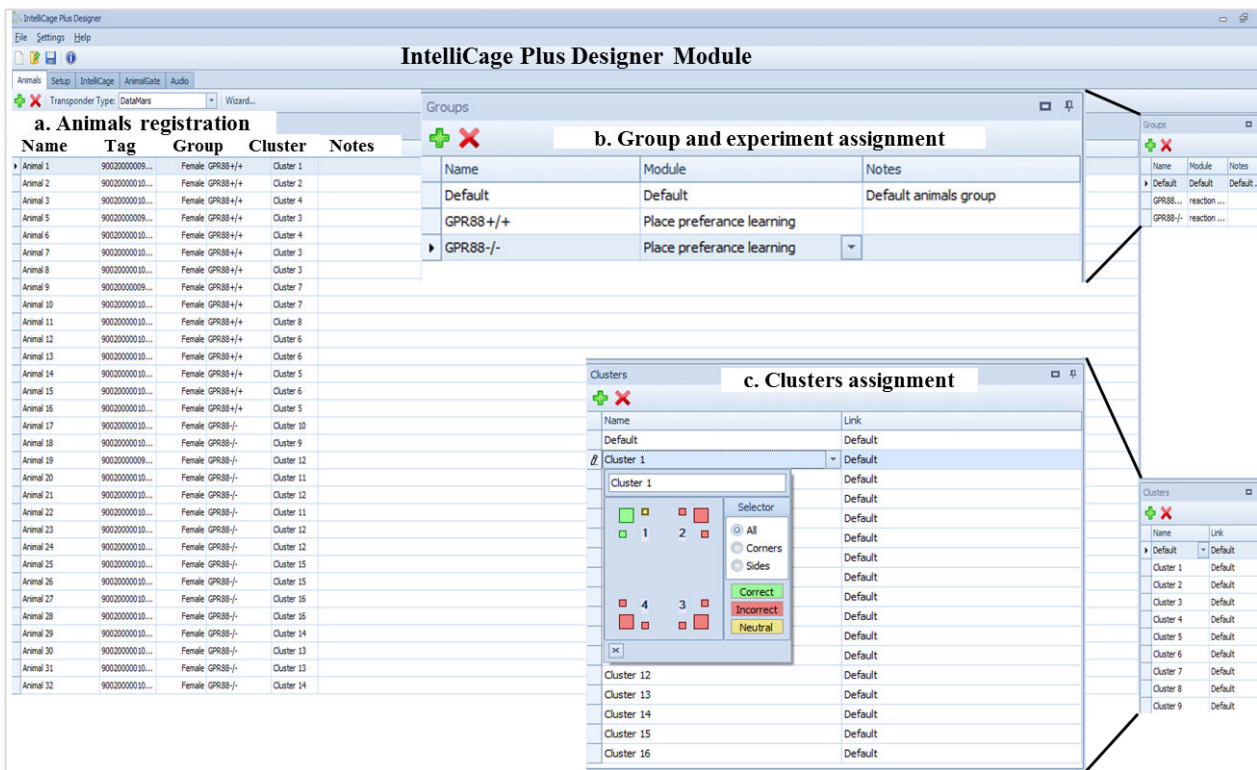


Figure 1: IntelliCage Plus Designer Module – animal and clusters registration: a) animal registration tab: to register all animals with specific tag and cluster, b) animal groups assignment tab, and selection of the specific session of the experiment and c) design and assignment of clusters for mice.

There are several steps required to follow prior to start an experiment as described below:

a) Animal registration: In order to perform an experiment, the very first step is to register all RFID implanted animals. The "Animals" tab in the main "Designer" window allows creating an animal list with corresponding RFID tags. It is also possible to assign the gender, name of the group and cluster for each animal. Figure 1a shows, all RFID implanted animals with the specific tag numbers, group names and assigned clusters.

b) Groups and experiment assignment: In the 'Groups' panel (Figure 1b) experimental groups can be added or removed, simply by pressing the 'add' (green 'plus' sign) button. Furthermore, experiments can be chosen from the 'module' section of the same panel. For example, figure 1b shows, there 2 groups of animals (Gpr88^{+/+} - CTRL and Gpr88^{-/-} group) have been registered for the 'place preference learning' experiment.

c) Clusters assignment: 'Clusters' panel is used to add or cross out clusters which represent the status of the cage components for an animal that is assigned to this cluster (Figure 1c). The larger squares represent the 4 corners of the IntelliCage and the two smaller squares per large one represent the two sides (left/right) of each corner. Each corner as well as side has three different color conditions: green (correct), red (incorrect), or yellow (neutral). The default setting for all corners and sides is the neutral condition. These three colors control the actions that the "Controller" module exerts in response to the behavior of each animal within each corner and side. This allows the experimenter to control the animal's behavior differentially, depending on the color condition of the actual corner and side where an animal performs a behavior.

After the registration of animals, groups, experiment and clusters, any designed experiment can be run and monitored online via the 'controller'.

The experimenter can implement any simple to complex tasks while designing an experiment to investigate the animal's behavior. Figure 1 shows different units of the IntelliCage designer tab, providing several options that can be implemented to design an experiment.

The 'Unit' section contains all the control elements that can be used to design the experimental modules by dragging them into the module Space and define their properties. There are four classes in total in the unit:

Tasks: Tasks contain the actions that the program can perform (Figure 2, panel: a).

Utils: All utility functions that control the information flow are listed here (Figure 2, panel: b).

Reporters: They can be used to keep track or count behavioral patterns that are not or difficult to extract from the data by a posteriori filtering (Figure 2, panel: c) and

Events: events contain all behavioral phenomena which the IntelliCage system can sense (Figure 2, panel: d).

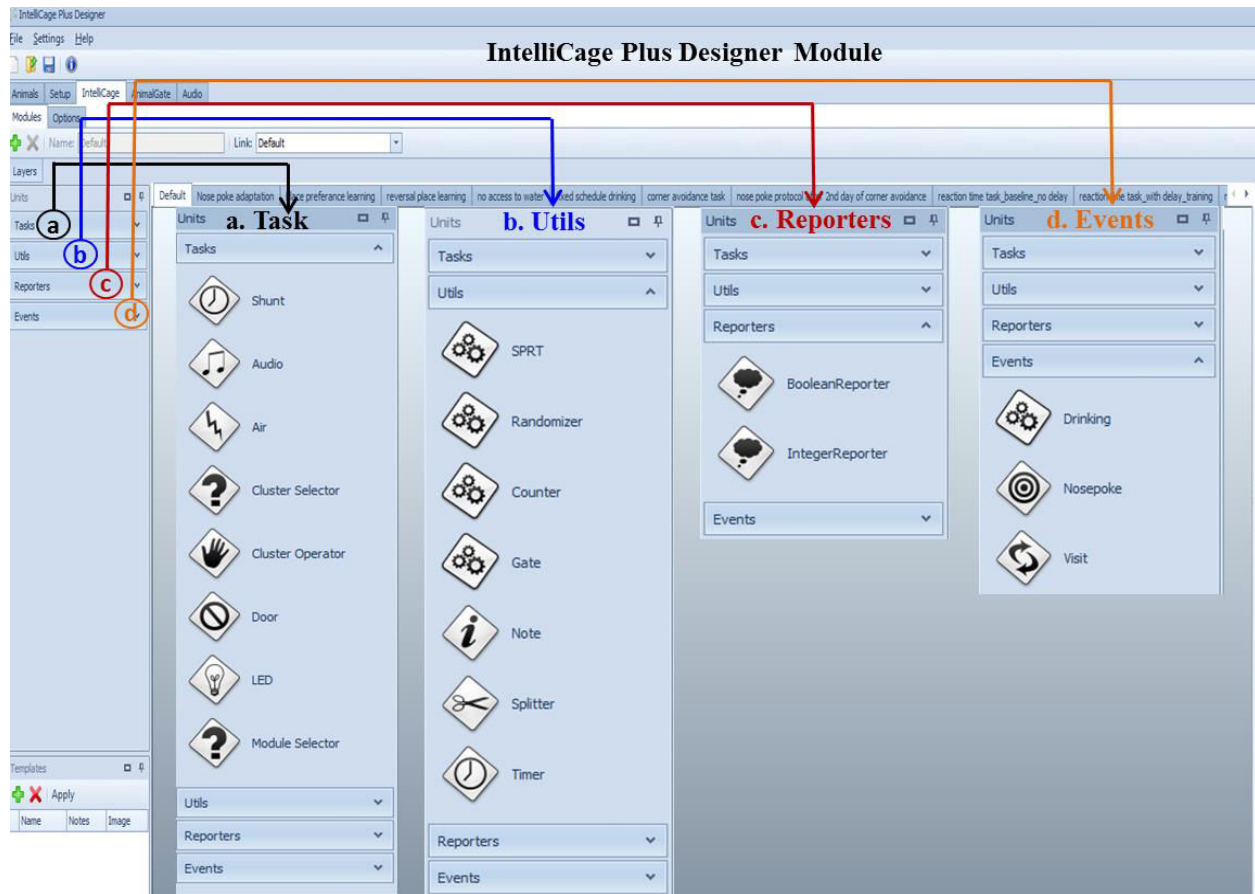


Figure 2: IntelliCage Plus Designer Module – IntelliCage tab to design the experiment: this tab provides several units allowing the experimenter to implement different conditions according to the experiment requirements a) Task, b) Utils, c) Reporters and d) Events.

These units can be used to design an experiment. For example, how the ‘place preference learning’ experiment was designed in my study using several above discussed units is described below.

The main purpose of this experiment was to test how quick the mice learn the rewarded location (with sucrose) in the IntelliCage and thus to investigate the cognitive performance of mice. A bottle of sucrose solution and water was placed in left and right side of each corner of the IntelliCage respectively. Each mouse was given access to water/sucrose only to a specific corner, assigned as ‘correct’ and furthermore sucrose side as ‘correct’ and water side as ‘neutral’. Door

in the correct corner could be opened to drink water/sucrose in response to nose-pokes for 5s (arrow 1, 2 and 3 represents these tasks in figure 3). Door was closed at the end of each visit (arrow 4 in figure 3) and thus each mouse had to perform the task from the beginning to drink again. All other corners were set as incorrect. All these activities were saved by the ‘controller’ of the IntelliCage as following:

Correct/incorrect visit/nose-poke: When a mouse visited and nose-poked in the correct corner or any of the other 3 incorrect corners.

Correct/neutral lick: When a mouse licked sucrose/water.

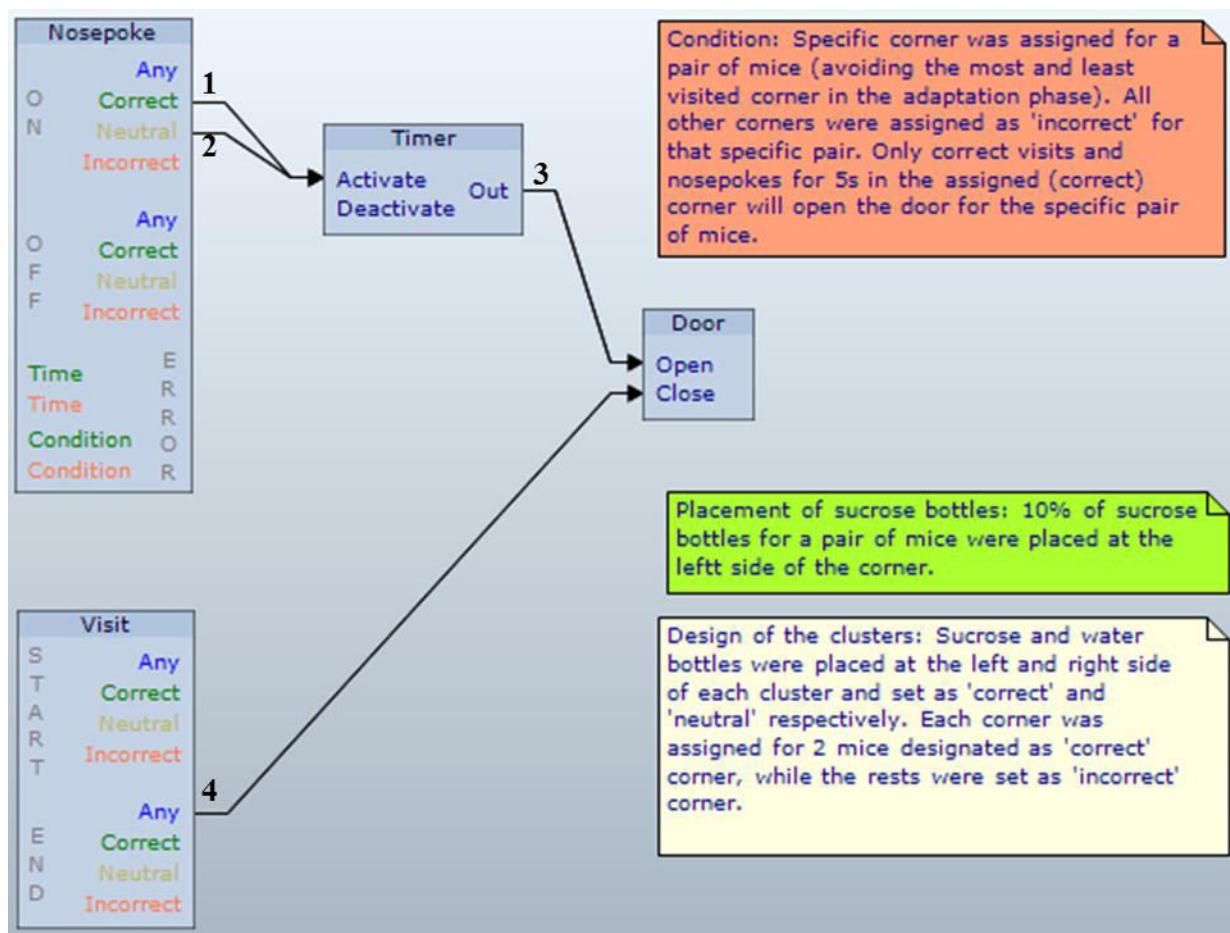


Figure 3: Design of the ‘place preference learning’ experiment: this tab provides several units allowing the experimenter to implement different conditions according to the experiment requirements a) Task, b) Utils, c) Reporters and d) Events.

These saved data were extracted by the ‘analyzer’ for further analyses.

4.4.4.3 Behavioral experiments with IntelliCage

Several experiments were carried out using IntelliCage in my study. One week before the behavioral tests mice were housed together, in the same groups as during the subsequent experimental procedures. To individually identify animals in the IntelliCage system all mice were subcutaneously injected with glass-covered microtransponders (11.5 mm length, 2.2 mm diameter; Trovan, ID-100) under isoflurane anesthesia. Microtransponders emit a unique animal identification code when activated by a magnetic field of the IntelliCage antennas. After transpondering procedure, all mice were moved from the housing facilities to the experimental rooms and adapted to the light-dark (LD) cycles (Light cycle: 7 am to 7 pm and dark cycle: 7 pm to 7 am).

7 to 8 weeks old, 16 CTRL and 16 *Gpr88*^{-/-} female mice were subjected to the 22-day IntelliCage protocol, divided into five phases: free adaptation, nose-poke adaptation, place preference learning, reversal learning and fixed schedule drinking.

Free adaptation: All mice were introduced to the IntelliCages separated according to the genotype (8 mice per IntelliCage). All doors were open and access to water was unrestricted so that mice could explore the IntelliCage and get adapted with the new environment. This adaptation phase is necessary in order to evaluate the spontaneous patrolling behavior of mice.

Nose-poke adaptation: The purpose of this phase was to train the mice how to open closed door in response to nose-pokes to drink. All doors were initially closed; thus no mice had free access to water bottles like the previous phase. But the doors could be opened once per visit only with nose pokes for 5 seconds (Task required to open the door in order to drink can be varied according to the design of the experiment by the experimenter. For example, door opens in response to 10 consecutive nose-pokes).

Place preference learning: This phase was carried out to evaluate the cognitive performance. During this phase access to the drinking bottles was restricted to only one of the IntelliCage learning chambers for each mouse and could be accessible by a nose-poke. Each mouse had access only to the target corner avoiding the most visited one during the ‘nose-poke adaptation’ phase. Each of the corner was provided with a bottle of water (right side) – assigned as ‘incorrect corner’ (corner with no reward) and sucrose (left side) – assigned as ‘correct corner’ (corner with reward).

Reversal learning: During this phase, rewarded location corner for each mouse was switched to the opposite as compared to the previous phase. Rest of the procedures were designed as same as the place preference learning phase.

Fixed schedule drinking: The purpose of this phase was to train the mice to drink in a fixed schedule. All sucrose bottles were subsequently replaced with water bottles. During this session, mice had access to water with doors opening in response to nose pokes only between the hours of 11:00–12:00 and 16:00–17:00. All doors were closed for the rest hours of the day.

4.4.4 IntelliCage data analysis

At first, all recorded experimental data were extracted using the IntelliCage ‘analyzer’ software. Data were then checked for outliers (> 3 times the standard deviation from the strain mean) for each phase of the experiment. One mouse was removed for outlying in the number of visits and nose-pokes in the free adaptation phase. Another one was removed from the experiment from nose-poke adaptation phase as it was not drinking anymore. A third one was removed during the fixed schedule drinking as it was outlying in the time spent in the corner. Mouse removed once in any phase, was automatically removed for the following phases. Then, the two cages housing CTRL mice and the two cages housing $Gpr88^{-/-}$ mice were compared to each other based on the total number of visits and nose-pokes in the first 2 phases. The two cages housing CTRL mice were indistinguishable to the two cages housing $Gpr88^{-/-}$ mice. Thus the mice were regrouped genotype-wise for the analysis. Data were analyzed using IBM SPSS statistic 20 (IBM, Armonk, NY, USA) to run two or three factors repeated-measures (RM) ANOVA. Whenever sphericity was violated a Greenhouse-Geisser correction was applied. For Pairwise comparison, a Sidak’s multiple comparison correction was applied when significant ANOVA results between factors were revealed. For mean comparison, one way ANOVA were performed when normality and equality of the variance were met, otherwise a non-parametric Mann-Whitney U-test was applied. An error probability level of $p < 0.05$ was accepted as statistically significant. All values are represented by means \pm S.E.M.

4.5 Principles of MRI

4.5.1 MR imaging

The encoding of the spatial information of the MRI signal requires three gradients, one for slice selection (along the z-axis) and two for frequency and phase encoding (along the x-y plane). The additional magnetic field of the *slice selection* gradient G_{slice} , varying linearly with position, is applied perpendicular to the desired slice plane resulting in a resonance frequency variation of the protons proportional to G_{slice} . An RF wave with the same frequency as that of the protons in a desired slice plane is applied simultaneously with G_{slice} . The RF pulse covers a certain bandwidth, which depends on the shape of the pulse and its duration, and the RF pulse bandwidth and the G_{slice} strength determines the slice thickness. The *phase encoding* takes place before the signal is recorded in the presence of the gradient G_{phase} which is applied for a limited time period in the certain direction. During that time, G_{phase} modifies the spin resonance frequencies, inducing spin dephasing and the rate of dephasing will depend on the location of the individual spin and the strength of the gradient. Interrupting G_{phase} , dephasing persists resulting in all the protons precessing in the same frequency but in different phases which lasts until the signal is recorded. Data can only be collected for one phase direction and multiple phase encoding steps can be obtained by changing either the duration or the amplitude of the phase gradient. The whole process is repeated n times for a resolution of n pixels in the y-direction and multiple phase

encoding steps can be achieved by acquiring multiple echoes or by subsequent excitations of the same slice. A *frequency encoding* gradient, which is also the read out gradient (G_{read}), is applied orthogonal to G_{phase} (e.g. horizontal or x-direction) while simultaneously receiving the signal. Spins precess location and tissue dependent at different resonance frequencies throughout the time G_{read} is applied. Frequency encoding only takes a few milliseconds (ms) of signal reading and the acquired MR signal corresponds to the overlap of the signals of all excited spins along the read out direction.

The raw data of detected signals, encoded in frequencies and phases, is collected during image acquisition in a temporary image space, an abstract 2D data collection matrix called *k-space*. *k-space* has 2 axes: k_x (each row or line) corresponds to a single phase direction (which is different line by line) and k_y (each column) is assigned to different precession frequencies collected during one phase encoding step. It is a graphic matrix of digitized MR data that represents the MR image before Fourier transformation is performed. Combining both phase and frequency information allows the creation of a grid in which each pixel possesses a distinct combination of phase and frequency codes. The data therefore represent many sine waves which build the MR image. The sampling density of k-space is dependent on the sampling rates of the readout gradient in x-direction and the number of phase encoding steps in y-direction (matrix size). The sampling rate should be at least twice the highest frequency within the signal in order to correctly compute the frequency of the signal (Nyquist-Theorem). So, the sampling rates in k-space define the maximal resolvable encoded frequency and therefore the spatial expansion (field of view, FOV) of the MR image. Furthermore, dividing the FOV by the matrix size gives the in-plane voxel size, and the depth of the voxel is determined by the slice thickness. To calculate the final MR image, k-space is mathematically processed using the inverse 2D *Fourier transform*. The Fourier transform is a mathematical procedure that decomposes a time varying signal into a sum of sine waves of different frequencies, phases and amplitude. This happens during MR data acquisition as described above where the time-varying MR signal intensity is obtained as a function of frequency. For generation of the MR image, the *inverse* Fourier transform is used, where the spatial frequency is decomposed into a variation of intensity (gray levels or proton density) over distance (the time domain becomes space domain) as for the MR image, the spatial distribution of tissue-specific proton density is of interest. Changes in spatial frequency therefore correspond to the rate at which image intensity values are changed in space and image features that change in intensity over short image distances or over long image distances correspond to high spatial frequencies or low spatial frequencies respectively. Thereby, most image information is available from the center of k-space containing low-spatial-frequency information (encoded by low-amplitude or short-duration gradient events) corresponding to general shape, contrast intensity of the image; whereas the periphery of k-space contains high-spatial-frequency information (encoded by high-amplitude or long-duration gradient events) corresponding to the details and sharpness of the image (resolution).

4.5.2 Relevant basic pulse sequences

There are number of different steps that make up an MR pulse sequence.

- Excitation of the target area
 - Switching on the slice-selection gradient,
 - Delivering the excitation pulse (RF pulse),
 - Switching off the slice-selection gradient.
- Phase encoding
 - Switching on the phase-encoding gradient repeatedly, each time with a different strength, to create the desired number of phase shifts across the image.
- Formation of the echo or MR signal
 - Generating an echo.
- Collection of the signal
 - Switching on the frequency-encoding or readout gradient,
 - Recording the echo.

These steps are repeated many times, depending on the desired image quality. A wide variety of sequences are used in medical MR imaging. Basics of some of those sequences are described below.

Spin echo (SE) sequences use a slice-selective 90° RF pulse for excitation, after which transverse magnetization decays with T_{2^*} . Dephasing occurs because some spins precess faster than others as a result of the static magnetic field inhomogeneities that are always present. This is why after half of the TE has elapsed, a 180° RF pulse is delivered to reverse or refocus the spins: those spins that were ahead before are now behind and vice versa. However, the spins that are now behind will catch up as they are still exposed to the same field inhomogeneities that caused the phase differences in the first place. Thus, after the second half of the TE interval has passed, all spins meet once again in phase. This is the moment at which the echo forms. The 180° refocusing pulse then serves to eliminate the effects of static magnetic field inhomogeneities (T_{2^*}) but cannot compensate for variable field inhomogeneities that underlie spin-spin interaction (T_2). Therefore, the magnetization decay that occurs after excitation is slower as it is a function of T_2 rather than T_{2^*} . Because of this decay, the transverse magnetization component is smaller at the time the echo is collected than immediately after excitation though the decrease in signal is less pronounced than it would be without application of the 180° refocusing pulse. SE sequences are characterized by an excellent image quality precisely because the effects of static field inhomogeneities are eliminated by application of the 180° refocusing pulse. The tradeoff is a fairly long scan time, which makes the sequence highly sensitive to motion artifacts. SE sequences are still used as the standard sequences for acquiring T1-weighted or PD-weighted images.

Gradient echo (GE) sequences employ the gradient coils for producing an echo rather than pairs of RF pulses. This is done by first applying a frequency-encoding gradient with negative polarity

to destroy the phase coherence of the precessing spins (dephasing). Subsequently, the gradient is reversed and the spins rephase to form a gradient echo. Since no 180° refocusing pulse is needed to generate GEs, very short TR can be achieved. As TR is a major determinant of the overall scan time of a GE sequence (and of most other sequences) much faster imaging is possible compared with SE and IR sequences, which is the most important advantage of GE imaging. As a result, GE sequences are less frequently troubled by motion artifacts and are thus preferred whenever a short scan time is desirable. A disadvantage of a short TR is that the time available for T_1 relaxation is also short. This may lead to saturation and reduce the signal to noise ratio (SNR) when a large flip angle is used. In the absence of 180° RF pulse, static field inhomogeneities are not compensated and the signal decays with T_2^* . The image contrast resulting from differences in the T_2^* decay of various tissues is called T_2^* contrast. The T_2^* contrast of GE images is affected by TE, which should be as short as possible to achieve optimal T_1 weighting (to minimize T_2^* contrast and to reduce susceptibility effects). Conversely, a longer TE is selected to accentuate T_2^* contrast. T_1 effects are minimized by simultaneously using a long TR. T_2^* -weighted images are useful to detect calcifications or deposits of blood products in tissues with a very short T_2 such as connective tissues. ***Echo planar imaging (EPI)*** uses the basis of GE sequence. A single excitation of the spins is followed by rapid switching of a strong frequency encoding gradient (Gread) to rapidly alternate between positive and negative values several times, forming multiple gradient echoes. Hereby each echo is encoded differently for spatial coordinates (a different degree of phase-encoding) allowing the sampling of several k-space lines within one shot. This ultrafast technique diminishes motion artifacts and enables the investigation of rapidly occurring changes in physiology (via DTI or rsfMRI).

4.5.3 Resting-state functional magnetic resonance imaging (rsfMRI)

Resting-state functional magnetic resonance imaging (rsfMRI) measures spontaneous low frequency fluctuations (0.01 - 0.1 Hz) in the blood oxygen level dependent (BOLD) signal to investigate the functional architecture of the brain at rest or in a state in the absence of any task or stimulation (Biswal et al., 1995; Lowe et al., 2000; Ogawa et al., 1990). Based on the ratio of oxygenated (diamagnetic) to deoxygenated (paramagnetic) hemoglobin in the blood (Pauling and Coryell, 1936), it is an indirect measurement of brain activity by detecting associated changes in blood flow. As neuronal activity increases, so do the metabolic demands for oxygen and nutrients triggering an increase in blood velocity and dilation of vessels, called the hemodynamic response (Kim and Ogawa, 2012). This leads to an over compensation resulting in increased oxygenation levels. Compared to an initial situation, where the paramagnetic nature of deoxygenated hemoglobin causes distortions in the magnetic field that results in a T_2^* decrease and thus a faster decay of the signal, a higher concentration of the oxyhemoglobin leads to increased T_2^* relaxation time and therefore a peak in T_2^* BOLD signal that takes place about 4-6 seconds following the neural activation (Buxton et al., 2004; Shmuel and Leopold, 2008). A GE-EPI sequence is made predominantly T_2^* weighted by using a low flip angle, long TE and TR (Chavhan et al., 2009). Although the BOLD signal is an indirect measurement of neural activity, it has been shown for simultaneously performed fMRI and electrophysiology experiments that the

BOLD signal corresponds to local electrical field potentials (Logothetis et al., 2001) which is likely to reflect changes in post-synaptic activity and thus neural firing. However, a distinction between excitation or inhibition is not possible, as both mechanisms consume energy (Logothetis and Wandell, 2004). Additionally, the hemodynamic response has been shown to vary both across subjects and across regions of the brain within the same subject, possibly depending on differences in vascularization patterns (Borowsky and Collins, 1989; Logothetis and Wandell, 2004), so the interpretation of the BOLD signal and its changes has to be conducted carefully.

Still, BOLD contrast not only depends on the oxygen consumption but a variety and interplay of physiological parameters can influence it. For example CO₂, a potent vasodilator which is increasing cerebral blood flow and hence the BOLD signal (Birn et al., 2006). Furthermore, respiration can change the arterial level of CO₂ and changing levels of CO₂ trigger chemoreflexes that change the depth and rate of subsequent breaths thus forming a feedback cycle (Birn et al., 2006). Additionally, partial pressure of CO₂ influences as well cerebral blood volume (Grubb et al., 1974), regions of high blood volume often show synchronized cardiac pulsations (Birn et al., 2006) and the heart rate of mice is influenced by the level of consciousness and body temperature. Taken together, monitoring of constant blood oxygen level, respiration, heart rate and body temperature is of high importance which has been implemented by using a pulse oximeter clipped to one hind paw; by using a pressure sensitive pad placed underneath the abdomen; using ECG electrodes on two front paws; and using a rectal temperature probe, respectively. Altered level of consciousness can influence the resting-state network pattern and activity (Guldenmund et al., 2012). Therefore, the choice and use of anesthesia is fundamental during imaging sessions of animals. For example, thiopental reduces blood pressure and flow in the cortex and is suggested to alter the feedback in neurovascular coupling leading to an increase in the magnitude and a reduction in the frequency of slow (< 0.1 Hz) fMRI BOLD signal fluctuations (Kiviniemi et al., 2000). Isoflurane is a vasodilator (Farber et al., 1997), allowing the hemodynamic fluctuations to effectively spread through larger areas and its usage was shown to result in less well-localized FC patterns (Williams et al., 2010). Another anesthetic used for animal imaging is medetomidine (MD), an α_2 -adrenergic receptor agonist and thus a favorable sedative suppressing alertness, arousal and hyperactivity (Nasrallah et al., 2012). However, it shows vasoconstrictive effects and may alter the coupling between neural activities and BOLD by stimulating cardiac output, blood pressure and cerebral blood flow (Nasrallah et al., 2012). Using MD sedated rats, a significant dose-dependent suppression of interhemispheric correlation has been demonstrated but not for the functional connectivity in the caudate putamen, a region with lower α_2 -receptor density suggesting a potential role of the adrenergic system in the functional connectivity (Nasrallah et al., 2012). Nevertheless, in the clinic, benefits of MD include among others blood pressure stabilization and sedation without respiratory depression or significant cognitive impairment (Pan et al., 2015). In rodents, no intubation is required and no catheterization is needed since it is administered subcutaneously (Zhao et al., 2008). Comparative investigation of stimulation-induced and resting-state fMRI signal during MD sedation demonstrated that observed low frequency fluctuation in rats reflect functional connectivity (Zhao et al., 2008).

4.5.4 T₂-weighted MRI

Different tissue types have different T₁ and T₂ values which facilitate the distinction between white matter (WM), gray matter (GM), and cerebrospinal fluid (CSF) in brain imaging. Tissues with short T₁ recover faster and their longitudinal magnetization values are larger, producing a stronger signal and brighter spot on the MR image. Tissues with short T₂ cause the signal to decay very rapidly and therefore have smaller signals and appear darker than materials with longer T₂ values. Furthermore, characteristic of the sample can be emphasized by altering TR and how soon after excitation data collection is started (TE). T₁ is coupled with TR whereas T₂ is depended on TE and by choosing certain TR or TE values, either T_{1w} (short TR and short TE), T_{2w} (long TR and long TE) or proton density weighted (long TR and short TE – minimally T_{2w} where the signal intensity is direct proportional to the proton density) images can be obtained. For a given imaging sequence all three type of contrast can contribute to the tissue contrast, but usually only one is emphasized. In T_{2w} imaging, contrast is predominantly caused by differences in T₂ values of the tissues and a long TE and a long TR are necessary to obtain a T₂ weighting. Tissues with long T₂ will give high signal intensity in the image while tissues with short T₂ times will appear hypointens (e.g. white matter with its high content of myelin). T_{2w} images are widely used for diagnosis, e.g. multiple sclerosis lesion detection which appear hyperintense. But quantitative characterization of white matter pathology is difficult as areas of oedemas, gliosis, demyelination or axonal loss cannot be distinguished from each other. Rapid Acquisition with Relaxation Enhancement (RARE) sequence, (Hennig et al., 1986) is used to acquire the high resolution T_{2w} morphological images. It is a modified multiple spin echo sequence, where a train of echoes is created by a number of refocusing pulses. As a different phase encoding gradient is applied to each echo, more than one *k-space* line can be collected per repetition. The number of excitations required to collect the full data set are reduced and the speed up factor (or turbo factor) is equal to the number of refocusing pulses applied.

4.5.5 Diffusion tensor magnetic resonance imaging (DT-MRI) and fiber tracking

Diffusion tensor imaging (DTI) is a technique that can measure macroscopic axonal organization in brain. DTI uses the motion of water molecules as a probe to infer the neuroanatomy. Mobility of water molecules can be characterized by a physical constant, the *diffusion coefficient* (*D*). The diffusivity depends on the size of the molecules, the temperature and the viscosity of the medium. Diffusion of molecules can be restricted by macromolecules or membranous boundaries (e.g. myelin sheath of axons) and therefore oriented along given direction (as for nerve fibers), which would be referred to as *anisotropic diffusion*. On the contrary, if diffusion is free (unrestricted) and the same in all spatial directions, it is termed *isotropic diffusion* (e.g. in cerebrospinal fluid). DTI uses the anisotropy to estimate the axonal organization of the brain. Therefore, tissues can be differentiated according to their cellular structure and moreover, diffusion data can additionally provide indirect information about certain pathological modifications (e.g. infarction, tumors, edema, plaques), where diffusivity is changed. Highlighting the differences in water molecule

mobility, irrespective of their direction of displacement, is called *diffusion-weighted Imaging* (DWI). Hereby, a spin echo sequence is adapted to diffusion imaging by adding two strong-pulsed magnetic field gradients (= diffusion gradients) before and after the 180° RF pulse, with a duration δ and a time difference Δ (= diffusion time). After dephasing by the first gradient, only the spins of the immobile water molecules are rephased by the second gradient, whereas diffusing spins move away and are not rephased, resulting in a decrease of the signal. Diffusion sequences are T₂ weighted sequences with induced diffusion weighting by applying diffusion gradients in at least three spatial directions (\cong three repetitions of the acquisition). The degree of diffusion weighting of the final image is hereby described by the *b-value* (or b-factor, unit: second/mm²) which depends on the characteristics of the diffusion gradients: amplitude, time of applied gradients and duration between the paired gradients (Le Bihan et al., 1986). To remove T₂ information and to measure the diffusion coefficient, at least two measurements at different b values are required (typically b-factor = 0 s/mm² for T₂-weighted and b-factor = 1000 s/mm² for diffusion weighting). DTI is a type of mathematical processing of DWI datasets for an indirect measurement of the degree of anisotropy and structural orientation. By performing at least six diffusion weighted measurements along non-collinear directions, it is possible to calculate for each voxel a 3D ellipsoid (diffusion tensor) which represents the average diffusion distance in each direction (Basser et al., 1994). Hereby, the lengths of the longest, middle, and shortest axes are called eigenvalues (e_1, e_2, e_3), representing the magnitude of diffusion, and their orientation is described by the eigenvectors, ($\lambda_1, \lambda_2, \lambda_3$). The eigenvectors and eigenvalues are independent of the direction of the applied gradients in MRI. Using eigenvectors, different parameters can be determined that provide valuable information about the brain structure. For example, *Axial diffusivity*, provides the diffusion rate along the main axis of diffusion, or in the case of CNS environment the diffusion parallel to fiber tracts ($D_{||} = \lambda_1$); *radial diffusivity* is the rate of diffusion in the transverse direction or perpendicular to fiber tracts ($D_{\perp} = (\lambda_2 + \lambda_3)/2$); or *fractional anisotropy (FA)* (degree of diffusion anisotropy with values between 0 ($\lambda_1 \cong \lambda_2 \cong \lambda_3$; isotropic or equally restricted diffusion) and 1 (restricted diffusion along one direction, i.e. $\lambda_1 > \lambda_2 \cong \lambda_3$). As cerebral anatomy shows strong correlation between orientations of the main eigenvector and direction of WM tracts, tractography methods with different fiber tracking algorithms have been developed to display fiber tract orientation (Mori et al., 2001). Tractography (*fiber tracking*) is the 3D reconstruction of fiber tract trajectories and basic colors give information how fibers are oriented (red: mediolateral (x-axis), green: dorsoventral (y-axis) and blue: rostrocaudal (z-axis)). Fiber tracking is an approximation of neuronal pathways by converting discrete voxel information into continuous tracking lines that finally form fiber tracts.

Remodeling of Sensorimotor Brain Connectivity in *Gpr88*-Deficient Mice

Tanzil Mahmud Arefin,¹⁻⁴ Anna E. Mechling,^{1,2} Aura Carole Meirsman,^{5,6} Thomas Bienert,¹ Neele Saskia Hübner,^{1,2} Hsu-Lei Lee,¹ Sami Ben Hamida,^{5,7} Aliza Ehrlich,^{5,7} Dan Roquet,⁸ Jürgen Hennig,¹ Dominik von Elverfeldt,¹ Brigitte Lina Kieffer,^{5,7} and Laura-Adela Harsan^{1,8,9}

Abstract

Recent studies have demonstrated that orchestrated gene activity and expression support synchronous activity of brain networks. However, there is a paucity of information on the consequences of single gene function on overall brain functional organization and connectivity and how this translates at the behavioral level. In this study, we combined mouse mutagenesis with functional and structural magnetic resonance imaging (MRI) to determine whether targeted inactivation of a single gene would modify whole-brain connectivity in live animals. The targeted gene encodes GPR88 (G protein-coupled receptor 88), an orphan G protein-coupled receptor enriched in the striatum and previously linked to behavioral traits relevant to neuropsychiatric disorders. Connectivity analysis of *Gpr88*-deficient mice revealed extensive remodeling of intracortical and cortico-subcortical networks. Most prominent modifications were observed at the level of retrosplenial cortex connectivity, central to the default mode network (DMN) whose alteration is considered a hallmark of many psychiatric conditions. Next, somatosensory and motor cortical networks were most affected. These modifications directly relate to sensorimotor gating deficiency reported in mutant animals and also likely underlie their hyperactivity phenotype. Finally, we identified alterations within hippocampal and dorsal striatum functional connectivity, most relevant to a specific learning deficit that we previously reported in *Gpr88*^{-/-} animals. In addition, amygdala connectivity with cortex and striatum was weakened, perhaps underlying the risk-taking behavior of these animals. This is the first evidence demonstrating that GPR88 activity shapes the mouse brain functional and structural connectome. The concordance between connectivity alterations and behavior deficits observed in *Gpr88*-deficient mice suggests a role for GPR88 in brain communication.

Keywords: default mode network; *Gpr88*; mouse brain functional connectivity

Introduction

NEURONS FORM STRUCTURAL and functional networks that drive brain function and behavior (Van Essen, 2013). Connectome genetics, or the analysis of brain connectivity in relation to gene expression and function, addresses how disease

genes influence brain connectivity in humans (Richiardi et al., 2015; Thompson et al., 2013), and also links gene transcriptional patterns with neural network activities in both humans and mice (Richiardi et al., 2015). These studies, however, remain correlative in nature. Deep understanding of cognitive and behavioral development, adaptation, or dysfunction also

¹Department of Radiology, Medical Physics, Medical Center University of Freiburg, Faculty of Medicine, University of Freiburg, Freiburg, Germany.

²Faculty of Biology, University of Freiburg, Freiburg, Germany.

³Bernstein Center Freiburg, University of Freiburg, Freiburg, Germany.

⁴Bernard and Irene Schwartz Center for Biomedical Imaging, Department of Radiology, New York University School of Medicine, New York, New York.

⁵Département de Médecine Translationnelle et Neurogénétique, Institut de Génétique et de Biologie Moléculaire et Cellulaire, INSERM U-964, CNRS UMR-7104, Université de Strasbourg, Illkirch-Graffenstaden, France.

⁶Neuroscience Paris Seine, Institut de Biologie Paris Seine, CNRS UMR 8246/INSERM U1130/Université Pierre et Marie Curie, Paris, France.

⁷Douglas Mental Health Institute, Department of Psychiatry, McGill University, Montreal, Quebec, Canada.

⁸Engineering Science, Computer Science and Imaging Laboratory (ICube), Integrative Multimodal Imaging in Healthcare, University of Strasbourg—CNRS, Strasbourg, France.

⁹Department of Biophysics and Nuclear Medicine, Faculty of Medicine, University Hospital Strasbourg, Strasbourg, France.

requires adapted approaches to identify molecular and network determinants of healthy and pathological brains. Our recent work, allying targeted mouse mutagenesis and fine-grained magnetic resonance (MR)-based neuroimaging of live animals, revealed a gene-to-network signature for the mu opioid receptor with predominant alteration of pain/aversion networks (Mechling et al., 2016). This proof-of-principle study, based on open-ended whole-brain connectivity analysis, demonstrates the power of combined gene knockout/MRI to decipher consequences of a single gene inactivation on brain networks and potentially predict behavioral outcomes of genetic dysfunction. In this study, we developed a similar approach to tackle the function of the orphan *Gpr88* (G protein-coupled receptor 88) receptor gene, encoding another G protein-coupled receptor whose ligand remains unknown, and discovered brain network mechanisms underlying major GPR88-controlled behaviors.

GPR88 is a striatal-enriched G protein-coupled receptor, expressed in rodents, monkeys, and humans during development and in adulthood (Massart et al., 2016). In humans, the *Gpr88* gene was associated with bipolar disorders and schizophrenia (Del Zompo et al., 2014), and the potential of GPR88 as a target to treat psychiatric disorders has attracted increasing interest. In mice, deletion of the *Gpr88* gene has been studied with a primary focus on striatal-mediated behaviors, and null mutant mice show motor coordination deficits (Logue et al., 2009; Meirsman et al., 2016a; Quintana et al., 2012), reduced prepulse inhibition (Logue et al., 2009), stereotypies (Meirsman et al., 2016a), and modified cue-based learning (Meirsman et al., 2016a; Quintana et al., 2012). Recently, we found that *Gpr88* knockout mice also show improved hippocampal-dependent learning and reduced anxiety levels (Meirsman et al., 2016b). This receptor therefore controls a much larger behavior repertoire than anticipated and, beyond motor activity, also engages spatial learning, emotional processing, and the evaluation of environmental stimulus value. In this study, we examined *Gpr88* knockout mice using combined resting-state functional MR imaging (rsfMRI)/diffusion tensor imaging (DTI) in live animals to identify neural networks depending on *Gpr88* gene activity and used open-ended whole-brain connectivity analysis to determine predominant alterations that would predict major functions of *Gpr88* related to neuropsychiatric conditions.

Materials and Methods

Additional detailed methods are provided in the Supplementary Data (Supplementary Data are available online at www.liebertpub.com/brain).

MRI experiments

Animals. MRI was performed on two groups ($n = 14$ /group) of 7–8-week-old live adult male mice (74.9% C57B/6J, 25% 129/SvPas, 0.05% FVB/N, 0.05% SJL/J): wild-type control mice (CTRL: $n = 14$) and the *Gpr88* knockout group (*Gpr88*^{-/-}: $n = 14$), respectively. All animal experiments were performed in accordance with the guidelines and ethics on animal experimentation established by the German and French laws: ethical allowance 35_9185.81/G-13/15 from Regierungspräsidium Freiburg, Germany, and CREMEAS, 2003-10-08-[1]-58, Strasbourg-France, respectively.

Animal preparation. The animals were briefly anesthetized with isoflurane during imaging preparation (stereotaxic fixation of the mouse head, attachment of physiological monitoring devices). To avoid the inhibitory effects of isoflurane on the blood oxygen level-dependent (BOLD) signal, anesthesia was further switched to medetomidine (MD—Domitor; Pfizer, Karlsruhe, Germany). Moderate MD sedation was initially induced by a subcutaneous (s.c.) bolus injection (0.3 mg MD/kg body weight in 100 μ L 0.9% NaCl solution); 15 min later, the animals received a continuous s.c. infusion of MD through an MRI-compatible catheter (0.6 mg/kg body weight in 200 μ L/h) subcutaneously inserted at the mouse shoulder level. After rsfMRI acquisition, MD infusion was stopped and replaced by anesthesia through isoflurane (~ 1.5 vol%) for further scanning performed on respiration triggering. Isoflurane induces a deeper anesthesia, important for avoiding the movement artifacts for diffusion imaging. Mouse physiological conditions (including temperature, respiration, and blood oxygen saturation) were monitored continually during the imaging session.

MRI data acquisition. Mouse brain MRI data were acquired with a 7 T small-bore animal scanner (Biospec 70/20, Bruker, Germany) and a mouse head adapted CryoCoil (MRI CryoProbe, Bruker, Germany).

- rsfMRI: Data were acquired with T₂*-weighted, single-shot, gradient-echo echo-planar imaging (GE-EPI) sequence (echo time [TE]/repetition time [TR] = 10 ms/1700 ms). The mouse brain (excluding the cerebellum) was covered using 12 axial slices of 0.7 mm thickness, with a field of view (FOV) of 19.2 \times 12 mm² and an acquisition matrix of 128 \times 80, which resulted in a planar resolution of 150 \times 150 μ m². Two hundred volumes were recorded in an interlaced manner for each run.
- T₂: High-resolution morphological images were acquired using Turbo rapid acquisition with relaxation enhancement (RARE) T₂ sequence (TE/TR = 50 ms/6514 ms, two averages at RARE factor of 4). The whole brain, including cerebellum, was covered using 48 slices (0.3 mm slice thickness) at planar spatial resolution of 51 \times 51 μ m² with an FOV of 1.3 \times 1.0 cm² and an acquisition matrix of 256 \times 196.
- High-angular resolution diffusion imaging (HARDI) was performed using four-shot DTI-EPI sequence. Twenty-five axial slices of 0.5 mm thickness were acquired at a resolution of 94 \times 94 μ m² with an FOV of 1.5 \times 1.2 cm² and an acquisition matrix of 160 \times 128, covering the equivalent partition of the brain as for the rsfMRI scan (TE/TR = 27 ms/3750 ms); $\Delta = 10$ ms, diffusion gradient duration (δ) = 4 ms, b factor of 1000 s/mm², 30 noncollinear diffusion gradient directions.

MRI data preprocessing. Imaging data were preprocessed (Mechling et al., 2016) using MATLAB (The MathWorks, Natick, MA) along with the fMRI tool of statistical parametric mapping SPM8* and its SPM Mouse[†] toolbox (Sawiak et al., 2013), which includes functions for realignment, coregistration, and segmentation of mouse brain data (see detailed procedure in Supplementary Data: “Data preprocessing”). Briefly, the

*www.fil.ion.ucl.ac.uk/spm

†www.spmmouse.org

preprocessing pipeline included an initial realignment of the 200 volumes of rsfMRI data to the first one using a least square approach and a six-parameter rigid body transformation in space to correct for motion in each single scan. The coregistration function also was used to align the rsfMRI (first time point) volumes of each mouse to its respective A_0 images obtained from HARDI (HARDI acquisition with a diffusion weighting factor $b_{\text{factor}} = 0 \text{ mm}^2/\text{s}$ —no diffusion gradient applied) and T_2 image volume. SPM Mouse brain template was further refined by including additional high-resolution mouse brain images to create a tissue probability map (TPM) template. We used this template for spatial normalization and alignment of rsfMRI mouse brain images, morphological T_2 -weighted images, the A_0 images, and the parametric maps derived from diffusion tractography (fiber density [FD] and fractional anisotropy maps). We applied a Gaussian smoothing with a kernel of full width at half maximum of $0.4 \times 0.4 \times 1 \text{ mm}^3$ to all TPM-aligned rsfMRI image volumes (Mechling et al., 2014). Furthermore, the whole brain was parceled using an in-house-developed MATLAB and Allen Mouse Brain Atlas (AMBA) (Lein et al., 2007). The AMBA was aligned and resliced to our template using the SPM8 toolbox, changing its initial resolution to our template's resolution of $165 \times 230 \times 135$ voxels with a voxel size of $0.07 \times 0.07 \times 0.07 \text{ mm}^3$.

MRI data postprocessing

Resting-state functional magnetic resonance imaging

Independent component analysis. High-dimensional (100 components) spatial group independent component analysis (ICA) (Calhoun et al., 2001) using the MATLAB-based toolbox GIFT (group ICA of fMRI toolbox—v1.3i, www.nitrc.org/projects/gift) was carried out on 28 combined control (CTRL) and $Gpr88^{-/-}$ datasets. Infomax algorithm was used to decompose the entire BOLD data set into spatially independent components (ICs) without any hypothesis paradigms (Hyvärinen and Oja, 2000). We further investigated the robustness of the identified components using ICASSO algorithm (Himberg et al., 2004).

Estimation of the number of components is an important step while decomposing the entire BOLD signal into spatially ICs or sources. Underestimation of the components may result in mixing various components (Margulies et al., 2010; van de Ven et al., 2004), whereas overestimation can result in splitting reliable networks (Esposito et al., 2003; Moritz et al., 2005), decreasing the stability of IC estimates (Li et al., 2007). Therefore, we used ICASSO algorithm (Himberg et al., 2004) to assess the stability pattern by bootstrapping and randomizing initial conditions for different numbers of ICs. The quality index I_q (values ranging from 0 to 1) was used as a quantitative measure of robustness of the identified components evaluating compactness and isolation of each cluster (Huebner et al., 2016; Mechling et al., 2014). We verified the consistency of the results when progressively achieving a high spatial definition (in accordance to fine anatomical details) of the functional clustering patterns with 10, 15, 20, 40, 60, 80, 100, and 120-ICASSO, respectively. Using the percentage of components revealing quality index (I_q) > 0.75 as a stability criterion, we observed a clear degradation of the IC estimates for 120-ICASSO, justifying our choice of 100-ICASSO analysis.

The mean resulting patterns were displayed as spatial color-coded z -maps onto T_2 -weighted morphological images (threshold $|z| > 3$, corresponding to $p < 0.00135$) and on coregistered AMBA (Lein et al., 2007). The color coding represents the dependence of the time course in each voxel compared with the mean time course of the respective component in arbitrary units. Coregistration with AMBA allowed for automatic identification of anatomic brain areas covered by IC patterns. From the 100-ICASSO results, 12 artifactual components related to cerebrospinal fluid, vascular, or movement-related pseudo activations were excluded from analysis after visual inspection and overlay on AMBA. From these aggregate components and the original data, we computed spatial, back-reconstructed, individual subject components using a spatial-temporal regression approach (see also Supplementary Data). We further used the back-reconstructed, individual spatial maps to create incidence maps for each IC. Relevant examples are the incidence maps illustrating the patterns of SS, CP, ACB, and AMY functional clusters (Supplementary Fig. S1c; Supplementary Data are available online at www.liebertpub.com/brain). The incidence maps illustrate the spatial distribution and the reproducibility of the IC pattern over each animal group (CTRL and $Gpr88^{-/-}$). The color-coded incidence of a voxel reflects in how many of the animals it was found to belong. These examples show low intragroup variability of ICA patterns and extremely high similarity between group patterns.

The results substantiate our further approach of using the meaningful 88 group ICASSO functional clusters (Supplementary Fig. S2) as nodes in the generation of mouse brain functional connectivity matrices (MBFC) of CTRL and $Gpr88^{-/-}$ groups of animals through partial correlation (PC). Conducting the 100-ICASSO separately on each animal group would have eventually resulted in slightly different nodes of connectivity and difficulties to directly compare the group results.

Pearson PC analysis. The PC coefficients (Pearson) between each pair of ICs derived with ICASSO were calculated and used to create an 88×88 adjacency PC matrix for each animal as well as two average matrices, representative for each experimental group (group-specific PC matrices: Fig. 1a). Each element of the matrix represented the strength of direct connectivity between two components (nodes). The PC matrices were then normalized using Fisher's z -transformation. The significance of positive and negative correlations between pairs of components was further assessed by using a two-sided one-sample t -test and thresholding at $p < 0.05$.

Direct intergroup (CTRL vs. $Gpr88^{-/-}$) statistical comparison of the group matrices was further performed. The functional connectivity (FC) alterations between groups were considered significant after assessment using a two-sample t -test ($p < 0.01$; false discovery rate [FDR] corrected). A group comparison matrix (GCM) was generated (Fig. 1b) that color coded the statistically significant intergroup differences of connectivity. GCM was further used to count the significantly changed connections for each node (IC) and we further ranked nodes on the basis of highest number of such statistically significant differences in connectivity across the two genotypes (Fig. 1c).

Seed-based correlation analysis. To evaluate the alterations of functional networks, several brain areas that showed high number of correlation alterations between groups were

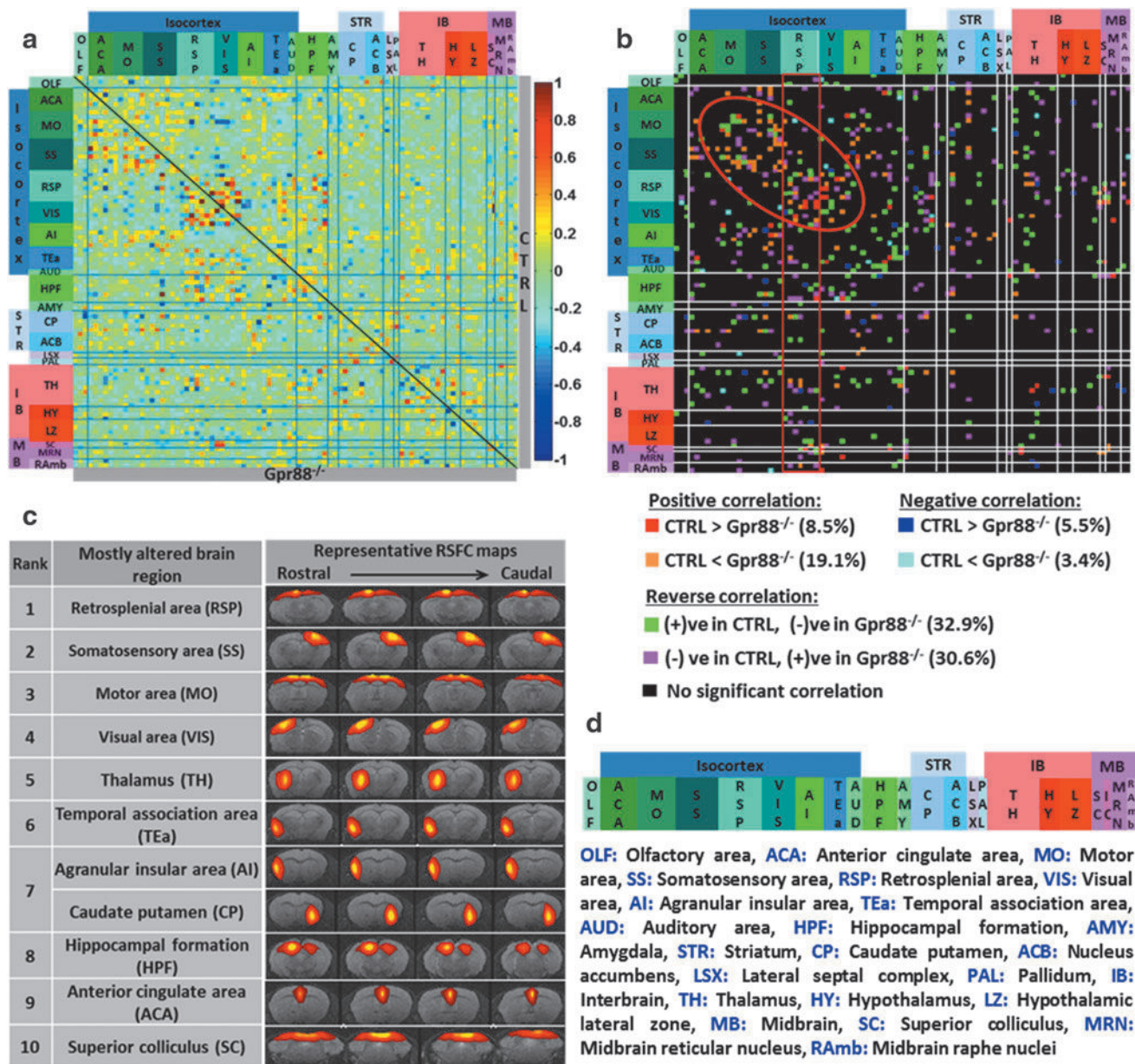


FIG. 1. Quantitative mapping of functional network alterations in *Gpr88*^{-/-} mice reveals a strong *Gpr88*-dependent activity signature in live animals: **(a)** Group-specific resting-state FC matrices (CTRL above and *Gpr88*^{-/-} group below the diagonal), including both positive and negative internodal correlations (derived via partial correlation methods). The nodes were defined through functional segregation using 100-ICASSO. Functional nodes were grouped and assigned to corresponding anatomical regions through coregistration on the Allen Mouse Brain Atlas **(d)**. **(b)** Direct intergroup (CTRL vs. *Gpr88*^{-/-}) statistical comparison of connectivity matrices (two-sample *t*-test, $p < 0.01$, FDR corrected) is shown as a 2D matrix. The *Gpr88* genetic inactivation induced widespread modifications of internode connectivity. The red circle points to the cluster of strong intracortical FC remodeling in the absence of *Gpr88*, whereas the red square points to extensive significant FC alterations of the RSP area connectivity. **(c)** Nodes of brain area with highest number of statistically significant connectivity changes are ranked (two-sample *t*-test, $p < 0.01$, FDR corrected). Their functional pattern is overlaid on four T₂-weighted anatomical images. From top to bottom: retrosplenial area (RSP), somatosensory area (SS), motor area (MO), visual area (VIS), thalamus (TH), temporal association area (TEa), superior colliculus (SC), caudate-putamen (CP), agranular insular area (AI), hippocampal formation (HPF), and anterior cingulate area (ACA). **(d)** Assignment of brain regions from rostral to caudal direction and their corresponding localization on the sagittal mouse brain template adapted from the Allen Mouse Brain Atlas. The anatomical overlap of components was identified using a MATLAB-based and in-house-developed postprocessing tool, which is based on coregistration of the data on the Allen Mouse Brain Atlas (AMBA) (Lein et al., 2007) (<http://mouse.brain-map.org/static/atlas>). We assigned the component to the region or anatomical subdivision (in case of large areas) with maximum overlap. Nevertheless, components are partly touching other regions (subdivisions). CTRL, control; FC, functional connectivity; FDR, false discovery rate; GPR88, G protein-coupled receptor 88; RSP, retrosplenial.

selected as the regions of interest (ROIs). As all the data were normalized onto AMBA, each ROI was extracted using this atlas and used as the seed region to perform FC analysis of preprocessed rsfMRI data. Correlation coefficients were then computed (two-tailed *t*-test, $p < 0.001$) between the seed region and the averaged time series of the remaining whole brain for each group and were converted to *z* values using Fisher's *r*-to-*z* transformation. We further performed voxel-level general linear model ($p < 0.001$) corrected for multiple comparisons using a random field theory approach (Worsley et al., 1996) to statistically evaluate FC remodeling on the group level for each specific seed.

Diffusion-based tractography. Modifications in the brain structural connectivity were assessed using HARDI and further tractography using a global fiber tracking approach (Harsan et al., 2013; Reisert et al., 2011). FD maps were used to measure brain microstructural modifications. Statistically significant differences were evaluated using a two-sample *t*-test ($p < 0.05$, familywise error [FWE] corrected) (detailed procedure is described in Supplementary Data).

Results

GPR88 expression in the mouse brain

We verified the expression pattern of GPR88 in the control (CTRL) mice by *in situ* hybridization (Supplementary Fig. S1a). We observed the receptor expressed in the layers 4 and 5 of the somatosensory cortex (SS), caudate-putamen (CP), amygdala, nucleus accumbens (ACB), and olfactory tubercle (OT) in support of several previously reported literatures (Becker et al., 2008; Ghatge et al., 2007; Massart et al., 2016; Mizushima et al., 2000; Van Waes et al., 2011).

Elementary functional clusters identified through group 100 ICA

We applied high-dimensional, data-driven spatial ICA (using 100 components) combined with ICASSO on rsfMRI datasets from CTRL and *Gpr88*^{-/-} animal groups. Eighty-eight reliable functional clusters were identified whose spatial pattern covered neuroanatomical regions defined by the Allen Mouse Brain Atlas (AMBA) (Supplementary Fig. S2). We further validated the reproducibility of the group ICASSO patterns in each animal and in each experimental group through back reconstruction (see the Materials and Methods section and Supplementary Fig. S1b, c). The results demonstrated low intragroup variability of the component pattern and extremely high similarity between groups. We could associate the spatial pattern of some of these components with areas strongly expressing *Gpr88* receptors in normal conditions (Supplementary Fig. S1b). Both left and right hemispheric patterns were obtained and presented in Supplementary Figure S1 for cortical (SS) and subcortical areas (CP, ACB, and AMY). We further used the 88 group ICASSO functional clusters (Supplementary Fig. S2) as nodes in the generation of resting-state brain FC (rsFC) matrices of CTRL (Fig. 1a—above the diagonal) and *Gpr88*^{-/-} (Fig. 1a—below the diagonal) groups of animals (two-sided one-sample *t*-test, $p < 0.05$) (see the Materials and Methods section). All these nodes correspond to anatomically well-defined brain regions and were rearranged according to their association with brain areas in the rostrocaudal axis (Fig. 1d).

Deletion of *GPR88* receptor induces extensive FC remodeling of the mouse brain

We quantitatively evaluated the impact of GPR88 receptor deletion on the mouse brain FC using direct statistical intergroup comparison of CTRL and *Gpr88*^{-/-} MBFC matrices (see the Materials and Methods section and Fig. 1b). We detected significant and widespread alterations of internode connectivity (Fig. 1b; two-sample *t*-test, $p < 0.01$, FDR corrected). The 2D matrix representation (Fig. 1b) captured the causal effect of targeted *Gpr88* gene disruption at the level of whole brain networks. The extent of *Gpr88*-dependent connective activity appeared surprisingly broad within cortical areas, particularly retrosplenial (RSP), sensory areas (somatosensory [SS], and motor cortex [MO]), as well as the visual cortex (VIS) (Fig. 1b, red circle). Furthermore, to define the *Gpr88* signature on the mouse brain connectome, we ranked the brain areas on the basis of the number of statistically significant differences ($p < 0.01$, FDR corrected) in connectivity across the two genotypes (Fig. 1c). There was a clear dominance of connectivity changes for cortical-related nodes, with seven nodes from the top 10 being associated with isocortex. RSP showed the strongest remodeling (rank 1, Fig. 1c) of connectivity. Along with this area—classically included in the default mode network (DMN) across species (Raichle, 2015), VIS (rank 4, Fig. 1c), thalamus (TH, rank 5, Fig. 1c), temporal association area (TEa, rank 6, Fig. 1c), hippocampal formation (HPF, rank 8, Fig. 1c), and anterior cingulate area (ACA, rank 9, Fig. 1c) are brain regions present in the top 10 of our hierarchy. They were previously described as part of a DM-like network in the C57Bl/6 mouse strain (Liska et al., 2015; Hübner et al., 2017). This result suggests a strong modification of resting-state brain activity in *Gpr88*^{-/-} mice involving DMN.

Additional to this network, the intergroup comparison of FC matrices revealed significant changes (two-sample *t*-test, $p < 0.01$, FDR corrected) of the MO (rank 3, Fig. 1c) and the sensory (SS, rank 2; and VIS, rank 4, Fig. 1c) cortical connectivity, as well as the subcortical striatal (particularly involving the caudate-putamen [CP], rank 7, Fig. 1c) and HPF (rank 8, Fig. 1c) circuitries. Moreover, superior colliculus (SC) of the midbrain area—a major node for mediating sensorimotor transformations (Simon, 2008), was ranked tenth among the most altered brain regions (SC, rank 10, Fig. 1c). All together, these findings suggest several salient features of the *Gpr88*^{-/-} mouse brain architecture. These are massive intracortical and cortico-subcortical rsFC modifications, particularly involving DMN core areas along with the sensorimotor and cortico-striatal pathway. To further strengthen these findings, we performed seed analysis using the brain areas highlighted in the ICASSO-based ranking and anatomically defining the seeds on the basis of coregistration with the AMBA (see the Methods section).

Altered DMN patterns in *Gpr88*^{-/-} mice

The RSP was ranked on top of substantial FC differences across CTRL and *Gpr88*^{-/-} mice. We selected bilateral RSP as a seed region for mapping its connectivity patterns across the whole brain (two-tailed *t*-test, $p < 0.001$) and identify the DMN. Similar to previous work using the seed-based correlation approach (Hübner et al., 2017; Sforzini et al., 2014), our results support the idea of a mouse DMN network with

RSP as a core area. Its positive connections with the medial and caudal ACA, HPF, TEa, and VIS system (Fig. 2a) portray, in the CTRL group, similarities with the posterior DMN obtained for humans (Di and Biswal, 2014). Relative to this CTRL pattern, RSP in the $Gpr88^{-/-}$ group exhibited clearly reduced FC with ACA, TEa, and massive decreased FC with TH (Fig. 2a vs. b, c). This result demonstrates modification of the DMN in mice lacking the GPR88 receptor. This major modification, which we did not observe in mu opioid receptor knockout mice in our previous work (Mechling et al., 2016), is consistent with the large extent of behavioral alterations reported in $Gpr88^{-/-}$ mice.

Remodeling of motor and sensory cortical rsFC in $Gpr88^{-/-}$ mice

Sensory (SS) and motor (MO) areas were ranked second and third in the quantification of FC alterations of $Gpr88^{-/-}$ mice. Seed-based analysis using MO as ROI revealed extensive cortical and subcortical rsFC modifications in the $Gpr88^{-/-}$ group (Fig. 3a). We quantified the group statistical significance of the alterations using voxel-level general linear modeling corrected for multiple comparisons using the random field theory approach ($p < 0.001$, see the Materials and Methods section). When compared with the CTRL group, $Gpr88^{-/-}$ MO showed salient features of reduced (Fig. 3b, CTRL > $Gpr88^{-/-}$) or stronger (Fig. 3b, CTRL < $Gpr88^{-/-}$) rsFC with specific brain areas.

From positive correlation analysis (Fig. 3a, correlations from 0 to 1, and Fig. 3b—positive correlation), the $Gpr88^{-/-}$ group showed decreased (CTRL > $Gpr88^{-/-}$) FC between MO and orbitofrontal cortex, agranular insular area (AI), and

limbic areas (prelimbic cortex—PL, infralimbic cortex—ILA, nucleus accumbens—ACB), as well as caudal RSP and parietal cortex (PTLp). However, stronger rsFC (Fig. 3b, positive correlation CTRL < $Gpr88^{-/-}$) was quantified between MO and CP and MO and SS, as well as within the MO. These strong modifications of striato-motor connectivity are particularly relevant to highest $Gpr88$ expression in the striatum and the hyperactive phenotype observed in this model (Logue et al., 2009; Meersman et al., 2016a; Quintana et al., 2012). Negative correlation analysis (Fig. 3a, correlations from -1 to 0, and Fig. 3b—anticorrelations) revealed reduced MO connectivity with amygdala (AMY) and posterior thalamic nuclei (TH) (Fig. 3b, anticorrelation CTRL > $Gpr88^{-/-}$), while stronger anticorrelations in the $Gpr88^{-/-}$ group compared with CTRL were obtained with HPF and midbrain (MB) areas, including superior colliculus (SC) or periaqueductal gray (PAG).

Along with remodeled MO connectivity, the $Gpr88^{-/-}$ SS cortex showed significant rsFC alterations (Fig. 3c, d). From positive correlation analysis (Fig. 3c, correlations from 0 to 1, and Fig. 3d—positive correlation), the $Gpr88^{-/-}$ group revealed decreased rsFC (CTRL > $Gpr88^{-/-}$) between SS and the mid-caudal isocortex, including MO, RSP, and VIS areas. Stronger rsFC (Fig. 3d, positive correlation CTRL < $Gpr88^{-/-}$) was quantified between SS and rostral isocortex, including MO and ACA. These intracortical modifications of rsFC in the $Gpr88^{-/-}$ group correlate with modifications of the brain connectivity matrix derived from ICASSO analysis (Fig. 1b). Negative correlation analysis (Fig. 3c, correlations from -1 to 0, and Fig. 3d—anticorrelations) revealed reduced SS connectivity with AMY, TH, hypothalamus (HY), and MB areas (Fig. 3d, anticorrelation CTRL > $Gpr88^{-/-}$), while

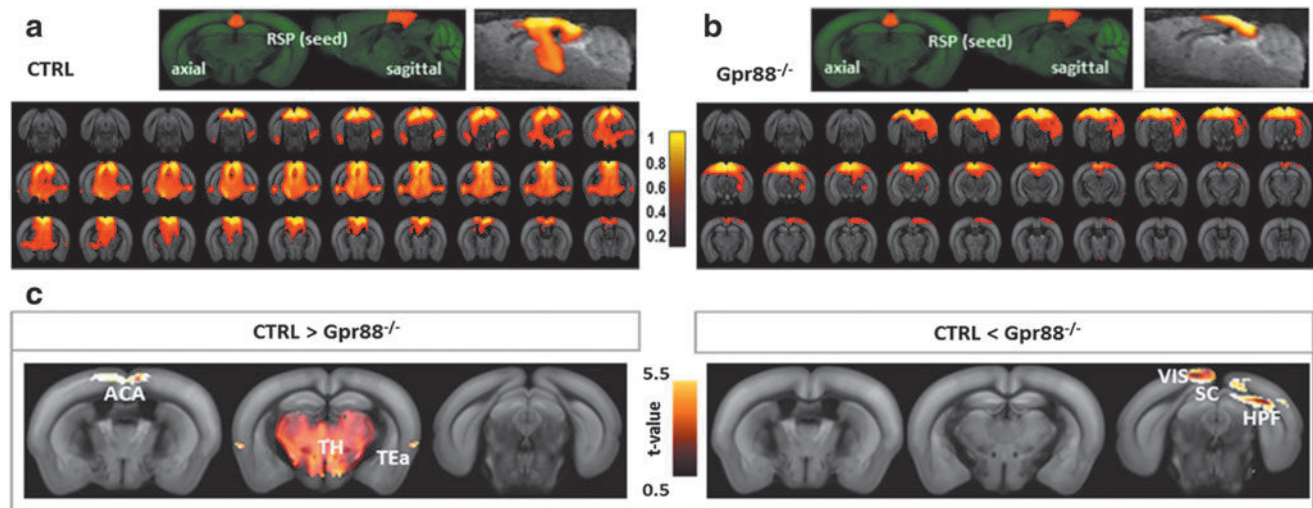


FIG. 2. $Gpr88$ deletion strongly reshapes the DMN pattern, defined as positive RSP cortex FC: (a) DMN pattern in the CTRL animal group. RSP cortex demonstrated strong coherent fluctuations of the BOLD signal with rostromedial ACA, TEa, and VIS areas, HPF, and thalamus. (b) Altered DMN pattern in the $Gpr88^{-/-}$ mouse brains is characterized by abolished FC of RSP with rostral ACA, TEa, and subcortical brain regions (HPF and TH), but strong connections mostly with the VIS area, including superior colliculus. (c) Statistically significant differences in the DMN patterns when comparing CTRL and $Gpr88^{-/-}$ groups (GLM, $p < 0.001$, corrected). The left panel shows the brain regions positively correlated with RSP for which correlations are significantly stronger in the CTRL than in the $Gpr88^{-/-}$ group. The right panel shows areas with FC stronger in the mutant group compared with the CTRL. The color scale at the middle indicates the corresponding T-value. BOLD, blood oxygen level-dependent; DMN, default mode network; GLM, general linear modeling.

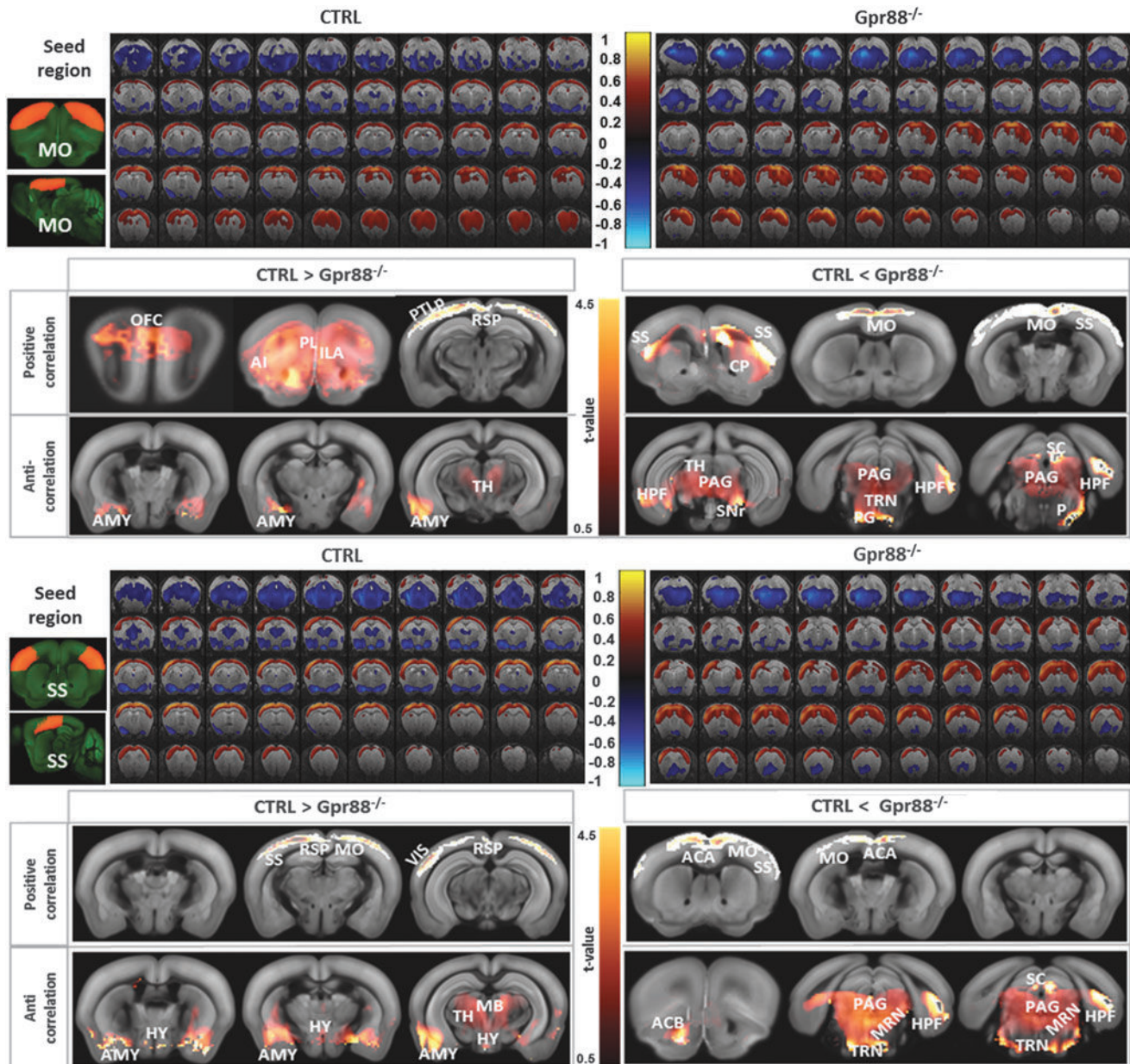


FIG. 3. Remodeled sensory-motor FC underscores the hyperactive or distracted behavior in mutant mice: BOLD rsfMRI correlation maps for (a) MO and (c) SS. Corresponding correlation maps of the CTRL and *Gpr88*^{-/-} groups were overlaid on atlas brain slices (two-tailed *t*-test, *p* < 0.001). The color scale indicates the correlation value (positive correlations from 0 to +1: dark red to yellow and negative correlations from 0 to -1: dark blue to turquoise). (b, d) Comparative analysis of the statistically significant FC (GLM, *p* < 0.001, corrected) resulting from the seed regions: MO and SS, respectively. The left panel shows positive and anticorrelated brain regions with the respective seed, stronger in the CTRL than *Gpr88*^{-/-} group. The right panel shows more strongly correlated regions in the mutant group compared with the CTRL. The color scale at the middle indicates the corresponding *T*-value. rsfMRI, resting-state functional magnetic resonance imaging.

stronger anticorrelations in the *Gpr88*^{-/-} group were obtained between SS and ACB, HPF, and MB areas, including SC or PAG (Fig. 3d, anticorrelation CTRL < *Gpr88*^{-/-}).

Modified caudate-putamen and HPF connectivity in *Gpr88*^{-/-} mice

Other brain areas were ranked high in the quantification of FC alterations in mutant mice. Notable are caudate-

putamen (CP) and HPF, where *Gpr88* is highly enriched for the former and virtually absent for the latter. Our previous behavioral study investigated whether altered striatal function would translate into a modification of hippocampal/striatal balance in learning (Meirman et al., 2016a). A dedicated, dual-solution cross-maze task revealed that *Gpr88*^{-/-} mice perform better in the allocentric versus egocentric component of the task for both acquisition and reversal learning, demonstrating facilitation of hippocampus-dependent behavior at the

expense of striatal-dependent responses (Meirsmann et al., 2016a). We therefore compared FC across these two brain structures using seed-based correlation analysis.

From *positive correlation analysis* (Fig. 4a, correlations from 0 to 1, and Fig. 4b—positive correlation), the $Gpr88^{-/-}$ CP showed strongly decreased rsFC toward HPF, TH, and MB. CP rsFC was, however, increased in the $Gpr88^{-/-}$ mice (Fig. 4b, positive correlation CTRL < $Gpr88^{-/-}$) toward ACA and rostral subcortical area, including septal

complex (S), pallidum (PAL), bed nuclei of the stria terminalis (BST), and AI. *Negative correlation analysis* (Fig. 4a, correlations from -1 to 0, and Fig. 4b—anticorrelations) revealed reduced CP connectivity with AMY, entorhinal (ENT), and VIS cortices, as well as SC and pontine olivary nuclei (P), in the $Gpr88^{-/-}$ group. However, stronger anti-correlations were obtained in the $Gpr88^{-/-}$ group between CP and ACB, as well as MO, SS, ACA, and PTLp cortical areas.

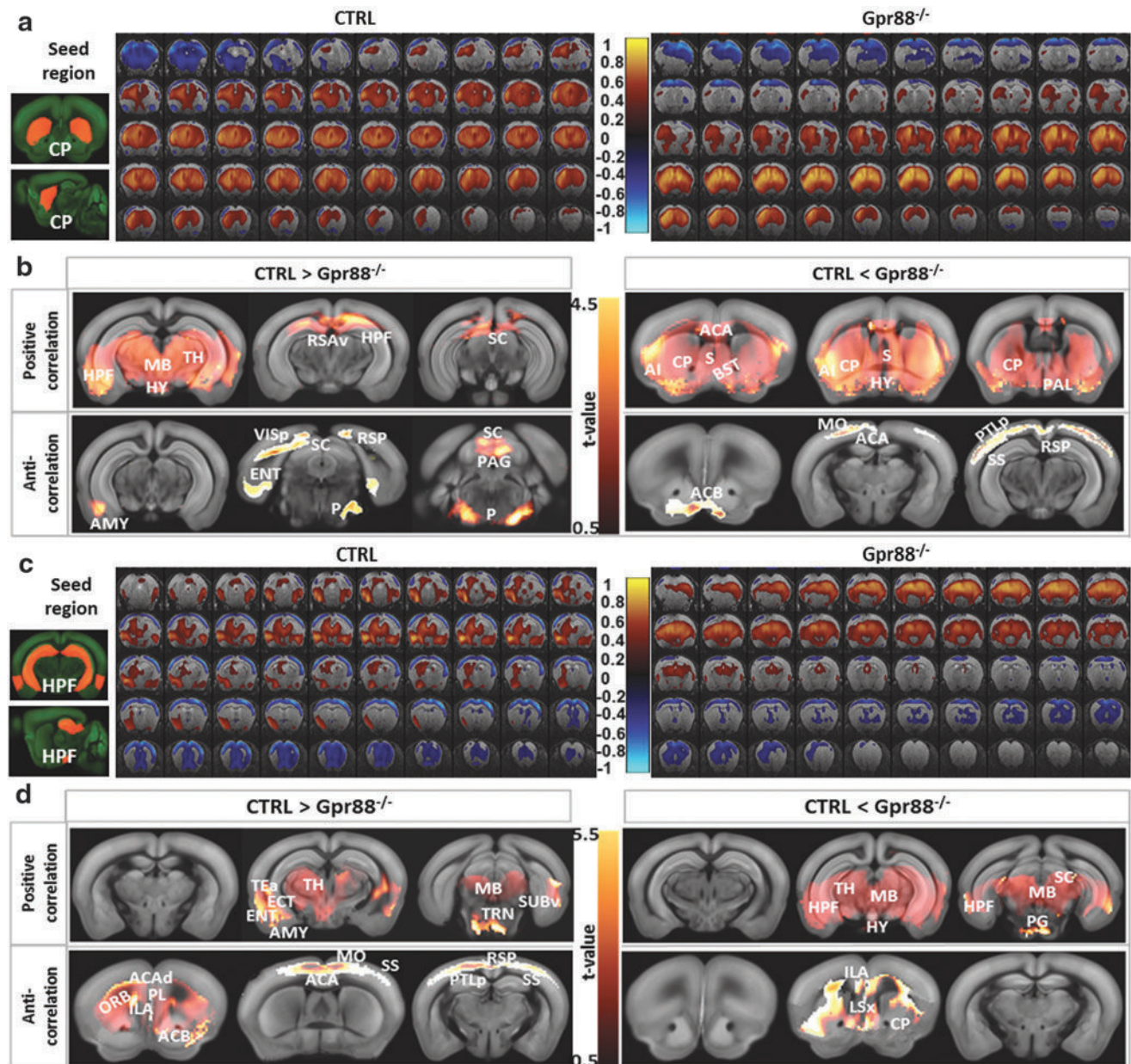


FIG. 4. FC patterns of dorsal striatum (CP) (a, b) and hippocampal formation (HPF) (c, d) are altered in $Gpr88^{-/-}$ mouse brains: BOLD rsfMRI correlation maps for (a) CP and (c) HPF. Corresponding correlation maps of the CTRL and $Gpr88^{-/-}$ groups were overlaid on T_2 -weighted anatomical brain slices (two-tailed t -test, $p < 0.001$). The color scale indicates the correlation value (positive correlations from 0 to +1: dark red to yellow and negative correlations from 0 to -1: dark blue to turquoise). (b, d) Detailed analysis of the statistically significant FC modifications (GLM, $p < 0.001$, corrected) of CP and HPF in the $Gpr88^{-/-}$ group. The left panel shows positive and anticorrelated brain regions with the respective seed stronger in the CTRL than $Gpr88^{-/-}$ group, while the right panel shows more strongly correlated regions in the mutant group compared with the CTRL. The color scale at the middle indicates the corresponding T -value.

Seed-based correlation analysis quantified strong hippocampal connectivity alterations in the *Gpr88*^{-/-} group. *Positive correlation analysis* (Fig. 4c, correlations from 0 to 1, and Fig. 4d—positive correlation) showed decreased positive correlations between HPF and AMY, ENT, and TEa, as well as rostral TH and MB in the *Gpr88*^{-/-} group. Meanwhile, HPF increased its positive rsFC toward caudal TH nuclei, SC, rostral MB, and pontine gray (PG) (Fig. 4d—positive correlation CTRL < *Gpr88*^{-/-}). *Negative correlation analysis* (Fig. 4b, correlations from -1 to 0, and Fig. 4d—anticorrelations) of HPF network indicated decreased connectivity between HPF and frontal limbic system, including orbital (ORB), PL, and ACB areas, as well as ACA, MO, SS, RSP, and PTLp cortical regions, in the *Gpr88*^{-/-} mice. Increased anticorrelated rsFC was, however, quantified between HPF and CP, lateral septal nuclei (LSX), and ILA (Fig. 4d—anticorrelation CTRL < *Gpr88*^{-/-}). Altogether, the extensive striato-hippocampal rsFC modifications corroborate the modified striato-hippocampal learning phenotype that we previously described for *Gpr88*^{-/-} mice (Meersman et al., 2016a).

Structural connectivity assessment

To noninvasively verify if *Gpr88* gene deletion impacted the underlying microstructure of brain functional networks, we used DTI and fiber tractography-derived parameters (FD) for measuring structural connectivity modifications (Fig. 6). Significant increase of FD values was detected in *Gpr88*^{-/-} animals compared with the CTRL group (voxel-wise statistical group comparison, $p < 0.05$, FWE corrected, contrast CTRL < *Gpr88*^{-/-}) in brain areas with altered rsFC. These areas included CP, MO, SS, HPF, parts of TH, and MB. No significant changes could be detected when examining the CTRL > *Gpr88*^{-/-} for FD contrast. For generation of FD maps, we used a global fiber-tracking algorithm that was previously validated for mouse and human DTI data (see the Materials and Methods section). A similar pattern of significant modifications was also quantified when performing group statistics on the fractional anisotropy maps (data not shown) derived after calculation of the diffusion tensor.

Discussion

During rest, endogenous fluctuations in low-frequency BOLD signals are synchronized between different regions—widely distributed throughout the brain, forming dynamic FC networks (Cabral et al., 2014). The genetic and molecular factors that regulate the development and behavior of these networks remain undefined. In this study, we focused on the *Gpr88* gene and discovered significant modifications of brain connective patterns in live *Gpr88*^{-/-} mice. This gene encodes an orphan G protein-coupled receptor whose ligand remains unknown and is expressed as early as embryonic day 16 in the rat (Massart et al., 2016) and P0 in the mouse (our unpublished data). Altered FC in mutant mice may therefore result either from the lack of GPR88 receptor activity during development, and thus reflect compensatory modifications, or from the absence of tonic GPR88 activity in the adult, or both. Inducible gene knockout approaches in the future should clarify respective contributions of early and adult GPR88 expression. The strong modifications of connective patterns observed in adult *Gpr88*^{-/-}

mice may potentially underpin behavioral alterations of these mutant mice. Table 1 summarizes behavioral phenotypes reported for *Gpr88*^{-/-} mice, which relate to altered rsFC observed in this study, and the relevant connectivity alterations are summarized in Figure 5.

The repertoire of *Gpr88*^{-/-} mice behavioral phenotypes was often discussed with respect to dysfunctions of cell types and brain areas expressing *Gpr88* in normal conditions. Particularly, the aberrant activation of striatal GABAergic medium spiny neurons (Quintana et al., 2012)—in the absence of a functional GPR88 receptor—was suggested to be a major contributor to behavioral deficits observed in *Gpr88*^{-/-} mice. However, one has to consider that such perturbations of brain activity are not confined to a single locus, instead they spread along axonal pathways to influence other regions' activity and alter the way these areas communicate with each other. This rsfMRI study allowed a whole brain and hypothesis-free analysis of brain connectivity, unraveling the intrinsic mouse brain functional communication and highlighting the complex highly organized topology of functional networks as previously observed in rodents (Biswal et al., 1995; Liang et al., 2011; Ma et al., 2016; Smith et al., 2013; Zerbi et al., 2015; Zhang et al., 2010), with its central player, the DMN (Raichle et al., 2001). Defined as a set of brain regions that show high neuronal activity during rest (Fox and Raichle, 2007; Raichle, 2015), DMN raised a lot of interest as it was demonstrated that its coherent activity is perturbed in pathological conditions, including psychiatric disorders (Raichle, 2015; Zhou et al., 2014). We and other groups found the DM-like network in the healthy mouse brain (Grandjean et al., 2016; Hübner et al., 2017; Sforzini et al., 2014) to be modified in mouse models of brain pathologies (Grandjean et al., 2016; Hübner et al., 2017). In this study, we show that *Gpr88* deletion in mice strongly perturbs the coherent activity of DMN, with major impact on the connectivity of RSP, the core player of this network. RSP connectivity with mid-rostral part of DMN, including the medial and anterior cingulate cortex as well as cortico-subcortical DMN subcomponents and temporal association area, is strongly suppressed in the *Gpr88*^{-/-} brains.

These large alterations of DMN upon deletion of the *Gpr88* gene are consistent with broad behavioral alterations mentioned in this mouse model and relate to patterns observed in human studies of psychiatric and neurologic disorders. Indeed FC modifications in the DMN have been reported, for instance, in bipolar disorder (Brady et al., 2016; Öngür et al., 2010; Wang et al., 2016), schizophrenia (Garrity et al., 2007; Kühn and Gallinat, 2012; Whitfield-Gabrieli and Ford, 2012), or attention-deficit/hyperactivity disorder (ADHD) (Castellanos and Proal, 2012; Castellanos et al., 2008; Fair et al., 2010; Fassbender et al., 2009; Hoekzema et al., 2014; Sonuga-Barke and Castellanos, 2007; Sun et al., 2012; Uddin et al., 2008). Emerging studies propose ADHD as a DMN disorder (Castellanos and Proal, 2012; Castellanos et al., 2008; Fair et al., 2010; Fassbender et al., 2009; Sonuga-Barke and Castellanos, 2007), and decreased DMN rsFC for adults (Castellanos et al., 2008; Hoekzema et al., 2014; Uddin et al., 2008) as well as adolescents suffering from ADHD (Sun et al., 2012) was reported. *Gpr88* receptor, as well as the behavioral traits of the *Gpr88*^{-/-} mice, was associated over time with the pathophysiology of such disorders (Del Zompo et al., 2014; Logue et al., 2009). This broad impact of *Gpr88* deletion on the

TABLE 1. SUMMARY BEHAVIORAL DEFICITS REPORTED IN GPR88^{-/-} MICE

System	Behavioral test	Behavior results
Sensorimotor gating deficit	Prepulse inhibition of the acoustic startle response assay	Sensorimotor gating deficit (Logue et al., 2009)
Motor deficits and hyperactivity	Stereotypy	Increased stereotypy (Meirsmann et al., 2016a)
	Rotarod Grip test Basal locomotor activity	Impaired motor coordination or strength (Quintana et al., 2012) No difference in muscle strength (Meirsmann et al., 2016a) Increased basal locomotor activity in novel and familiar environments (Quintana et al., 2012)
Learning deficiency	Basal locomotor activity	Increased locomotor activity and lack of habituation to a novel environment. (Meirsmann et al., 2016a)
	Basal locomotor activity	Increased locomotor activity (Meirsmann et al., 2016b)
	Operant behavior, two-way active avoidance procedure	Impaired avoidance learning, acquisition, and integration of visual or auditory cues (Quintana et al., 2012)
	Morris water maze	Visuospatial memory and learning were intact (Quintana et al., 2012)
	A water-based U maze	Impairments in cue-based learning (Quintana et al., 2012)
	Rotarod	Motor coordination and learning impairment (Meirsmann et al., 2016a)
	Y-maze	Increased exploration in new environments (Meirsmann et al., 2016a)
	Novel object recognition test	Improved learning and recognition memory (Meirsmann et al., 2016a)
Risk-taking behavior	Dual-solution cross-maze task	Improved ability to distinguish between goal-directed responses and habitual behavior (Meirsmann et al., 2016a)
	Fear conditioning	Impaired contextual fear and cue-related fear expression (Meirsmann et al., 2016b)
	Elevated-plus maze test	Reduced anxiety levels (Meirsmann et al., 2016a)
	Elevated-plus maze test	Decreased anxiety behaviors (Meirsmann et al., 2016b)
	Light-dark test	Exhibit increased risk-taking behaviors (Meirsmann et al., 2016b)
	Marble-burying test	Lower anxiety behaviors (Meirsmann et al., 2016a)
	Marble-burying test	Decreased threat avoidance and more risk-taking behaviors (Meirsmann et al., 2016b)
	Nest building	Decreased anxiety (Meirsmann et al., 2016a)
	Novelty preference	Increased novelty approach/low anxiety behaviors (Meirsmann et al., 2016b)
	Novelty-suppressed feeding test	Decreased conflict anxiety (Meirsmann et al., 2016a)
Novelty-suppressed feeding test	Increased novelty approach/low anxiety behaviors (Meirsmann et al., 2016b)	
Social interaction test	Increased social behaviors (Meirsmann et al., 2016b)	

Mutant mouse phenotypes are displayed in relation to brain connectivity domains as represented in Figure 5.

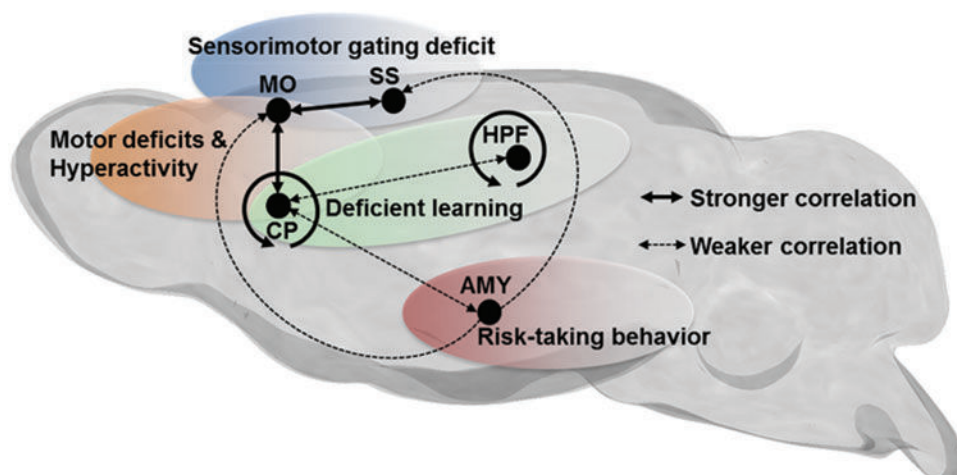


FIG. 5. Schematic representation of dominant resting-state FC alterations in *Gpr88*^{-/-} mice, associated with specific behavioral deficits previously reported for these mutant mice, and summarized in Table 1. Bold lines represent stronger correlations between regions, whereas dashed lines represent weaker correlations.

topology of resting-state connectivity has to be considered in a developmental context as well, as in normal brain, *Gpr88* shows differential expression over time in various brain areas. It is therefore likely that the global remodeling observed here results from the lack of GPR88 during development, at least for a large part.

Beside a strongly modified DMN pattern, we show extensive alterations of whole brain *Gpr88*^{-/-} FC matrix (Fig. 1) and, most interestingly, within intracortical connectivity. Indeed, recent work demonstrates intracellular redistribution of GPR88 during cortical lamination in the normal brains (Massart et al., 2016). In the cortical plate of the developing cortex, GPR88 presents a classical G protein-coupled receptor (GPCR) plasma membrane/cytoplasmic localization that shifts, on the day of birth, to nuclei of neurons progressively settling during postnatal development in layers V to II. It is likely that *Gpr88* influences, to some extent, the development of intracortical functional communication and that deletion of the receptor in *Gpr88*^{-/-} mice leads to remodeling of cortical functional pathways, as seen here. Particularly clear is the alteration of somatomotor connectivity (SS-MO) and SS-MO-ACA functional connections linked with the observed sensorimotor gating deficiency (Logue et al., 2009; Meirsman et al., 2016a) and risk-taking behavior (Meirsman et al., 2016b) of *Gpr88*^{-/-} mice. Sensorimotor gating is the process of screening or gating of the sensory and motor/cognitive information to enable uninterrupted processing of the most salient aspects of the external and internal environment (Butler et al., 1990). Sensorimotor gating deficiency reflects

central inhibitory functioning deficiency and underlies symptoms of ADHD (Holstein et al., 2013) in adults and schizophrenia patients (Braff and Geyer, 1990; Geyer et al., 2001). Prepulse inhibition is a well-validated operational measure of sensorimotor gating in humans and animals (Geyer et al., 2001) that is found to be disrupted in *Gpr88*^{-/-} mice (Logue et al., 2009). Beyond the widespread whole-brain functional disconnections detected in schizophrenic patients (Liang et al., 2006; Welsh et al., 2010), several studies report specific rsFC disruption in DMN and sensorimotor networks (Kaufmann et al., 2015; Tang et al., 2012) similar to our findings in mice lacking the GPR88 receptor. These connectivity features are suggestive of inhibitory control deficits, hyperactivity, and impulsivity symptoms, as seen in human ADHD (Choi et al., 2013; McLeod et al., 2014; Mostert et al., 2016; Tian et al., 2008). Most remarkably, the cortico-striatal connectivity (particularly MO-striatum FC) is strongly perturbed in *Gpr88*^{-/-} mice, congruent to the cardinal resting-state network perturbations observed in ADHD (Castellanos and Proal, 2012; Castellanos et al., 2006; Oldehinkel et al., 2016).

Striatal *Gpr88*^{-/-} FC changes are paralleled by structural modification of the striato-cortical pathways (Fig. 6), revealed in our study through DTI and high-resolution fiber mapping (Harsan et al., 2013). This modified striatocortical circuitry structure (especially the CP-MO altered component) is consistent with rsFC data and may underpin the hyperactive behavior described in the *Gpr88*^{-/-} model (Meirsman et al., 2016a; Quintana et al., 2012). The involvement of *Gpr88* in shaping

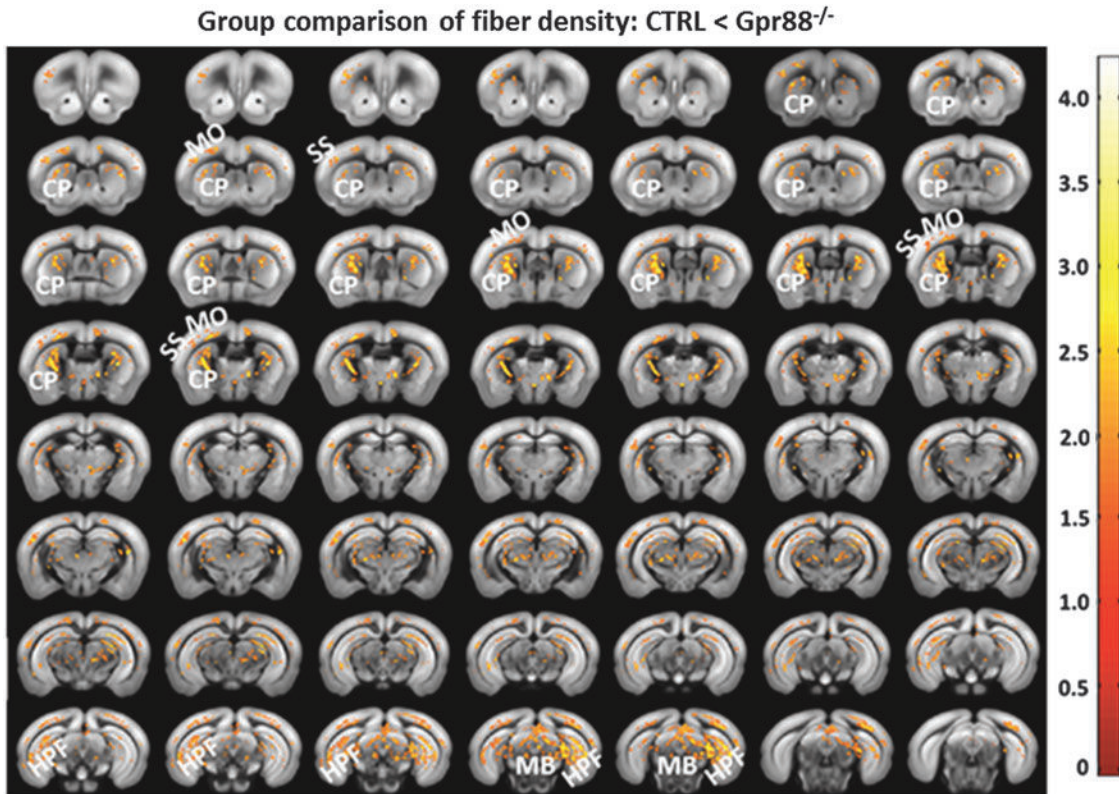


FIG. 6. Significant alterations of the fiber density in *Gpr88*^{-/-} mice: Statistical significance was evaluated using a two-sample *t*-test ($p < 0.05$, FWE corrected). The panel shows the regions with higher fiber density in the mutant mice compared with the CTRL. Corresponding *T*-value scale is shown. FWE, familywise error.

striatal connections and therefore underlying hyperactive features is supported by the most abundant expression of the receptor in this brain area, including CP (Ghate et al., 2007; Mizushima et al., 2000) and ACB.

Our analysis also indicates that amygdala connectivity to somatosensory and motor cortical area as well as caudate-putamen is weakened in *Gpr88* knockout mice. This observation is consistent with the notion that amygdala might now drive increased risk-taking (RT) behavior in a potentially dangerous environment, leading to an apparent reduced anxiety in *Gpr88*^{-/-} mice (Meirsman et al., 2016b). This phenotype was previously associated with altered gene transcription, dopamine levels, and neuronal morphology in amygdala (Alisch et al., 2014; Yokoyama et al., 2005) and consistent with the rsFC patterns reported in young adult RT behavior (Cox et al., 2010; DeWitt et al., 2014; Touroutoglou et al., 2014). In addition, hypersynchrony of the BOLD signal in the striatum of *Gpr88*^{-/-} mice, as observed in our study (Fig. 4a, b), has been reported earlier as a major contributor to adolescent RT behavior (Galvan, 2010).

The striatum, densely populated by GPR88 receptors in normal animals, showed perturbed functional cross talk not only with the hippocampus but also the prefrontal cortex, limbic area, and MB in *Gpr88*^{-/-} mice. Additionally, HPF rsFC was altered. These striatal and hippocampal FC perturbations might underlie the modified learning phenotype of *Gpr88*^{-/-} mice, observed in a behavioral test that specifically addresses the striatum-hippocampus balance in learning (Meirsman et al., 2016a; Quintana et al., 2012). The dorsal striatum (CP), a major hub of the basal ganglia network, is involved in several functional domains, including learning, cognition, and motivation (Mestres-Missé et al., 2012; Miyachi et al., 2002; Yin et al., 2009). In rodents, CP lesions disrupt acquisition of habits and impair goal-directed learning (Yin et al., 2004, 2005). Human neuroimaging studies also report the involvement of CP activity in the development of habits and goal-directed behavior (Liljeholm et al., 2011; Tanaka et al., 2008; Tricomi et al., 2009). Hippocampus, on the other hand, plays crucial roles in working and episodic memory (Aggleton and Brown, 2006; Cabeza and Nyberg, 2000). Our study therefore reveals a particular deficit in the striatal-hippocampal dialog at the neural network level, which likely explains the preferred allocentric (hippocampus) versus egocentric (striatum) behavioral strategy adopted by mutant mice in performing the cross-maze task (Meirsman et al., 2016a).

Thus far, the intrinsic functional architecture revealed spatially distinct brain regions that exhibit altered rsFC in the *Gpr88*^{-/-} mice, concordant with hyperactive characteristics of mutant mice and evocative of connectivity alterations observed in ADHD patients. In humans, disrupted functional communications between brain regions is often accompanied by microstructural abnormalities in the white matter, which are thought to contribute to behavioral functioning in ADHD (Nagel et al., 2011). Therefore, we also measured the microstructural integrity in the *Gpr88*^{-/-} mouse brain through DTI and fiber tractography (Harsan et al., 2013) and mapped the FD, one of the primary indices used to quantitatively measure structural integrity (Konrad and Eickhoff, 2010; Nagel et al., 2011), with diffusion-based tractography. FD values were significantly higher in *Gpr88*^{-/-} mice (two-sample *t*-test, $p < 0.05$, FWE corrected) particularly along the

striato-cortical pathway (Fig. 6) linking the striatum (CP) and cortical areas, like MO and SS. Former studies report disturbed structural connectivity of the cortico-striatal network in both adults and children with ADHD in comparison with healthy subjects (Konrad and Eickhoff, 2010; Tamm et al., 2012). Taken together, functional and structural connectivity modifications in the sensorimotor and cortico-striatal circuitry observed in *Gpr88*^{-/-} mice are consistent with the prevailing neurobiological hypothesis of ADHD, which identifies these networks as a probable substrate for cognitive and behavioral impairments seen in ADHD patients (Bush et al., 2005; Castellanos and Proal, 2012; Castellanos et al., 2006; Holstein et al., 2013; Oldehinkel et al., 2016; van Ewijk et al., 2012).

Conclusion

In conclusion, we provide here the first evidence of *Gpr88* involvement in reshaping the mouse brain functional and structural circuitry. The remodeled network architecture and topology underlie the large behavior deficits described in mice lacking a functional GPR88 receptor. Our study therefore suggests GPR88 as an influential player in brain connectivity and likely a susceptibility gene for psychiatric conditions in humans.

Acknowledgments

This project was funded with support from the NeuroTime Erasmus+: Erasmus Mundus program of the European Commission. This publication/communication reflects the views only of the author, and the Commission cannot be held responsible for any use that may be made of the information contained therein. This study was supported by the ATHOS Consortium (Fonds Unique Interministériel, Région Alsace, Domain Therapeutics Illkirch, France, and Prestwick Chemicals Illkirch, France). The authors also thank the National Institutes of Health (NIH-NIAAA No. 16658 and NIH-NIDA No. 005010) for financial support. The authors acknowledge the funding grants from Brain Links Brain Tools (BLBT) cluster of excellence from Freiburg (MouseNet 31 project).

Author Disclosure Statement

No competing financial interests exist.

References

- Aggleton JP, Brown MW. 2006. Interleaving brain systems for episodic and recognition memory. *Trends Cogn Sci* 10:455–463.
- Alisch RS, Chopra P, Fox AS, Chen K, White ATJ, Roseboom PH, et al. 2014. Differentially methylated plasticity genes in the amygdala of young primates are linked to anxious temperament, an at risk phenotype for anxiety and depressive disorders. *J Neurosci* 34:15548–15556.
- Becker JaJ, Befort K, Blad C, Filliol D, Ghate A, Dembele D, et al. 2008. Transcriptome analysis identifies genes with enriched expression in the mouse central extended amygdala. *Neuroscience* 156:950–965.
- Biswal B, Yetkin FZ, Haughton VM, Hyde JS. 1995. Functional connectivity in the motor cortex of resting human brain using echo-planar MRI. *Magn Reson Med* 34:537–541.
- Brady RO, Tandon N, Masters GA, Margolis A, Cohen BM, Keshavan M, Öngür D. 2016. Differential brain network

- activity across mood states in bipolar disorder. *J Affect Disord* 207:367–376.
- Braff DL, Geyer MA. 1990. Sensorimotor gating and schizophrenia. Human and animal model studies. *Arch Gen Psychiatry* 47:181–188.
- Bush G, Valera EM, Seidman LJ. 2005. Functional neuroimaging of attention-deficit/hyperactivity disorder: a review and suggested future directions. *Biol Psychiatry* 57:1273–1284.
- Butler RW, Braff DL, Rausch JL, Jenkins MA, Sprock J, Geyer MA. 1990. Physiological evidence of exaggerated startle response in a subgroup of Vietnam veterans with combat-related PTSD. *Am J Psychiatry* 147:1308–1312.
- Cabeza R, Nyberg L. 2000. Imaging cognition II: an empirical review of 275 PET and fMRI studies. *J Cogn Neurosci* 12:1–47.
- Cabral J, Kringelbach ML, Deco G. 2014. Exploring the network dynamics underlying brain activity during rest. *Prog Neurobiol* 114:102–131.
- Calhoun VD, Adali T, Pearlson GD, Pekar JJ. 2001. A method for making group inferences from functional MRI data using independent component analysis. *Hum Brain Mapp* 14:140–151.
- Castellanos FX, Margulies DS, Kelly C, Uddin LQ, Ghaffari M, Kirsch A, et al. 2008. Cingulate-precuneus interactions: a new locus of dysfunction in adult attention-deficit/hyperactivity disorder. *Biol Psychiatry* 63:332–337.
- Castellanos FX, Proal E. 2012. Large-scale brain systems in ADHD: beyond the prefrontal-striatal model. *Trends Cogn Sci* 16:17–26.
- Castellanos FX, Sonuga-Barke EJS, Milham MP, Tannock R. 2006. Characterizing cognition in ADHD: beyond executive dysfunction. *Trends Cogn Sci* 10:117–123.
- Choi J, Jeong B, Lee SW, Go HJ. 2013. Aberrant development of functional connectivity among resting state-related functional networks in medication-naïve ADHD children. *PLoS One* 8:e83516.
- Cox CL, Gotimer K, Roy AK, Castellanos FX, Milham MP, Kelly C. 2010. Your resting brain CAREs about your risky behavior. *PLoS One* 5:e12296.
- Del Zompo M, Deleuze JF, Chillotti C, Cousin E, Niehaus D, Ebstein RP, et al. 2014. Association study in three different populations between the GPR88 gene and major psychoses. *Mol Genet Genomic Med* 2:152–159.
- DeWitt SJ, Aslan S, Filbey FM. 2014. Adolescent risk-taking and resting state functional connectivity. *Psychiatry Res Neuroimaging* 222:157–164.
- Di X, Biswal BB. 2014. Modulatory interactions between the default mode network and task positive networks in resting-state. *PeerJ* 2:e367.
- Esposito F, Seifritz E, Formisano E, Morrone R, Scarabino T, Tedeschi G, Cirillo S, Goebel R, Di Salle F. 2003. Real-time independent component analysis of fMRI time-series. *Neuroimage* 20:2209–2224.
- Fair DA, Posner J, Nagel BJ, Bathula D, Dias TGC, Mills KL, et al. 2010. Atypical default network connectivity in youth with attention-deficit/hyperactivity disorder. *Biol Psychiatry* 68:1084–1091.
- Fassbender C, Zhang H, Buzy WM, Cortes CR, Mizuiri D, Beckett L, Schweitzer JB. 2009. A lack of default network suppression is linked to increased distractibility in ADHD. *Brain Res* 1273:114–128.
- Fox MD, Raichle ME. 2007. Spontaneous fluctuations in brain activity observed with functional magnetic resonance imaging. *Nat Rev Neurosci* 8:700–711.
- Galvan A. 2010. Adolescent development of the reward system. *Front Hum Neurosci* 4:6.
- Garrity AG, Pearlson GD, McKiernan K, Lloyd D, Kiehl KA, Calhoun VD. 2007. Aberrant “default mode” functional connectivity in schizophrenia. *Am J Psychiatry* 164:450–457.
- Geyer MA, Krebs-Thomson K, Braff DL, Swerdlow NR. 2001. Pharmacological studies of prepulse inhibition models of sensorimotor gating deficits in schizophrenia: a decade in review. *Psychopharmacology (Berl.)* 156:117–154.
- Ghate A, Befort K, Becker JAJ, Filliol D, Bole-Feysot C, Demebele D, et al. 2007. Identification of novel striatal genes by expression profiling in adult mouse brain. *Neuroscience* 146:1182–1192.
- Grandjean J, Azzinnari D, Seuwen A, Sigrist H, Seifritz E, Pryce CR, Rudin M. 2016. Chronic psychosocial stress in mice leads to changes in brain functional connectivity and metabolite levels comparable to human depression. *Neuroimage* 142:544–552.
- Harsan LA, Dávid C, Reisert M, Schnell S, Hennig J, von Elverfeldt D, Staiger JF. 2013. Mapping remodeling of thalamocortical projections in the living reeler mouse brain by diffusion tractography. *Proc Natl Acad Sci U S A* 110: E1797–E1806.
- Himberg J, Hyvärinen A, Esposito F. 2004. Validating the independent components of neuroimaging time series via clustering and visualization. *Neuroimage* 22:1214–1222.
- Hoekzema E, Carmona S, Ramos-Quiroga JA, Richarte Fernández V, Bosch R, Soliva JC, et al. 2014. An independent components and functional connectivity analysis of resting state fMRI data points to neural network dysregulation in adult ADHD. *Hum Brain Mapp* 35:1261–1272.
- Holstein DH, Vollenweider FX, Geyer MA, Csomor PA, Belsner N, Eich D. 2013. Sensory and sensorimotor gating in adult attention-deficit/hyperactivity disorder (ADHD). *Psychiatry Res* 205:117–126.
- Hübner N, Mechling AE, Lee HL, Reisert M, Bienert T, Hennig J, et al. 2017. The connectomics of brain demyelination: functional and structural patterns in the cuprizone mouse model. *Neuroimage* 146:1–18.
- Hyvärinen A, Oja E. 2000. Independent component analysis: algorithms and applications. *Neural Netw* 13:411–430.
- Kaufmann T, Skátun KC, Alnæs D, Doan NT, Duff EP, Tønnesen S, et al. 2015. Disintegration of sensorimotor brain networks in schizophrenia. *Schizophr Bull* 41:1326–1335.
- Konrad K, Eickhoff SB. 2010. Is the ADHD brain wired differently? A review on structural and functional connectivity in attention deficit hyperactivity disorder. *Hum Brain Mapp* 31:904–916.
- Künn S, Gallinat J. 2012. The neural correlates of subjective pleasantness. *Neuroimage* 61:289–294.
- Lein ES, Hawrylycz MJ, Ao N, Ayres M, Bensinger A, Bernard A, et al. 2007. Genome-wide atlas of gene expression in the adult mouse brain. *Nature* 445:168–176.
- Li Y-O, Adali T, Calhoun VD. 2007. Estimating the number of independent components for functional magnetic resonance imaging data. *Hum Brain Mapp* 28:1251–1266.
- Liang M, Zhou Y, Jiang T, Liu Z, Tian L, Liu H, Hao Y. 2006. Widespread functional disconnectivity in schizophrenia with resting-state functional magnetic resonance imaging. *Neuroreport* 17:209–213.
- Liang Z, King J, Zhang N. 2011. Uncovering intrinsic connective architecture of functional networks in awake rat brain. *J Neurosci* 31:3776–3783.

- Liljeholm M, Tricomi E, O'Doherty JP, Balleine BW. 2011. Neural correlates of instrumental contingency learning: differential effects of action-reward conjunction and disjunction. *J Neurosci* 31:2474–2480.
- Liska A, Galbusera A, Schwarz AJ, Gozzi A. 2015. Functional connectivity hubs of the mouse brain. *Neuroimage* 115: 281–291.
- Logue SF, Grauer SM, Paulsen J, Graf R, Taylor N, Sung MA, et al. 2009. The orphan GPCR, GPR88, modulates function of the striatal dopamine system: a possible therapeutic target for psychiatric disorders? *Mol Cell Neurosci* 42:438–447.
- Ma Z, Perez P, Ma Z, Liu Y, Hamilton C, Liang Z, Zhang N. 2016. Functional atlas of the awake rat brain: a neuroimaging study of rat brain specialization and integration. *Neuroimage*. pii: S1053-8119(16)30315-9.
- Margulies DS, Böttger J, Long X, Lv Y, Kelly C, Schäfer A, Goldhahn D, Abbushi A, Milham MP, Lohmann G, Villringer A. 2010. Resting developments: a review of fMRI post-processing methodologies for spontaneous brain activity. *MAGMA* 23:289–307.
- Massart R, Mignon V, Stanic J, Munoz-Tello P, Becker JAJ, Kieffer BL, et al. 2016. Developmental and adult expression patterns of the G-protein-coupled receptor GPR88 in the rat: establishment of a dual nuclear-cytoplasmic localization. *J Comp Neurol* 524:2776–2802.
- McLeod KR, Langevin LM, Goodyear BG, Dewey D. 2014. Functional connectivity of neural motor networks is disrupted in children with developmental coordination disorder and attention-deficit/hyperactivity disorder. *Neuroimage Clin* 4:566–575.
- Mechling AE, Arefin T, Lee HL, Bienert T, Reisert M, Ben Hamida S, et al. 2016. Deletion of the mu opioid receptor gene in mice reshapes the reward-aversion connectome. *Proc Natl Acad Sci U S A* 113:11603–11608.
- Mechling AE, Hübner NS, Lee HL, Hennig J, von Elverfeldt D, Harsan LA. 2014. Fine-grained mapping of mouse brain functional connectivity with resting-state fMRI. *Neuroimage* 96:203–215.
- Meirsmann AC, Le Merrer J, Pellissier LP, Diaz J, Clesse D, Kieffer BL, Becker JAJ. 2016a. Mice lacking GPR88 show motor deficit, improved spatial learning, and low anxiety reversed by delta opioid antagonist. *Biol Psychiatry* 79:917–927.
- Meirsmann AC, Robé A, de Kerchove d'Exaerde A, Kieffer BL. 2016b. GPR88 in A2AR neurons enhances anxiety-like behaviors. *eNeuro* 3. DOI:10.1523/ENEURO.0202-16.2016
- Mestres-Missé A, Turner R, Friederici AD. 2012. An anterior-posterior gradient of cognitive control within the dorsomedial striatum. *Neuroimage* 62:41–47.
- Miyachi S, Hikosaka O, Lu X. 2002. Differential activation of monkey striatal neurons in the early and late stages of procedural learning. *Exp Brain Res* 146:122–126.
- Mizushima K, Miyamoto Y, Tsukahara F, Hirai M, Sakaki Y, Ito T. 2000. A novel G-protein-coupled receptor gene expressed in striatum. *Genomics* 69:314–321.
- Moritz CH, Carew JD, McMillan AB, Meyerand ME. 2005. Independent component analysis applied to self-paced functional MR imaging paradigms. *Neuroimage* 25:181–192.
- Mostert JC, Shumskaya E, Mennes M, Onnink AMH, Hoogman M, Kan CC, et al. 2016. Characterising resting-state functional connectivity in a large sample of adults with ADHD. *Prog Neuropsychopharmacol Biol Psychiatry* 67:82–91.
- Nagel BJ, Bathula D, Herting M, Schmitt C, Kroenke CD, Fair D, Nigg JT. 2011. Altered white matter microstructure in children with attention-deficit/hyperactivity disorder. *J Am Acad Child Adolesc Psychiatry* 50:283–292.
- Oldehinkel M, Beckmann CF, Pruim RHR, van Oort ESB, Franke B, Hartman CA, et al. 2016. Attention-deficit/hyperactivity disorder symptoms coincide with altered striatal connectivity. *Biol Psychiatry Cogn Neurosci Neuroimaging* 1:353–363.
- Öngür D, Lundy M, Greenhouse I, Shinn AK, Menon V, Cohen BM, Renshaw PF. 2010. Default mode network abnormalities in bipolar disorder and schizophrenia. *Psychiatry Res* 183:59–68.
- Quintana A, Sanz E, Wang W, Storey GP, Güler AD, Wanat MJ, et al. 2012. Lack of GPR88 enhances medium spiny neuron activity and alters motor- and cue-dependent behaviors. *Nat Neurosci* 15:1547–1555.
- Raichle ME. 2015. The brain's default mode network. *Annu Rev Neurosci* 38:433–447.
- Raichle ME, MacLeod AM, Snyder AZ, Powers WJ, Gusnard DA, Shulman GL. 2001. A default mode of brain function. *Proc Natl Acad Sci U S A* 98:676–682.
- Reisert M, Mader I, Anastasopoulos C, Weigel M, Schnell S, Kiselev V. 2011. Global fiber reconstruction becomes practical. *Neuroimage* 54:955–962.
- Richiardi J, Altmann A, Milazzo AC, Chang C, Chakravarty MM, Banaschewski T, et al. 2015. Correlated gene expression supports synchronous activity in brain networks. *Science* 348:1241–1244.
- Sawiak SJ, Wood NI, Williams GB, Morton AJ, Carpenter TA. 2013. Voxel-based morphometry with templates and validation in a mouse model of Huntington's disease. *Magn Reson Imaging* 31:1522–1531.
- Sforazzini F, Schwarz AJ, Galbusera A, Bifone A, Gozzi A. 2014. Distributed BOLD and CBV-weighted resting-state networks in the mouse brain. *Neuroimage* 87:403–415.
- Simon SS. 2008. Merging of the senses. *Front Neurosci* 2:13–14.
- Smith SM, Beckmann CF, Andersson J, Auerbach EJ, Bijsterbosch J, Douaud G, et al. 2013. Resting-state fMRI in the Human Connectome Project. *Neuroimage* 80:144–168.
- Sonuga-Barke EJS, Castellanos FX. 2007. Spontaneous attentional fluctuations in impaired states and pathological conditions: a neurobiological hypothesis. *Neurosci Biobehav Rev* 31:977–986.
- Sun L, Cao Q, Long X, Sui M, Cao X, Zhu C, et al. 2012. Abnormal functional connectivity between the anterior cingulate and the default mode network in drug-naïve boys with attention deficit hyperactivity disorder. *Psychiatry Res* 201:120–127.
- Tamm L, Barnea-Goraly N, Reiss AL. 2012. Diffusion tensor imaging reveals white matter abnormalities in Attention-Deficit/Hyperactivity Disorder. *Psychiatry Res* 202:150–154.
- Tanaka SC, Balleine BW, O'Doherty JP. 2008. Calculating consequences: brain systems that encode the causal effects of actions. *J Neurosci* 28:6750–6755.
- Tang Y, Wang L, Cao F, Tan L. 2012. Identify schizophrenia using resting-state functional connectivity: an exploratory research and analysis. *Biomed Eng Online* 11:50.
- Thompson PM, Ge T, Glahn DC, Jahanshad N, Nichols TE. 2013. Genetics of the connectome. *Neuroimage* 80:475–488.
- Tian L, Jiang T, Liang M, Zang Y, He Y, Sui M, Wang Y. 2008. Enhanced resting-state brain activities in ADHD patients: a fMRI study. *Brain Dev* 30:342–348.
- Touroutoglou A, Bickart KC, Barrett LF, Dickerson BC. 2014. Amygdala task-evoked activity and task-free connectivity independently contribute to feelings of arousal. *Hum Brain Mapp* 35:5316–5327.
- Uddin LQ, Kelly AMC, Biswal BB, Margulies DS, Shehzad Z, Shaw D, et al. 2008. Network homogeneity reveals decreased

- integrity of default-mode network in ADHD. *J Neurosci Methods* 169:249–254.
- van de Ven VG, Formisano E, Prvulovic D, Roeder CH, Linden DEJ. 2004. Functional connectivity as revealed by spatial independent component analysis of fMRI measurements during rest. *Hum Brain Mapp* 22:165–178.
- Van Essen DC. 2013. Cartography and connectomes. *Neuron* 80:775–790.
- van Ewijk H, Heslenfeld DJ, Zwiers MP, Buitelaar JK, Oosterlaan J. 2012. Diffusion tensor imaging in attention deficit/hyperactivity disorder: a systematic review and meta-analysis. *Neurosci Biobehav Rev* 36:1093–1106.
- Van Waes V, Tseng KY, Steiner H. 2011. GPR88- a putative signaling molecule predominantly expressed in the striatum: cellular localization and developmental regulation. *Basal Ganglia* 1:83–89.
- Wang Y, Zhong S, Jia Y, Sun Y, Wang B, Liu T, et al. 2016. Disrupted resting-state functional connectivity in nonmedicated bipolar disorder. *Radiology* 280:529–536.
- Welsh RC, Chen AC, Taylor SF. 2010. Low-frequency BOLD fluctuations demonstrate altered thalamocortical connectivity in schizophrenia. *Schizophr Bull* 36:713–722.
- Whitfield-Gabrieli S, Ford JM. 2012. Default mode network activity and connectivity in psychopathology. *Annu Rev Clin Psychol* 8:49–76.
- Worsley KJ, Marrett S, Neelin P, Vandal AC, Friston KJ, Evans AC. 1996. A unified statistical approach for determining significant signals in images of cerebral activation. *Hum Brain Mapp* 4:58–73.
- Yin, HH, Knowlton BJ, Balleine BW. 2004. Lesions of dorsolateral striatum preserve outcome expectancy but disrupt habit formation in instrumental learning. *Eur J Neurosci* 19:181–189.
- Yin HH, Mulcare SP, Hilário MRF, Clouse E, Holloway T, Davis MI, et al. 2009. Dynamic reorganization of striatal circuits during the acquisition and consolidation of a skill. *Nat Neurosci* 12:333–341.
- Yin HH, Ostlund SB, Knowlton BJ, Balleine BW. 2005. The role of the dorsomedial striatum in instrumental conditioning. *Eur J Neurosci* 22:513–523.
- Yokoyama M, Suzuki E, Sato T, Maruta S, Watanabe S, Miyaoka H. 2005. Amygdalic levels of dopamine and serotonin rise upon exposure to conditioned fear stress without elevation of glutamate. *Neurosci Lett* 379:37–41.
- Zerbi V, Grandjean J, Rudin M, Wenderoth N. 2015. Mapping the mouse brain with rs-fMRI: an optimized pipeline for functional network identification. *Neuroimage* 123:11–21.
- Zhang N, Rane P, Huang W, Liang Z, Kennedy D, Frazier JA, King J. 2010. Mapping resting-state brain networks in conscious animals. *J Neurosci Methods* 189:186–196.
- Zhou F, Zhuang Y, Gong H, Wang B, Wang X, Chen Q, et al. 2014. Altered inter-subregion connectivity of the default mode network in relapsing remitting multiple sclerosis: a functional and structural connectivity study. *PLoS One* 9:e101198.

Address correspondence to:

Laura-Adela Harsan
 Engineering Science, Computer Science
 and Imaging Laboratory (ICube)
 Integrative Multimodal Imaging in Healthcare
 UMR 7357/University of Strasbourg—CNRS
 4 Rue Kirschleger
 Strasbourg 67000
 France

E-mail: harsan@unistra.fr

Archival Report

Increased Alcohol Seeking in Mice Lacking *Gpr88* Involves Dysfunctional Mesocorticolimbic Networks

Sami Ben Hamida, Sueli Mendonça-Netto, Tanzil Mahmud Arefin, Md. Taufiq Nasseef, Laura-Joy Boulos, Michael McNicholas, Aliza Toby Ehrlich, Eleanor Clarke, Luc Moquin, Alain Gratton, Emmanuel Darcq, Laura Adela Harsan, Rafael Maldonado, and Brigitte Lina Kieffer

ABSTRACT

BACKGROUND: Alcohol use disorder (AUD) is devastating and poorly treated, and innovative targets are actively sought for prevention and treatment. The orphan G protein-coupled receptor GPR88 is enriched in mesocorticolimbic pathways, and *Gpr88* knockout mice show hyperactivity and risk-taking behavior, but a potential role for this receptor in drug abuse has not been examined.

METHODS: We tested *Gpr88* knockout mice for alcohol-drinking and -seeking behaviors. To gain system-level understanding of their alcohol endophenotype, we also analyzed whole-brain functional connectivity in naïve mice using resting-state functional magnetic resonance imaging.

RESULTS: *Gpr88* knockout mice showed increased voluntary alcohol drinking at both moderate and excessive levels, with intact alcohol sedation and metabolism. Mutant mice also showed increased operant responding and motivation for alcohol, while food and chocolate operant self-administration were unchanged. Alcohol place conditioning and alcohol-induced dopamine release in the nucleus accumbens were decreased, suggesting reduced alcohol reward in mutant mice that may partly explain enhanced alcohol drinking. Seed-based voxelwise functional connectivity analysis revealed significant remodeling of mesocorticolimbic centers, whose hallmark was predominant weakening of prefrontal cortex, ventral tegmental area, and amygdala connectional patterns. Also, effective connectivity from the ventral tegmental area to the nucleus accumbens and amygdala was reduced.

CONCLUSIONS: *Gpr88* deletion disrupts executive, reward, and emotional networks in a configuration that reduces alcohol reward and promotes alcohol seeking and drinking. The functional connectivity signature is reminiscent of alterations observed in individuals at risk for AUD. The *Gpr88* gene, therefore, may represent a vulnerability/resilience factor for AUD, and a potential drug target for AUD treatment.

Keywords: Amygdala, Ethanol voluntary drinking, *Gpr88* knockout mice, Operant self-administration, Orphan G protein-coupled receptor, Prefrontal cortex, Resting-state functional magnetic resonance imaging, Ventral tegmental area

<https://doi.org/10.1016/j.biopsych.2018.01.026>

Alcohol use disorder (AUD) is a chronic relapsing disorder, characterized by excessive alcohol drinking and loss of control over consumption, and has dramatic consequences for individuals' health and productivity, their families, and society. Only few treatments are available (1–3), which target glutamatergic, gamma-aminobutyric acidergic, dopaminergic, or opioid systems; efficacy is low and variable; and the search for novel therapeutic strategies is largely open. AUD is a multifactorial condition involving both population-level (cultural and societal factors) (4) and individual-level (genetics) (5) characteristics, and family studies demonstrate that AUD is partly heritable, with genetics explaining 50% to 60% of phenotypic variability (6). Accordingly, neuroimaging studies show premorbid differences in brain

structure and function for individuals with AUD family history considered at risk for AUD (7). Overall, AUD shows high heterogeneity (8) and psychiatric comorbidity (9), and innovative biomarkers and drug targets are actively sought to address vulnerability factors and prevention, and to develop effective personalized treatments (8–10). In rodent research, gene knockout approaches have identified a number of genes that causally contribute to alcohol drinking-related behaviors (11,12). Here, we demonstrate that the *Gpr88* gene, which encodes an orphan G protein-coupled receptor (GPR) (13) expressed only in the brain (GPR88, no known native ligand) is a novel target for alcohol research.

At the neurobiological level, alcohol acts as a complex drug that modifies the activity of multiple molecular targets and

triggers broad alterations of gene expression and synaptic plasticity in neural networks responsible for reward, mood, and decision making (12,14,15). Remarkably, *Gpr88* is essentially expressed in these brain circuits (16). The *Gpr88* transcript is most enriched in the striatum of both rodent (17) and human (18) brains, and also in the central amygdala (19,20) and cortex (21), although with lower density. *Gpr88* transcript levels are altered upon pharmacological treatment using antidepressants (22) and mood stabilizers (23,24), as well as chronic exposure to drugs of abuse, including alcohol (25). To our knowledge, however, a potential role of this receptor in drug consumption, seeking, and dependence has not been examined.

Functional studies of GPR88 have used genetic approaches, as GPR88 drugs (26,27) with effective in vivo activity are lacking. *Gpr88* gene knockout in the mouse leads to a range of phenotypes consistent with the strong striatal GPR88 expression. In brief, these include altered dopamine (DA) signaling and enhanced medium spiny neuron excitability, increased basal activity and locomotor responses to psychostimulants, increased stereotypies and motor coordination deficits, and altered cue-based and procedural learning (28–30). Sensorimotor gating (28) and sensory processing (18) deficits are also observed in *Gpr88* knockout mice, possibly related to cortical GPR88 expression. Finally, these mutant mice display reduced anxiety-related responses together with increased approach behaviors, leading to a risk-taking phenotype (30), and perseverative (30) and compulsive-like behavior (Ben Hamida *et al.*, Ph.D., unpublished data, September 2017). In sum, the *Gpr88* expression pattern overlapping brain networks of addiction, and the phenotypic traits of *Gpr88* knockout mice involving dysfunctional motivation, mood regulation, and higher-order integration, prompted us to hypothesize that GPR88 may contribute to alcohol-drinking behaviors.

In this report, we show that deletion of the *Gpr88* gene leads to enhanced alcohol-drinking and -seeking behaviors. Tackling mechanisms underlying this behavior, we next show lower alcohol-induced conditioned place preference (CPP) associated with reduced augmentation of extracellular DA levels by alcohol in the nucleus accumbens (NAC), suggesting that alcohol reward is decreased in mutant mice. Extending our study to the broader circuits of addiction, using resting-state functional magnetic resonance imaging (Rs-fMRI) in live animals, we finally demonstrate altered functional connectivity (FC) within the mesocorticolimbic circuitry of live knockout mice, in a pattern reminiscent to network alterations observed in individuals at risk for AUD. Together, our data identify a circuit mechanism subserving GPR88-regulated alcohol drinking and strongly suggest that deficient GPR88 signaling is a risk factor for AUD.

METHODS AND MATERIALS

Mice

Male *Gpr88*^{-/-} mice were produced as previously described (30) (more details in the Supplement).

Drugs and Treatments

For information on drugs and treatments, see the Supplement.

Behavioral Procedures

Two-bottle choice (continuous and intermittent access) was performed as reported previously (31,32), and measures of sucrose, quinine, and saccharin consumption are described in the Supplement. Blood alcohol concentrations were measured as described in Zapata *et al.* (33) and details are in the Supplement. Loss of righting reflex; operant behavior to obtain alcohol, chocolate pellets, and food; and CPP are described in the Supplement.

In Vivo Microdialysis

Microdialysis was performed as described previously (34).

Resting-State Functional Magnetic Resonance Imaging

MRI data acquisition and Rs-fMRI analysis were conducted as described in Mechling *et al.* (35) and Arefin *et al.* (36), and effective FC analysis as in Friston *et al.* (37). Detailed methods for both the mouse experiment and human data analysis are provided in the Supplemental Materials and Methods.

RESULTS

Deletion of *Gpr88* Increases Voluntary Alcohol Consumption

We first measured the level of moderate voluntary alcohol intake in *Gpr88* knockout (*Gpr88*^{-/-}) mice and their wild-type littermates (*Gpr88*^{+/+}) using a 10% alcohol continuous access two-bottle-choice drinking paradigm in the home cage. Deletion of the *Gpr88* gene increased daily alcohol consumption compared with *Gpr88*^{+/+} mice (Figure 1A, left panel; see statistics in Supplemental Table S1). The mean daily alcohol intake during the entire experiment was also significantly higher in mutant mice (Figure 1A, right panel) (39.9%; *p* < .001). Water intake was comparable in both groups (Figure 1B).

Next, we used a 20% alcohol intermittent two-bottle-choice drinking procedure to test whether the *Gpr88* gene deletion also alters excessive alcohol intake, a hallmark of AUD. This procedure led to an enhanced mean daily alcohol intake in both *Gpr88*^{-/-} (76.3%) and *Gpr88*^{+/+} (57%) mice compared with a moderate dose in the procedure, and this increase was more pronounced in *Gpr88*^{-/-} mice (Figure 1C, left panel; see statistics in Supplemental Table S1). Over the entire experiment, the mean daily alcohol intake was also significantly higher in *Gpr88*^{-/-} mice compared with *Gpr88*^{+/+} control mice (Figure 1C, right panel) (63.3%; *p* < .001). Finally, similar to our finding for moderate drinking, no difference in water consumption was found across genotypes (Figure 1D). These results together demonstrate that the *Gpr88* gene deletion increases both moderate and excessive voluntary alcohol drinking. Heterozygous *Gpr88* mice (*Gpr88*^{+/-}) were also evaluated in the 20% alcohol intermittent two-bottle-choice drinking procedure. We found increased alcohol consumption, similar to total *Gpr88*^{-/-} mice (Supplemental Figure S1A, B), indicating that a partial deletion of *Gpr88* is sufficient to alter the alcohol-drinking behavior.

Finally, we found that sucrose intake (Supplemental Figure S1C), taste palatability (Figure 1E, F), sedative alcohol effects (Figure 1G), alcohol metabolism (Figure 1H), and body

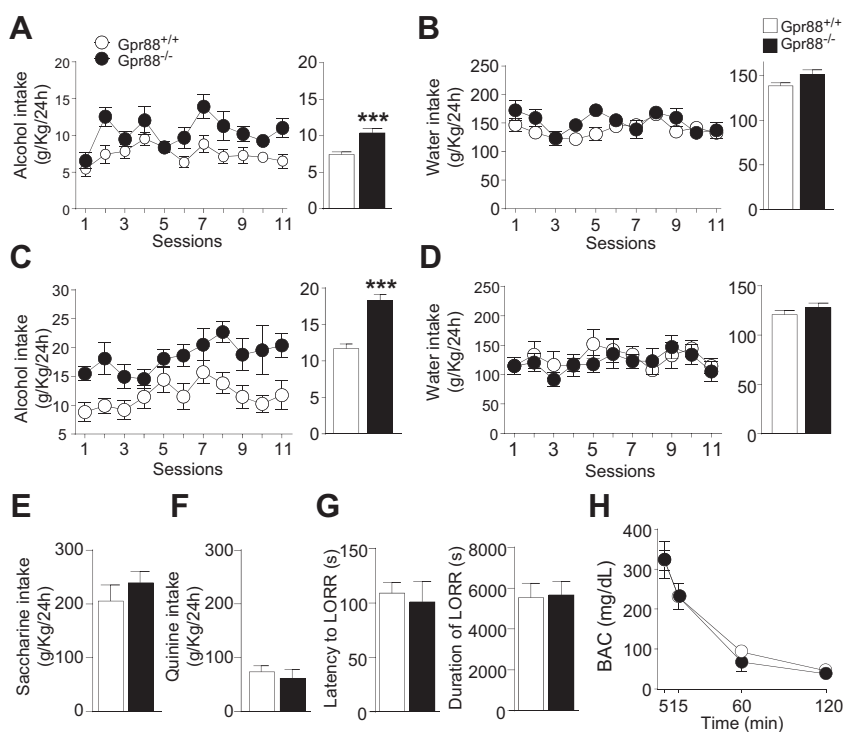
High Alcohol Drinking in *Gpr88* Knockout Mice

Figure 1. *Gpr88* knockout mice show increased alcohol drinking, with no change of taste palatability, alcohol sedation, and metabolism. (A–D) In the two-bottle-choice drinking paradigm, *Gpr88* knockout mice consume more alcohol than control mice, while water intake is unchanged. Mice were first offered continuous access to (A) 20% alcohol (v/v) and (B) water in their home cages for 11 consecutive days (11 sessions). Next, mice underwent intermittent access procedure to (C) 20% alcohol or (D) water for 1 month (12 sessions). (Left panel) Curves represent the mean (\pm SEM) alcohol or water intake per session; (right panel) histograms show mean (\pm SEM) daily alcohol or water consumption during the entire experiment. (E, F) In the two-bottle choice procedure, no difference is detected between mutant and control mice for the consumption of (E) sweet (saccharin) or (F) bitter (quinine) solutions. (G) Both latency and duration of the loss of righting reflex (LORR) are identical for mutant mice and their control counterparts upon alcohol injection (3.2 g/kg, 20% v/v solution, intraperitoneal), as are (H) blood alcohol concentration (BAC) levels. (A–D) $n = 11$ –17 for each group; (E–G) $n = 7$ –11 for each group; (H) $n = 3$ for each group. *** $p < .001$ compared with the control group. Statistical analysis is shown in Supplemental Table S1.

weights (Supplemental Figure S1D) are comparable in the mutant and control groups (details in Supplement), suggesting that higher alcohol consumption in *Gpr88* knockout mice is mostly due to enhanced appetitive properties of alcohol (38).

Deletion of *Gpr88* Increases Alcohol Operant Seeking and Motivation

To test this, we examined both drug seeking (lever press) and drug taking (licks) using operant alcohol self-administration (SA) (see Figure 2A and Supplemental Table S2 for statistical analysis). *Gpr88*^{-/-} and control mice were first subjected to a saccharine fading procedure. When alcohol concentration reached 10%, saccharine was omitted and alcohol SA was examined under fixed ratio (FR) 3 (sessions 36–40) and FR5 (sessions 41–46) schedules of reinforcement. During these sessions, *Gpr88*^{-/-} mice made a significantly higher number of lever presses for alcohol on the active lever compared with *Gpr88*^{+/+} control mice in both FR schedules (Figure 2C, left panel) (FR3 [$t_{18} = 2.0$, $p = .05$], FR5 [$t_{18} = 2.4$, $p < .05$]). In accordance to previous findings of hyperactivity (28–30), *Gpr88*^{-/-} mice also showed increased activity on the inactive lever in both FR schedules (Figure 2C, right panel) (FR3 [$t_{18} = 3.6$, $p < .01$], FR5 [$t_{18} = 3.2$, $p < .01$]), although the level of responding remained substantially lower than for the active level. Also, importantly, when tested for SA of 10% alcohol (sessions 36–46), mutant mice showed increased number of licks compared with their control counterparts in both FR schedules (Figure 2E) (FR3 [$t_{18} = 1.7$, $p = .1$], FR5 [$t_{18} = 2.2$, $p < .05$]), leading to more alcohol consumption and indicating that both seeking and taking were increased.

The observation of both higher lever pressing and licking in mutant mice led us to hypothesize that these mice have a stronger motivation for alcohol drinking. To test this, we conducted a progressive ratio schedule of reinforcement session. *Gpr88*^{-/-} mice showed a significantly higher breaking point compared with control mice (Figure 2F) ($t_{18} = 1.7$, $p < .05$), demonstrating that motivation to obtain the alcohol reward is enhanced in mutant mice.

Next, we examined whether the alcohol phenotype is substance specific. *Gpr88*^{-/-} mice were measured for operant responding for food under FR1 schedule and for highly palatable chocolate-flavored pellets under FR1, FR3, and FR5 schedules. The criteria for acquisition of food operant responding were reached after the same number of sessions in both genotypes (Figure 2G). In addition, knockout animals acquired and maintained operant responding for food (Figure 2H) and chocolate pellets (Figure 2I and Supplemental Figure S2) similarly to control animals. Motivation for natural rewards as measured in progressive ratio training was also preserved in *Gpr88*^{-/-} mice (Figure 2J). These data suggest that the general motivational state of mutant animals remains unchanged.

In conclusion, operant SA experiments reveal that deletion of the *Gpr88* gene increases incentive properties of alcohol, and that this phenotype is not generalizable to all appetitive substances.

Deletion of *Gpr88* Decreases Alcohol-Induced Reward

To understand mechanisms underlying increased alcohol seeking and drinking, we examined whether rewarding properties

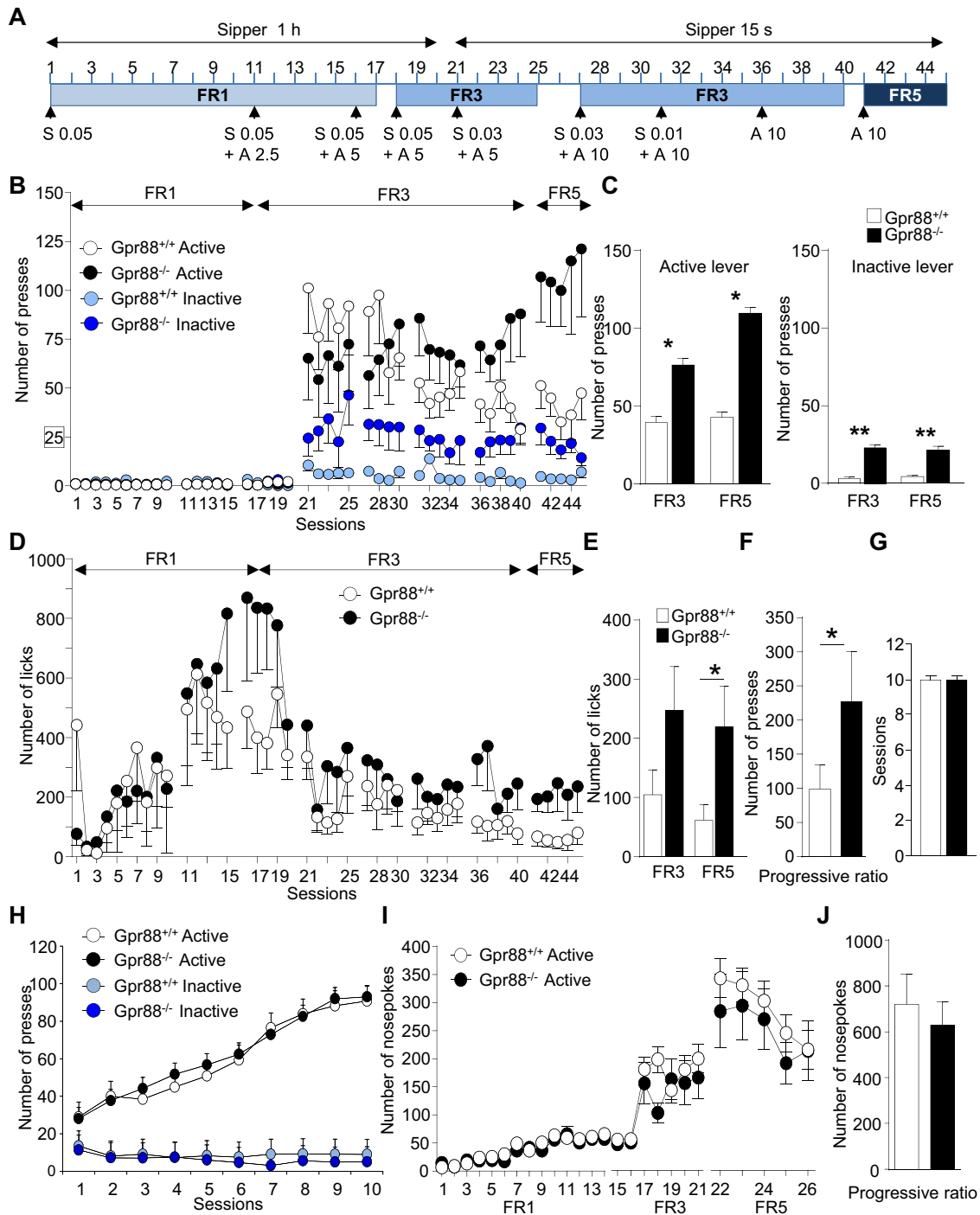


Figure 2. *Gpr88* knockout mice show increased alcohol-seeking and alcohol-taking behavior, with no change in food and chocolate self-administration. **(A)** Experimental timeline and history of reinforcement schedules for the acquisition and maintenance of alcohol self-administration. Alcohol was self-administered using a saccharin fading procedure on a fixed ratio (FR) 1 schedule of reinforcement for sessions 1 to 17, then FR3 for sessions 18 to 41 and FR5 for sessions 41 to 45. Over sessions alcohol concentration (A) (v/v) was gradually increased to reach 10% while saccharin concentration (S) (w/v) was progressively eliminated. Over successive training sessions the sipper access time was reduced from 60 minutes to 15 seconds to encourage the mice to elevate the frequency of responding. **(B)** Overall, the number of lever presses during 60-minute sessions was higher in mutant mice compared with control mice for both active and inactive levers. Also, **(C)** average daily active (left) and inactive (right) lever presses for 10% alcohol (sessions 36–45) were higher for *Gpr88* knockout mice under both FR3 (sessions 36–40) and FR5 (sessions 41–45) schedules. **(D)** Number of licks per session for the whole experiment and **(E)** average daily licks for 10% alcohol under FR3 and FR5 schedules were also higher in mutant mice. **(F)** The number of active lever responses under the progressive ratio schedule of reinforcement is shown, indicating a higher breaking point for mutant animals. **(G–H)** Operant food self-administration does not differ

High Alcohol Drinking in *Gpr88* Knockout Mice

of alcohol are altered in mutant mice using alcohol-induced CPP (39) (Figure 3A). No side preference was observed for any genotype during conditioning (data not shown). After conditioning, CPP scores differed between mutant and control animals. Two-way analysis of variance revealed a significant effect of genotype ($F_{1,46} = 6.8, p < .05$) and treatment ($F_{1,46} = 17.7, p < .001$), and no significant interaction ($F_{1,46} = 0.76, p = .39$). Despite the lack of interaction in the more stringent analysis, planned comparison analysis showed that both *Gpr88*^{+/+} ($t_{21} = 3.7, p < .01$) and *Gpr88*^{-/-} ($t_{25} = 2.5, p < .05$) mice showed a significant alcohol-induced CPP and that mutant mice spent less time in the alcohol-paired compartment than wild-type littermates ($t_{23} = 2.4, p < .05$). These data indicate that mutant mice show reduced development and/or expression of alcohol CPP, an indicator of reduced alcohol reward.

Drug reward is typically associated with drug-induced DA release in the NAC. Therefore, we tested consequences of the *Gpr88* gene deletion on basal and alcohol-enhanced extracellular levels of NAC DA (Figure 3B) in response to two alcohol doses (1.8 and 3.2 g/kg). The mean baseline dialysate DA concentration was not significantly different between the groups (*Gpr88*^{+/+} 0.098 ± 0.014 nM, *Gpr88*^{-/-} 0.102 ± 0.022 nM), and systemic injection of saline did not alter DA for any group (*Gpr88*^{+/+} 0.081 ± 0.008 nM, *Gpr88*^{-/-} 0.085 ± 0.007 nM). Alcohol administration increased extracellular DA in both *Gpr88*^{-/-} and *Gpr88*^{+/+} mice. Notably, however, *Gpr88*^{-/-} mice exhibited significantly lower DA-elevating response to the high alcohol dose, and areas under the curve for cumulative dialysates following alcohol injection (inserts for Figure 3B) showed a lower increase of DA levels in mutant mice for the two alcohol doses (see complete statistical analysis in Supplemental Table S3).

Together, the significant reduction of both alcohol place conditioning and NAC DA response to alcohol strongly suggests that alcohol reward is diminished in mutant mice, a mechanism that could contribute partly to their enhanced alcohol consumption.

Deletion of *Gpr88* Weakens FC of the Mesocorticolimbic Circuitry

In addition to their alcohol phenotype, *Gpr88* knockout mice show a number of other behavioral deficits (28–30). Most likely, therefore, reduced alcohol reward is not the only mechanism underlying high alcohol seeking and taking in these animals. To gain a broader circuit-level view of brain function deficits, which may lead to the high alcohol-drinking phenotype, we compared the FC patterns of key mesocorticolimbic players in live mutant mice and their control counterparts (Figure 4).

Rs-fMRI is based on the statistical analysis of low-frequency fluctuations in blood oxygen level-dependent signals at rest (40) and is now highly used in human research emotional responses. We have adapted Rs-fMRI to mice (41),

and our initial data-driven analysis of mice lacking the mu opioid receptor gene revealed major reshaping of reward/aversion networks (35), consistent with the known role of this receptor in pain and drug abuse. Very recently, we also used Rs-fMRI to compare whole-brain FC of *Gpr88*^{-/-} and *Gpr88*^{+/+} mice (36), and here, we further analyzed the Rs-fMRI datasets using seed-based analysis with a focus on key mesocorticolimbic centers (16), and mapped their connectivity patterns across the whole brain.

We selected four seeds most relevant to the high alcohol-seeking and -drinking behavior of mutant mice. These include the prefrontal cortex (PFC), as a key center for executive functions; the ventral tegmental area (VTA) and NAC, considered the core of reward circuitry; and the amygdala (AMY), which is central to mood. RsFC data from *Gpr88*^{-/-} and *Gpr88*^{+/+} mice were acquired and preprocessed as described previously (35) (and see Methods and Materials). Bilateral seeds were anatomically defined by coregistration with the Allen Mouse Brain Atlas, and voxelwise seed-based correlation analysis was conducted for each seed. The correlation maps revealed well-detectable cortical and subcortical RsFC modifications in the *Gpr88*^{-/-} group for the PFC, VTA, and AMY, while group differences for the NAC seed were less obvious (Supplemental Figure S3).

We further quantified the statistical significance of connectivity alterations in *Gpr88*^{-/-} mice using a voxel-level general linear model corrected for multiple comparisons ($p < .001$), and significant group differences are mapped in Figure 4A for both positive (from 0 to +1) and negative (from -1 to 0) correlations. For all the seeds (PFC, NAC, VTA, and AMY), voxelwise FC was predominantly weakened (*Gpr88*^{-/-} mice < control mice) in mutant mice, with only rare and mainly cortical strengthened correlated targets (*Gpr88*^{-/-} mice > control mice). See the Supplemental Results for a detailed description.

Network diagrams in Figure 4B summarize significant voxelwise modifications observed for each of the four PFC, NAC, VTA and AMY seeds, with a focus on their correlated activity with selected brain areas. These include 1) the four seeds; 2) the somatosensory area, which is related to sensorimotor gating deficiency reported in mutant animals (18); 3) the motor area, which is pivotal for sensorimotor integration and the control of voluntary movements (42) and likely contributes to the hyperactivity phenotype of *Gpr88*^{-/-} mice (29,30,36,43); and 4) the hippocampal formation and caudate putamen, both relevant to a specific learning deficit that we previously reported in *Gpr88*^{-/-} animals (29,30,43). Together, this analysis reveals a dysfunctional RsFC pattern within the mesocorticolimbic network.

FC analysis provides information on whole-brain connective patterns for selected seeds, without addressing how these brain regions may influence each other. Effective

between *Gpr88*^{-/-} mice and their controls (see Supplemental Methods and Materials). The number of (G) sessions required for the mice to reach the criteria and (H) lever presses for food pellets across the 10 sessions of a FR1 procedure were identical across genotypes. (I–J) Operant self-administration of chocolate flavor pellets did not differ between *Gpr88*^{-/-} mice and their control counterparts. (I) Animals were trained under FR1 (sessions 1–14), FR3 (sessions 15–21), and FR5 (sessions 22–26) schedules of reinforcement in 20-minute daily sessions during 26 sessions. (J) The number of nose-poke responses under the progressive ratio schedule of reinforcement is shown, indicating a similar breaking point for both genotypes. Data are mean ± SEM. * $p < .05$ and ** $p < .01$ compared with control group. (A–H) $n = 10$ for each group; (I, J) $n = 10–11$ for each group. For panels (B) and (D), statistical analysis is shown in Supplemental Table S2.

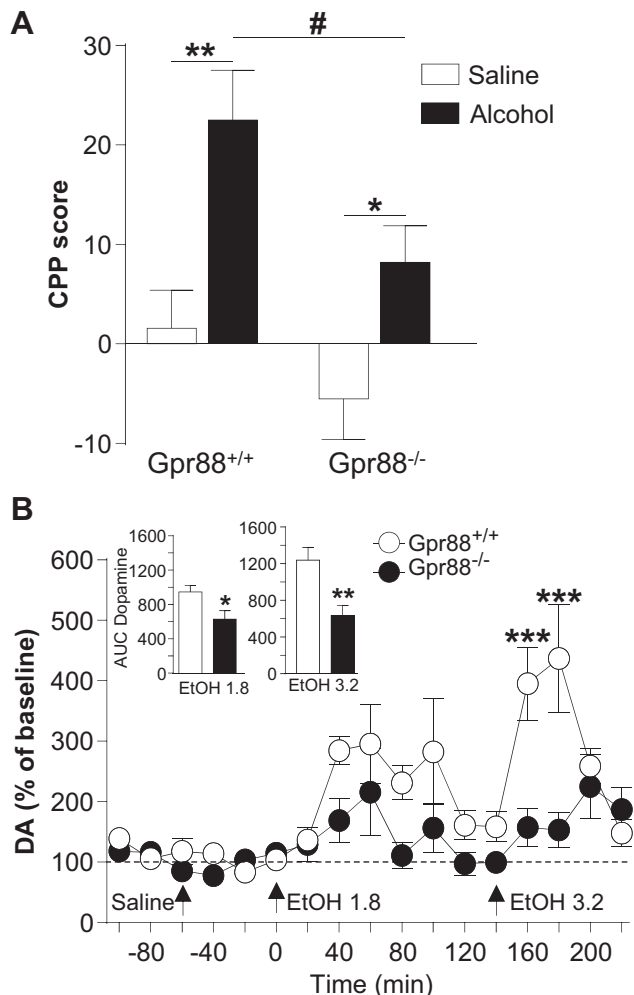


Figure 3. *Gpr88* knockout mice show lower place conditioning to alcohol and reduced alcohol-induced dopamine (DA) release in the nucleus accumbens. **(A)** Alcohol conditioned place preference (CPP) was induced by alternating alcohol (1.8 g/kg, intraperitoneal) or saline administration in the drug- or non-drug-paired compartment for 5 minutes (daily sessions, 8 days total). CPP scores are expressed as the percent of time spent in the alcohol- or saline-paired compartment during post-minus preconditioning session, and show the expression of alcohol CPP for the two genotypes, with a significantly lower score for mutant mice. **(B)** Extracellular DA and 3,4-dihydroxyphenylacetic acid levels were determined by *in vivo* microdialysis and high-performance liquid chromatography. After the collection of basal fractions, saline and both alcohol concentrations (1.8 and 3.2 g/kg) were administered at times of 0, 60, and 140 minutes, respectively. Alcohol-induced changes in DA were normalized to the percent change over baseline, and insets show the area under the curve (AUC) of cumulative dialysate DA and 3,4-dihydroxyphenylacetic acid levels from the four samples following alcohol injection (ethanol [EtOH] 1.8 g/kg; 0–80 minutes; EtOH 3.2 g/kg; 140–200 minutes). Data are mean \pm SEM. **(A)** $n = 11$ –14 for each group; **(B)** $n = 11$ for each group. * $p < .05$, ** $p < .01$, and *** $p < .001$ compared with control group. # $p < .05$ for alcohol *Gpr88*^{+/+} vs. alcohol *Gpr88*^{-/-} group.

connectivity (EF) further evaluates the causal influence of one region of interest on other regions within a predefined small network (44). To gain further insight into abnormal patterns of distributed activity in the mesocorticolimbic circuitry of mutant

mice, we measured statistical dependencies within and among regional dynamics of the four PFC, NAC, VTA, and AMY seeds, as described previously (37). Spectral dynamic causal modeling was performed using datasets from *Gpr88*^{-/-} mice and their wild-type littermates. We specified a model (Figure 4C) in which connected regions are based on known anatomical projections for the four seeds (45,46), hence unreported or minor physical projections were deleted (NAC to PFC, NAC to AMY, AMY to VTA). Average EF parameters (t test, $p < .001$, false discovery rate corrected) of the model are shown for wild-type (control) and mutant (*Gpr88*^{-/-}) mice (left and middle panels). In general, EF strength values were lower in the *Gpr88*^{-/-} group for all the selected directions, with the exception of the NAC-to-VTA direction. Group comparison (right panel) showed significantly reduced EF strength in mutant animals for both VTA-to-AMY and VTA-to-NAC connections (paired t test, $p < .05$).

Therefore, in addition to reducing correlated activities within mesocorticolimbic circuitry (FC analysis), deletion of the *Gpr88* gene limits information flow from the VTA to the NAC and AMY. The latter finding is in line with reduced DA release in the NAC upon alcohol treatment in mutant mice.

DISCUSSION

In this study, we first demonstrate that genetic deletion of *Gpr88* in mice increases alcohol-seeking and -taking behavior. We next show that alcohol reward is reduced in these mice and that further, FC is weakened throughout reward, executive, and emotional networks that are all involved in substance abuse disorders.

A first conclusion from this study is that activity of the GPR88 protein, an orphan G protein-coupled receptor encoded by the *Gpr88* gene, influences behaviors related to AUD. Mice lacking *Gpr88* exhibited higher levels of voluntary alcohol drinking and higher alcohol intake in operant SA, which together indicate significant alteration of processes that promote approach behaviors to alcohol. These phenotypes could not be attributed to a general modification of appetitive learning or taste sensitivity, as no genotype differences in daily sucrose intake were found. Also, both mutant and control mice similarly acquired and maintained stable operant responding for food and chocolate pellets, and showed comparable preference for nonalcohol tastes (saccharine and quinine). In addition, food and chocolate operant responding as well as sucrose intake were unchanged, indicating that neither hyperactivity nor generalized responding to rewarding stimuli could explain the higher motivation for alcohol in SA experiments. Future studies will determine whether *Gpr88* knockout mice also show enhanced preference and/or intake behavior for other drugs of abuse.

The progressive ratio break point during alcohol SA, considered a measure of motivation for the reward, was also enhanced in *Gpr88*^{-/-} mice. Increased motivation for alcohol may be due to higher or lower rewarding effects of alcohol, as SA studies show that higher drug-seeking behavior can be associated with either higher or lower drug reward [see (47–50)]. Here we find that, parallel to increased motivation for alcohol, mutant mice show reduced alcohol place preference in a conditioning paradigm, and also, importantly, reduced DA

extracellular levels release in the NAC upon alcohol administration. Because extracellular DA levels in the NAC classically reflect drug reward related to abuse potential (51–53), we propose that alcohol reward is indeed reduced in *Gpr88*^{-/-} mice. This, in turn, would contribute to augmenting both voluntary intake and operant responding for alcohol, to reach in mutant mice alcohol-rewarding effects similar to those achieved by control animals. Paralleling our findings, previous rodent studies showed that reduced drug reward together with reduced drug-induced DA responses is associated to higher motivation for cocaine (48,49). In humans, both reduced DA response to a psychostimulant (54) and low response to an alcohol challenge in young humans with a family history of AUD (55) are predictive of a higher risk for addiction. The *Gpr88* knockout mouse phenotype may therefore be interpreted along a similar line (56).

This mechanism, however, is unlikely to be the only cause for higher alcohol seeking and taking in *Gpr88* knockout mice, and a second conclusion from this study is that GPR88 is critical in regulating functional activity of a number of brain networks. Rs-fMRI is increasingly used in human research to address how disease conditions and genes influence FC of brain networks (57,58). RsFC alterations are associated with many brain disorders [see for example (59–63)], including drug abuse (64,65), and have already provided a host of information and biomarkers for alcohol research (7). In a prior study (36), and further in this study, we have investigated the *Gpr88*^{-/-} mice phenotype at the brain circuitry level using Rs-fMRI neuroimaging adapted to mice (35). Our initial structural and functional analysis provided evidence for altered cortical microstructure, as well as cortical remodeling in live mutant animals (36). In particular, Rs connective patterns of sensorimotor cortical areas were significantly altered, consistent with sensory processing and sensorimotor gating deficits, as well as hyperactivity in these mice (18,28–30). Also, amygdala connectivity with motor and sensory cortices was modified, and we suggested that these alterations may subserve enhanced exploratory and “risk-taking” phenotypes in these animals (30). The same AMY-motor area/somatosensory area modifications may also contribute to increased alcohol-drinking behavior observed in this study.

In this study, we have focused analysis of Rs-fMRI data on mesocorticolimbic networks. The most salient finding is a broad reduction of brainwide FC for the VTA, PFC, and AMY seeds, providing circuit-level mechanisms to explain excessive

alcohol seeking and taking in mutant animals. First, VTA seed-based connectivity showed decreased correlation/anti-correlation with voxels covering the NAC and AMY regions and, further, information flow from VTA to NAC (EF) was significantly reduced in *Gpr88*^{-/-} mice. These data are consistent with neurochemical analysis showing a lower increase of NAC DA levels upon alcohol treatment, and support the notion that reduced alcohol reward in mutant mice promotes increased alcohol-drinking behavior. Second, the PFC seed also showed reduced FC with voxels belonging to the NAC and AMY seeds, as well as the somatosensory area, motor area, caudate putamen, and hippocampal formation, which remarkably correlate with previously reported behavioral deficits of *Gpr88*-deficient mice (28–30,43). This finding strongly suggests that top-down controls are disrupted in mutant mice, a hallmark of behavioral modification in addiction research (66). Third, the AMY seed showed strong abnormalities, as correlated voxels were reduced with the PFC and caudate putamen. Conversely, the PFC and VTA seeds showed either decreased or increased FC with voxels belonging to the AMY. Also, EF from the VTA to the AMY was strongly reduced, and together, these multiple modifications of AMY FC are suggestive of altered emotional processing. In sum, the genetic deletion of *Gpr88* leads to significant modifications of brain networks contributing to reward processing, executive controls, and emotional regulation, and all concur to regulate addiction-related behaviors. Whether GPR88 activity regulates neuronal connectivity and effectiveness of these circuits during development, and/or is an active brain modulator in the adult, remains to be established. The observation of developmental stage-dependent *Gpr88* expression (18,21) certainly includes the former. In the future inducible gene knockout experiments may clarify the respective contributions of developmental and tonic GPR88 activities in shaping addiction-related networks. Alternatively, pharmacology may adequately address this question, should specific and bioavailable agonists/antagonists become available.

Our behavioral, neurochemical, and functional connectivity analyses of *Gpr88* knockout mice together suggest that deletion of the *Gpr88* gene creates an alcohol vulnerability phenotype in mice. This endophenotype, and in particular the brain-level functional architecture of mutant mice, is reminiscent of dysfunctional connectivity reported in individuals with a family history of AUD but who are not alcoholics (7,67), or abstinent individuals with high risk of relapse (68,69). Review of the human

indicates the corresponding *t* values. **(B)** Schematic representation of major significant FC modifications for each of the four selected seeds (PFC, VTA, NAC, and AMY) with the other regions of the mesocorticolimbic circuit, and also including the caudate putamen (CP), hippocampal formation (HPF), motor area (MO), and somatosensory area (SS) related to previously described behavioral and cognitive characteristics of mutant mice. The seed used for the voxelwise analysis is shown in red; the three other mesocorticolimbic regions are shown in yellow; and CP, HPF, MO, and SS are in gray. Dashed and solid lines represent weakened (*Gpr88*^{-/-} < CTRL) or strengthened (*Gpr88*^{-/-} > CTRL) FC, respectively. White lines represent FC with mesocorticolimbic regions, and gray lines show FC with CP, HPF, MO, and SS. Hallmarks of the *Gpr88* mesocorticolimbic signature are weaker PFC-AMY, VTA-NAC, and altered VTA-AMY FC. **(C)** Effective connectivity analysis using spectral dynamic causal modeling shows significant modification of information flow from VTA to NAC and VTA to AMY in mutant mice. Optimal causal models are shown for CTRL (left) and *Gpr88*^{-/-} (middle) mice. Numbers represent mean strengths of directional information transfer using Bayesian parameter averaging following *t* test (*p* < .001, false discovery rate [FDR] correction). Group comparison is shown in the right panel, with numbers indicating *p* values. Asterisks show the significant group difference directions by paired *t* test at *p* < .05. *n* = 14 for each group. ACA, anterior cingulate area; ACA_d, anterior cingulate area–dorsal part; ACA_v, anterior cingulate area–ventral part; aco, anterior commissure; AI, agranular insular area; AUD, auditory area; ECT, ectornal cortex; ENT, entornal area; GP, globus pallidus; HY, hypothalamus; LSX, lateral septal complex; MB, midbrain; OFC, orbitofrontal cortex; OT, olfactory tubercle; P, pons; PG, pontine gray; PRN, pontine reticular nucleus; PTL_p, posterior parietal association area; RSP, retrosplenial area; RSP_v, retrosplenial area–ventral part; SC, superior colliculus; TEa, temporal association area; TH, thalamus; TRN, tegmental reticular nucleus; VIS, visual area.

High Alcohol Drinking in *Gpr88* Knockout Mice

Rs-fMRI literature for alcohol research (see [Supplemental Materials and Methods](#)) identifies a complex set of brain network abnormalities in at-risk individuals, which we summarize in [Figure 5A](#). These include predominant alterations of networks responsible for reward/emotion processing and inhibitory controls, generally considered risk markers for substance abuse in the human neuroimaging literature (70). Although the reductionist mouse model does not, by far, recapitulate the complexity of human brain connectivity, homologous deficits of Rs brain connectivity can be noted for the *Gpr88* knockout mouse model and humans at risk (see [Figure 5B](#)). In particular, our study shows altered correlated activity of NAC with cortical areas in *Gpr88* knockout animals (weaker with PFC and motor area, and stronger with motor area). Impaired Rs

synchrony between the NAC and executive brain centers was also reported in youths with a family history of alcoholism (71). Notable also is the strong reduction of PFC-AMY synchrony in our study, and findings of poorer AMY-frontal cortex Rs connectivity in vulnerable individuals (72,73). In brief, the impaired interplay among reward, emotional, and executive functioning in *Gpr88* mutant mice also characterizes the premorbid condition of at-risk human subjects. Our study represents a first step toward the establishment of translatable FC signatures, or biomarkers that may also provide mechanistic clues for abnormal alcohol-related behavior.

In conclusion, our study positions the *Gpr88* gene as a target for alcohol research. In the future, this gene may be considered a risk factor, though the search for genetic association with alcoholism has not yet started. The combined gene/connectome information may also be useful for diagnostic and prevention. Finally, current drug development efforts will likely provide GPR88 drugs that may hold promise for the treatment of alcohol and drug addiction.

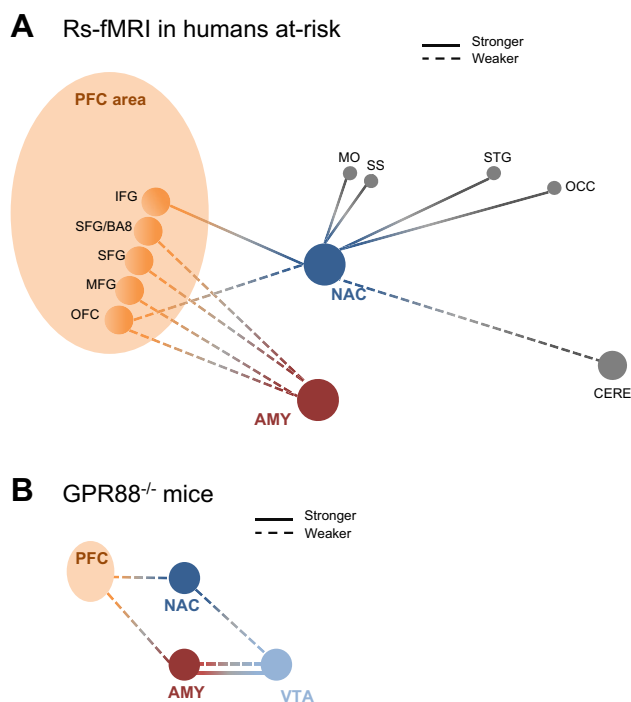


Figure 5. Review of the human resting-state functional magnetic resonance imaging (Rs-fMRI) literature identifies a complex set of network abnormalities in individuals at risk for alcohol use disorder (71–74), with homology to the *Gpr88* knockout mice functional connectivity (FC) signature. **(A)** Summary of the human Rs-fMRI imaging literature. Dashed and solid lines represent weakened and strengthened FC, respectively. Prefrontal cortex (PFC) (orange), nucleus accumbens (NAC) (blue), amygdala (AMY) (red), and cerebellum (CERE) (gray) seeds are shown. Lateralization details: the left NAC showed increased FC with the left superior temporal gyrus (STG) and right/left inferior frontal gyrus (IFG) (71). The right NAC showed decreased FC with the right CERE and left orbitofrontal cortex (OFC) (71). The left AMY showed decreased FC with the left superior frontal gyrus (SFG) and left SFG/Brodman area 8 (BA8), and right middle frontal gyrus (MFG) (72). The right AMY showed decreased FC with the right MFG (72). **(B)** Summary of FC modifications in this study. The RsFC signature of the *Gpr88* gene is adapted from [Figure 4](#). The scheme highlights homology with human findings in panel **(A)**, namely reduced PFC-NAC and PFC-AMY correlations. The altered connective pattern for the ventral tegmental area (VTA) reported in this study has been described in the human literature. MO, motor cortex; OCC, right occipital cortex; SS, somatosensory cortex.

ACKNOWLEDGMENTS AND DISCLOSURES

This work was supported by National Institutes of Health/National Institute of Drug Abuse Grant No. 05010 (to BLK); National Institute on Alcohol Abuse and Alcoholism Grant No. 16658 (to BLK); the Canada Fund for Innovation and the Canada Research Chairs (to BLK); Spanish Ministerio de Economía y Competitividad-MINECO Grant No. #SAF2014-59648-P/FEDER (to RM); Instituto de Salud Carlos III RETICS-RTA Grant No. RD12/0028/0023/FEDER (to RM); Ministerio de Sanidad, Servicios Sociales e Igualdad, Plan Nacional sobre Drogas Grant No. PNSD-2013-068 (to RM); Generalitat de Catalunya AGAUR Grant No. 2014-SGR-1547 (to RM); a 2015 Catalan Institution for Research and Advanced Studies Academia Award (to RM); the Brazilian government's CAAP scholarship (Programa Ciência Sem Fronteiras) (to SM-N); and the NeuroTime Erasmus+: Erasmus Mundus program of the European Commission. This publication/communication reflects the views only of the authors, and the Commission cannot be held responsible for any use which may be made of the information contained therein.

We thank the staff at the animal facility of the Neurophenotyping Center Douglas Research Center (Montreal, Quebec, Canada), as well as the Institut de Génétique et de Biologie Moléculaire et Cellulaire and the Mouse Clinic Institute (Illkirch-Graffenstaden, France) for technical support and housing of the animals. We are grateful to Audrey Matifas, Elise Le Marchand, Thomas Favier, Gilles Duval, Dzemailj Memedov, Aude Villemain, Eujin Kim, Annie Saless, Karine Lachapelle, and Aimee Lee Luco for animal care and genotyping.

The authors report no biomedical financial interests or potential conflicts of interest.

ARTICLE INFORMATION

From the Département de Médecine Translationnelle et Neurogénétique (SBH, L-JB, ATE, BLK), Institut de Génétique et de Biologie Moléculaire et Cellulaire, Institut National de la Santé et de la Recherche Médicale U-964, Centre National de la Recherche Scientifique UMR-7104, University of Strasbourg, Illkirch-Graffenstaden; Engineering Science, Computer Science and Imaging Laboratory (HLA), Integrative Multimodal Imaging in Healthcare, University of Strasbourg – Centre National de la Recherche Scientifique; and Department of Biophysics and Nuclear Medicine (HLA), Faculty of Medicine, University Hospital Strasbourg, Strasbourg, France; Douglas Mental Health Institute (SBH, MTN, L-JB, MM, ATE, EC, LM, AG, ED, BLK), Department of Psychiatry, McGill University, Montreal, Quebec, Canada; Departament de Ciències Experimentals i de la Salut (SM-N, RM), Universitat Pompeu Fabra, Barcelona, Spain; Department of Radiology (TMA, HLA), Medical Physics, Medical Center University of Freiburg, Faculty of Medicine; and Bernstein Center Freiburg (TMA), University of Freiburg, Freiburg, Germany; and the Bernard and Irene Schwartz Center for

Biomedical Imaging (TMA), Department of Radiology, New York University School of Medicine, New York, New York.

Address correspondence to Brigitte Lina Kieffer, Ph.D., Douglas Hospital Research Center, Perry Pavilion Room E-3317.1, 6875 boulevard LaSalle, Montreal (Quebec) H4H 1R3, Canada; E-mail: brigitte.kieffer@douglas.mcgill.ca.

Received Jul 17, 2017; revised and accepted Jan 22, 2018.

Supplemental material cited in this article is available online at <https://doi.org/10.1016/j.biopsych.2018.01.026>.

REFERENCES

- Maisel NC, Blodgett JC, Wilbourne PL, Humphreys K, Finney JW (2013): Meta-analysis of naltrexone and acamprosate for treating alcohol use disorders: When are these medications most helpful? *Addiction* 108:275–293.
- Johnson BA (2010): Medication treatment of different types of alcoholism. *Am J Psychiatry* 167:630–639.
- Muller CA, Geisel O, Pelz P, Higl V, Kruger J, Stickel A, *et al.* (2015): High-dose baclofen for the treatment of alcohol dependence (BACLAD study): A randomized, placebo-controlled trial. *Eur Neuropsychopharmacol* 25:1167–1177.
- Castro FG, Barrera M Jr, Mena LA, Aguirre KM (2014): Culture and alcohol use: Historical and sociocultural themes from 75 years of alcohol research. *J Stud Alcohol Drugs Suppl* 17(suppl 17):36–49.
- Buscemi L, Turchi C (2011): An overview of the genetic susceptibility to alcoholism. *Med Sci Law* 51(suppl 1):S2–S6.
- Reilly MT, Noronha A, Goldman D, Koob GF (2017): Genetic studies of alcohol dependence in the context of the addiction cycle. *Neuropharmacology* 122:3–21.
- Cservenka A (2016): Neurobiological phenotypes associated with a family history of alcoholism. *Drug Alcohol Depend* 158:8–21.
- Heilig M, Goldman D, Berrettini W, O'Brien CP (2011): Pharmacogenetic approaches to the treatment of alcohol addiction. *Nat Rev Neurosci* 12:670–684.
- Helton SG, Lohoff FW (2015): Pharmacogenetics of alcohol use disorders and comorbid psychiatric disorders. *Psychiatry Res* 230:121–129.
- Heilig M, Sommer WH, Spanagel R (2016): The need for treatment responsive translational biomarkers in alcoholism research. *Curr Top Behav Neurosci* 28:151–171.
- Mayfield J, Arends MA, Harris RA, Blednov YA (2016): Genes and alcohol consumption: Studies with mutant mice. *Int Rev Neurobiol* 126:293–355.
- Ron D, Barak S (2016): Molecular mechanisms underlying alcohol-drinking behaviours. *Nat Rev Neurosci* 17:576–591.
- Davenport AP, Alexander SP, Sharman JL, Pawson AJ, Benson HE, Monaghan AE, *et al.* (2013): International Union of Basic and Clinical Pharmacology. LXXXVIII. G protein-coupled receptor list: Recommendations for new pairings with cognate ligands. *Pharmacol Rev* 65:967–986.
- Spanagel R (2009): Alcoholism: A systems approach from molecular physiology to addictive behavior. *Physiol Rev* 89:649–705.
- Mulholland PJ, Chandler LJ, Kalivas PW (2016): Signals from the Fourth Dimension Regulate Drug Relapse. *Trends Neurosci* 39:472–485.
- Koob GF, Volkow ND (2016): Neurobiology of addiction: A neuro-circuitry analysis. *Lancet Psychiatry* 3:760–773.
- Mizushima K, Miyamoto Y, Tsukahara F, Hirai M, Sakaki Y, Ito T (2000): A novel G-protein-coupled receptor gene expressed in striatum. *Genomics* 69:314–321.
- Ehrlich AT, Semache M, Bailly J, Wojcik S, Arefin TM, Colley C, *et al.* (2017): Mapping GPR88-Venus illuminates a novel role for GPR88 in sensory processing [published online ahead of print Nov 6]. *Brain Struct Funct*.
- Becker JA, Befort K, Blad C, Filliol D, Ghate A, Demebele D, *et al.* (2008): Transcriptome analysis identifies genes with enriched expression in the mouse central extended amygdala. *Neuroscience* 156:950–965.
- Befort K, Filliol D, Ghate A, Darq E, Matifas A, Muller J, *et al.* (2008): Mu-opioid receptor activation induces transcriptional plasticity in the central extended amygdala. *Eur J Neurosci* 27:2973–2984.
- Massart R, Mignon V, Stanic J, Munoz-Tello P, Becker JA, Kieffer BL, *et al.* (2016): Developmental and adult expression patterns of the G-protein-coupled receptor GPR88 in the rat: Establishment of a dual nuclear-cytoplasmic localization. *J Comp Neurol* 524:2776–2802.
- Conti B, Maier R, Barr AM, Morale MC, Lu X, Sanna PP, *et al.* (2007): Region-specific transcriptional changes following the three antidepressant treatments electro convulsive therapy, sleep deprivation and fluoxetine. *Mol Psychiatry* 12:167–189.
- Ogden CA, Rich ME, Schork NJ, Paulus MP, Geyer MA, Lohr JB, *et al.* (2004): Candidate genes, pathways and mechanisms for bipolar (manic-depressive) and related disorders: An expanded convergent functional genomics approach. *Mol Psychiatry* 9:1007–1029.
- Brandish PE, Su M, Holder DJ, Hodor P, Szumiloski J, Kleinhanz RR, *et al.* (2005): Regulation of gene expression by lithium and depletion of inositol in slices of adult rat cortex. *Neuron* 45:861–872.
- Le Merrer J, Befort K, Gardon O, Filliol D, Darq E, Demebele D, *et al.* (2012): Protracted abstinence from distinct drugs of abuse shows regulation of a common gene network. *Addict Biol* 17:1–12.
- Dzierba CD, Bi Y, Dasgupta B, Hartz RA, Ahuja V, Cianchetta G, *et al.* (2015): Design, synthesis, and evaluation of phenylglycinols and phenyl amines as agonists of GPR88. *Bioorg Med Chem Lett* 25:1448–1452.
- Jin C, Decker AM, Huang XP, Gilmour BP, Blough BE, Roth BL, *et al.* (2014): Synthesis, pharmacological characterization, and structure-activity relationship studies of small molecular agonists for the orphan GPR88 receptor. *ACS Chem Neurosci* 5:576–587.
- Logue SF, Grauer SM, Paulsen J, Graf R, Taylor N, Sung MA, *et al.* (2009): The orphan GPCR, GPR88, modulates function of the striatal dopamine system: A possible therapeutic target for psychiatric disorders? *Mol Cell Neurosci* 42:438–447.
- Quintana A, Sanz E, Wang W, Storey GP, Guler AD, Wanat MJ, *et al.* (2012): Lack of GPR88 enhances medium spiny neuron activity and alters motor- and cue-dependent behaviors. *Nat Neurosci* 15:1547–1555.
- Meirsman AC, Le Merrer J, Pellissier LP, Diaz J, Clesse D, Kieffer BL, *et al.* (2016): Mice lacking GPR88 show motor deficit, improved spatial learning, and low anxiety reversed by delta opioid antagonist. *Biol Psychiatry* 79:917–927.
- Warnault V, Darq E, Levine A, Barak S, Ron D (2013): Chromatin remodeling—a novel strategy to control excessive alcohol drinking. *Transl Psychiatry* 3:e231.
- Simms JA, Steensland P, Medina B, Abernathy KE, Chandler LJ, Wise R, *et al.* (2008): Intermittent access to 20% ethanol induces high ethanol consumption in Long-Evans and Wistar rats. *Alcohol Clin Exp Res* 32:1816–1823.
- Zapata A, Gonzales RA, Shippenberg TS (2006): Repeated ethanol intoxication induces behavioral sensitization in the absence of a sensitized accumbens dopamine response in C57BL/6J and DBA/2J mice. *Neuropsychopharmacology* 31:396–405.
- Charbogne P, Gardon O, Martin-Garcia E, Keyworth HL, Matsui A, Mechling AE, *et al.* (2017): Mu opioid receptors in gamma-aminobutyric acidergic forebrain neurons moderate motivation for heroin and palatable food. *Biol Psychiatry* 81:778–788.
- Mechling AE, Arefin T, Lee HL, Bienert T, Reisert M, Ben Hamida S, *et al.* (2016): Deletion of the mu opioid receptor gene in mice reshapes the reward-aversion connectome. *Proc Natl Acad Sci U S A* 113:11603–11608.
- Arefin TM, Mechling AE, Meirsman C, Bienert T, Hübner N, Lee HL, *et al.* (2017): Remodeling of sensorimotor brain connectivity in *Gpr88* deficient mice. *Brain Connect* 7:526–540.
- Friston KJ, Kahan J, Biswal B, Razi A (2014): A DCM for resting state fMRI. *Neuroimage* 94:396–407.
- Samson HH, Slawecki CJ, Sharpe AL, Chappell A (1998): Appetitive and consummatory behaviors in the control of ethanol consumption: a measure of ethanol seeking behavior. *Alcohol Clin Exp Res* 22:1783–1787.
- Gremel CM, Cunningham CL (2007): Role of test activity in ethanol-induced disruption of place preference expression in mice. *Psychopharmacology (Berl)* 191:195–202.

High Alcohol Drinking in *Gpr88* Knockout Mice

40. Fox MD, Raichle ME (2007): Spontaneous fluctuations in brain activity observed with functional magnetic resonance imaging. *Nat Rev Neurosci* 8:700–711.
41. Mechling AE, Hubner NS, Lee HL, Hennig J, von Elverfeldt D, Harsan LA (2014): Fine-grained mapping of mouse brain functional connectivity with resting-state fMRI. *Neuroimage* 96:203–215.
42. Sanes JN, Donoghue JP (2000): Plasticity and primary motor cortex. *Annu Rev Neurosci* 23:393–415.
43. Meirsmann AC, Robe A, de Kerchove d'Exaerde A, Kieffer BL (2016): GPR88 in A2AR neurons enhances anxiety-like behaviors. *eNeuro* 3.
44. Friston KJ (2011): Functional and effective connectivity: A review. *Brain Connect* 1:13–36.
45. Russo SJ, Nestler EJ (2013): The brain reward circuitry in mood disorders. *Nat Rev Neurosci* 14:609–625.
46. Oh SW, Harris JA, Ng L, Winslow B, Cain N, Mihalas S, *et al.* (2014): A mesoscale connectome of the mouse brain. *Nature* 508:207–214.
47. Berridge KC, Robinson TE, Aldridge JW (2009): Dissecting components of reward: 'Liking', 'wanting', and learning. *Curr Opin Pharmacol* 9:65–73.
48. Lack CM, Jones SR, Roberts DC (2008): Increased breakpoints on a progressive ratio schedule reinforced by IV cocaine are associated with reduced locomotor activation and reduced dopamine efflux in nucleus accumbens shell in rats. *Psychopharmacology (Berl)* 195: 517–525.
49. Song R, Zhang HY, Li X, Bi GH, Gardner EL, Xi ZX (2012): Increased vulnerability to cocaine in mice lacking dopamine D3 receptors. *Proc Natl Acad Sci U S A* 109:17675–17680.
50. Blum K, Gardner E, Oscar-Berman M, Gold M (2012): "Liking" and "wanting" linked to reward deficiency syndrome (RDS): Hypothesizing differential responsivity in brain reward circuitry. *Curr Pharm Des* 18:113–118.
51. Howe MW, Tierney PL, Sandberg SG, Phillips PE, Graybiel AM (2013): Prolonged dopamine signalling in striatum signals proximity and value of distant rewards. *Nature* 500:575–579.
52. Adamantidis AR, Tsai HC, Boutrel B, Zhang F, Stuber GD, Budygin EA, *et al.* (2011): Optogenetic interrogation of dopaminergic modulation of the multiple phases of reward-seeking behavior. *J Neurosci* 31:10829–10835.
53. Abrahao KP, Quadros IM, Andrade AL, Souza-Formigoni ML (2012): Accumbal dopamine D2 receptor function is associated with individual variability in ethanol behavioral sensitization. *Neuropharmacology* 62:882–889.
54. Casey KF, Benkelfat C, Cherkasova MV, Baker GB, Dagher A, Leyton M (2014): Reduced dopamine response to amphetamine in subjects at ultra-high risk for addiction. *Biol Psychiatry* 76: 23–30.
55. Schuckit MA (1994): Low level of response to alcohol as a predictor of future alcoholism. *Am J Psychiatry* 151:184–189.
56. de Wit H, Phillips TJ (2012): Do initial responses to drugs predict future use or abuse? *Neurosci Biobehav Rev* 36:1565–1576.
57. Richiardi J, Altmann A, Milazzo AC, Chang C, Chakravarty MM, Banaschewski T, *et al.* (2015): BRAIN NETWORKS. Correlated gene expression supports synchronous activity in brain networks. *Science* 348:1241–1244.
58. Fornito A, Zalesky A, Breakspear M (2015): The connectomics of brain disorders. *Nat Rev Neurosci* 16:159–172.
59. Takamura T, Hanakawa T (2017): Clinical utility of resting-state functional connectivity magnetic resonance imaging for mood and cognitive disorders. *J Neural Transm (Vienna)* 124:821–839.
60. Hull JV, Jacokes ZJ, Torgerson CM, Irimia A, Van Horn JD (2016): Resting-state functional connectivity in autism spectrum disorders: A review. *Front Psychiatry* 7:205.
61. Tahmasian M, Bettray LM, van Eimeren T, Drzezga A, Timmermann L, Eickhoff CR, *et al.* (2015): A systematic review on the applications of resting-state fMRI in Parkinson's disease: Does dopamine replacement therapy play a role? *Cortex* 73:80–105.
62. Colombo B, Rocca MA, Messina R, Guerrieri S, Filippi M (2015): Resting-state fMRI functional connectivity: a new perspective to evaluate pain modulation in migraine? *Neurol Sci* 36(suppl 1):41–45.
63. Vargas C, Lopez-Jaramillo C, Vieta E (2013): A systematic literature review of resting state network–functional MRI in bipolar disorder. *J Affect Disord* 150:727–735.
64. Ma X, Qiu Y, Tian J, Wang J, Li S, Zhan W, *et al.* (2015): Aberrant default-mode functional and structural connectivity in heroin-dependent individuals. *PLoS One* 10:e0120861.
65. Fedota JR, Stein EA (2015): Resting-state functional connectivity and nicotine addiction: Prospects for biomarker development. *Ann N Y Acad Sci* 1349:64–82.
66. Baler RD, Volkow ND (2006): Drug addiction: The neurobiology of disrupted self-control. *Trends Mol Med* 12:559–566.
67. Squeglia LM, Cservenka A (2017): Adolescence and drug use vulnerability: Findings from neuroimaging. *Curr Opin Behav Sci* 13:164–170.
68. Volkow ND, Baler RD (2013): Brain imaging biomarkers to predict relapse in alcohol addiction. *JAMA Psychiatry* 70:661–663.
69. Camchong J, Stenger A, Fein G (2013): Resting-state synchrony during early alcohol abstinence can predict subsequent relapse. *Cereb Cortex* 23:2086–2099.
70. Heitzeg MM, Cope LM, Martz ME, Hardee JE (2015): Neuroimaging risk markers for substance abuse: Recent findings on inhibitory control and reward system functioning. *Curr Addict Rep* 2:91–103.
71. Cservenka A, Casimo K, Fair DA, Nagel BJ (2014): Resting state functional connectivity of the nucleus accumbens in youth with a family history of alcoholism. *Psychiatry Res* 221:210–219.
72. Cservenka A, Fair DA, Nagel BJ (2014): Emotional processing and brain activity in youth at high risk for alcoholism. *Alcohol Clin Exp Res* 38:1912–1923.
73. Peters S, Peper JS, Van Duijvenvoorde AC, Braams BR, Crone EA (2017): Amygdala-orbitofrontal connectivity predicts alcohol use two years later: A longitudinal neuroimaging study on alcohol use in adolescence. *Dev Sci* 20:12448.
74. Peters S, Jolles DJ, Van Duijvenvoorde AC, Crone EA, Peper JS (2015): The link between testosterone and amygdala-orbitofrontal cortex connectivity in adolescent alcohol use. *Psychoneuroendocrinology* 53:117–126.



Lack of anticipatory behavior in *Gpr88* knockout mice revealed by automatized home cage phenotyping

Gregoire Maroteaux^{1*}, Tanzil Mahmud Arefin^{2,3,6*}, Laura-Adela Harsan^{3,4,5}, Emmanuel Darcq¹, Sami Ben Hamida^{1,2*} and Brigitte Lina Kieffer^{1,2*#}

¹Douglas Mental Health Institute, Department of Psychiatry, McGill University, Montreal, Quebec, Canada

²IGBMC, Institut de Génétique et de Biologie Moléculaire et Cellulaire, INSERM U-964, CNRS UMR-7104, Université de Strasbourg, 67400 Illkirch-Graffenstaden, France

³Departments of Radiology, Medical Physics, Medical Center University of Freiburg, Faculty of Medicine, University of Freiburg, Freiburg, Germany

⁴Engineering science, computer science and imaging laboratory (ICube), Integrative Multimodal Imaging in Healthcare, University of Strasbourg – CNRS, Strasbourg, France

⁵Department of Biophysics and Nuclear Medicine, Faculty of Medicine, University Hospital Strasbourg, Strasbourg, France

⁶Present address: Bernard and Irene Schwartz Center for Biomedical Imaging, Department of Radiology, New York University School of Medicine, New York, NY 10016, USA.

* co-first authors and co-last authors

Corresponding author: Brigitte L. Kieffer, PhD

Douglas Hospital Research Center, Perry Pavilion Room E-3317.1, 6875 boulevard LaSalle, Montreal (Quebec) H4H 1R3, Canada.

Phone: 514 761-6131 ext: 3175 Fax: 514 762-3033.

E-mail address: brigitte.kieffer@douglas.mcgill.ca

This article has been accepted for publication and undergone full peer review but has not been through the copyediting, typesetting, pagination and proofreading process which may lead to differences between this version and the Version of Record. Please cite this article as doi: 10.1111/gbb.12473

Abstract

Mouse models are widely used to understand genetic bases of behavior. Traditional testing typically requires multiple experimental settings, captures only snapshots of behavior, and involves human intervention. The recent development of automated home cage monitoring offers an alternative method to study mouse behavior in their familiar and social environment, and over weeks. Here we used the IntelliCage system to test this approach for mouse phenotyping, and studied mice lacking the *Gpr88* that have been extensively studied using standard testing.

We monitored mouse behavior over 22 days in 4 different phases. In the free adaptation phase, *Gpr88*^{-/-} mice showed delayed habituation to the home cage, and increased frequency of same corner returns behavior in their alternation pattern. In the following nose-poke adaptation phase, non-habituation continued, however mutant mice acquired nose-poke conditioning similarly to controls. In the place learning and reversal phase, *Gpr88*^{-/-} mice developed preference for the water/sucrose corner with some delay, but did not differ from controls for reversal. Finally, in a fixed schedule-drinking phase, control animals showed higher activity during the hour preceding water accessibility, and reduced activity after access to water was terminated. Mutant mice did not show this behavior, revealing lack of anticipatory behavior.

Our data therefore confirm hyperactivity, non-habituation and altered exploratory behaviors that were reported previously. Learning deficits described in other settings were

barely detectable, and a novel phenotype was discovered. Home cage monitoring therefore extends previous findings and reveals yet another facet of GPR88 function that deserves further investigation.

Keywords. Intellicage System, GPR88, Long-term Phenotyping, Automated, Female Mice, Non-habituation, Hyperactivity, Perseveration, Learning, Anticipatory Behavior

Introduction

Psychiatric disorders are complex multi-factorial-dependent disorders (Karl and Arnold, 2014; Kim and Leventhal, 2015). Their diagnosis, treatment and recovery are long lasting processes and sensitive to environmental factors. Rodents have been used since decades to model behavioral dysfunctions related to mental disorders, and mouse models in particular are instrumental to understand genetic bases of psychiatric illnesses (Leung and Jia, 2016). Unfortunately, most standard behavioral testing modalities, which are used to investigate mouse models in psychiatry, take only snapshots of their behavior (Barnes, 1979; Crawley and Goodwin, 1980; Hall, 1932; Pellow et al., 1985). Further, in order to describe the effect of genetic background, mutation or drug on behavior, a battery of tests is required to tap into different aspects of behavior such as motor, sensory, cognitive and circadian functions (Rogers et al., 1999). The succession of tests in those batteries involves several major confounders such as repetitive human handling, testing during mice's rest period, in a new environment and often single-housing the animals. Those external stressors in turn influence the rodent behavioral responses, and should be carefully taken into account as they are source of variations that may lead to misinterpretations (Crabbe et al., 1999; Turner and Burne, 2013; Wahlsten, 2010; Würbel, 2002).

A solution to reduce confounding factor effects is to observe mouse behavior in their home cage. The recent development of automated home cage monitoring systems allows repetitive, objective, and consistent measurement of mice behavior, over days or even weeks, rather than minutes. Plus, continuous recording allows investigation of multi-dimensional

Accepted Article

aspects of behavior, in a freely moving animal, from basal activity and everyday life pattern, to challenged behavior (de Visser et al., 2006; Endo et al., 2012; Maroteaux et al., 2012). Under such conditions, animal motivation is intrinsic; the animal is not forced to react to a novel environment and handling does not bias animal responses. Over the last decade long-term home cage monitoring has been developed by several companies with different monitoring techniques (de Visser et al., 2006; Galsworthy et al., 2005). To investigate mice in a social and environmentally familiar situation (Galsworthy et al., 2005), and reduce the influence of external factors, we chose to undertake the characterization of *Gpr88* deficient mice using the IntelliCage system. This automated home cage monitors group-housed mice implanted with radio frequency identification chips and allows investigating multi-dimensional aspects of mice behavior (habituation, baseline and challenged behavior). Behavioral phenotypes have already been reported for *Gpr88* deficient mice using standard behavioral testing (Logue et al., 2009; Meirsman et al., 2016a, 2016b; Quintana et al., 2012). The goal of this study was to determine whether longitudinal IntelliCage-based investigations would confirm previous findings and uncover novel aspects of GPR88 function.

GPR88 is an orphan G protein-coupled receptor, classically described as striatal-enriched receptor (Ghate et al., 2007; Logue et al., 2009; Massart et al., 2009; Mizushima et al., 2000; Van Waes et al., 2011), with detectable expression also in the cortex and central amygdala (Becker *et al.*, 2008, Befort *et al.*, 2008). Behavioral analysis of *Gpr88* deficient mice was therefore developed using standard behavioral testing paradigms known to engage areas of highest GPR88 density. Related to striatal function, repeated exposure of *Gpr88* deficient mice to a novel environment, or housing in a uncomfortable situation, triggered non-habituation

Accepted Article

hyperactivity (Meirsman et al., 2016a; Quintana et al., 2012). Mutant mice also showed difficulties in ending behavioral sequences, including foraging time and circling, impaired procedural learning on the rotarod (Meirsman et al., 2016a) and altered hippocampus/striatal-dependent behaviors in the dual solution cross maze task (Meirsman et al., 2016a). Possibly related to receptor expression in other brain areas, those mice finally exhibited sensorimotor gating alteration with decreased pre-pulse inhibition (Logue et al., 2009), as well as low levels of anxiety (Meirsman et al., 2016a). Standard behavioral testing, therefore, detected multiple and complex phenotypes in these mice, providing an attractive knockout model for subsequent analysis. Here we tested female mice lacking *Gpr88* in the group-housed and stress-reduced conditions of the IntelliCage system. Animals were monitored during—several weeks and challenged throughout five behavioral phases including habituation, nose-poke adaptation, place and reversal learning and fixed schedule drinking. Together our data confirm the non-habituation phenotype, as well as altered exploratory behaviors that were described previously (Meirsman et al., 2016a), and also reveal a yet unreported phenotype that involves the lack of anticipation.

Material and methods

Animals

Total *Gpr88*^{-/-} knockout mice were produced as previously described (Meirsman et al., 2016a). Briefly, *Gpr88*-floxed mice were crossed with CMV-Cre mice expressing Cre recombinase under the cytomegalovirus promoter. This led to germ-line deletion of *Gpr88* exon 2 under a mixed

background (13.96% C57B1/6N; 60.94% C57B1/6J; 0.05% FVB/N; 25% 129/SvPas; 0.05% SJL/J). Mutant mice were then fully backcrossed on the hybrid 50%C57B1/6J-129/50%SvPas background, and the Cre transgene was no longer maintained once excision had occurred on both alleles. Current breeding involves heterozygous matings, and animals used in the experiments are wild-type and homozygous littermates. All mice were bred at Institut Clinique de la Souris-Institut de Génétique et Biologie Moléculaire et Cellulaire, France. Animals were group-housed under 12 h light/dark cycle. Female *Gpr88*^{-/-} (n = 16) and controls *Gpr88*^{+/+} (n = 16). Mice were 8-10 weeks old at the time of the experiments. Temperature and humidity were controlled and food and water were available ad libitum. All animal procedures in this report were conducted in accordance with the European Communities Council Directive of 24 November 1986 (86/609/EEC) and approved by both the Comité Régional d’Ethique en Matière d’Expérimentation Animale de Strasbourg (CREMEAS, 2003-10-08-[1]-58) and the local ethical comity (Comité d’Ethique en Experimentation Animale IGBMC-ICS).

IntelliCage study

The IntelliCage apparatus (NewBehavior AG, Zurich, Switzerland, www.newbehavior.com) consists of a polycarbonate cage (20.5 cm high × 58 × 40 cm at top, 55 × 37.5 cm at bottom) with a conditioning chamber in each of the 4 corners (Fig. 1B). Each chamber allows access to two water bottles for drinking one each side, by means of closable round opening. Sensors at these opening allow registering nose-pokes (Fig. 1C). The conditioning corners are accessible via a ring containing a transponder reader antenna and presence is confirmed by temperature-differential sensor. A visit is defined by antenna reading and the presence of signal. A nose-

Accepted Article

poke is counted each time the mouse inserted its nose in the round opening, whether the door opened or not. Licks are registered by a lickometer, each time a mouse touches the drinking spout. The apparatus is controlled by the IntelliCage software 2.1, described previously (Krackow et al., 2010; Voikar et al., 2010). The study was done with female mice as they have a greater compatibility in a social home cage setting and the long-term monitoring will most likely cancel most of the fluctuation due to their 5-days long estrous cycle (Kobayashi et al., 2013).

General procedures

One week before the start of the experiment, mice were implanted subcutaneously with Radio frequency identification transponders (Planet ID GmbH, Essen, Germany) under isoflurane inhalation anesthesia.

Description of the 22 days protocol (Figure 1):

Free adaptation phase

Mice were separated in groups of 8 animals with identical genotype and placed in 4 IntelliCages. During the 1st four days, all four corners and door were opened, giving access to 2 water bottles per corner. Food was accessible *ad libitum*. The alternation pattern was defined on four consecutive visits as follow: 1) spontaneous corner alternations (SCA) were counted if three first corner visits out of a four were different, 2) alternate corner returns (ACR) were counted when a mouse visited the same corner two times, with a different corner in-between and 3) Same corner returns (SCR) were counted when a mouse visited the same corner two times in a row. As mice could visit the corners at their own rhythm, we started the analysis for

Accepted Article

spontaneous alternations using a number of visits threshold of 100 (not a time threshold). This number was chosen to be high enough to establish a percentage and also not too large to remain in the acclimation phase for the mouse (one mouse was removed as it took over two days to reach 100 visits). The last mouse reached 100 visits 11h after the beginning of the free adaptation phase. The analysis was then done on all the corner visits of the free adaptation phase.

Nose-poke adaptation

During the three following days, all doors were closed and could be opened once per visit in response to a minimum of successive 5s nose-poke giving access to the water spouts.

Sucrose preference and reversal

During the 3 following days, water was replaced by a 8% sucrose solution in one bottle of each corner. To prevent learning by imitation, cage mates were divided in 4 pairs, each pair of mice had a designated corner (correct corner) in which they could access water or sucrose in response to a 5s nose-poke. The correct corner was set as the opposite corner (in the diagonal) for the three following days in the reversal phase.

Fixed schedule drinking

Sucrose solution was replaced by water (2 water bottles per corner, as in the first two phases). During the 9 following days, water access was restricted to two one-hour time periods during the light phase (11 am and 4 pm). Mice still had to nose-poke in order to open access to the spout,

but any nose-poke outside those 2 hours did not give access to the spout. We studied this phase during dark and light phase to observe the influence on the daily rhythm, and we also focused on the one-hour period before, during and after the access to water in order to analyze the anticipatory and persistent behavior of mice.

Statistical analysis

In a first step, data were checked for outliers (> 3 times the standard deviation from the strain mean) for each phase of the experiment. One mouse was removed for outlying in the number of visits and nose-pokes in the free adaptation phase. Another one was not drinking anymore in the nose-poke adaptation phase and was removed. A third animal was outlying in time spent in the corner during fixed schedule drinking and was also removed. Once removed in one phase, outlier mice were automatically removed for the following phases.

In a second step, the two cages housing *Gpr88*^{+/+} mice and the two cages housing *Gpr88*^{-/-} mice were compared to each other for total number of visits and nose-pokes in the first in habituation and nose-poke adaptation phases. The two cages housing *Gpr88*^{+/+} mice were indistinguishable, as were the two cages housing *Gpr88*^{-/-} mice. Thus, mice were regrouped genotype-wise for the analysis.

Data were analyzed using IBM SPSS statistic 20 (IBM, Armonk, NY, USA) to run two or three factors repeated-measures (RM) ANOVA. Whenever sphericity was violated a Greenhouse-Geisser correction was applied. For post-hoc and planned pairwise comparison, we used a Sidak's multiple comparison correction was applied when significant ANOVA results between factors were revealed. For mean comparison, one-way ANOVA were performed when

normality and equality of the variance were met, otherwise a non-parametric Mann-Whitney U-test was applied. An error probability level of $p < 0.05$ was accepted as statistically significant. All values are represented by means \pm S.E.M.

Results

We monitored spontaneous activity of group-housed *Gpr88*^{-/-} female, and their controls, using IntelliCages with saw dust-covered floor to reduce external stressors. The experimental design allowed animal monitoring under basal conditions (free adaptation), during conditioning (nose-poke adaptation; place learning then reversal learning) and in challenging conditions (fixed schedule drinking) in that order. Activity was recorded for each mouse using RFID tracking to register individual visits of the conditioning corners. The five phases of the protocol lasted 22 days in total, and are detailed in Figure 1.

Free adaptation phase – Gpr88^{-/-} mice show delayed habituation and altered exploratory behavior

Prior to any challenge, it is essential to characterize responses to the novel environment, here the IntelliCage, and baseline activity of the animals. Plus, GPR88 deficiency affects striatal function impairing locomotor activity (Do et al., 2012; Meirsmann et al., 2016a; Quintana et al., 2012). During the free adaptation phase, mice could freely explore the new cage for 4 days and had access to all eight water bottles. Overall, diurnal activity was similar for the two groups. Peaks of activity were observed during the active dark periods and deeps in the activity were

obvious during the resting light periods (Figure 2A). Analysis was then further performed separately for dark and light periods. In Figure S1A, cumulative raw data are shown and the number of licks shows that *Gpr88*^{-/-} mice took more time to start drinking from the water bottles.

Dark period. In Figure 2B, two-ways RM-ANOVA revealed an effect of Time on the number of visits ($p < 0.001$) but not on the number of nose-pokes and licks during the active phase. Genotype had an effect on the number of nose-pokes ($p = 0.023$) but not on the number of visits and licks. Interaction between Time and Genotype had an effect on all three parameters ($p_{\text{visits}} = 0.003$, $p_{\text{nose-pokes}} = 0.002$ and $p_{\text{licks}} = 0.02$). Pairwise comparison tests yielded a significant decrease in the number of visits (Dark1 (D1) vs. D4, $p < 0.001$), nose-pokes (D1 vs. D4, $p = 0.017$) and licks (D1 to D3, $p = 0.032$) for *Gpr88*^{+/+} mice, showing a clear adaptation to the new environment. In contrast, *Gpr88*^{-/-} mice began with a lower number of visits on D1 ($p < 0.01$) and a similar number of nose-pokes was observed for the two groups. Further, *Gpr88*^{-/-} mice did not decrease their number of visits and nose-pokes over time, and therefore showed a higher number of visits ($p = 0.026$) and nose-pokes ($p = 0.012$) on D4 compared to *Gpr88*^{+/+} mice. Moreover, *Gpr88*^{-/-} mice showed no significant difference in the number of licks between D1 and 3 and a significant increase in D4 ($p = 0.043$). Together, data from the dark period of the free adaptation phase reveal a clear difference between genotypes in adapting to the new environment, with *Gpr88*^{+/+} but not *Gpr88*^{-/-} mice showing habituation to the environment after four days.

Light period. In Figure 2C, two-ways RM-ANOVA revealed an effect of Time on the number of visits ($p < 0.001$), nose-pokes ($p < 0.001$) and licks ($p = 0.044$) but no effect of Genotype. Interaction between Time and Genotype showed an effect in the number of nose-

Accepted Article

pokes ($p = 0.004$) and licks ($p = 0.008$) but not in the number of visits. Pairwise comparison tests revealed a stable number of nose-pokes and licks throughout the free adaptation phase for *Gpr88*^{+/+} mice, and a significant increase of nose-pokes (L1 vs. L3, $p < 0.001$) and licks (L1 vs. L3, $p = 0.014$) for *Gpr88*^{-/-} mice. Thus, in their resting period, *Gpr88*^{-/-} mice do not differ from *Gpr88*^{+/+} mice, except for the number of licks that was higher in *Gpr88*^{+/+} mice on L1 ($p = 0.034$) and L2 ($p = 0.025$).

Spontaneous alternations. To test hippocampal-dependent navigation, as was done previously using a Y-maze (Meirsman et al., 2016a), we used the four identical corners of the IntelliCage to quantify spontaneous alternations over the first hundred visits of each mouse to stay in the acclimation phase. As for the Y-maze, we divided the alternation in 3 groups 1) spontaneous corner alternation (SCA), 2) alternate corner return (ACR) and 3) same corner return (SCR). Two-way ANOVA on the number of alternations revealed no effect of Genotype but an effect of the type of alternation ($p = 0.043$) and an interaction between both factors ($p = 0.004$). Pairwise comparison tests revealed that *Gpr88*^{+/+} mice made a significantly higher number of spontaneous corner alternations compared to alternate corner returns ($p = 0.028$), same corner returns ($p = 0.011$), and compared to *Gpr88*^{-/-} mice ($p = 0.007$) (Figure 2D). Thus, although there was no significant difference in the total number of alternations between the groups ($p = 0.066$) (Figure 2E), *Gpr88*^{+/+} mice displayed an exploration behavior going successively in each corner, whereas *Gpr88*^{-/-} mice displayed an increase sequence of repeated actions by visiting the same corner several times in a row. We also characterized the alternation pattern of visits over the entire free adaptation phase. As shown in Figure 2F, two-way ANOVA on the number of alternations revealed an effect of Genotype ($p = 0.008$), of the type of

Accepted Article

alternation ($p = 0.003$) and an interaction between both factors ($p = 0.011$). Pairwise comparison tests revealed that *Gpr88*^{+/+} mice displayed the three types of alternations to similar levels, and made significantly more spontaneous corner alternations ($p = 0.002$) and alternate corner returns ($p = 0.015$) than *Gpr88*^{-/-} mice. In contrast, *Gpr88*^{-/-} mice made significantly more same corner returns than spontaneous corner alternations ($p = 0.001$) and alternate corner return ($p < 0.001$). Total alternations over the 4 days of free adaptation phase were also lower for *Gpr88*^{-/-} mice ($p = 0.04$) (Figure 2G). Again, therefore, *Gpr88*^{+/+} mice displayed a randomized visit behavior with no difference in the alternation pattern, whereas *Gpr88*^{-/-} mice showed an altered exploratory behavior with more same corner returns.

Taken together, data from the free adaptation phase show a clear habituation pattern for *Gpr88*^{+/+} mice, including decreasing number of visits, nose-pokes and licks along dark periods. *Gpr88*^{-/-} mice did not display this habituation pattern, as shown by stable number of visits and increased number of nose-pokes throughout this phase. Further, *Gpr88*^{-/-} mice displayed a preference to return to the previously visited corner (for statistical detail see Supplementary Table 1). Observations from this phase confirm non-habituation behaviors, which we previously described for *GPR88*^{-/-} mice (Meirsmann et al., 2016a) and an exploratory behavior distinct from control mice.

Nose-poke adaptation - *Gpr88*^{-/-} mice remain more active 7 days after entering the IntelliCage

Following the Free adaptation phase and prior to any behavioral tests in the IntelliCage, female mice were exposed to three days of behavioral training, in which they needed to perform a 5s nose-poke per visit to access the water bottles, the nose-poke adaptation phase.

Dark period. In Figure 3A, Two-way RM-ANOVA revealed an effect of Time on the number of visits ($p = 0.001$) and nose-pokes ($p = 0.004$), but not on the number of licks. Genotype had an effect on the number of nose-pokes ($p = 0.041$) and licks ($p = 0.006$) but not on the number of visits. Interaction between Time and Genotype had an effect on all three parameters ($p_{\text{visits}} < 0.001$, $p_{\text{nose-pokes}} = 0.023$ and $p_{\text{licks}} = 0.018$). Pairwise comparison tests revealed a significant decrease in the number of visits (D5 vs. D7, $p = 0.014$), and no significant changes in the number of nose-pokes and licks for *Gpr88*^{+/+} mice. Whereas, *Gpr88*^{-/-} mice showed a trend to decrease their number of visits (D5 vs. D7, $p = 0.053$), a steep decrease followed by an increase in the number of nose-pokes (D5 vs. D6, $p < 0.001$ and D6 vs. D7, $p = 0.009$) and licks (D5 vs. D6, $p = 0.004$ and D6 vs. D7, $p = 0.003$). Thus, there was a higher number of visits ($p = 0.008$), nose-pokes ($p = 0.047$) and licks ($p = 0.011$) on D7 for *Gpr88*^{-/-} mice compared to their controls.

Light period. In Figure 3B, Two-way RM-ANOVA revealed an effect of Time on the number of visits ($p < 0.001$), nose-pokes ($p < 0.001$) but not licks, no effect of the Genotype and no Interaction between Time and Genotype on all three parameters.

Overall. In Figure 3C, *Gpr88*^{-/-} mice showed a higher total number of licks ($p = 0.009$) and nose-pokes ($p = 0.05$).

Taken together, these data show a stabilization of control mice behavior after habituation phase, whereas *Gpr88*^{-/-} mice still showed more activity with significantly higher numbers of

visits, nose-pokes and licks on D7 during the dark. Notably however, and as for control mice, mutant animals showed no difficulty in acquiring 5s nose-poke conditioning to obtain water (for statistical detail see Supplementary Table 2)

Place learning and reversal - Gpr88^{-/-} mice show delayed preference learning but reversal learning is intact

GPR88 deficiency affects learning and memory in different classical paradigms (Meirsman et al., 2016a; Quintana et al., 2012). Here, *Gpr88^{-/-}* mice were tested for place learning and reversal procedures. These tasks consisted in two phases of three days each in the IntelliCage protocol (Figure 1A). First, in the place learning phase, the water of one bottle was replaced by an 8% sucrose solution in each corner. Pairs of cage-mates were assigned to one corner (correct corner) in which they could access water or sucrose in response to a consecutive 5s nose-poke. The other corners were accessible but access to the bottles was blocked. Second, in the reversal phase, the corner with accessible bottles was switched to the opposite side for each pairs of cage-mates. For each phase, we analyzed the total number of visits, nose-pokes and lick per dark and light periods. We also analyzed the correct number of visits and nose-pokes, defined as visits or nose-pokes in the corner with access to bottles, as well as the percentage of correct visits (% visits) and nose-pokes (% nose-pokes). The licks were separated in total lick and sucrose licks. For the percentage of licks on the sucrose side (% sucrose licks), the data are shown per day (not per dark and light periods) because several mice (8 per group) did not perform licks during the light phase (Figure 4F and 4M).

Place learning. The total number of visits (Figure 4A), nose-pokes (Figure 4C) and licks (Figure 4E) in all corners during the place learning phase were not different between the two genotypes. Similarly, the number of visits and nose-pokes in the correct corners and licks in the sucrose side were not significantly different between the two genotypes. Two-ways RM-ANOVA revealed an effect of Time on the percentage of nose-pokes in the correct corner ($p = 0.007$) with no effect of the percentage of correct visits. No effect of Genotype or interactions was detected for the two parameters. Further, pairwise comparison revealed lower % visits ($p = 0.014$, Figure 4B) and % nose-pokes ($p = 0.009$, Figure 4D) in the correct corner for *Gpr88*^{-/-} mice on D9 compared to their wild-type littermates. Indeed, *Gpr88*^{+/+} mice displayed a preference to visit the correct corner with more than 34% on D9 (chance level of visit is 25%), whereas *Gpr88*^{-/-} mice were only at 25.8% correct visits. Finally, both groups displayed a similar preference to lick (Figure 4E) on the sucrose side (> 60% for each day of the experiment) over the three days of the experiment (Figure 4F). Taken together, these data show that the development of the preference for the correct corner was slightly delayed in *Gpr88*^{-/-} mice, yet the preference for sucrose was similar in the two groups.

Reversal. Our previous study showed enhanced behavioral flexibility of *Gpr88*^{-/-} mice in a cross-maze (Meirsman et al., 2016a). To challenge this phenotype, we tested reversal learning after the place learning phase was completed. In the reversal phase, the two groups displayed a similar number of total visits (Figure 4G), as well as correct number of visits (Figure 4H) and sucrose licks (Figure 4M). Also, *Gpr88*^{-/-} mice displayed significantly more total number of nose-pokes ($p = 0.028$) (Figure 4J) and total number of licks ($p = 0.047$) (Figure 4L). Further, the two groups showed a percentage of correct visits and nose-pokes above 30% and 40%

Accepted Article

respectively, and a preference for the sucrose solution higher than 67%, during the reversal phase (Figure 4H, 4K and 4M). Next, we tested whether place reversal learning and strategy switching occurred immediately after the corner switch, we specifically analyzed the percentage of correct visits in the reversal corner over the first 25, 50, 100 and 200 corner visits (Figure 4I). A Two-ways RM-ANOVA revealed an effect of the number of visits on the Percentage of correct visits ($p < 0.001$) but no Genotype or interaction effect. This result shows that both groups increased their percentage of new correct corner visits in D11.

Altogether, data from place learning and reversal indicate that *Gpr88*^{-/-} mice are capable to learn the task, although with some delay, and show no obvious behavioral flexibility abnormality (for statistical details see Supplementary Table 3) and for the full dataset -% visits to correct and incorrect corners during both learning and reversal phases- see **Supplementary Figure 2**).

Fixed schedule drinking - Gpr88^{-/-} mice show altered anticipatory and persistent behavior

Gpr88^{-/-} mice show striatal alteration of basal dopamine and an enhanced amphetamine-induced hyper-locomotion (Logue et al., 2009) suggesting a modification in reward-related responses. To test temporal learning abilities as well as motivation for a natural reward, we used the Fixed Schedule drinking task. During 9 days mice had access to water bottles for one hour twice a day, starting at 11am and 4pm (light phase). The rest of the time, doors in front of the spouts remained closed.

12 hours bins. Prior to the statistical analysis, we controlled whether all the mice were activating the lickometer during the two access hours. As shown in Figure S3A, three-way RM-

ANOVA revealed an effect of Days ($p < 0.001$), and Hour ($p < 0.001$), but not Genotype on the number of licks. Interactions effect were also found between Days and Hour ($p < 0.001$) and Days x Hour x Genotype ($p = 0.004$) but not Days and Genotype. Pairwise comparison tests revealed no difference in the number of licks for hour 11am and hour 4pm between the two genotypes. However, both genotypes displayed a significantly higher number of licks in hour 11am compared to 4pm ($p < 0.001$ for both). In addition, an average of 86% ($\pm 10\%$) of all mice went to drink on hour 11am, against only 43% ($\pm 5\%$) on hour 4pm over the nine days of experiment. The difference between 11 am vs 4 pm strongly suggests that all mice were drinking sufficiently, despite restricted access to water.

In this task however, *Gpr88*^{-/-} mice showed a different response compared to their counterparts. Two-ways RM-ANOVA revealed a significant effect of Time, Genotype and interaction on the number of visits (Figure 5A; $p_{\text{time}} < 0.001$, $p_{\text{genotype}} = 0.016$ and $p_{\text{interaction}} < 0.001$) and nose-pokes (Figure S3B; $p_{\text{time}} < 0.001$, $p_{\text{genotype}} < 0.01$ and $p_{\text{interaction}} < 0.001$) in the corner. Pairwise comparison tests revealed that control mice modified their corner visit activity after three days, as the difference between dark and light periods disappeared ($p > 0.05$ from days 16 to 22) (Figure 5A), with no significant changes in the number of nose-pokes (Figure S3B). *Gpr88*^{-/-} mice also decreased their number of corner visits during the dark period. However, a marked difference remained between dark and light periods ($p < 0.01$ from days 14 to 22) (Figure 5A). Also, the difference in nose-poke number between dark and light periods decreased until D16 and then stabilized ($p > 0.1$) (Figure S3B). While observing only the active periods (dark periods) in Figure S3C, a two-way RM-ANOVA, on the number of visits, showed an effect of the Days ($p < 0.001$), of Genotype ($p < 0.001$) and an interaction between both ($p =$

0.006). Pairwise comparison revealed a significant decrease in the number of visits on D15 for both *Gpr88*^{+/+} ($p = 0.036$) and *Gpr88*^{-/-} mice ($p = 0.022$) followed by slow decrease before stabilization of the number of visits until D18 for *Gpr88*^{+/+} mice and D19 for *Gpr88*^{-/-} mice. Overall, *Gpr88*^{-/-} mice displayed a significantly higher number of visits during the dark periods ($p < 0.001$) (Figure 5B), and lower number of visits in the light periods ($p < 0.01$) (Figures 5C & S3D). At 11 am, more than 80% mice accessed the water bottles on average over the 9 days of the experiment, whereas less than 50% mice made licks at 4 pm (Figures S3A, E & F), making statistics less robust for the latter time period. We therefore focused on the 11 am period and compared the number of visits and nose-pokes one hour before (hour 10), during (hour 11) and after (hour 12) mice had access to the water, during the 9 days of the experiment.

Hours before water access. During hours preceding water access, *Gpr88*^{-/-} mice showed a different response compared to their counterparts. Two-way RM-ANOVA on the number of visits showed a significant interaction between Days and Genotype for the three hours before water access (p 's < 0.05) (Figure 5D). During the fourth (-4h) and fifth hours (-5h) before water access period both genotypes visited the corners equally over days of the experiment. However, overall the number of visits increased in *Gpr88*^{+/+} mice compared to *Gpr88*^{-/-} mice during the 3 hours preceding water access (p 's < 0.05). Two-way RM-ANOVA on the number of nose-pokes only revealed an interaction between Days and Genotype two hours before water access ($p < 0.05$). (Figure 5E). Pairwise comparison revealed differences between the two groups only at the beginning of the phase, on day 14 ($p < 0.05$) and 15 ($p < 0.001$).

Hour during water access. As showed in Figure 5D, during the hour when water was accessible, two-way RM-ANOVA on the number of visits showed no effect of the Genotype, a

Accepted Article

significant effect of Days ($p < 0.001$) and an significant interaction between Days x Genotype factors ($p < 0.001$). Two-way RM-ANOVA on the number of nose-pokes showed an effect of Days only ($p = 0.004$), with no Genotype or interaction effect for the two factors. Pairwise comparison tests on the number of visits revealed a difference between the groups only on day 14 ($p = 0.001$), showing that when water was accessible, both groups had a similar visit behavior during almost the entire experiment.

Hour after water access. During the 2 hours following water access, two-way RM-ANOVA on the number of visits showed a significant interaction between Days and Genotype factors (p 's < 0.05) (Figure 5D). Pairwise comparison tests revealed that for the first hour following water access time a higher number of visits for *Gpr88*^{-/-} from day 15 to 19 compared to *Gpr88*^{+/+} mice ($p < 0.05$, except at day 17 $p = 0.07$). However, for the second hour after water access period, only higher visits for *Gpr88*^{-/-} were observed on day 15 and 16 compared to *Gpr88*^{+/+} mice. Two-way RM-ANOVA on the number of nose-pokes also showed a significant interaction between Days and Genotype factors ($p = 0.002$) between the two factors an hour after water access (+1h) but not on the second hour (+2h) (Figure 5E). Pairwise comparison tests revealed that for the first hour following water access time a higher number of nose-pokes for *Gpr88*^{-/-} from day 15 to 19 compared to *Gpr88*^{+/+} mice ($p < 0.05$, except at day 17 $p = 0.07$).

Taken together, these data first indicate that *Gpr88*^{-/-} mice show a delay in adjusting their behavior to the new rule (late stabilization of the number of corner visits during the dark phase). Further, and contrary to control mice also, mutant animals did not seem to develop an anticipatory behavior (higher number of visits) in the time period preceding the water-accessible

hour. Finally, mutant mice were more persistent (higher number of visits) to visit corners after water was not accessible anymore (for statistical detail see Supplementary Table 4).

Discussion

Previous studies of Gpr88 null mutant mice were done using standard behavioral tests, which provide snapshots of individual mouse behavior in novel testing environments, (Logue et al., 2009 ; Meirsman et al., 2016a; Quintana et al., 2012). In this study, we performed longitudinal analysis of group-housed mutant females in an automated home cage system. We designed a 22-days protocol in the IntelliCage apparatus where mouse behavior was monitored in 4 different phases: 1) Free adaptation: *Gpr88*^{-/-} mice showed delayed habituation to the home cage, and altered exploratory behavior in their alternation pattern; 2) Nose-poke adaptation: non-habituation in *Gpr88*^{-/-} mice continued through this phase, however mutant mice acquired the 5s nose-poke conditioning similarly to their control counterparts; 3) Place learning and reversal: *Gpr88*^{-/-} mice showed a slight delay in developing preference for the water/sucrose accessible corner, but showed no difference from controls in the reversal phase; 4) Fixed schedule drinking: *Gpr88*^{-/-} mice showed delayed adaptation to the fixed drinking hour with an elevated light/dark activity along the entire phase. Importantly in this phase, control animals showed higher activity during the hour preceding accessibility to water, and highly reduced activity after access to water was terminated, while on the contrary, mutant mice showed a lack of anticipatory behavior followed by persistent higher activity after water was not available anymore.

Results from the IntelliCage study are summarized in Table 1 and confronted to published data using conventional testing methods. In order to be able to compare data from the IntelliCage set-up to those from conventional testing, we have classified behavioral responses collected throughout the five IntelliCage phases in five phenotypic categories: hyperactivity (section 1), non-habituation (section 2), altered exploratory behavior (section 3), learning (section 4) and anticipatory behavior (section 5). While the three former are fully concordant with already reported phenotypes, the learning phenotype appears complex and is refined in this study, and the lack of anticipatory behavior is novel.

The IntelliCage protocol confirms hyperactivity, non-habituation and altered exploratory behavior in *Gpr88* deficient mice

In previous reports, deletion of *Gpr88* in mice was reported to caused hyperactivity, non-habituation and repetitive exploratory behavior (detailed in Table 1, first three sections). This phenotype was reported through different tests and in both males and females. Our data using group-housed females in a home cage environment are in line with these results. In the five different phases of the protocol, *Gpr88*^{-/-} mice showed a higher number of visits, nose-pokes and/or licks (Table 1). Under IntelliCage conditions also, the *Gpr88* deletion effect could not be detected during the light (resting) phase, hyperactivity was only observed during the active phase (dark phase) and did not affect diurnal rhythm (Figure 2A). Further, *Gpr88*^{-/-} mice showed a non-habituation behavior, with no decrease in the number of visits after the free adaptation, more same corner returns and maintained a marked light-dark rhythm in the fixed schedule (Figures 2B, E, G and 5A). Finally, the higher percentage of same corner returns (Figures 2E

and 2G) can be interpreted as an altered exploratory behavior, as detected in *Gpr88*^{-/-} mice in our previous study (Meirsman et al., 2016a). Together, data throughout the IntelliCage protocol strengthen the characterization of *Gpr88*^{-/-} mice displaying a non-habituating hyperactivity and confirm the tendency to repeat certain behaviors. Compared to standard behavioral test, automated home cage recording brings advantages in behavioral screening in that, with only one experiment using relatively few animals (n = 16/group) and time, we could reproduce previous findings that necessitated ten different assays (Meirsman et al., 2016a). Of note, our data are focused on female animals, whereas previous standard testing used both males and females and showed few statistical gender differences, such as nest building, startle response and rotarod (Logue et al., 2009; Meirsman et al., 2016a; Quintana et al., 2012). Hence, it would be interesting to repeat this IntelliCage experiment with groups of male siblings raised together.

The Intellicage long-lasting protocol reveals only subtle learning deficit

The total deletion of *Gpr88* in mice affects several forms of learning, which involve both striatal and hippocampal function (see Meirsman et al., 2016a; Quintana et al., 2012 and Table 1). In a first study (Quintana et al., 2012), *Gpr88*^{Cre/Cre} mice showed normal turned-based (egocentric) learning involving the striatum (Rubio et al., 2012) but cue-based (allocentric) learning involving the hippocampus was delayed (Kleinknecht et al., 2012). In a further study using different testing paradigms (Meirsman et al., 2016a), we reported facilitated hippocampal-dependent behaviors in *Gpr88*^{-/-} mice, based on less repetitive arm re-entries in the Y-maze, higher preference for the displaced object in the novel object recognition test, and a faster acquisition and behavioral shift in the dual solution task using a cross-maze, all requiring hippocampal

Accepted Article

integrity (Kleinknecht et al., 2012; Oliveira et al., 2010). In the IntelliCage, learning occurs in yet another different experimental setting, and likely recruits striatal and hippocampal functions differently from the previous studies. In this case, *Gpr88*^{-/-} mice mutant mice showed slightly delayed place learning, and reversal learning was intact indicating that spatial cues remain correctly interpreted (Figure 4). In fact, the learning phenotype of mutant mice in the IntelliCage set-up remained extremely subtle. It seems therefore that, despite previous evidence of altered striatal/hippocampal balance in *Gpr88*^{-/-} mice (Meirsmann et al., 2016a), the non-stressful home cage conditions allowed optimal learning performance in mutant mice. This is clear evidence that the IntelliCage system offers a very distinct environmental and emotional context for animal testing, compared to conditions of traditional behavioral analyses.

The IntelliCage system reveals delayed anticipatory behavior in Gpr88 deficient mice

The longitudinal aspect of the IntelliCage protocol allowed analyzing the behavior before and after the one-hour water access in the fixed schedule-drinking phase. The need to drink water was comparable in the two groups because, when water was accessible, no major difference was observed between the groups in number of visits, nose-pokes and licks at both 11 am or 4 pm (Figure 5D & E and Fig. S3A), suggesting that thirst-activated circuits in the hypothalamus (Oka et al., 2015) are unaffected in mice lacking *Gpr88*. Interestingly however, after four days, control mice increased their number of visits during the hour preceding water access, which may be interpreted as an anticipation of the up-coming event (water access), whereas *Gpr88*^{-/-} mice did not show this behavior (Figure 5D). This interpretation is based on the fact that, although the 24h water deprivation step does not produce robust physiological changes

(Bekkevold et al., 2013), mice are subjected to 19-hour water deprivation for nine consecutive days and that, under these conditions, drinking water is considered an innately rewarding behavior (Rolls and Rolls, 1982).

Reward anticipation neural networks involve both the striatum and cortical regions including visual association cortex and the somatosensory cortex (Jia et al., 2016) and the fact that *Gpr88*^{-/-} mice did not anticipate the water access suggests a possible alteration of this neural network. This is consistent with the prominent expression of GPR88 in both striatum and cortex (Massart et al., 2009, Massart et al., 2016). This conclusion also fully accords our recent discovery of specific GPR88 expression in layer 4 of the somatosensory cortex, paralleling delayed sensory processing in *Gpr88*^{-/-} mice (Ehrlich et al., 2017), as well as our recent fMRI data from *Gpr88*^{-/-} mice indicating disrupted functional connectivity predominantly at the level motor and sensory cortices, as well as the striatum in live mutant mice (Arefin et al., 2017). In further support of our interpretation, the ventral striatum was shown activated in response to ingestive behavior (Pitchers et al., 2010; Yoshida et al., 1992), and dopamine levels in lateral hypothalamic area and the nucleus accumbens are associated with anticipatory and consummatory phases of feeding (Legrand et al., 2015). Altogether therefore, we propose that GPR88 plays a role in reward anticipation, involving striatum-cortex communication. This function has not been described as yet, and was revealed by refined temporal data analysis from the IntelliCage approach. Further experiments using highly palatable food schedule in the IntelliCage (similar to Hsu et al., 2010) or selected standard testing paradigms (5-choice serial reaction time task) and conditional knockout approaches (see for example Meirnsman et al.,

2016b) will further investigate this aspect of Gpr88 knockout mice behavior, and determine the exact brain site for this particular GPR88 function.

Conclusion

Standard behavioral testing is designed to study hypothesis-driven behavioral modifications, and provide reasonable interpretations in the least amount of time. A large number of classical testing paradigms are based on the behavioral reaction to a novel environment (e. g. open-field, elevated plus maze) for a short time period (minutes to maximum one hour). Thus, standard testing provides no baseline condition, and reactions are always recorded in response to challenging conditions, hence in a state of arousal (“stress”) of the animal. However, psychiatric diseases are chronic illnesses and their diagnosis, treatment and recovery are long lasting processes and depend on the environmental factors including pharmacotherapies. Their complexity compels the development of long-term, unbiased behavior assays taking place in familiar environment for the mice. In Long-term-based behavioral analysis, such as IntelliCage, the animal is constantly monitored, allowing a multidimensional behavioral profiling. Through the development of an IntelliCage protocol, we were able to observed hyperactivity (Figure 2, 3, 4 and 4), non-habituation (Figure 2 and 5), altered exploratory behavior (Figure 2 and 5) and learning alteration (Figure 4), that were previously described using ten different classical behavioral tests (Table 1). Home cage monitoring therefore extends the characterization of these mutant mice, revealing another facet of GPR88 function, and providing yet another useful endophenotypic profile in the context of genetic mouse models for neuropsychiatric disorders.

Acknowledgements

This project was funded by the ATHOS Consortium (Fonds Unique Interministériel, Région Alsace, Domain Therapeutics Illkirch, France and Prestwick Chemicals Illkirch, France) and the the National Institutes of Health (NIH-NIAAA #16658 and NIH-NIDA #005010). GM was supported by the Bourgeois Chair for Pervasive Developmental Disorders and TA was supported by the NeuroTime Erasmus+: Erasmus Mundus program of the European Commission. BK is grateful to the Canada Research Chairs.

References

- Arefin, T., Mechling, A.E., Meirman, C.A., Bienert, T., Huebner, N.S., Lee, H.-L., Ben Hamida, S., Ehrlich, A., Roquet, D., Hennig, J., von Elverfeldt, D., Kieffer, B.L., Harsan, L.-A., 2017. Remodeling of Sensorimotor Brain Connectivity in Gpr88 deficient mice. *Brain Connect.* <https://doi.org/10.1089/brain.2017.0486>
- Barnes, C.A., 1979. Memory deficits associated with senescence: a neurophysiological and behavioral study in the rat. *J. Comp. Physiol. Psychol.* 93, 74–104.

- Bekkevold, C.M., Robertson, K.L., Reinhard, M.K., Battles, A.H., Rowland, N.E., 2013. Dehydration Parameters and Standards for Laboratory Mice. *J. Am. Assoc. Lab. Anim. Sci.* JAALAS 52, 233–239.
- Crabbe, J.C., Wahlsten, D., Dudek, B.C., 1999. Genetics of mouse behavior: interactions with laboratory environment. *Science* 284, 1670–1672.
- Crawley, J., Goodwin, F.K., 1980. Preliminary report of a simple animal behavior model for the anxiolytic effects of benzodiazepines. *Pharmacol. Biochem. Behav.* 13, 167–170.
- de Visser, L., van den Bos, R., Kuurman, W.W., Kas, M.J.H., Spruijt, B.M., 2006. Novel approach to the behavioural characterization of inbred mice: automated home cage observations. *Genes Brain Behav.* 5, 458–466. <https://doi.org/10.1111/j.1601-183X.2005.00181.x>
- Do, J., Kim, J.-I., Bakes, J., Lee, K., Kaang, B.-K., 2012. Functional roles of neurotransmitters and neuromodulators in the dorsal striatum. *Learn. Mem. Cold Spring Harb.* N 20, 21–28. <https://doi.org/10.1101/lm.025015.111>
- Ehrlich, A.T., Semache, M., Bailly, J., Wojcik, S., Arefin, T.M., Colley, C., Gouill, C.L., Gross, F., Lukashova, V., Hogue, M., Darcq, E., Harsan, L.-A., Bouvier, M., Kieffer, B.L., 2017. Mapping GPR88-Venus illuminates a novel role for GPR88 in Sensory Processing. (in revision).
- Endo, T., Kakeyama, M., Uemura, Y., Hajjima, A., Okuno, H., Bito, H., Tohyama, C., 2012. Executive Function Deficits and Social-Behavioral Abnormality in Mice Exposed to a Low Dose of Dioxin In Utero and via Lactation. *PLOS ONE* 7, e50741. <https://doi.org/10.1371/journal.pone.0050741>
- Galsworthy, M.J., Amrein, I., Kuptsov, P.A., Poletaeva, I.I., Zinn, P., Rau, A., Vyssotski, A., Lipp, H.-P., 2005. A comparison of wild-caught wood mice and bank voles in the Intellicage: assessing exploration, daily activity patterns and place learning paradigms. *Behav. Brain Res.* 157, 211–217. <https://doi.org/10.1016/j.bbr.2004.06.021>
- Ghate, A., Befort, K., Becker, J. a. J., Filliol, D., Bole-Feysot, C., Demebele, D., Jost, B., Koch, M., Kieffer, B.L., 2007. Identification of novel striatal genes by expression profiling in adult mouse brain. *Neuroscience* 146, 1182–1192. <https://doi.org/10.1016/j.neuroscience.2007.02.040>
- Hall, C., 1932. A study of the rat's behavior in a field. A contribution to method in comparative psychology. *Univ. Calif. Publ. Psychol.* 6, 1–12.
- Hsu, C.T., Patton, D.F., Mistlberger, R.E., Steele, A.D., 2010. Palatable meal anticipation in mice. *PLoS One* 5. <https://doi.org/10.1371/journal.pone.0012903>
- Jia, T., Macare, C., Desrivieres, S., Gonzalez, D.A., Tao, C., Ji, X., Ruggeri, B., Nees, F., Banaschewski, T., Barker, G.J., Bokde, A.L.W., Bromberg, U., Büchel, C., Conrod, P.J., Dove, R., Frouin, V., Gallinat, J., Garavan, H., Gowland, P.A., Heinz, A., Ittermann, B., Lathrop, M., Lemaitre, H., Martinot, J.-L., Paus, T., Pausova, Z., Poline, J.-B., Rietschel, M., Robbins, T., Smolka, M.N., Müller, C.P., Feng, J., Rothenfluh, A., Flor, H., Schumann, G., IMAGEN Consortium, 2016. Neural basis of reward anticipation and its genetic determinants. *Proc. Natl. Acad. Sci. U. S. A.* 113, 3879–3884. <https://doi.org/10.1073/pnas.1503252113>
- Karl, T., Arnold, J.C., 2014. Schizophrenia: a consequence of gene-environment interactions? *Front. Behav. Neurosci.* 8. <https://doi.org/10.3389/fnbeh.2014.00435>

- Kim, Y.S., Leventhal, B.L., 2015. Genetic Epidemiology and Insights into Interactive Genetic and Environmental Effects in Autism Spectrum Disorders. *Biol. Psychiatry* 77, 66–74. <https://doi.org/10.1016/j.biopsych.2014.11.001>
- Kleinknecht, K.R., Bedenk, B.T., Kaltwasser, S.F., Grünecker, B., Yen, Y.-C., Czisch, M., Wotjak, C.T., 2012. Hippocampus-dependent place learning enables spatial flexibility in C57BL6/N mice. *Front. Behav. Neurosci.* 6, 87. <https://doi.org/10.3389/fnbeh.2012.00087>
- Kobayashi, Y., Sano, Y., Vannoni, E., Goto, H., Suzuki, H., Oba, A., Kawasaki, H., Kanba, S., Lipp, H.-P., Murphy, N.P., Wolfer, D.P., Itohara, S., 2013. Genetic dissection of medial habenula-interpeduncular nucleus pathway function in mice. *Front. Behav. Neurosci.* 7, 17. <https://doi.org/10.3389/fnbeh.2013.00017>
- Krackow, S., Vannoni, E., Codita, A., Mohammed, A.H., Cirulli, F., Branchi, I., Alleva, E., Reichelt, A., Willuweit, A., Voikar, V., Colacicco, G., Wolfer, D.P., Buschmann, J.-U.F., Safi, K., Lipp, H.-P., 2010. Consistent behavioral phenotype differences between inbred mouse strains in the IntelliCage. *Genes Brain Behav.* 9, 722–731. <https://doi.org/10.1111/j.1601-183X.2010.00606.x>
- Legrand, R., Lucas, N., Breton, J., Déchelotte, P., Fetissov, S.O., 2015. Dopamine release in the lateral hypothalamus is stimulated by α -MSH in both the anticipatory and consummatory phases of feeding. *Psychoneuroendocrinology* 56, 79–87. <https://doi.org/10.1016/j.psyneuen.2015.02.020>
- Leung, C., Jia, Z., 2016. Mouse Genetic Models of Human Brain Disorders. *Front. Genet.* 7, 40. <https://doi.org/10.3389/fgene.2016.00040>
- Logue, S.F., Grauer, S.M., Paulsen, J., Graf, R., Taylor, N., Sung, M.A., Zhang, L., Hughes, Z., Pulito, V.L., Liu, F., Rosenzweig-Lipson, S., Brandon, N.J., Marquis, K.L., Bates, B., Pausch, M., 2009. The orphan GPCR, GPR88, modulates function of the striatal dopamine system: a possible therapeutic target for psychiatric disorders? *Mol. Cell. Neurosci.* 42, 438–447. <https://doi.org/10.1016/j.mcn.2009.09.007>
- Maroteaux, G., Loos, M., van der Sluis, S., Koopmans, B., Aarts, E., van Gassen, K., Geurts, A., Largaespada, D.A., Spruijt, B.M., Stiedl, O., Smit, A.B., Verhage, M., 2012. High throughput phenotyping of avoidance learning in mice discriminates different genotypes and identifies a novel gene. *Genes Brain Behav.* <https://doi.org/10.1111/j.1601-183X.2012.00820.x>
- Massart, R., Guilloux, J.-P., Mignon, V., Sokoloff, P., Diaz, J., 2009. Striatal GPR88 expression is confined to the whole projection neuron population and is regulated by dopaminergic and glutamatergic afferents. *Eur. J. Neurosci.* 30, 397–414. <https://doi.org/10.1111/j.1460-9568.2009.06842.x>
- Meirsman, A.C., Le Merrer, J., Pellissier, L.P., Diaz, J., Clesse, D., Kieffer, B.L., Becker, J.A.J., 2016a. Mice Lacking GPR88 Show Motor Deficit, Improved Spatial Learning, and Low Anxiety Reversed by Delta Opioid Antagonist. *Biol. Psychiatry*. <https://doi.org/10.1016/j.biopsych.2015.05.020>
- Meirsman, A.C., Robé, A., de Kerchove d'Exaerde, A., Kieffer, B.L., 2016b. GPR88 in A2AR Neurons Enhances Anxiety-Like Behaviors. *eNeuro* 3. <https://doi.org/10.1523/ENEURO.0202-16.2016>

- Mizushima, K., Miyamoto, Y., Tsukahara, F., Hirai, M., Sakaki, Y., Ito, T., 2000. A novel G-protein-coupled receptor gene expressed in striatum. *Genomics* 69, 314–321. <https://doi.org/10.1006/geno.2000.6340>
- Oka, Y., Ye, M., Zuker, C.S., 2015. Thirst driving and suppressing signals encoded by distinct neural populations in the brain. *Nature* 520, 349–352. <https://doi.org/10.1038/nature14108>
- Oliveira, A.M.M., Hawk, J.D., Abel, T., Havekes, R., 2010. Post-training reversible inactivation of the hippocampus enhances novel object recognition memory. *Learn. Mem. Cold Spring Harb. N* 17, 155–160. <https://doi.org/10.1101/lm.1625310>
- Pellow, S., Chopin, P., File, S.E., Briley, M., 1985. Validation of open:closed arm entries in an elevated plus-maze as a measure of anxiety in the rat. *J. Neurosci. Methods* 14, 149–167.
- Pitchers, K.K., Balfour, M.E., Lehman, M.N., Richtand, N.M., Yu, L., Coolen, L.M., 2010. Neuroplasticity in the Mesolimbic System Induced by Natural Reward and Subsequent Reward Abstinence. *Biol. Psychiatry, Metabotropic Glutamate Receptor Agonist Modulation of Alcohol Consumption* 67, 872–879. <https://doi.org/10.1016/j.biopsycho.2009.09.036>
- Quintana, A., Sanz, E., Wang, W., Storey, G.P., Güler, A.D., Wanat, M.J., Roller, B.A., La Torre, A., Amieux, P.S., McKnight, G.S., Bamford, N.S., Palmiter, R.D., 2012. Lack of GPR88 enhances medium spiny neuron activity and alters motor- and cue-dependent behaviors. *Nat. Neurosci.* 15, 1547–1555. <https://doi.org/10.1038/nn.3239>
- Rogers, D.C., Jones, D.N., Nelson, P.R., Jones, C.M., Quilter, C.A., Robinson, T.L., Hagan, J.J., 1999. Use of SHIRPA and discriminant analysis to characterise marked differences in the behavioural phenotype of six inbred mouse strains. *Behav. Brain Res.* 105, 207–217.
- Rolls, B.J., Rolls, E.T., 1982. Thirst. CUP Archive.
- Rubio, S., Begega, A., Méndez, M., Méndez-López, M., Arias, J.L., 2012. Similarities and differences between the brain networks underlying allocentric and egocentric spatial learning in rat revealed by cytochrome oxidase histochemistry. *Neuroscience* 223, 174–182. <https://doi.org/10.1016/j.neuroscience.2012.07.066>
- Turner, K.M., Burne, T.H.J., 2013. Interaction of genotype and environment: effect of strain and housing conditions on cognitive behavior in rodent models of schizophrenia. *Front. Behav. Neurosci.* 7, 97. <https://doi.org/10.3389/fnbeh.2013.00097>
- Van Waes, V., Tseng, K.Y., Steiner, H., 2011. GPR88 - a putative signaling molecule predominantly expressed in the striatum: Cellular localization and developmental regulation. *Basal Ganglia* 1, 83–89. <https://doi.org/10.1016/j.baga.2011.04.001>
- Voikar, V., Colacicco, G., Gruber, O., Vannoni, E., Lipp, H.-P., Wolfer, D.P., 2010. Conditioned response suppression in the IntelliCage: assessment of mouse strain differences and effects of hippocampal and striatal lesions on acquisition and retention of memory. *Behav. Brain Res.* 213, 304–312. <https://doi.org/10.1016/j.bbr.2010.05.019>
- Wahlsten, D., 2010. *Mouse Behavioral Testing: How to Use Mice in Behavioral Neuroscience*. Academic Press.
- Würbel, H., 2002. Behavioral phenotyping enhanced—beyond (environmental) standardization 1, 3–8.

Yoshida, M., Yokoo, H., Mizoguchi, K., Kawahara, H., Tsuda, A., Nishikawa, T., Tanaka, M., 1992. Eating and drinking cause increased dopamine release in the nucleus accumbens and ventral tegmental area in the rat: measurement by in vivo microdialysis. *Neurosci. Lett.* 139, 73–76.

Figure legends

Figure 1. The IntelliCage system. A. Schematic representation of the IntelliCage five-phase protocol. 1) Free adaptation: all four corners and door were opened, giving access to 2 water bottles (blue circles) per corner (D1 to L4). 2) Nose-poke adaptation: all doors were closed and could be opened once per visit in response to a minimum of successive 5s nose-poke (D5 to L7). 3) Place learning: one bottle of each corner was replaced with an 8% sucrose solution (green circle). Each pair of mice had a designated corner (correct corner) in which they could access water or sucrose in response to a 5s nose-poke. The other corners were accessible but not the bottles (red circles) (D8 to L10). 4) Reversal Learning: the correct corner was set as the opposite corner (D11 to L13). 5) Fixed schedule drinking (FSD): water access was restricted to two one-hour time periods during the light phase (11 am and 4 pm) (D14 to L22). Timeline: grey and white rectangles correspond to dark (D) and light (L) periods, respectively and yellow rectangles represent the change of protocol period; blue arrows show hours of accessible water in the FSD. **B.** Conditioned chamber: accessible via a ring containing a transponder reader antenna and presence is confirmed by temperature-differential sensor. **C.** 5s Nose-poke water access.

Figure 2. Free adaptation. A. Total corner visits per hour over 4 days: both groups displayed a contrasted activity between dark and light periods. **B.** Number of visits (left), nose-pokes (middle) and licks (right) during the dark period. **C.** Number of visits (left), nose-pokes (middle) and licks (right) during the light period. **D.** Distribution of alternation types over the first hundred

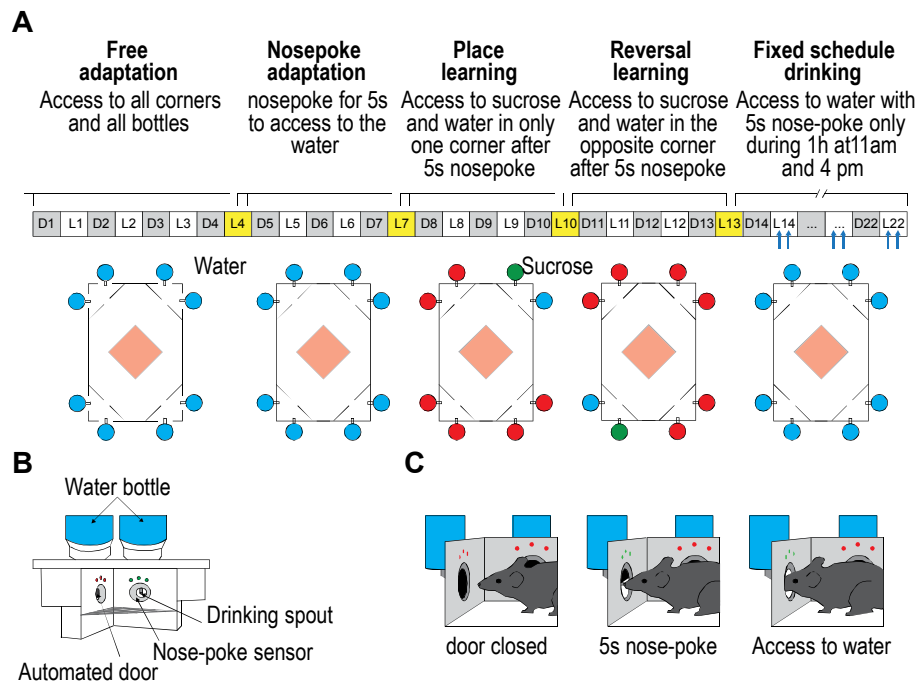
visits. Spontaneous corner alternation (SCA), alternate corner returns (ACR) and same corner returns (SCR). **E.** Total number of alternations over the first hundred visits. **F.** Distribution of alternation types over four days. **G.** Total number of alternation over four days. Black bars, *Gpr88*^{+/+} mice; white bars, *Gpr88*^{-/-} mice; grey bars, dark periods. Numbers in bar graphs represent the n for each group. All graphs show means ± S.E.M, except for cumulative plots that show individual data. Statistical significance shown here are pairwise comparison, *p<0.05, **p<0.01. (for statistical details see Supplementary Table 1).

Figure 3. Nose-poke adaptation. **A.** Number of visits (left), nose-pokes (middle) and licks (right) during the dark period. **B.** Number of visits (left), nose-pokes (middle) and licks (right) during the light period. **C.** Total number of visits (left), nose-pokes (middle) and licks (right). Black, *Gpr88*^{+/+} mice; white, *Gpr88*^{-/-} mice. Grey bars represent dark periods. Numbers in bar graphs represent the N for each group. All graphs presents means ± S.E.M, except for the cumulative plot which represents individual data. Statistical significance shown here are pairwise comparison, *p<0.05, **p<0.01. (for statistical detail see Supplementary Table 2).

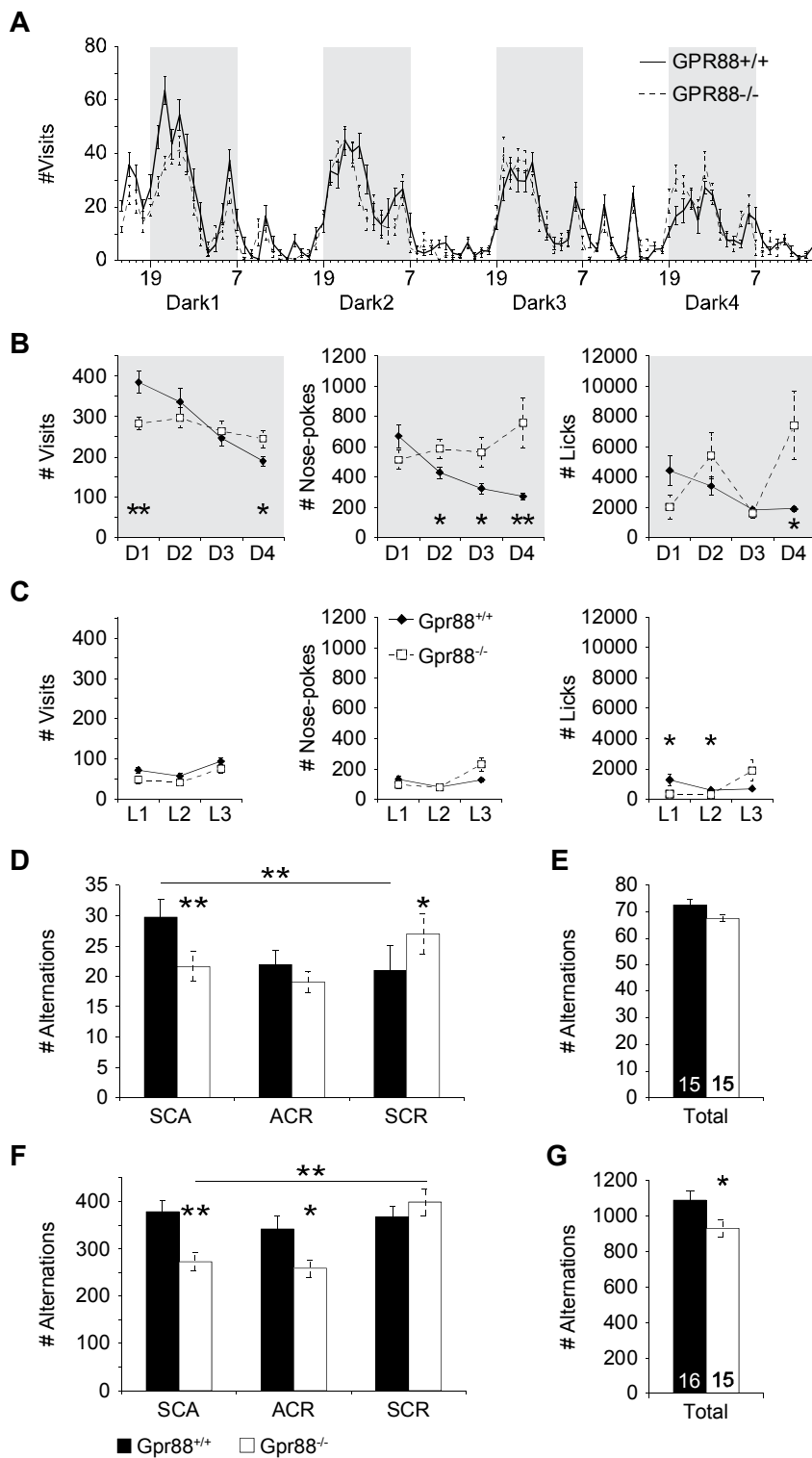
Figure 4. Place learning A-F. **A.** Number of total and correct visits. **B.** Percentage of visits in the correct corner per 12h. **C.** Number of total nose-pokes. **D.** Percentage of nose-pokes in the correct corner per 12h. **E.** Number of total licks. **F.** Percentage of licks in the sucrose side per day. **Reversal G-M.** **G.** Number of total visits. **H.** Percentage of visits in the correct corner per 12h. **I.** Percentage of correct visits in the first 25, 50, 100, 200 visits and over all visits of the reversal phase. **J.** Number of total nose-pokes. **K.** Percentage of nose-pokes in the correct

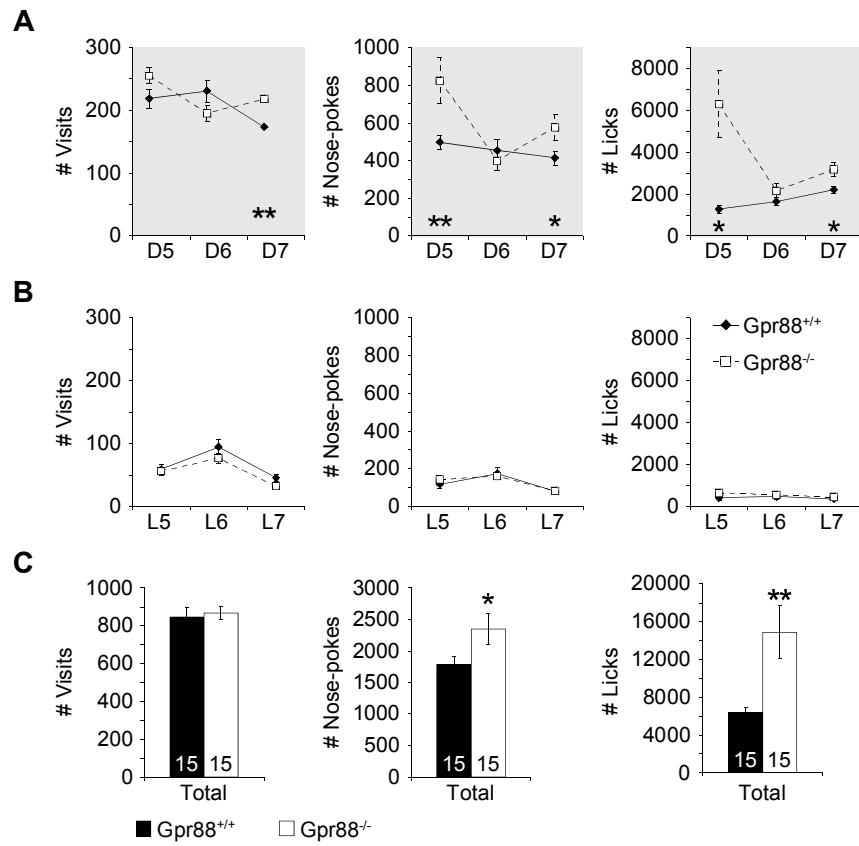
corner per 12h. **L.** Number of total licks. **M.** Percentage of licks in the sucrose side per day. Black, $Gpr88^{+/+}$ mice; white $Gpr88^{-/-}$ mice. Grey bars represent dark periods. Horizontal dashed lines represent chance level (25% for correct visits and nose-poke, 50% for nose-pokes and licks in sucrose side). All graphs presents means and \pm S.E.M. Histograms show total numbers with the upper bar and correct number with the mid bar. Statistical significance shown here are pairwise comparison, $*p<0.05$, $**p<0.01$. (for statistical detail see Supplementary Table 3).

Figure 5. Fixed schedule drinking. **A.** Number of visits in 12h bins in periods Dark 14 to Light 22. **B.** Total Number of visits during the dark period. **C.** Total Number of visits during the light period. **D.** Number of visits per day during the 5 hours before (-5h to -1h), during (water access) and 2 hours (+1h and + 2h) after water accessibility. **E.** Number of nose-pokes per day during the 5 hours before (-5h to -1h), during (water access) and 2 hours (+1h and + 2h) after water accessibility. Black, $Gpr88^{+/+}$ mice; White $Gpr88^{-/-}$ mice. Grey bars represent dark periods. All graphs presents means \pm S.E.M. Statistical significance shown here are pairwise comparison $*p<0.05$, $**p<0.01$, $***p<0.001$ (for statistical detail see Supplementary Table 4).

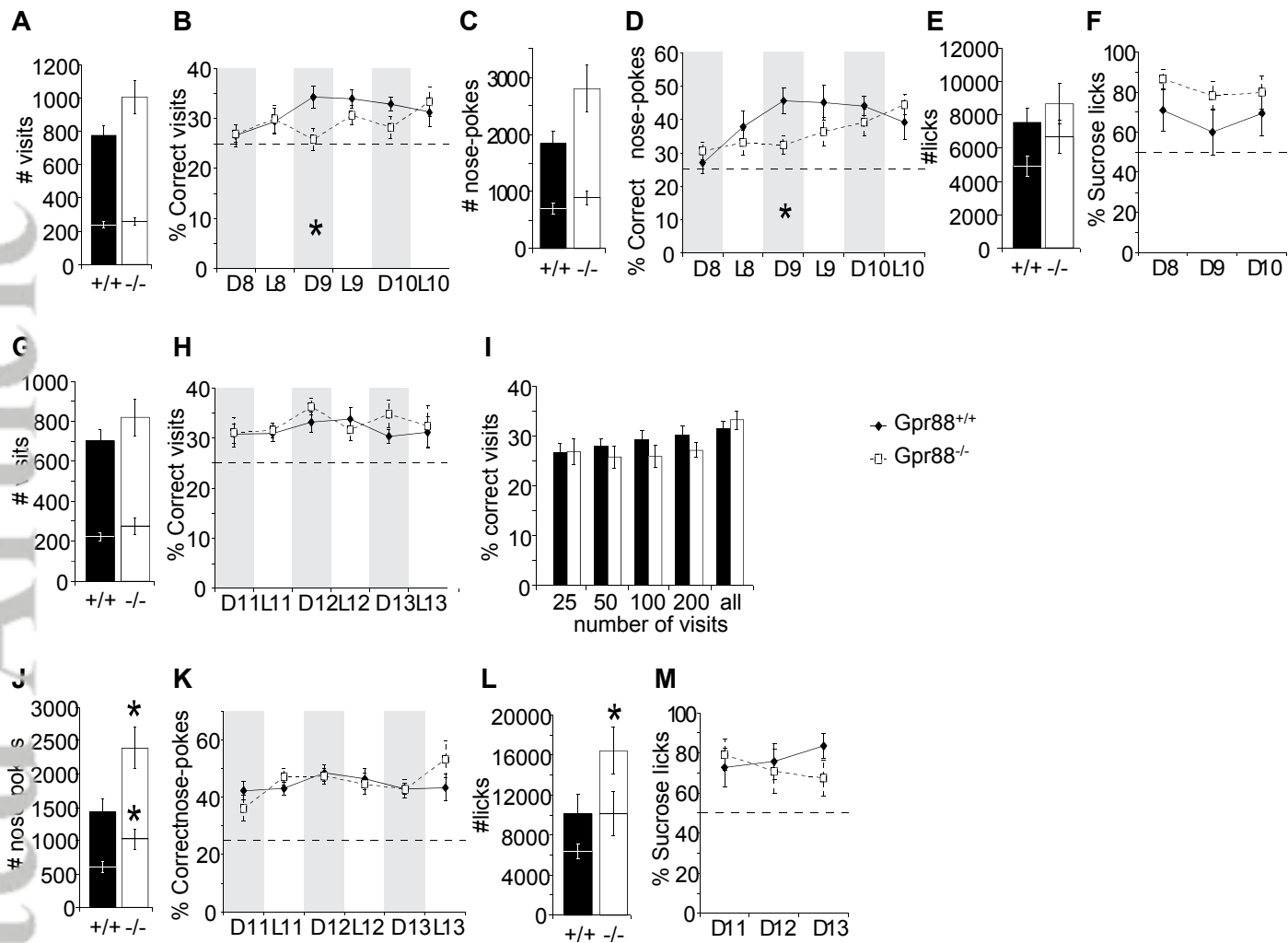


Maroteaux et al Figure 1

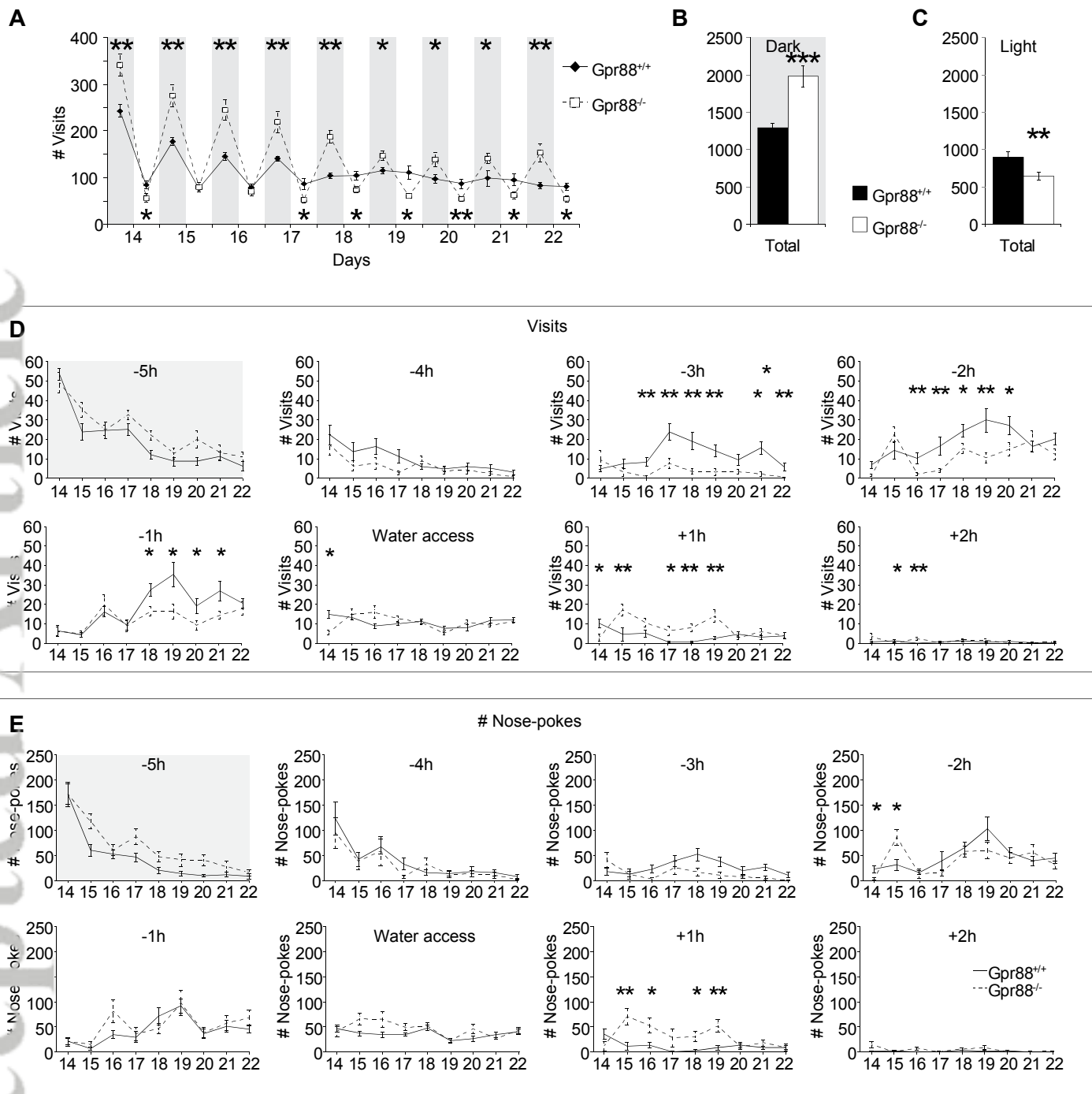




Maroteaux et al Figure 3



Maroteaux et al Figure 4



Maroteaux et al Figure 5

Table 1. Summary table (left) and comparison to phenotypes previously describe using traditional behavioral testing (right).

	IntelliCage findings in this study		Previous studies using conventional testing		
	Phase	Parameter (-/- compared to +/+)	Behavioral test	Parameter (-/- compared to +/+)	References
Hyperactivity	Free adaptation	higher number nose-pokes during the dark phase	Open-field	longer distance moved under 3mg/kg Amphetamine	Logue et al., 2009
	Nose-poke adaptation	higher number of visits, nose-pokes and Licks	Y-maze	higher number of arm entries	Meirsman et al., 2016
	Place learning & reversal fixed schedule drinking	higher number of nose-pokes higher number of visits during the dark phase	object recognition grid floor home cage 48h	higher number of visits to object longer distance moved during dark period	Meirsman et al., 2016 Quintana et al. 2012
Non-habituation	Free adaptation	stable number of visits	Open-field	no decrease of activity after repeated exposure	Meirsman et al., 2016
	fixed schedule drinking	keep a dark-light pattern delayed stabilization of visits			
Altered exploratory behavior	Free adaptation	higher number of same corner returns	Stereotypies	More burying duration and more circling	Meirsman et al., 2016
	fixed schedule drinking	higher perseverative visits and nose-pokes after access to water	Stereotypies	more climbing and sniffing licking and gnawing under 0.3mg/kg apomorphine	Logues et al., 2009
Learning	Place learning & reversal	preference development delayed	dual solution cross-maze task	faster acquisition and shift	Meirsman et al., 2016
			Morris water maze	longer latency to escape	Quintana et al. 2012
			water U-maze	delayed development of the correct choice	Quintana et al. 2012
Anticipatory behavior	fixed schedule drinking	no visit increase before water access	Unprecedented		

Deletion of the mu opioid receptor gene in mice reshapes the reward–aversion connectome

Anna E. Mechling^{a,b}, Tanzil Arefin^{a,c}, Hsu-Lei Lee^a, Thomas Bienert^a, Marco Reisert^a, Sami Ben Hamida^{d,e}, Emmanuel Darcq^e, Aliza Ehrlich^{d,e}, Claire Gaveriaux-Ruff^d, Maxime J. Parent^f, Pedro Rosa-Neto^f, Jürgen Hennig^a, Dominik von Elverfeldt^a, Brigitte Lina Kieffer^{d,e,1,2}, and Laura-Adela Harsan^{a,g,h,1,2}

^aAdvanced Molecular Imaging Center, Medical Physics, University Medical Center Freiburg, 79106 Freiburg, Germany; ^bFaculty of Biology, University of Freiburg, 79104 Freiburg, Germany; ^cBernstein Center for Computational Neuroscience, University of Freiburg, 79104 Freiburg, Germany; ^dDepartment of Translational Medicine and Neurogenetics, Institut de Génétique et de Biologie Moléculaire et Cellulaire, Illkirch-Griffenstaden 67400, France; ^eDepartment of Psychiatry, Douglas Hospital Research Center, School of Medicine, McGill University, Montreal, QC, Canada H3A 1A1; ^fTranslational Neuroimaging Laboratory, Douglas Hospital Research Center, McGill University, Montreal, QC, Canada H3A 1A1; ^gEngineering Science, Computer Science, and Imaging Laboratory, Integrative Multimodal Imaging in Healthcare, UMR 7357, University of Strasbourg, CNRS, 67000 Strasbourg, France; and ^hDepartment of Biophysics and Nuclear Medicine, University Hospital Strasbourg, 67000 Strasbourg, France

Edited by Marcus E. Raichle, Washington University in St. Louis, St. Louis, MO, and approved July 19, 2016 (received for review February 4, 2016)

Connectome genetics seeks to uncover how genetic factors shape brain functional connectivity; however, the causal impact of a single gene's activity on whole-brain networks remains unknown. We tested whether the sole targeted deletion of the mu opioid receptor gene (*Oprm1*) alters the brain connectome in living mice. Hypothesis-free analysis of combined resting-state fMRI diffusion tractography showed pronounced modifications of functional connectivity with only minor changes in structural pathways. Fine-grained resting-state fMRI mapping, graph theory, and intergroup comparison revealed *Oprm1*-specific hubs and captured a unique *Oprm1* gene-to-network signature. Strongest perturbations occurred in connective patterns of pain/aversion-related nodes, including the mu receptor-enriched habenula node. Our data demonstrate that the main receptor for morphine predominantly shapes the so-called reward/aversion circuitry, with major influence on negative affect centers.

mouse brain connectivity | resting-state functional MRI | diffusion tensor imaging | mu opioid receptor | reward/aversion network

Neuronal connectivity is at the foundation of brain function (1) and the concept that brain connectivity patterns are dynamically shaped by experience, pathology, and genetics has gained increasing importance. In humans, MRI has opened the era of connectome/imaging genetics to elucidate how genetic factors affect brain organization and connectivity in healthy individuals and disease, and to correlate genotype to phenotype (2). However, the causal impact of a single gene on overall functional connectivity (FC) remains largely unknown, and animal research is best suited to this goal. Here we tested whether combined functional/structural MRI in live animals (3–8) coupled to open-ended postprocessing analysis would reveal connectivity alterations upon targeted inactivation of a single gene. The mu opioid receptor (MOR) mediates the remarkably potent analgesic and addictive properties of opiates, like morphine (9), and belongs to the endogenous opioid system that controls sensory, emotional, and cognitive processes. This receptor is broadly distributed throughout the nervous system (10). It is a key component to facilitate reward (11) and relieves the negative experience of pain (12–14). In this report we show that targeted deletion of the MOR gene (*Oprm1*) significantly alters the brain connectome in living mice and predominantly reshapes the so-called reward/aversion network involved in pain, depression, and suicide (15).

Results and Discussion

Fine-Grained Mapping of the Mouse Brain Functional Connectome. In a first step, we established fine-grained mapping of the mouse brain functional connectome (MBFC) in control and *Oprm1*^{−/−} living mice. Using data-driven spatial independent component analysis (100-ICASSO) (4) of combined blood oxygenation level-dependent (BOLD) resting-state functional MRI (rsfMRI)

datasets (*Materials and Methods, Data Analysis*), we identified 87 functional components, the patterns of which covered neuroanatomical regions defined by automatic coregistration on the Allen Mouse Brain Atlas (AMBA; mouse.brain-map.org/static/atlas) (Fig. S1). We tested the reproducibility of the group ICASSO [a tool for reliability investigation of independent component analysis (ICA) estimates] patterns in each animal and in each experimental group separately via back-reconstruction (*SI Materials and Methods, Statistical and Algorithmic Reliability of Group ICA Results* and Fig. S2). These examples illustrate low intragroup variability of the ICA patterns and extremely high similarity between group patterns, supporting our further approach of using the 87 group ICA functional clusters (ICASSO components) as nodes in the generation of brain FC matrices of both *Oprm1*^{−/−} and a control (Ctrl) group of animals (*Materials and Methods, Data Analysis* and *SI Materials and Methods*). These matrices, including both, correlations (positive) and anticorrelations (negative) between brain nodal activities (Fig. S3), were further used to examine whether global topological properties and organizational principles of the MBFC (4, 16) are modified in *Oprm1*^{−/−} mice using graph theory (17). We probed small-world network hallmarks (*SI Materials and Methods, Assessment of Global*

Significance

Mice manipulated by targeted deletion of a specific brain gene show diverse pathological phenotypes, apparent, for example, in behavioral experiments. To explain observed findings, connectome genetics attempts to uncover how brain functional connectivity is affected by genetics. However the causal impact of a single gene on whole-brain networks is still unclear. Here the sole targeted deletion of the mu opioid receptor gene (*Oprm1*), the main target for morphine, induced widespread remodeling of brain functional connectome in mice. The strongest perturbations occurred within the so-called reward/aversion-circuitry, predominantly influencing the negative affect centers. We present a hypothesis-free analysis of combined structural and functional connectivity data obtained via MRI of the living mouse brain, and identify a specific *Oprm1* gene-to-network signature.

Author contributions: J.H., B.L.K., and L.-A.H. designed research; A.E.M., T.A., A.E., and L.-A.H. performed research; H.-L.L., T.B., M.R., C.G.-R., P.R.-N., J.H., and D.v.E. contributed new reagents/analytic tools; A.E.M., S.B.H., E.D., M.J.P., B.L.K., and L.-A.H. analyzed data; and A.E.M., J.H., B.L.K., and L.-A.H. wrote the paper.

The authors declare no conflict of interest.

This article is a PNAS Direct Submission.

¹B.L.K. and L.-A.H. contributed equally to this work.

²To whom correspondence may be addressed. Email: harsan@unistra.fr or Brigitte.Kieffer@douglas.mcgill.ca.

This article contains supporting information online at www.pnas.org/lookup/suppl/doi:10.1073/pnas.1601640113/-DCSupplemental.

Topological Features of the MBFC in Ctrl and Oprm1^{-/-} Mice) and found similar features (Fig. S3) for both genotypes: a short average path length between all node pairs with high local clustering. We also tested modular properties (17) of the MBFC, a key feature of mammalian brain networks (18), and found partitioning into four stable functional modules (*SI Materials and Methods, Assessment of Global Topological Features of the MBFC in Ctrl and Oprm1^{-/-} Mice*) in both animal groups, indicating again that general organization principles of the MBFC are preserved in *Oprm1^{-/-}* mice.

However, this global analysis revealed that the recruitment of brain regions as network hubs (4, 19), defined as functional nodes showing above-mean normalized connectivity strength and diversity (*SI Materials and Methods, Assessment of Global Topological Features of the MBFC in Ctrl and Oprm1^{-/-} Mice*), was significantly modified in *Oprm1^{-/-}* mice. In the positive correlation analysis (Fig. S4), several components lost their hub status in *Oprm1^{-/-}* mice, suggesting decreased relay function in brain structures involved in positive affect and motivational processes [nucleus accumbens (ACB), prefrontal cortex (PFC)], as well as negative sensory and emotional experiences [midbrain reticular nucleus (MRN), periaqueductal gray (PAG), habenula (HB), somatosensory areas (SS)]. Concurrently, other nodes appeared as functional hubs in *Oprm1^{-/-}* mice only [caudoputamen (CP), bed nuclei of stria terminalis (BST), hippocampal formation (HPF) and peri-HPF cortex, thalamus (TH), superior colliculus (SC)/PAG, MRN/SC/PAG], which, without exception, covered areas integrated into the so-called core aversion-related network (20, 21). In addition, connectivity of PAG, which is a major opioid-sensitive pain-modulatory structure in both rodents (14,

22) and humans (23) and is engaged in aversive learning (24), appeared entirely remodeled in mutant mice (Fig. S4 B and C). Finally, the application of stronger exclusion criteria (combined positive and negative correlations) (Fig. S5) designated the ventromedial rostral MRN/PAG as the sole remaining *Oprm1*-dependent functional hub. Together, these substantial hub alterations suggest facilitated communication across pain/aversion-processing centers and perhaps less-efficient integration of reward-related information.

Quantitative Intergroup Comparison of Ctrl and *Oprm1^{-/-}* Functional Connectomes Reveals an *Oprm1^{-/-}*-Specific Fingerprint.

In a second step, we quantified remodeling of the *Oprm1^{-/-}* functional connectome using a direct statistical intergroup comparison of Ctrl and *Oprm1^{-/-}* MBFC matrices (*Materials and Methods, Direct Intergroup (Ctrl. vs. Oprm1^{-/-}) Statistical Analysis of MBFC* and Fig. 1). We detected significant and widespread alterations of internode connectivity (Fig. 1) [$P < 0.05$, false-discovery rate (FDR)-corrected]. The 2D-matrix representation (Fig. 1A) captured the causal effect of targeted *Oprm1* gene disruption at the level of whole-brain networks, and the extent of *Oprm1*-dependent connective activity appeared surprisingly broad. To establish characteristic features of this *Oprm1* FC signature, we ranked nodes on the basis of highest number of statistically significant differences in connectivity across the two genotypes (*Materials and Methods, Direct Intergroup (Ctrl. vs. Oprm1^{-/-}) Statistical Analysis of MBFC* and Fig. 1D). There was a clear dominance of connectivity changes for pain/aversion-related nodes [PAG, hippocampal region (HIP), amygdala (AMY), SS, anterior cingulate areas (ACA), MRN, HB], with the first top 10 of this hierarchy being core players of the

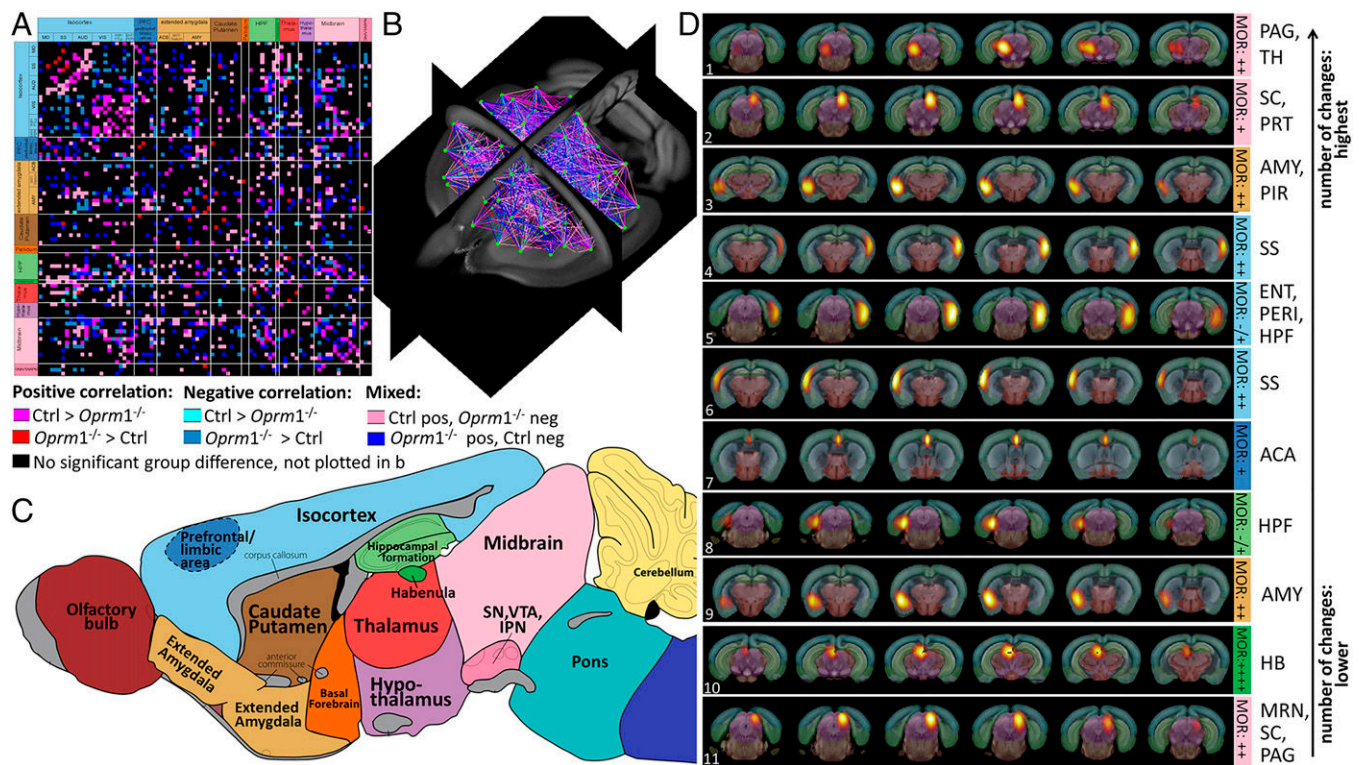


Fig. 1. Quantitative mapping of functional network alterations in *Oprm1^{-/-}* mice reveals a MOR-dependent activity signature in live animals. (A–C) Direct intergroup (Ctrl vs. *Oprm1^{-/-}*) statistical comparison of connectivity matrices ($P < 0.05$, FDR-corrected) is shown as a 2D-matrix (A) or a 3D view (B). Functional nodes were grouped and color-coded as assigned in the sagittal brain view from C. The *Oprm1* genetic inactivation induced widespread modifications of internode connectivity. (D) Nodes with the highest number of statistically significant connectivity changes are ranked. Their functional pattern is overlaid on the Allen Brain Atlas, for precise anatomical identification. The top-10 nodes correspond to brain areas associated with pain/aversion processing or double players involved in both pain and reward (PAG/TH, SC/PRT, bilateral AMY, bilateral SS, and MRN/SC/PAG, ACA, HPF, HB). Information on MOR density (10) is included [from low “-/+” barely detectable in the entorhinal area (ENT)/perihinal area (PERI) cortex and HPF to “++++” highest expression in HB].

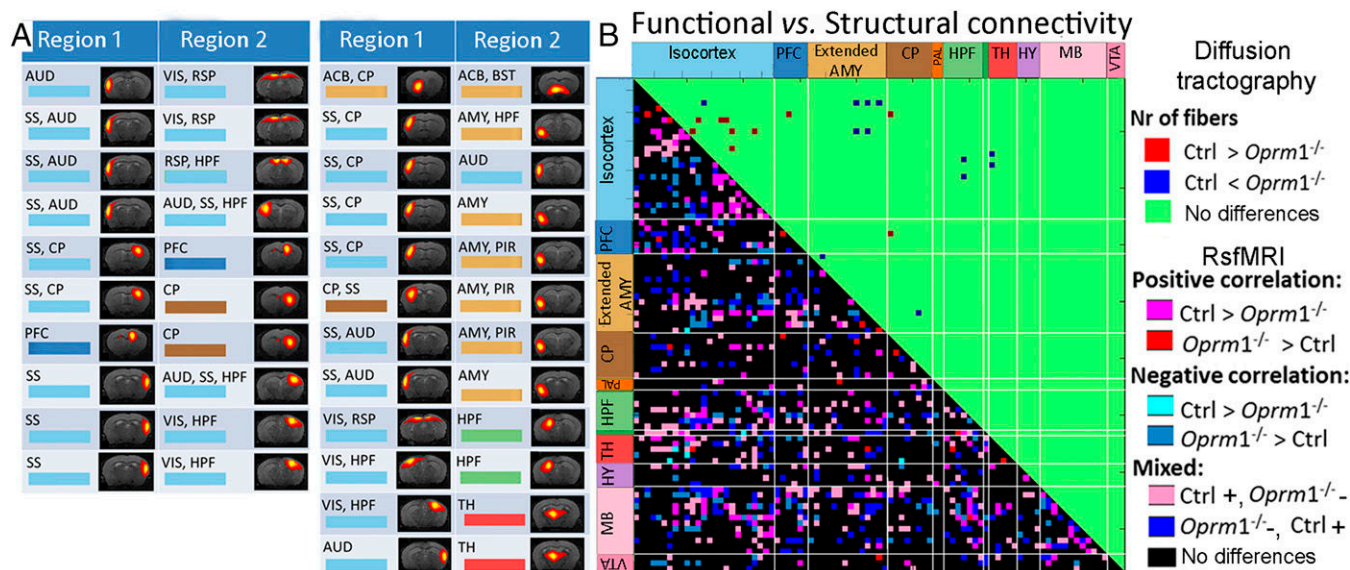


Fig. 4. Limited alteration of tractography-based structural compared with FC in *Oprm1*^{-/-} mice. (A) Modifications of internode structural connectivity: changes were assessed based on the number of fibers directly connecting functional nodes of the brain connectivity matrix (between region 1 and region 2). (Left) Significant change in fiber numbers Ctrl > *Oprm1*^{-/-}. (Right) Significant change in fiber numbers *Oprm1*^{-/-} > Ctrl. (B) Direct comparison of significant functional and structural connectivity showed widespread FC modifications in mutant mice, whereas structural adaptations were limited. The few alterations of structural connectivity determined from tractography included SS, AMY, and ACB, as well as SS-AMY connections. Diffusion tractography also showed remodeling within ACB (A, first row right) in MOR depleted brains but no modification for midbrain centers (i.e., PAG).

the pivotal role of MOR in both pain and pleasure (Dataset S1 and references therein), recognized as intermingled processes at circuit level (40) and for pathology (41).

In our analysis, the major influence of *Oprm1* inactivation on aversion/pain-related, rather than reward connectivity, may reflect a stronger inhibitory MOR tone or developmental influence on negative affect centers, at least under resting-state conditions. From an evolutionary perspective, pain represents a key signal for survival, and successful coping with a pain stimulus is essential to gain a selective advantage (42). Despite the antique notion that pain and pleasure form a continuum, it is only recently that the rewarding value of pain relief has been recognized (40, 41). The key implication of MOR activity in dampening physical, emotional, and social pain, evidenced in human PET imaging studies (see ref. 43 and references therein), and our own FC analysis of live *Oprm1*-deficient mice, together suggest that pain relief may be a primary MOR function.

Importantly, our data unequivocally reveal pronounced causal effects of a single gene on whole-brain FC in live animals, with subtle modifications of the tractography-based structural connectome. This report is among the very first studies (44) that open the way to targeted connectome genetics (2) in basic research and, to the best of our knowledge, this is the first hypothesis-free analysis of combined rsfMRI/diffusion tractography data in the mouse, leading to the identification of a specific gene-to-network signature.

Materials and Methods

Ethics. All experiments were performed in accordance with the German and French laws and guidelines regarding ethics on animal experimentation (ethics allowance 35_9185.81/G-13/15).

Animal Preparation, Anesthesia, and Physiological Parameters. Animal preparation, anesthesia, and physiological parameters during imaging are described in the first part of *SI Materials and Methods*. The rsfMRI data were acquired under continuous Medetomidine (MD, an α -2 adrenergic agonist) sedation through a MRI compatible catheter (initial intraperitoneal injection of 0.3 mg MD per kilogram body weight in 100 μ L 0.9% NaCl-solution followed by subcutaneous infusion of 0.6 mg per kilogram body weight in 200 μ L/h). MD was selected among other anesthetics based on previous reports suggesting minimal impact on FC (5, 45–47).

Mouse Brain MRI Data Acquisition. Mouse brain MRI data acquisition (see also *SI Materials and Methods*) was performed with a 7T animal scanner (Biospec 70/20) and a mouse head-adapted cryocool (both from Bruker). rsfMRI data were collected (30 min after MD bolus injection) using single-shot Gradient Echo Echo Planar Imaging (EPI) [12 axial slices, 200 volumes, image resolution 150 \times 150 \times 700 μ m³, echo time (TE)/repetition time (TR) = 10 ms/1,700 ms]. High-resolution morphological imaging was done using Turbo RARE T₂ (51 \times 51 \times 300 μ m³, TE/TR = 50 ms/6,514 ms). HARDI was performed using a four-shot Diffusion Tensor Imaging-EPI (DTI-EPI) sequence (15 axial slices, resolution of 94 \times 94 \times 500 μ m³, TE/TR = 27 ms/3,750 ms); Δ = 10 ms, diffusion gradient duration (δ) = 5 ms, $b_{\text{factor}} = 1,000$ s/mm², 30 diffusion gradient directions.

Data Analysis. The data preprocessing pipeline is described in *SI Materials and Methods*.

rsfMRI data analysis. Identification of elementary functional clusters as nodes of the MBFC matrix was performed via high-dimensional ICA (100 components). Spatial group ICA (48) via the MATLAB based toolbox GIFT (Group ICA of fMRI Toolbox, v1.3i, www.nitrc.org/projects/gift/) was carried out on all of the mouse brain rsfMRI data (*Oprm1*^{-/-} and Ctrl mice) using the Infomax algorithm. ICASSO (49) was used to assess pattern stability for the identified components (*SI Materials and Methods*, *Statistical and Algorithmic Reliability of Group ICA Results*). The mean resulting patterns were displayed as spatial color-coded z-maps onto T₂ weighted images and on coregistered AMBA (50) (see, for example, Figs. 1–3, Figs. S1, S4, and S5, and Movies S1–S3). Coregistration with AMBA allowed for automatic identification of anatomic brain areas covered by IC patterns. From the 100-ICASSO results, 13 artifactual components were excluded from analysis. The meaningful 87 functional clusters were further used as nodes (Fig. S1) in the generation of the MBFC matrix, via partial correlation (PC).

PC analysis (*SI Materials and Methods*, *Partial Pearson Correlation*) was performed for each experimental group (*Oprm1*^{-/-} and Ctrl) separately. The time courses associated with each relevant independent component (IC, node) obtained from 100-ICASSO were used in PC analysis using an in-house developed MATLAB tool (4). The PC coefficients (Pearson) between each pair of IC were calculated and used to create a 87 \times 87 adjacency PC matrix for each animal, as well as two average matrices, representative for each experimental group (*Oprm1*^{-/-} and Ctrl) (Fig. S3E; see also and histogram display of correlation coefficients in Fig. S3F). Each element of the matrix represented the strength of direct connectivity between two components (nodes). The PC matrices were then normalized using Fisher's z transformation. The significance of positive and negative correlations between pairs of components was further assessed via a two-sided one-sample *t* test, for $P < 0.05$ (4). This procedure generated a weighted undirected matrix

(WUM) for each group, containing statistically relevant/significant correlation values. For 3D visualization of the MBFC, a Matlab-based toolbox was developed (*SI Materials and Methods, Visualization of Results*).

Assessment of global topological features of the MBFC in Ctrl and *Oprm1*^{-/-} mice is described in *SI Materials and Methods*.

Direct intergroup (Ctrl vs. *Oprm1*^{-/-}) statistical analysis of MBFC. The analysis of the FC remodeling of the *Oprm1*^{-/-} mouse brain was done via direct statistical comparison between the PC matrices (unthresholded z matrices) generated for each experimental group. We tested the hypothesis that there are no differences in connectivity between the two groups via a two-sided two-sample t test (similar variation within each group). The hypothesis was rejected at a significance level of 0.05, under FDR control for multiple comparisons.

A group comparison matrix (GCM) was generated (Fig. 2A) that color-coded the statistically significant intergroup differences of connectivity. Each node was associated to a broader brain area, based on the anatomical overlapping assigned via coregistration of the ICA results on the AMBA. The GCM was arranged to cluster the connectivity changes in association to anatomical areas (Fig. 1A and C and Fig. S1). Three-dimensional visualization of

the changed connections was also generated (Fig. 1B). The color-code associated with the GCM was maintained for the 3D displays. Only nodes showing changes in their FC are plotted. The GCM was further used to count the significantly changed connections for each node (IC) and we further ranked nodes on the basis of highest number of such statistically significant differences in connectivity across the two genotypes (Fig. 1D).

Mouse brain tractography-based structural network analysis. Mouse brain tractography-based structural network analysis are detailed in *SI Materials and Methods, Mouse Brain Structural Network Analysis*.

ACKNOWLEDGMENTS. We thank Robin Simpson for his help in creating Movie S1. This work was supported by the French Academy of Sciences and the NIH (National Institute on Alcohol Abuse and Alcoholism Grant 16658); the Centre National de la Recherche Scientifique, Institut National de la Santé et de la Recherche Médicale; Strasbourg University; and grants from the Brain Links Brain Tools cluster of excellence from Freiburg (MouseNet) and European Research Area Network (ERANET-Neuron), AF12-NEUR0008-01-WM2NA.

- Van Essen DC (2013) Cartography and connectomes. *Neuron* 80(3):775–790.
- Thompson PM, Ge T, Glahn DC, Jahanshad N, Nichols TE (2013) Genetics of the connectome. *Neuroimage* 80:475–488.
- Harsan LA, et al. (2013) Mapping remodeling of thalamocortical projections in the living reeler mouse brain by diffusion tractography. *Proc Natl Acad Sci USA* 110(19):E1797–E1806.
- Mechling AE, et al. (2014) Fine-grained mapping of mouse brain functional connectivity with resting-state fMRI. *Neuroimage* 96:203–215.
- Grandjean J, Schroeter A, Batata I, Rudin M (2014) Optimization of anesthesia protocol for resting-state fMRI in mice based on differential effects of anesthetics on functional connectivity patterns. *Neuroimage* 102(Pt 2):838–847.
- Gozzi A, Schwarz AJ (2016) Large-scale functional connectivity networks in the rodent brain. *Neuroimage* 127:496–509.
- Stafford JM, et al. (2014) Large-scale topology and the default mode network in the mouse connectome. *Proc Natl Acad Sci USA* 111(52):18745–18750.
- Zerbi V, et al. (2014) Resting-state functional connectivity changes in aging apoE4 and apoE-KO mice. *J Neurosci* 34(42):13963–13975.
- Matthes HW, et al. (1996) Loss of morphine-induced analgesia, reward effect and withdrawal symptoms in mice lacking the mu-opioid-receptor gene. *Nature* 383(6603):819–823.
- Erbas E, et al. (2015) A mu-opioid receptor brain atlas reveals neuronal co-occurrence in subcortical networks. *Brain Struct Funct* 220(2):677–702.
- Le Merrer J, Becker JA, Befort K, Kieffer BL (2009) Reward processing by the opioid system in the brain. *Physiol Rev* 89(4):1379–1412.
- Leknes S, Tracey I (2008) A common neurobiology for pain and pleasure. *Nat Rev Neurosci* 9(4):314–320.
- Navratilova E, Porreca F (2014) Reward and motivation in pain and pain relief. *Nat Neurosci* 17(10):1304–1312.
- Fields H (2004) State-dependent opioid control of pain. *Nat Rev Neurosci* 5(7):565–575.
- Elman I, Borsook D, Volkow ND (2013) Pain and suicidality: Insights from reward and addiction neuroscience. *Prog Neurobiol* 109:1–27.
- Liang Z, Li T, King J, Zhang N (2013) Mapping thalamocortical networks in rat brain using resting-state functional connectivity. *Neuroimage* 83:237–244.
- Bullmore E, Sporns O (2009) Complex brain networks: Graph theoretical analysis of structural and functional systems. *Nat Rev Neurosci* 10(3):186–198.
- Fornito A, Zalesky A, Breakspear M (2015) The connectomics of brain disorders. *Nat Rev Neurosci* 16(3):159–172.
- Liska A, Galbusera A, Schwarz AJ, Gozzi A (2015) Functional connectivity hubs of the mouse brain. *Neuroimage* 115:281–291.
- Hayes DJ, Northoff G (2011) Identifying a network of brain regions involved in aversion-related processing: A cross-species translational investigation. *Front Integr Neurosci* 5:49.
- Hayes DJ, Northoff G (2012) Common brain activations for painful and non-painful aversive stimuli. *BMC Neurosci* 13:60.
- Linnman C, Moulton EA, Barmettler G, Becerra L, Borsook D (2012) Neuroimaging of the periaqueductal gray: State of the field. *Neuroimage* 60(1):505–522.
- Wager TD, Scott DJ, Zubieta JK (2007) Placebo effects on human mu-opioid activity during pain. *Proc Natl Acad Sci USA* 104(26):11056–11061.
- Roy M, et al. (2014) Representation of aversive prediction errors in the human periaqueductal gray. *Nat Neurosci* 17(11):1607–1612.
- Forkmann K, et al. (2013) Pain-specific modulation of hippocampal activity and functional connectivity during visual encoding. *J Neurosci* 33(6):2571–2581.
- Neugebauer V (2015) Amygdala pain mechanisms. *Handbook Exp Pharmacol* 227:261–284.
- Bushnell MC, Ceko M, Low LA (2013) Cognitive and emotional control of pain and its disruption in chronic pain. *Nat Rev Neurosci* 14(7):502–511.
- Hikosaka O (2010) The habenula: from stress evasion to value-based decision-making. *Nat Rev Neurosci* 11(7):503–513.
- Russo SJ, Nestler EJ (2013) The brain reward circuitry in mood disorders. *Nat Rev Neurosci* 14(9):609–625.
- Borsook D, et al. (2007) Reward-aversion circuitry in analgesia and pain: Implications for psychiatric disorders. *Eur J Pain* 11(1):7–20.
- Lammel S, et al. (2012) Input-specific control of reward and aversion in the ventral tegmental area. *Nature* 491(7423):212–217.
- Gardon O, et al. (2014) Expression of mu opioid receptor in dorsal diencephalic conduction system: New insights for the medial habenula. *Neuroscience* 277:595–609.
- Reisert M, et al. (2011) Global fiber reconstruction becomes practical. *Neuroimage* 54(2):955–962.
- Loseth GE, Ellingsen DM, Leknes S (2014) State-dependent mu-opioid modulation of social motivation. *Front Behav Neurosci* 8:430.
- Navratilova E, et al. (2015) Endogenous opioid activity in the anterior cingulate cortex is required for relief of pain. *J Neurosci* 35(18):7264–7271.
- Kieffer BL, Gavériaux-Ruff C (2002) Exploring the opioid system by gene knockout. *Prog Neurobiol* 66(5):285–306.
- Contet C, Kieffer BL, Befort K (2004) Mu opioid receptor: A gateway to drug addiction. *Curr Opin Neurobiol* 14(3):370–378.
- Moles A, Kieffer BL, D'Amato FR (2004) Deficit in attachment behavior in mice lacking the mu-opioid receptor gene. *Science* 304(5679):1983–1986.
- Becker JA, et al. (2014) Autistic-like syndrome in mu opioid receptor null mice is relieved by facilitated mGluR4 activity. *Neuropsychopharmacology* 39(9):2049–2060.
- Navratilova E, Atcherley CV, Porreca F (2015) Brain circuits encoding reward from pain relief. *Trends Neurosci* 38(11):741–750.
- Elman I, Borsook D (2016) Common brain mechanisms of chronic pain and addiction. *Neuron* 89(1):11–36.
- Fields HL (2014) Neuroscience. More pain; less gain. *Science* 345(6196):513–514.
- Hsu DT, et al. (2015) It still hurts: Altered endogenous opioid activity in the brain during social rejection and acceptance in major depressive disorder. *Mol Psychiatry* 20(2):193–200.
- Zhan Y, et al. (2014) Deficient neuron-microglia signaling results in impaired functional brain connectivity and social behavior. *Nat Neurosci* 17(3):400–406.
- Weber R, Ramos-Cabrer P, Wiedermann D, van Camp N, Hoehn M (2006) A fully noninvasive and robust experimental protocol for longitudinal fMRI studies in the rat. *Neuroimage* 29(4):1303–1310.
- Pawela CP, et al. (2009) A protocol for use of medetomidine anesthesia in rats for extended studies using task-induced BOLD contrast and resting-state functional connectivity. *Neuroimage* 46(4):1137–1147.
- Nasrallah FA, Tay HC, Chuang KH (2014) Detection of functional connectivity in the resting mouse brain. *Neuroimage* 86:417–424.
- Calhoun VD, Adali T, Pearlson GD, Pekar JJ (2001) A method for making group inferences from functional MRI data using independent component analysis. *Hum Brain Mapp* 14(3):140–151.
- Himberg J, Hyvärinen A, Esposito F (2004) Validating the independent components of neuroimaging time series via clustering and visualization. *Neuroimage* 22(3):1214–1222.
- Lein ES, et al. (2007) Genome-wide atlas of gene expression in the adult mouse brain. *Nature* 445(7124):168–176.
- van de Ven VG, Formisano E, Prvulovic D, Roeder CH, Linden DE (2004) Functional connectivity as revealed by spatial independent component analysis of fMRI measurements during rest. *Hum Brain Mapp* 22(3):165–178.
- Margulies DS, et al. (2010) Resting developments: A review of fMRI post-processing methodologies for spontaneous brain activity. *MAGMA* 23(5–6):289–307.
- Esposito F, et al. (2003) Real-time independent component analysis of fMRI time-series. *Neuroimage* 20(4):2209–2224.
- Moritz CH, Carew JD, McMillan AB, Meyerand ME (2005) Independent component analysis applied to self-paced functional MR imaging paradigms. *Neuroimage* 25(1):181–192.
- Li YO, Adali T, Calhoun VD (2007) Estimating the number of independent components for functional magnetic resonance imaging data. *Hum Brain Mapp* 28(11):1251–1266.
- Smith SM, et al. (2011) Network modelling methods for FMRI. *Neuroimage* 54(2):875–891.
- Watts DJ, Strogatz SH (1998) Collective dynamics of 'small-world' networks. *Nature* 393(6684):440–442.
- Humphries MD, Gurney K, Prescott TJ (2006) The brainstem reticular formation is a small-world, not scale-free, network. *Proc Biol Sci* 273(1585):503–511.
- Newman ME (2006) Modularity and community structure in networks. *Proc Natl Acad Sci USA* 103(23):8577–8582.
- Rubinov M, Sporns O (2010) Complex network measures of brain connectivity: Uses and interpretations. *Neuroimage* 52(3):1059–1069.

Signatures du récepteur GPR88 sur la connectivité fonctionnelle et structurelle du cerveau chez la souris : implications pour le développement de la dépendance à l'alcool

Introduction:

Des études récentes ont démontré que des modifications pathologiques ou des mutations génétiques influencent l'architecture fonctionnelle et structurelle du cerveau (Cao et al., 2015; Mechling et al., 2016; Richiardi et al., 2015; Thompson et al., 2013). Ainsi, la cartographie de la connectivité structurelle et fonctionnelle nous offre un moyen de localiser les anomalies, d'identifier les régions cérébrales affectées par la pathologie et d'établir les patrons d'activité anormales dans les maladies psychiatriques (Biswal et al., 2010; Craddock et al., 2013; Sporns et al., 2005).

L'Imagerie par Résonance Magnétique Nucléaire à l'état de repos (rsfMRI) est une méthode qui détecte les fluctuations à basse fréquence (LFFs) de moins de 0.1 Hz dans le signal dépendant du niveau d'oxygène dans le sang (BOLD) et permet de mesurer l'activité fonctionnelle des neurones, ainsi que leur connectivité entre différentes régions du cerveau par la détection de synchronie temporelle du signal BOLD entre ces régions au repos (Biswal et al., 1995, 1997; Greicius et al., 2003). D'autre part, l'imagerie par diffusion de tenseur (DTI) est une modalité d'imagerie tridimensionnelle non-invasive qui mesure la diffusion des molécules d'eau comme indice de la microstructure cérébrale. En combinant l'information directionnelle et l'amplitude de la diffusion anisotrope de voxels individuels, il est possible de reconstituer la trajectoire des fibres nerveuses, une approche nommée tractographie. Ainsi, le DTI et la tractographie permettent de caractériser l'architecture des fibres et les modifications microstructurales induites par une pathologie ou un traitement. Les approches RsfMRI et DTI ont toutes deux été utilisées largement en imagerie cérébrale chez l'homme (Fair et al., 2007; Fox and Raichle, 2007; Alexander et al., 2007; Mori et al., 2001), les rongeurs (Jonckers et al., 2011; Mechling et al., 2014, 2016; Harsan et al., 2006, 2010, 2013) et les primates (Hutchison et al., 2012; Shi et al., 2013; Zhang et al., 2013).

Les récepteurs couplés aux protéines G (GPCRs) sont des médiateurs essentiels de l'action des hormones et neurotransmetteurs, et sont aussi des cibles privilégiées pour les traitements pharmacologiques. Les GPCRs du cerveau sont activés par des neurotransmetteurs peptidiques, aminergiques ou lipidiques, et leur stimulation induit une modification de l'activité neuronale.

GPR88 est un GPCR orphelin (ligand inconnu), fortement exprimé dans le striatum, ainsi que l'amygdale, le tubercule olfactif, l'olive inférieure et le néocortex (Ghate et al., 2007; Meirsmann et al., 2016a; Mizushima et al., 2000) chez les rongeurs, les primates et l'homme pendant le développement et chez l'adulte (Massart et al., 2009). Le striatum représente la voie d'entrée majeure des ganglions de la base (BG) et joue un rôle essentiel dans l'initiation et le développement de nombreux comportements. Le striatum reçoit des afférences excitatrices du cortex et du thalamus, ainsi que des afférences dopaminergiques modulatrices du cerveau médian et les neurones épineux (MSNs) qui le composent, modulés par l'activité d'interneurones GABAergiques locaux, projettent à leur tour vers ces régions. Les MSNs sont des deux types, les MSN exprimant les récepteurs à la dopamine D1 et ceux exprimant les récepteurs à la dopamine D2, formant la voie directe et indirecte, respectivement (Gerfen, 1992) et GPR88 est abondant dans les deux types de MSNs (Massart

et al., 2009). En conséquence, GPR88 est potentiellement impliqué dans des pathologies impliquant le striatum telles que la schizophrénie, la dépression, l'hyperactivité, les addictions et les syndromes bipolaires (Del Zompo et al., 2014; Ingallinesi et al., 2015; Logue et al., 2009; Massart et al., 2009; Meirsmann et al., 2016a; Quintana et al., 2012). Pourtant, bien des choses restent à clarifier quant à la fonction de ce récepteur au niveau cellulaire et physiologique et son rôle potentiel dans les pathologies cérébrales reste incertain.

Objectifs de la thèse:

Le premier objectif de ma thèse était de caractériser le rôle de GPR88 dans la communication neuronale chez l'animal vivant. Pour ce faire nous avons étudié par imagerie RsfMRI et DTI le cerveau de souris knockout dans lesquelles le gène codant pour GPR88 a été inactivé (souris *Gpr88^{-/-}*).

Le deuxième objectif était d'étudier le rôle de GPR88 dans le développement de l'alcoolisme. Dans ce but, nous avons évalué les comportements de consommation d'alcool chez les animaux *Gpr88^{-/-}*, ainsi que les modifications de connectivité structurelle et fonctionnelle après l'exposition alcoolique.

Enfin, dans un troisième objectif, nous avons caractérisé le comportement des animaux *Gpr88^{-/-}* à l'aide d'une approche innovante qui utilise des cages d'observation des animaux en groupe entièrement automatisée – les IntelliCages. Dans ces cages, chaque animal est identifié par une micropuce implantée. Son activité est enregistrée en continu pendant quatre phases consécutives, au cours desquelles on mesure l'apprentissage de tâches et les comportements opérants (adaptation libre, adaptation au nose-pokes, apprentissage de place and boisson à intervalles fixes).

Resultats:

La délétion du récepteur GPR88 dans les souris produit un remodelage prononcé des réseaux corticaux et sous-corticaux (Arefin et al., 2017). Les modifications les plus importantes ont été observées au niveau de la connectivité de plexus retrosplénial, un acteur majeur du réseau par défaut (default mode network ou DMN). De façon remarquable, les altérations du DMN sont reconnues comme un indice caractéristique de nombreuses maladies psychiatriques (Brady et al., 2016; Castellanos et al., 2008; Fair et al., 2010; Garrity et al., 2007). De plus, les réseaux corticaux somatosensoriels et moteurs sont fortement modifiés, ce qui est en accord avec le déficit de filtration sensorimotrice rapporté précédemment chez ces animaux, ainsi que leur phénotype hyperactif (Logue et al., 2009; Meirsmann et al., 2016a). Outre les régions corticales, avons aussi observé des altérations importantes dans la connectivité striatum-hippocampe, qui est probablement à l'origine d'une modification de l'équilibre entre les comportements allocentriques vs egocentriques que nous avons rapportée précédemment (Meirsmann et al., 2016a). Enfin, la connectivité du noyau amygdalien est fortement diminuée, en accord avec les comportements "à risque" que nous avons aussi rapporté récemment chez les souris *Gpr88^{-/-}* (Meirsmann et al., 2016b). Cette étude démontre donc que GPR88 est un régulateur majeur de la communication cérébrale, et identifie les mécanismes "réseau" qui soutendent les comportement régulés par ce récepteur. De plus, elle confirme et explicite plus avant le potentiel thérapeutique de GPR88 en tant que cible thérapeutique.

Les souris *Gpr88*^{-/-} consomment des quantités d'alcool plus élevées que leur contrôles, sans que la consommation d'eau ne soit affectée. Pour comprendre ce phénotype comportemental, nous avons développé l'étude de connectivité fonctionnelle chez les animaux qui ont consommé de l'alcool. Nous avons focalisé notre attention sur l'aire tegmentale ventral (VTA) et de l'amygdale central (CeA) et réalisé une étude de corrélation « voxelwise » pour ces régions (seed analysis). Notre quantification démontre des modifications majeures de la connectivité du VTA et de la CeA consécutives à l'exposition alcoolique à la fois chez les animaux *Gpr88*^{-/-} et leur contrôles. Ces modifications sont détectables à la fois en intra-seed et vers le cortex orbito-frontal, le striatum et le thalamus (two-sample t-test, $p < 0.001$). L'analyse des effets spécifiques liés à l'alcool et/ou au génotype est encore en cours, ainsi que celle du lien avec les données connues chez l'homme (Arefin et al., publication en préparation).

En ce qui concerne l'étude Intellicage, nous avons découvert que les souris *Gpr88*^{-/-} présentent un comportement altéré dans la phase d'habituation libre, et notamment une absence d'habituation en accord avec les études précédentes réalisées sur des animaux testés de façon individuelle. Nous n'avons pas observé de déficit dans les comportements opérants, ni dans l'apprentissage de place, indiquant que l'absence de GPR88 n'altère pas l'apprentissage dans nos conditions expérimentales. Au cours de la dernière phase, nous avons observé une différence significative dans les patrons d'activité circadienne, ainsi qu'un manque d'anticipation et une persistance dans les comportements qui n'avaient pas été rapportés lors des analyses comportementales classiques, soulignant le potentiel de l'approche Intellicage (Maroteaux et al., 2018).

Discussion:

Les gènes influencent le phénotype de manière complexe, en agissant notamment sur l'activité des réseaux neuronaux et, par voie de conséquence, en régulant les comportements. Dans le domaine de la psychiatrie, l'identification de ces mécanismes est essentielle pour le développement de nouvelles stratégies thérapeutiques. Les études récentes indiquent que l'activité de GPR88 a des conséquences sur un large répertoire de comportements, et l'implication de GPR88 dans les maladies mentales est très activement étudiée.

Notre analyse quantitative des réseaux neuronaux des souris *Gpr88*^{-/-} par Rs-fMRI a révélé que l'aire rétrospléniale (RSP) présente les perturbations les plus fortes dans sa connectivité avec le reste du cerveau. Le RSP est un élément central du DMN (Buckner et al., 2008), impliqué dans la cognition (Buckner et al., 2008; Raichle et al., 2001), et la perturbation de l'activité du DMN est connue pour être responsable de dysfonctionnements dans les maladies telles que la schizophrénie, l'autisme, l'hyperactivité avec déficit d'attention (ADHD) et la dépression (Buckner et al., 2008; Greicius et al., 2008). De plus, la délétion de GPR88 remodèle significativement la connectivité fonctionnelle dans les aires sensorielles et motrices, affectant en particulier la connectivité SS-MO et SS-MO-ACA en accord avec le déficit de filtration sensoriel, l'hyperactivité (Logue et al., 2009; Meirsmann et al., 2016a) et le comportement de prise de risque (Meirsmann et al., 2016a; 2016b) des animaux mutants. Aussi, l'analyse par « seeds » révèle des modifications importantes de la connectivité du striatum dorsal (DS) et de l'hippocampe (HP). Le DS est un centre majeur des ganglions de la base, et est impliqué dans l'apprentissage, la motivation et la cognition (Mestres-Missé et al., 2012; Yin et al., 2009). Chez les rongeurs, une lésion du DS perturbe à

la fois les comportements motivés et l'acquisition d'habitudes (Yin et al., 2004, 2005), et l'imagerie chez l'homme rapporte aussi une association entre l'activité fonctionnelle du DS et ces mêmes comportements (Liljeholm et al., 2011; Tanaka et al., 2008; Tricomi et al., 2009). L'hippocampe, par ailleurs, est critique pour différentes formes de mémoire (épisode et de travail) (Aggleton and Brown, 2006; Cabeza and Nyberg, 2000). Ainsi, la connectivité DS-HP aberrante et les perturbations de la connectivité de ces structures avec le cortex préfrontal, les aires limbiques et le cerveau médian sont très probablement à l'origine du phénotype des souris mutantes observées dans un comportement lié précisément à l'équilibre des fonctions striatales et hippocampiques (Meersman et al., 2016a). Une autre observation importante, la connectivité cortico-striatale est très perturbée (MO-CP-FC) avec un patron similaire aux modifications observées chez l'homme dans l'ADHD, dans plusieurs études à la fois chez l'adulte et l'enfant (Castellanos et al., 2006; Oldehinkel et al., 2016; Konrad and Eickhoff, 2010; Tamm et al., 2012). Enfin, nous avons aussi analysé les circuits de la récompense, au centre duquel se trouve le circuit dopaminergique mésolimbique (Kalivas and Volkow, 2005) fortement perturbé au cours du développement des addictions et de la dépendance aux drogues (Wolf et al., 2004; Zweifel et al., 2008; Koob and Le Moal, 2001). Des études électrophysiologiques récentes ont montré une forte perturbation de ce système dans les souris dépourvues de GPR88 (Quintana et al., 2012), ainsi qu'une modification du niveau d'expression de GPR88 en réponse à des drogues psychotropes (Befort et al., 2008; Conti et al., 2006). Nos résultats montrent une modification importante de la connectivité de l'aire tegmentale ventrale (Floresco and Tse, 2007), qui rassemble la majorité de neurones dopaminergiques du cerveau, ainsi que de celle de l'amygdale centrale impliquées dans les réponses exacerbées aux drogues et au stress. Ces modifications sont en accord avec notre observation d'une consommation excessive d'alcool chez ces souris.

En conclusion, notre étude combine la manipulation génétique et l'imagerie cérébrale pour étudier l'impact de l'activité du gène *Gpr88* sur la connectivité fonctionnelle du cerveau à l'échelle du cerveau entier et chez l'animal vivant. Nous avons établi une cartographie des modifications fonctionnelles et microstructurales. C'est la première étude qui démontre que l'activité du récepteur GPR88 module l'activité des réseaux neuronaux. La signature d'activité que nous observons est très similaire aux altérations observées dans le cerveau de patients atteint d'ADHD, et les études futures indiqueront si *Gpr88* est associé à cette maladie. De plus, nous avons montré que la régulation de l'activité cérébrale par GPR88 influe la consommation volontaire d'alcool, et cette observation a des implications pour le développement de traitements de l'alcoolisme. Plus généralement, notre étude confirme que GPR88 est une cible potentielle pour le traitement des maladies psychiatriques et apporte une vue très nouvelle de l'activité de ce récepteur.

References:

- Aggleton, J.P., Brown, M.W., 2006. Interleaving brain systems for episodic and recognition memory. *Trends Cogn. Sci.* 10, 455–463. doi:10.1016/j.tics.2006.08.003
- Arefin, T., Mechling, A.E., Meirsman, C.A., Bienert, T., Huebener, N.S., Lee H.L., Ben Hamida, S., Ehrlich, A., Roquet, D., Hennig, J., von Elverfeldt, D., Kieffer, B.L., Harsan, L.A., 2017. Remodeling of Sensorimotor Brain Connectivity in Gpr88 Deficient Mice. *Brain Connectivity*. doi:10.1089/brain.2017.0486 [Epub ahead of print]
- Arefin, T. M., Ben-Hamida, S., Bienert, T., Lee, H.-L., Hennig, J., von Elverfeldt, D., Kieffer, B.L., and Harsan, L.-A.. GPR88 signatures on the brain reward network connectivity after alcohol exposure in mice (*en cours de rédaction*).
- Alexander, A.L., Lee, J.E., Lazar, M., Field, A.S., 2007. Diffusion Tensor Imaging of the Brain. *Neurother. J. Am. Soc. Exp. Neurother.* 4, 316–329. doi:10.1016/j.nurt.2007.05.011
- Befort, K., Filliol, D., Ghate, A., Darcq, E., Matifas, A., Muller, J., et al., 2008. Mu-opioid receptor activation induces transcriptional plasticity in the central extended amygdala. *Eur. J. Neurosci.* 27, 2973–2984. doi:10.1111/j.1460-9568.2008.06273.x
- Biswal, B., Yetkin, F.Z., Haughton, V.M., Hyde, J.S., 1995. Functional connectivity in the motor cortex of resting human brain using echo-planar MRI. *Magn. Reson. Med.* 34, 537–541.
- Biswal, B.B., Van Kylen, J., Hyde, J.S., 1997. Simultaneous assessment of flow and BOLD signals in resting-state functional connectivity maps. *NMR Biomed.* 10, 165–170.
- Brady, R.O., Tandon, N., Masters, G.A., Margolis, A., Cohen, B.M., Keshavan, M., Öngür, D., 2016. Differential brain network activity across mood states in bipolar disorder. *J. Affect. Disord.* 207, 367–376. doi:10.1016/j.jad.2016.09.041
- Buckner, R.L., Andrews-Hanna, J.R., Schacter, D.L., 2008. The brain’s default network: anatomy, function, and relevance to disease. *Ann. N. Y. Acad. Sci.* 1124, 1–38. doi:10.1196/annals.1440.011
- Cao, M., Wang, Z., He, Y., 2015. Connectomics in psychiatric research: advances and applications. *Neuropsychiatr. Dis. Treat.* 11, 2801–2810. doi:10.2147/NDT.S63470
- Castellanos, F.X., Sonuga-Barke, E.J.S., Milham, M.P., Tannock, R., 2006. Characterizing cognition in ADHD: beyond executive dysfunction. *Trends Cogn. Sci.* 10, 117–123. doi:10.1016/j.tics.2006.01.011
- Castellanos, F.X., Margulies, D.S., Kelly, C., Uddin, L.Q., Ghaffari, M., Kirsch, A., et al., 2008. Cingulate-precuneus interactions: a new locus of dysfunction in adult attention-deficit/hyperactivity disorder. *Biol. Psychiatry* 63, 332–337. doi:10.1016/j.biopsych.2007.06.025
- Cabeza, R., Nyberg, L., 2000. Imaging cognition II: An empirical review of 275 PET and fMRI studies. *J. Cogn. Neurosci.* 12, 1–47.

- Conti, B., Maier, R., Barr, A.M., Morale, M.C., Lu, X., Sanna, P.P., Bilbe, G., Hoyer, D., Bartfai, T., 2006. Region-specific transcriptional changes following the three antidepressant treatments electro convulsive therapy, sleep deprivation and fluoxetine. *Mol. Psychiatry* 12, 167–189. doi:10.1038/sj.mp.4001897
- Craddock, R.C., Jabadi, S., Yan, C.-G., Vogelstein, J.T., Castellanos, F.X., Di Martino, A et al., 2013. Imaging human connectomes at the macroscale. *Nat. Methods* 10, 524–539. doi:10.1038/nmeth.2482
- Del Zompo, M., Deleuze, J.-F., Chillotti, C., Cousin, E., Niehaus, D., Ebstein, R.P., et al., 2014. Association study in three different populations between the GPR88 gene and major psychoses. *Mol. Genet. Genomic Med.* 2, 152–159. doi:10.1002/mgg3.54
- Fair, D.A., Dosenbach, N.U.F., Church, J.A., Cohen, A.L., Brahmbhatt, S., Miezin, F.M., Barch, et al., 2007. Development of distinct control networks through segregation and integration. *Proc. Natl. Acad. Sci. U. S. A.* 104, 13507–13512. doi:10.1073/pnas.0705843104
- Fair, D.A., Posner, J., Nagel, B.J., Bathula, D., Dias, T.G.C., Mills, K.L., Blythe, M.S., Giwa, A., Schmitt, C.F., Nigg, J.T., 2010. Atypical default network connectivity in youth with attention-deficit/hyperactivity disorder. *Biol. Psychiatry* 68, 1084–1091. doi:10.1016/j.biopsych.2010.07.003
- Floresco, S.B., Tse, M.T., 2007. Dopaminergic regulation of inhibitory and excitatory transmission in the basolateral amygdala-prefrontal cortical pathway. *J. Neurosci. Off. J. Soc. Neurosci.* 27, 2045–2057. doi:10.1523/JNEUROSCI.5474-06.2007
- Fox, M.D., Raichle, M.E., 2007. Spontaneous fluctuations in brain activity observed with functional magnetic resonance imaging. *Nat. Rev. Neurosci.* 8, 700–711. doi:10.1038/nrn2201
- Garrity, A.G., Pearlson, G.D., McKiernan, K., Lloyd, D., Kiehl, K.A., Calhoun, V.D., 2007. Aberrant “default mode” functional connectivity in schizophrenia. *Am. J. Psychiatry* 164, 450–457. doi:10.1176/ajp.2007.164.3.450
- Gerfen, C.R., 1992. The neostriatal mosaic: multiple levels of compartmental organization. *Trends Neurosci.* 15, 133–139.
- Ghate, A., Befort, K., Becker, J. a. J., Filliol, D., Bole-Feysot, C., Demebele, D., Jost, B., Koch, M., Kieffer, B.L., 2007. Identification of novel striatal genes by expression profiling in adult mouse brain. *Neuroscience* 146, 1182–1192. doi:10.1016/j.neuroscience.2007.02.040
- Greicius, M.D., Krasnow, B., Reiss, A.L., Menon, V., 2003. Functional connectivity in the resting brain: a network analysis of the default mode hypothesis. *Proc. Natl. Acad. Sci. U. S. A.* 100, 253–258. doi:10.1073/pnas.0135058100
- Greicius, M.D., Kiviniemi, V., Tervonen, O., Vainionpää, V., Alahuhta, S., Reiss, A.L., Menon, V., 2008. Persistent default-mode network connectivity during light sedation. *Hum. Brain Mapp.* 29, 839–847. doi:10.1002/hbm.20537

- Harsan, L.-A., Dávid, C., Reisert, M., Schnell, S., Hennig, J., von Elverfeldt, D., Staiger, J.F., 2013. Mapping remodeling of thalamocortical projections in the living reeler mouse brain by diffusion tractography. *Proc. Natl. Acad. Sci. U. S. A.* 110, E1797-1806. doi:10.1073/pnas.1218330110
- Harsan, L.-A., Paul, D., Schnell, S., Kreher, B.W., Hennig, J., Staiger, J.F., von Elverfeldt, D., 2010. In vivo diffusion tensor magnetic resonance imaging and fiber tracking of the mouse brain. *NMR Biomed.* 23, 884–896. doi:10.1002/nbm.1496
- Harsan, L.A., Poulet, P., Guignard, B., Steibel, J., Parizel, N., de Sousa, P.L., Boehm, N., Grucker, D., Ghandour, M.S., 2006. Brain dysmyelination and recovery assessment by noninvasive in vivo diffusion tensor magnetic resonance imaging. *J. Neurosci. Res.* 83, 392–402. doi:10.1002/jnr.20742
- Hutchison, R.M., Womelsdorf, T., Gati, J.S., Leung, L.S., Menon, R.S., Everling, S., 2012. Resting-state connectivity identifies distinct functional networks in macaque cingulate cortex. *Cereb. Cortex N. Y. N 1991* 22, 1294–1308. doi:10.1093/cercor/bhr181
- Ingallinesi, M., Le Bouil, L., Biguet, N.F., Thi, A.D., Mannoury la Cour, C., Millan, M.J., Ravassard, P., Mallet, J., Meloni, R., 2015. Local inactivation of Gpr88 in the nucleus accumbens attenuates behavioral deficits elicited by the neonatal administration of phencyclidine in rats. *Mol. Psychiatry* 20, 951–958. doi:10.1038/mp.2014.92
- Jonckers, E., Van Audekerke, J., De Visscher, G., Van der Linden, A., Verhoye, M., 2011. Functional connectivity fMRI of the rodent brain: comparison of functional connectivity networks in rat and mouse. *PLoS One* 6, e18876. doi:10.1371/journal.pone.0018876
- Kalivas, P.W., Volkow, N.D., 2005. The neural basis of addiction: a pathology of motivation and choice. *Am. J. Psychiatry* 162, 1403–1413. doi:10.1176/appi.ajp.162.8.1403
- Konrad, K., Eickhoff, S.B., 2010. Is the ADHD brain wired differently? A review on structural and functional connectivity in attention deficit hyperactivity disorder. *Hum. Brain Mapp.* 31, 904–916. doi:10.1002/hbm.21058
- Koob, G.F., Le Moal, M., 2001. Drug addiction, dysregulation of reward, and allostasis. *Neuropsychopharmacol. Off. Publ. Am. Coll. Neuropsychopharmacol.* 24, 97–129. doi:10.1016/S0893-133X(00)00195-0
- Liljeholm, M., Tricomi, E., O'Doherty, J.P., Balleine, B.W., 2011. Neural correlates of instrumental contingency learning: differential effects of action-reward conjunction and disjunction. *J. Neurosci. Off. J. Soc. Neurosci.* 31, 2474–2480. doi:10.1523/JNEUROSCI.3354-10.2011
- Logue, S.F., Grauer, S.M., Paulsen, J., Graf, R., Taylor, N., Sung, M.A., et al., 2009. The orphan GPCR, GPR88, modulates function of the striatal dopamine system: a possible therapeutic target for psychiatric disorders? *Mol. Cell. Neurosci.* 42, 438–447. doi:10.1016/j.mcn.2009.09.007
- Massart, R., Guilloux, J.-P., Mignon, V., Sokoloff, P., Diaz, J., 2009. Striatal GPR88 expression is confined to the whole projection neuron population and is regulated by

dopaminergic and glutamatergic afferents. *Eur. J. Neurosci.* 30, 397–414. doi:10.1111/j.1460-9568.2009.06842.x

Massart, R., Mignon, V., Stanic, J., Munoz-Tello, P., Becker, J.A.J., Kieffer, B.L., et al., 2016. Developmental and adult expression patterns of the G-protein-coupled receptor GPR88 in the rat: Establishment of a dual nuclear-cytoplasmic localization. *J. Comp. Neurol.* 524, 2776–2802. doi:10.1002/cne.23991

Maroteaux, Arefin TM., Harsan, L.-A., Emmanuel D., Ben Hamida, S., Kieffer, B., 2018. Lack of anticipatory behavior in Gpr88 knockout mice revealed by automated home cage phenotyping. *Genes Brain Behav.* In press

Mechling, A.E., Arefin, T., Lee, H.-L., Bienert, T., Reisert, M., Ben Hamida, S., Darcq, E., Ehrlich, A., Gaveriaux-Ruff, C., Parent, M.J., Rosa-Neto, P., Hennig, J., von Elverfeldt, D., Kieffer, B.L., Harsan, L.-A., 2016. Deletion of the mu opioid receptor gene in mice reshapes the reward-aversion connectome. *Proc. Natl. Acad. Sci. U. S. A.* 113, 11603–11608. doi:10.1073/pnas.1601640113

Mechling, A.E., Hübner, N.S., Lee, H.-L., Hennig, J., von Elverfeldt, D., Harsan, L.-A., 2014. Fine-grained mapping of mouse brain functional connectivity with resting-state fMRI. *NeuroImage* 96, 203–215. doi:10.1016/j.neuroimage.2014.03.078

Meersman, A.C., Le Merrer, J., Pellissier, L.P., Diaz, J., Clesse, D., Kieffer, B.L., Becker, J.A.J., 2016a. Mice Lacking GPR88 Show Motor Deficit, Improved Spatial Learning, and Low Anxiety Reversed by Delta Opioid Antagonist. *Biol. Psychiatry* 79, 917–927. doi:10.1016/j.biopsych.2015.05.020

Meersman, A.C., Robé, A., de Kerchove d'Exaerde, A., Kieffer, B.L., 2016b. GPR88 in A2AR Neurons Enhances Anxiety-Like Behaviors. *eNeuro* 3. doi:10.1523/ENEURO.0202-16.2016

Mestres-Missé, A., Turner, R., Friederici, A.D., 2012. An anterior-posterior gradient of cognitive control within the dorsomedial striatum. *NeuroImage* 62, 41–47. doi:10.1016/j.neuroimage.2012.05.021

Mizushima, K., Miyamoto, Y., Tsukahara, F., Hirai, M., Sakaki, Y., Ito, T., 2000. A novel G-protein-coupled receptor gene expressed in striatum. *Genomics* 69, 314–321. doi:10.1006/geno.2000.6340

Mori, S., Itoh, R., Zhang, J., Kaufmann, W.E., van Zijl, P.C., Solaiyappan, M., Yarowsky, P., 2001. Diffusion tensor imaging of the developing mouse brain. *Magn. Reson. Med.* 46, 18–23.

Oldehinkel, M., Beckmann, C.F., Pruim, R.H.R., Oort, E.S.B. van, Franke, B., Hartman, C.A., Hoekstra, P.J., Oosterlaan, J., Heslenfeld, D., Buitelaar, J.K., Mennes, M., 2016. Attention-Deficit/Hyperactivity Disorder Symptoms Coincide With Altered Striatal Connectivity. *Biol. Psychiatry Cogn. Neurosci. Neuroimaging* 1, 353–363. doi:10.1016/j.bpsc.2016.03.008

- Quintana, A., Sanz, E., Wang, W., Storey, G.P., Güler, A.D., Wanat, M.J., et al., 2012. Lack of GPR88 enhances medium spiny neuron activity and alters motor- and cue-dependent behaviors. *Nat. Neurosci.* 15, 1547–1555. doi:10.1038/nn.3239
- Raichle, M.E., MacLeod, A.M., Snyder, A.Z., Powers, W.J., Gusnard, D.A., Shulman, G.L., 2001. A default mode of brain function. *Proc. Natl. Acad. Sci. U. S. A.* 98, 676–682.
- Richiardi, J., Altmann, A., Milazzo, A.-C., Chang, C., Chakravarty, M.M., Banaschewski et al., Correlated gene expression supports synchronous activity in brain networks. *Science* 348, 1241–1244. doi:10.1126/science.1255905
- Shi, Y., Short, S.J., Knickmeyer, R.C., Wang, J., Coe, C.L., Niethammer, M., Gilmore, J.H., Zhu, H., Styner, M.A., 2013. Diffusion tensor imaging-based characterization of brain neurodevelopment in primates. *Cereb. Cortex N. Y. N 1991* 23, 36–48. doi:10.1093/cercor/bhr372
- Sporns, O., Tononi, G., Kötter, R., 2005. The human connectome: A structural description of the human brain. *PLoS Comput. Biol.* 1, e42. doi:10.1371/journal.pcbi.0010042
- Tamm, L., Barnea-Goraly, N., Reiss, A.L., 2012. Diffusion tensor imaging reveals white matter abnormalities in Attention-Deficit/Hyperactivity Disorder. *Psychiatry Res.* 202, 150–154. doi:10.1016/j.psychres.2012.04.001
- Tanaka, S.C., Balleine, B.W., O’Doherty, J.P., 2008. Calculating consequences: Brain systems that encode the causal effects of actions. *J. Neurosci. Off. J. Soc. Neurosci.* 28, 6750–6755. doi:10.1523/JNEUROSCI.1808-08.2008
- Thompson, P.M., Ge, T., Glahn, D.C., Jahanshad, N., Nichols, T.E., 2013. Genetics of the connectome. *NeuroImage* 80, 475–488. doi:10.1016/j.neuroimage.2013.05.013
- Tricomi, E., Balleine, B.W., O’Doherty, J.P., 2009. A specific role for posterior dorsolateral striatum in human habit learning. *Eur. J. Neurosci.* 29, 2225–2232. doi:10.1111/j.1460-9568.2009.06796.x
- van Ewijk, H., Heslenfeld, D.J., Zwiers, M.P., Buitelaar, J.K., Oosterlaan, J., 2012. Diffusion tensor imaging in attention deficit/hyperactivity disorder: a systematic review and meta-analysis. *Neurosci. Biobehav. Rev.* 36, 1093–1106. doi:10.1016/j.neubiorev.2012.01.003
- Wolf, M.E., Sun, X., Mangiavacchi, S., Chao, S.Z., 2004. Psychomotor stimulants and neuronal plasticity. *Neuropharmacology* 47 Suppl 1, 61–79. doi:10.1016/j.neuropharm.2004.07.006
- Yin, H.H., Knowlton, B.J., Balleine, B.W., 2004. Lesions of dorsolateral striatum preserve outcome expectancy but disrupt habit formation in instrumental learning. *Eur. J. Neurosci.* 19, 181–189.
- Yin, H.H., Mulcare, S.P., Hilário, M.R.F., Clouse, E., Holloway, T., Davis, M.I., Hansson, A.C., Lovinger, D.M., Costa, R.M., 2009. Dynamic reorganization of striatal circuits during the acquisition and consolidation of a skill. *Nat. Neurosci.* 12, 333–341. doi:10.1038/nn.2261

Yin, H.H., Ostlund, S.B., Knowlton, B.J., Balleine, B.W., 2005. The role of the dorsomedial striatum in instrumental conditioning. *Eur. J. Neurosci.* 22, 513–523. doi:10.1111/j.1460-9568.2005.04218.x

Zhang, D., Guo, L., Zhu, D., Li, K., Li, L., Chen, H., Zhao, Q., Hu, X., Liu, T., 2013. Diffusion tensor imaging reveals evolution of primate brain architectures. *Brain Struct. Funct.* 218, 1429–1450. doi:10.1007/s00429-012-0468-4

Zweifel, L.S., Argilli, E., Bonci, A., Palmiter, R.D., 2008. Role of NMDA receptors in dopamine neurons for plasticity and addictive behaviors. *Neuron* 59, 486–496. doi:10.1016/j.neuron.2008.05.028

Résumé

Les mutations génétiques et les conditions pathologiques affectent la connectivité fonctionnelle du cerveau. Nous avons combiné la mutagenèse chez la souris et l'analyse de connectivité fonctionnelle (CF) par imagerie en Résonance Magnétique Nucléaire (IRM) pour déterminer l'impact de la délétion du gène codant pour le récepteur orphelin GPR88 sur la CF du cerveau entier. En utilisant une approche non biaisée, nous avons découvert que la délétion génétique chez la souris altère fortement le Default Mode Network, une caractéristique de nombreuses maladies psychiatriques. Nous avons aussi observé des modifications importantes de la connectivité des cortex moteurs et somatosensoriels, et du striatum en accord avec le pattern d'expression du récepteur. Enfin, une analyse par régions d'intérêt montre une perturbation importante du réseau mesocorticolimbic, qui pourrait expliquer la tendance de ces animaux à consommer de fortes quantités d'alcool. La concordance entre les altérations de CF et celles du comportement des animaux GPR88 knockout positionnent ce récepteur comme une cible prometteuse pour le traitement de maladies psychiatriques.

Résumé en anglais

Pathological agitations of the brain and the expression or mutation of single gene affect overall brain connectivity. Here we combined mouse mutagenesis with functional and structural MRI and explored mouse whole brain connectivity maps non-invasively in response to the inactivation of Gpr88 gene. We perceived robust modifications in the default mode network which is considered a hallmark of many psychiatric conditions, followed by sensori-motor network allied to sensorimotor gating deficiency underlying hyperactivity phenotype in Gpr88^{-/-} mice. In addition, hippocampal and dorsal striatum functional connectivity perturbations might underlie learning deficiency and weakened amygdala connectivity with cortex and striatum might suggest triggering of risk-taking behavior previously observed in these animals. Moreover, Gpr88 deletion strongly modifies the reward network leading Gpr88^{-/-} mice vulnerable to alcohol intake. This is the first evidence of Gpr88 involvement in reshaping the mouse brain connectome. The concordance between connectivity alterations and behavior deficits posits Gpr88 as a potential target for psychiatric disorders.

Keywords: Gpr88, mouse brain functional and structural connectivity, default mode network